APPLICATIONS OF CHEMICAL PROTEOMICS IN DEFINING PRENYLATED PROTEOMES AND DISCOVERING NOVEL PRENYLATED PROTEINS

A DISSERTATION

SUBMITTED TO THE FACULTY OF THE GRADUATE SCHOOL

OF THE UNIVERSITY OF MINNESOTA

BY

KIALL FRANCIS GANDILAN SUAZO

IN PARTIAL FULFILLMENT OF THE REQUIREMENTS

FOR THE DEGREE OF

DOCTOR OF PHILOSOPHY

ADVISOR: PROF. MARK D. DISTEFANO

APRIL 2021

Acknowledgements

My pursuit of this PhD degree was indeed one of the biggest decisions I had to make. I would have not reached this far without the help, encouragement, and support of many people whom I am grateful to have known. I would like to take this opportunity to thank those who have been a part of this journey.

I would like to first thank my advisor, Dr. Mark D. Distefano, for trusting me with various projects and giving me opportunities to collaborate with many scientists inside and outside of the university. Coming from a place where I did not have much access to cutting-edge research and state-of-the-art facilities, he allowed and encouraged me to pursue scientific questions that were beneficial to our group's research, particularly those that have piqued my interests. Through his enthusiasm and undying curiosity, I learned how to think critically and devise strategies to tackle every scientific question I could think of. He always cared not only about my current progress in research but also with my future career plans by providing me helpful advice. He has prepared me to become the scientist I am today and I will forever be grateful for that. I would also like to thank my committee members Dr. Edgar Arriaga, Dr. Carrie Haskell-Luevano, and Dr. Ling Li.

I am grateful to have shared my experiences in doing research with the past and current members of the MDD group. I am grateful to have had Charuta Palsuledesai as my mentor, who initially trained me and kept me up to speed when I started working in the lab. The past members including Yi Zhang, Mohsen Mamoodi, Jeff Vervacke, Sudheer Chava,

Mina Ahmadi, and Matt Hammers have been great sources of helpful information on how to navigate in the lab and in graduate school, in general. I am also grateful to have Grace Mauger joining the MDD group with me in our first year. We definitely made a lot of memories—outside of the lab for my most part. The current lab members Kevin Park, Garrett Schey, Taysir Bader, Yiao Wang, and Shelby Auger have made this journey a lot more bearable. It was a pleasure to share the lab space and research projects with you. Our pre-Covid rendezvous were essential outlets to release the stress and tension in my projects when the results were frustrating and not going well. I would like to thank Pa Thao and Kevin Liu for giving me the opportunity to train them in the lab. It was a pleasure to work with you both and I am proud of what you have now become.

Working in multiple projects would have not been possible without the help of our collaborators. I would like to acknowledge all of my collaborators, particularly the Ling Li's lab, who have closely worked with us all through these years and have helped me expand my knowledge in biology. The Pomerantz, Carlson, and Hoye labs in our department were also generous in sharing reagents and lab equipment and I am grateful for their help.

My previous teachers and mentors from grade school, high school, and college have played key roles in leading me to my pursuit of this PhD degree. In particular, my high school chemistry and math teachers, Maam Ruby Dahilog and Julie Alas, respectively, has honed my interest in science and math, which has inspired me to take up a chemistry degree in college. I would like to thank Dr. Susan Arco for teaching and guiding me how to apply

my knowledge in organic chemistry for my undergraduate research. I am also extremely grateful for Dr. Aaron Villaraza who gave me the opportunity to conduct research for my MS degree and supported me to advance my career by pursuing this PhD in the United States.

Minnesota will always be my first home here in the United States. Several people have made my life outside work enjoyable and memorable. My Filipino friends Dr. Camille May, Mavic Punay, Dr. Geoffrey Li, Kenn Chua, Dr. Kurt See, Dr. Romel Dator, Dr. Morwena Solivio, and Dr. Jon Ramirez always felt like home. Thank you for making our little community a testament that wherever we Filipinos will be, we will always be there for each other. My bisdak friends, especially Zel Andales, who always made me feel comfortable and was always available when I needed a friend to hang out with or to talk to. Andrew Rabin has been my best friend here in Minnesota. Thank you for everything. To my former roommate, Dr. David Goldfeld, thank you for the five years of living with me. You have helped in many ways, especially in times I needed you to create programs that I could use in my research projects. I would also like to thank Jeff Dreblow for helping me get through the many times I almost gave up in life. Thank you for introducing me to ways on how I could take care of my mental health.

I would also like to thank my friends who greatly influenced my decision to leave my comfort zone and jump in the train to the daunting graduate school. To my buddies Marco Jacinto and Faye Carvajal-Calvary, thank you for the times you shared with me when we were preparing to the exams we needed to take in order to get into graduate

school. I will always cherish those memories with you. I would have not been more dedicated to apply to get in to programs if it were not for you. To my constants Herdeline Ardona, Maxx Arguilla, Daben Libardo, Jenny Obligacion, Arizza Ibanez, Joe Mapas, Jasmine Federizon, and Bobby Katigbak, thank you for the friendship and for constantly checking up on me. Our weekly zoom call has been the one thing I would look forward to every weekend and has been keeping me sane all though out this pandemic. Thank you for sharing your own experiences in pursuing your respective PhD degrees. Those have always made me feel I am not alone in this endeavour.

Finally, I would like to thank my family. Since I left home when I was 16 to pursue college, you have always been supportive of my decisions. Thank you mama, Phoebe Suazo, for always making ends meet for us. You always worked hard to help me get through school. We were never financially stable and yet you found ways to put my needs first. I would also like to thank my sister, Dr. Kharinine Escasinas for assisting my mom financially in supporting me to get through college. I dedicate this dissertation to you both.

Abstract

Since its development as a strategy to study biological systems, click chemistry has found its widespread use as a chemical tool in the discovery of post-translationally modified (PTM) proteins. In particular, the number of identified and validated lipid-modified proteins has dramatically increased over the last decade owing to the versatility and ease of use of this technique. Among these lipid PTMs, protein prenylation has benefited in uncovering new protein substrates, leading to the characterization and understanding of the functional role of this type of modification. This dissertation describes the development of a mass spectrometry-based chemical proteomics strategy that heavily relies on click chemistry to identify prenylated proteins in various systems, which allows for defining the prenylated proteomes and discovering novel prenylated proteins. The first chapter details a comprehensive literature review on the impact of click chemistry in revolutionizing the field of protein lipidation. Chapter 2 describes the development of chemical proteomics using probe analogue of isoprenoids to define the set of prenylated proteins in the malaria parasite, *Plasmodium falciparum*. Upon moving to eukaryotic systems, optimization of the probe and statin (enhancer of probe incorporation) treatments is described in Chapter 3. Our chemical proteomics approach was then successfully employed in various mammalian cell lines, enabling the validation of known and discovery of novel prenylated proteins. Moreover, the similarities and differences in brain-related cell lines were determined. Finally, an unusually prenylated protein, ALDH9A1, was discovered from these proteomic studies and tools in chemical and molecular biology were used to characterize and understand its occurrence. This dissertation highlights the

advantages of using chemical proteomics in studying protein prenylation and contributes to the growing picture of protein lipid modifications.

Table of Contents

List of Tables

List of Figures

Chapter 1: Click chemistry in protein-lipid modifications

1.1. Introduction

Protein lipid modification involves the attachment of hydrophobic groups to proteins via ester, thioester, amide or thioether linkages; this process occurs in eukaryotes but not prokaryotes.[1,2] The most common purpose of such modifications is to cause the association of the resulting proteins to various membranes where they can interact with other proteins involved in signal transduction pathways. Proteins containing such modifications are involved in a diverse range of cellular functions including cell division, subcellular organization, secretion and differentiation.[3–7] Due to their critical role in such processes, these lipid-modified proteins are often mutated in various diseases or targets for therapeutic intervention.[8–11] In addition, the consensus sequences that mark proteins for lipidation are often simple and can be incorporated into other proteins to render them membrane-bound or provide a new site for selective modification. That feature has been exploited for a myriad of applications ranging from protein immobilization to the creation of protein-drug

conjugates for therapeutic applications.[12,13] Click chemistry has played a key role in both illuminating features of protein lipid modification as well as exploiting it for the aforementioned alternative applications.[14–18]

In this chapter, the specific click chemical reactions that have been employed to study protein lipid modification and their use for specific labeling applications are described. That is followed by an introduction to the different types of protein lipid modifications that occur in biology. Finally, the roles of click chemistry in elucidating specific biological features including the identification of lipid-modified proteins, studies of their regulation, and their role in diseases are presented.

1.2. Protein lipid modifications

A large number of proteins synthesized within cells undergo post-translational modifications (PTMs) essential for their biological function, cellular localization and activity. More than 200 PTMs are currently known that diversify protein function and dynamically synchronize complex signaling networks.[19] Among these PTMs, protein lipidation involves the covalent attachment of small, hydrophobic molecules that promote stable membrane association of proteins, regulate protein trafficking, and mediate protein-protein interactions.[3] Lipid PTMs can be categorized into two types—those that occur on the cytosolic side of membranes and those that take place in the lumen of secretory organelles. There are three major protein lipidation processes known to occur in the cytoplasm or cytoplasmic face of membranes. The first two modify proteins with fatty acyl groups, palmitoyl and myristoyl, generally on thiols present in cysteine (*S*-acylation) and

N-terminal amines of glycine (*N*-myristoylation), respectively. The thioester bonds formed *in S*-acylated proteins are labile and are therefore reversible, as opposed to the amide bonds in *N*-myristoylated proteins that are thought to be stable and irreversible. The third major type of protein lipidation is *S*-prenylation where the thiols of cysteines present near the C-terminus of proteins are linked to an isoprenoid through a thioether bond. In contrast, lipidation of secreted proteins includes cholesterylation and the attachment of glycosylphosphatidylinositol (GPI) anchors. Cholesterylation involves the esterification of the carboxyterminus of proteins with a cholesteryl functional group, while modification with a GPI anchor appends a fatty acylated phosphatidyl inositol containing a glycan core and linked to the carboxyterminus of proteins through an amide bond with ethanolamine. An overview of the major cytoplasmic protein lipid modifications is presented below.

1.2.1. *S*-acylation (S-palmitoylation)

Protein *S*-acylation is the addition of fatty acids of varying carbon chain lengths (C14-C20) to a cysteine residue forming a thioester bond. In particular, protein is *S*-palmitoylation is the most common type of this modification (Fig. 1.1A). This lipid PTM is essential for stable anchoring, trafficking and localization of a plethora of membrane-associated proteins.[20] The discovery of a protein modified with a palmitoyl moiety was initially made via radiolabeling in virus-infected cells with [^{3}H] palmitate.[21] Soon thereafter, a number of other *S*-acylated proteins were reported including rhodopsin and p21 Ras protein.[22,23] The protein acyltransferase (PAT) enzymes that catalyze this thioester linkage formation were initially discovered in yeast,[24] and later found to bear a conserved aspartate-histidine-

histidine-cysteine (DHHC) motif in its cysteine-rich domain (CRD).[25] The first mammalian homolog identified contained a zinc finger domain,[26] which is a salient feature of all mammalian PATs reported to date. Hence, they are typically referred to as zDHHC-PATs. These enzymes are relatively ubiquitous as they localize in the golgi, endoplasmic reticulum (ER), and plasma membrane,[27] although recent findings indicate that they mainly reside in golgi membranes.[28] In both human and mouse genomes, bioinformatic analyses revealed that there are 23 proteins known to possess the DHHC-CRD motifs, raising the possibility of a large family of zDHHC-PATs.[29] Indeed, these 23 enzymes are recognized as fatty acyl transferases particularly for protein *S*-palmitoylation. However, the catalytic motif is not strictly constrained to the DHHC amino acid residues, as other motifs such as DHYC in yeast Akr1 and DQHC in mammalian zDHHC13 display efficient *S*-palmitoylation activity with their substrates.[30,31] Furthermore, zDHHC-PATs generally catalyze the transfer of fatty acids with varying lengths or containing unsaturated bonds, although palmitate-CoA is their preferred substrate.

The DHHC motif in PATs is highly conserved and usually necessary for catalysis, while the CRD is speculated to be important for zinc ion binding.[32,33] Although PATs have been studied for several years, until recently, no atomic structure was available and most studies relied mainly on predictive models. The recent breakthrough of successfully solving the crystal structures for human zDHHC20 and zebrafish zDHHC15 illuminated and supported the observed and predicted features of some zDHHCs crucial to understanding their structure and mechanism.[34,35] The crystal structures of these two zDHHCs revealed the projection of transmembrane domains (TMDs) and other key

intramolecular contacts that rationalize the exposure of the DHHC-CRD to the cytoplasm, as well as the placement of the active site at the cytoplasm-membrane interface (Fig. 1.1B). Their active sites also resemble a catalytic triad wherein the first His in the DHHC motif is polarized by the Asp to deprotonate the catalytic Cys, generating a thiolate for efficient

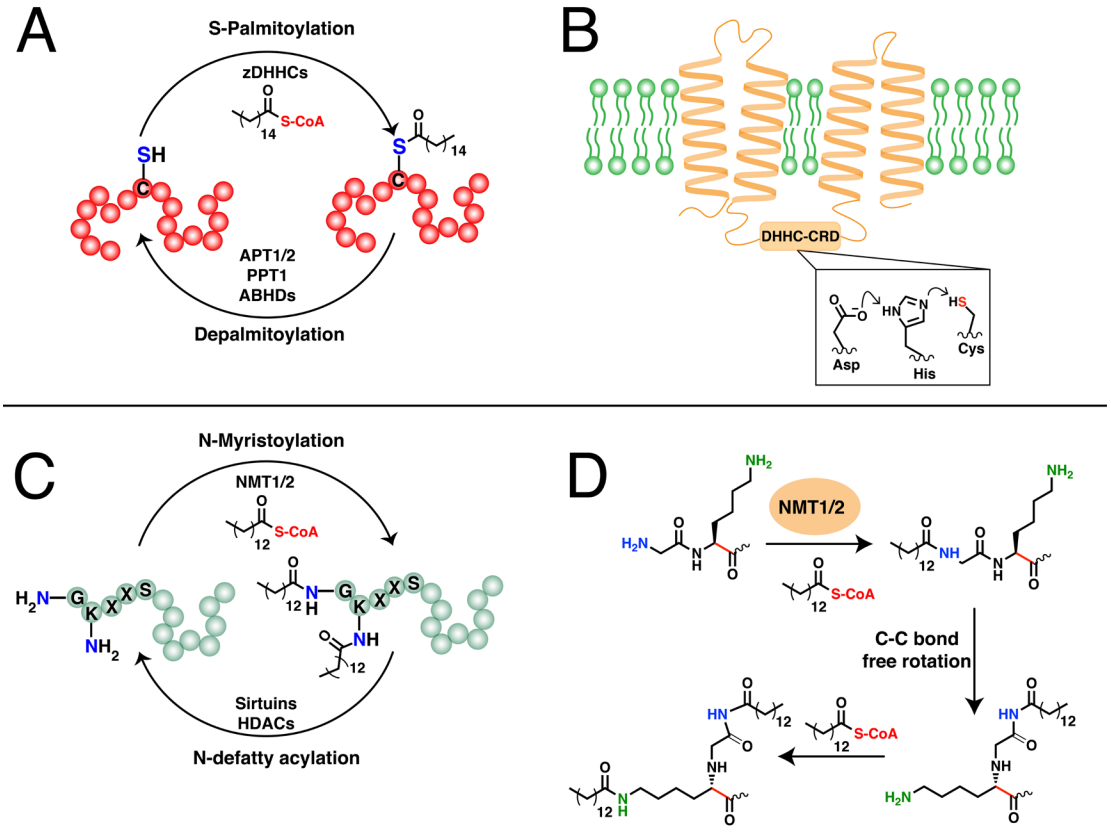

Figure 1.1. Fatty acylation on Proteins.

(A) The dynamic cycling of protein *S*-palmitoylation and depalmitoylation on cysteine residues. zDHHCs catalyze *S*-acylation on proteins particularly *S*-palmitoylation while APTs, PPT1, and ABHDs can remove these modifications. **(B)** A representative structure of a zDHHC-PAT embedded in a membrane through its transmembrane domains (TMDs). The DHHC active site is oriented towards the cytoplasm and resembles a catalytic triad that generates a thiolate nucleophile for activation of fatty acyl-CoAs. **(C)** The *N*-myristoylation and *N*-defatty acylation cycling of *N*-lipidated proteins. NMTs can catalyze both N-terminal and side-chain fatty acylation, although the lysine is typically adjacent to the N-terminal glycine. Sirtuins and HDACs can reverse this modification **(D)** The mechanism for the dual myristoylation on the N-terminus of myristoylated AFR6 GTPase. The free rotation of the C-C bond shown in red allows for dual myristoylation on the N-terminal glycine and the side-chain of the adjacent lysine.

nucleophilic attack on palmitoyl-CoA, and resulting in an auto-palmitoylated zDHHC enzyme with a concomitant release of CoA. The covalently attached palmitoyl moiety is then transferred to a bound protein substrate.[36] The auto-acylation mechanism is common among zDHHCs, however, not all seem to require such an intermediate. Depending on the mutations introduced into the positions in the active site, some zDHHCs remain functional and can still *S*-palmitoylate their protein substrates regardless of whether the machinery for auto-palmitoylation is present or not.[30,37,38] It is important to note that these crystal structures are for only two zDHHCs and may not necessarily be representative of other zDHHC family members. Factors such as structural and chemical requirements of individual zDHHCs, the mechanism of fatty acyl transfer, or the reactivity of the protein substrate's cysteine may play key roles into determining the precise mechanistic details of each zDHHC enzyme's reaction with their cognate substrates.[35]

Deducing substrate specificities across zDHHCs is non-trivial due to the lack of a consensus sequence within the substrates that these enzymes recognize. The functional redundancy observed among them coupled with the fact that they share the same substrates makes the generality of their substrate recognition mechanism implausible. Multiple factors may dictate the specificity of particular zDHHCs for their substrates such as the presence of specific binding domains and substrate proximity. For example, zDHHC13 and zDHHC17 contain ankyrin-repeat domains that interact with a consensus sequence present in SNAP23, SNAP25, and huntingtin.[37] On the other hand, zDHHC5 engages with its substrate GRIP1b through its PDZ motif, yet interacts with another substrate PLM through the enzyme's C-terminal 120-amino acid domain.[39,40] Clearly, these varying modes of

interaction between zDHHCs and their substrates requires further investigations to elucidate the distinctive substrate recognition features of individual enzyme-substrate pairs. Despite this lack of consensus, a powerful predictive tool, based on a clustering and scoring algorithm (CSS-Palm), was developed for global *in silico* screening of *S*-palmitoylation sites in proteomes.[41]

One characteristic feature of protein *S*-palmitoylation is its dynamic nature (Fig. 1.1A). Acyl protein thioesterases (APTs) and lysosomal protein palmitoylthioesterase-1 (PPT1) serve as deacylases/depalmitoylases that catalyze the cleavage of palmitate groups for protein cycling and degradation, respectively.[42] Members of the α/β-Hydrolase domain-containing (ABHDs) family of thioesterases were also found to catalyze depalmitoylation of mammalian proteins.[43] These depalmitoylases themselves require palmitoyl modification for proper localization and function. The plasma membrane localization of small GTPases and G proteins, for example, is controlled by a continuous *S*-palmitoylation-depalmitoylation cycle, manifesting the requirement of both zDHHCs and depalmitoylases for regulating localization, and in effect, the function of palmitoylated proteins.[44] However, the stability of the palmitate modification varies over a range of substrates, with most proteins remaining stably *S*-palmitoylated with others undergoing rapid dynamic cycling.[45]

The broad substrate scope of protein *S*-acylation/deacylation highlights its major role in mediating numerous and diverse biological processes. This includes regulation of intracellular signaling and trafficking, shaping of neuronal synaptic plasticity, and immunity against bacterial and viral infections, among others.[46–48] Dysregulation and perturbations in this lipidation pathway have been linked to a myriad of diseases including

neurological disorders and cancer.[49,50] In later sections, this review describes the impact of click chemistry as a valuable tool to characterize the role of *S*-acylation particularly of *S*-palmitoylation in regulating the biological functions of known and novel *S*-palmitoylated proteins, as well as the development of technological innovations based on the clickable analogues of palmitic acid.

1.2.2. *N*-Myristoylation

A second major type of fatty acylation is the covalent attachment of a myristoyl group, a saturated 14-carbon chain, onto the amine of an N-terminal glycine residue (Fig. 1.1C). Similar to *S*-acylation, the activated myristoyl-CoA form is used as a substrate to acylate proteins and form an amide bond catalyzed by *N*-myristoyltransferases (NMTs).[51] This lipidation is often critical for proper localization of modified proteins. However, *N*-myristoylation alone is generally insufficient to confer stable anchoring and is therefore usually present in tandem with a second membrane-targeting signal such as a polybasic region (PBR) or other lipid modifications including *S*-palmitoylation.[52,53] *N*-myristoylation can proceed either through co- or post-translational mechanisms. The co-translational mechanism occurs on nascent proteins with initial cleavage of Met catalyzed by MetAPs and subsequent glycine *N*-myristoylation on substrates with consensus N-terminal sequence of MG[^DEFRWY]X[^DEKR][*ACGST][*KR]X, where ^ denotes exclusion of the amino acids listed in that specific position, * indicates preferred residues, and X is any amino acid.[54] The transfer of the myristoyl moiety then takes place during translation. In contrast, post-translational modification has been observed in pro-apoptotic proteins that

are cleaved by caspases during apoptosis, revealing a new N-terminal glycine fated for myristoyl modification.[53] The NMTs themselves are truncated during apoptosis, which alters their cellular localization and influences their rates of activity and to some extent, their specificities towards their fragment substrates.[55]

NMT-mediated *N*-myristoylation follows a sequential ordered bi-bi mechanism where the initial binding of myristoyl-CoA elicits a conformational change that enables subsequent protein substrate binding.[56,57] Unlike *S*-palmitoylation where the palmitoyl group is transiently attached to zDHHCs prior to transfer, NMTs directly append the myristoyl group onto their substrates without participation of a covalent intermediate. A recent analysis of high-resolution structures of human NMT1 co-crystalized with myristoyl-CoA and substrate peptides allowed for atomic-level dissection of the molecular mechanism of NMT catalysis.[57] In these structures, an oxy-anion hole is present that activates the acyl group for efficient attack of the N-terminal amine from Gly1 of the substrate. The Ab-loop of NMT represents a fluid structure that promotes pre-organization of the substrates, which then triggers water-mediated deprotonation of the amino group by a carboxy catalytic base from Gln496, followed by nucleophilic attack of myristoyl-CoA. This concerted reaction is promoted by Thr282 that serves as a key residue in this mechanism. Importantly, the absence of a side chain on Gly permits free rotation of the N-terminal amine that is necessary for this mechanism, making it preferentially modified by NMTs over other amino acids. In addition, a hydrophilic pocket near the enzyme's active site interacts with the fifth amino acid of the substrate, favoring the polar residues Ser, Thr,

or Cys that occupy this position. These features serve as the basis for the specificity of NMTs toward N-terminal glycine-containing substrates.[58,59]

There is no evidence of innate expression of NMTs in prokaryotes and hence, they usually exploit host machinery to perform myristoyl modification required during infection.[60] In some cases, pathogenic eukaryotes require intracellular *N*-myristoylation for their survival and virulence, prompting efforts to design pathogen-specific NMT inhibitors as therapeutic agents.[52] Lower eukaryotes typically encode a single NMT gene while higher organisms express two characterized enzymes NMT1 and NMT2, which share approximately 77% sequence identity in the human homologs.[61] Although both NMTs generally have overlapping substrates, biochemical and kinetic assays suggest that their substrate affinities differ and are not functionally redundant.[62] Separate knockdowns of each enzyme resulted in differential effects in cell proliferation, embryonic development, and T-cell receptor signaling.[3] Furthermore, they behave differently during apoptosis—NMT1 translocates from the plasma membrane to the cytosol while NMT2 does the contrary.[55] These changes in their localization cause subtle differences in their substrate scope reflected by the downstream effects that ensue from the aberrations on the biological functions of their substrates.

While *N*-myristoylation is frequently ascribed to covalent attachment on an N-terminal glycine, N^{ε}-side chain fatty acylation on Lys residues was recognized as early as 1992.[63] The growing number of side-chain fatty acylated proteins identified has gained more attention over recent years and highlights their more frequent occurrence than was

previously thought. Members of the Ras family of small GTPases such as KRAS, RRAS2, and RalB are N^{ε}-fatty acylated on a Lys in their PBR, in addition to *S*-palmitoylation or *S*-prenylation on Cys residues.[64–66] NMTs were recently discovered as the first enzymes to catalyze such Lys modification, at least for ARF6 GTPase.[67] After the initial N-terminal *N*-myristoylation on Gly1 of ARF6, the lipid moiety shifts to a conformation that positions the side-chain amine of the adjacent Lys2 for efficient N^{ε}-myristoylation (Fig. 1.1D). High-resolution structures of Gly1-Lys2-containing peptides in NMTs reveal that the Lys2 amino side-chain directly interacts with the carboxy catalytic base for efficient deprotonation, as opposed to the observed water-mediated deprotonation of Gly1.[57] This possible dimyristoylation of ARF6 adds another layer to the intricacies of lipid modification and provides a rationale for its potentially unique regulation compared to other glycine-myristoylated members of the ARF family.[67] While this demonstrates the capability of NMTs to modify side-chain amines, the mechanism for the fatty acylation on Lys residues positioned within the protein sequence or in the C-terminal PBRs remains unknown.

For many years, dynamic lipid modification has been focused on *S*-palmitoylation until recently, when the unexpected hydrolytic removal of fatty acyl groups from N^{ε}-modified Lys residues was reported. The landmark discovery of sirtuins and histone deacetylases (HDACs) as lysine defatty-acylases broadened the paradigm to include the idea that Lys fatty acylation may also be dynamic.[68] This family of proteins were initially described as “erasers” of short acyl modifications (*e.g.* acetyl) that is essential mainly in regulating epigenetic processes.[69,70] However, recent studies provide evidence of their

ability to remove long-chain fatty acids from modified substrates associated with other biological processes. For example, SIRT6 and HDAC11 can efficiently cleave long-chain lipids from RRAS2 and serine methylhydroxytransferase (SHMT), respectively.[65,71] ARF6 itself is regulated by both NMTs and SIRT2, where NMT may myristoylate Lys2 in its GTP-bound active form while SIRT2 demyristoylates ARF6 while in its GDP-bound inactive state, thereby regulating another aspect of the GTPase cycle.[67] Other members of these family of hydrolyzing enzymes exhibit defatty-acylase activity but no current bonafide substrates have been identified to date.[68]

Being an important lipid modification, *N*-myristoylation is a key regulator of protein stability, activity, localization, and protein-protein interactions that are linked to multiple aspects of immunity, autophagy, infection, and cancer.[3,52,72–74] The use of click chemistry has enabled significant progress towards addressing numerous biological questions with substantial efforts focused on parasitic infections. A comprehensive description of those studies are discussed in Section 1.5.

1.2.3. *S*-Prenylation

While the previous two major types of lipidation are based on acylation, *S*-prenylation is the attachment of isoprenoids onto cysteine residues forming a thioether bond. It was first observed in fungi and much later found to be present in mammals.[75,76] There are now three recognized classes of protein *S*-prenylation. The first two involve a single addition of an isoprenoid either as a shorter-chain farnesyl or a longer-chain geranylgeranyl group from

the native substrates farnesyldiphosphate (FPP) or geranylgeranyldiphosphate (GGPP), respectively, catalyzed by farnesyltransferase (FTase) or geranylgeranyltransferase type I (GGTase-I) as shown in Fig. 1.2A.[77] The protein substrates for these enzymes are recognized through a C-terminal motif with a canonical sequence generalized as the Ca_1a_2X box. C is the cysteine that is modified with the prenyl group, a_1 and a_2 are generally hydrophobic amino acids, and X determines the fate of the protein substrate, either farnesylation or geranylgeranylation. Farnesylation is usually observed in proteins with alanine, methionine, serine, or glutamate at the X position, whereas hydrophobic residues leucine, isoleucine, and phenylalanine promote geranylgeranylation.[77] Although these general rules are widely acknowledged, some proteins are capable of bearing either type of *S*-prenylation. For example, the Rho GTPase RhoB terminating in CKVL exhibits a prenylation-dependent function, wherein it promotes cell growth when farnesylated but its geranylgeranylated form induces apoptosis.[78] Furthermore, the a_1 and a_2 positions are not strictly limited to hydrophobic amino acids as other polar or charged residues occupying these positions display efficient farnesylation activities.[79,80] Another feature of these protein substrates is a linker region containing small or flexible hydrophilic residues that often precedes the Ca_1a_2X box. This facilitates the accessibility of the C-terminus for prenyltransferases and may impact substrate reactivity.[81,82] Recent efforts to expand the existing accepted paradigm of protein *S*-prenylation have shown that proteins terminating in longer (CXXXX) or shorter (CXX) C-terminal motifs can be efficiently modified by the prenyltransferase enzymes.[83,84] Although these sequences have been shown to be substrates *in vitro* and within cells, there is no reported evidence of these types of modifications on endogenous proteins to date.

Singly prenylated proteins often undergo additional processing steps to increase their hydrophobicity. The -a_1a_2X tripeptide is cleaved off by the endoproteases Ras converting enzyme (RCE1) or Ste24 (Fig. 1.2A), followed by methylation with *S*-adenosyl methionine (SAM) on the exposed carboxyterminus catalyzed by isoprenylcysteine carboxyl methyltransferase (ICMT).[85,86] These mature forms of *S*-prenylated proteins are then usually directed to the plasma membrane tethered through the prenyl anchor. However, in several instances, the prenyl group is not sufficient for stable anchoring, similar to *N*-myristoylation. Thus, prenylated proteins may also possess a PBR or undergo *S*-palmitoylation.[87] In fewer cases, Ca_1a_2X-containing proteins circumvent the maturation process and are rather directed to a shunt pathway, thereby retaining their C-terminal Ca_1a_2X intact that is essential to their subsequent function.[88]

The third class of *S*-prenylation usually confers dual geranylgeranylation on two cysteine residues positioned near the C-terminus catalyzed by geranylgeranyltransferase type II (GGTase-II), also conveniently referred to as RabGGTase, since its currently known substrates are members of the Rab family of proteins (Fig. 1.2B). The Rab protein substrates are initially recruited by the Rab escort protein 1 or 2 (REP1 or REP2) recognized through their C-terminal interacting motif (CIM).[89] This pre-formed complex then associates with RabGGTase to install the prenyl modification. While most of these proteins terminate in -CC, -CXC, or CCXX motifs poised for dual cysteine *S*-prenylation, some of these Rabs terminate with Ca_1a_2X box motifs that are singly geranylgeranylated and are also subjected to the maturation process described above.[90] The dual

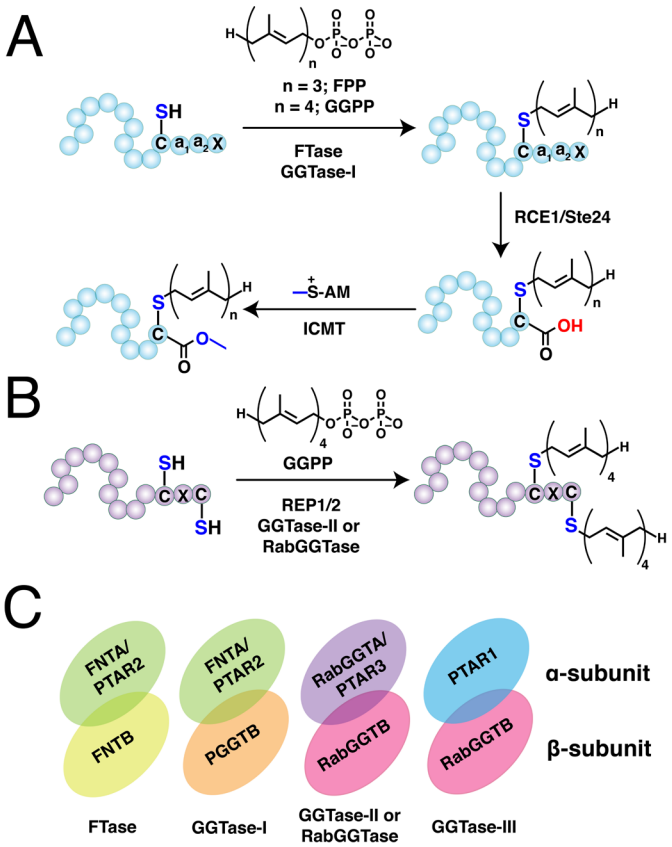

Figure 1.2. Protein Prenylation.

(A) Single prenylation on Ca_1a_2X box-containing proteins with farnesyl diphosphate (FPP) or geranylgeranyl diphosphate (GGPP) catalyzed by farnesyltransferase (FTase) or geranylgeranyltransferase type I (GGTase-I), respectively. The prenylated protein undergoes a maturation process involving cleavage of $-a_1a_2X$ tripeptide catalyzed by ras converting enzyme (RCE1) or sterile 24 (Ste24), followed by methylation of the exposed carboxy terminus by isoprenylcysteine methyl transferase (ICMT). **(B)** Dual geranylgeranylation on two proximal C-terminal cysteine residues in Rab proteins. The Rab substrate is initially recruited by the rab escort protein 1 or 2 (REP1/2) and subsequently geranylgeranylated by the geranylgeranyltransferase type II (GGTase-II) or RabGGTase. **(C)** Representation of the heterodimeric structures of prenyltransferases showing their α and β subunits. FTase and GGTase-I share a common α subunit but differs in their β that determines their reactivity and substrate specificity (*e. g.* FPP vs GGPP). GGTase-II and GGTase-III share a common β subunit for geranylgeranylation but differ in their α subunit that influences their substrate recognition.

geranylgeranylation on many of these Rabs might be required for proper localization function as monoprenylated variants of yeast Rab homologs failed to function both *in vitro* and *in vivo*.[91]

All three prenyltransferase enzymes are heterodimers consisting of α and β subunits, with the active site situated at the interface but mainly comprised of residues from the latter (Fig. 1.2C).[92] The β subunits also influence the preference of each enzyme for FPP versus GGPP. Both FTase and GGTase-I share a common α- subunit, FNTA (or prenyltransferase alpha subunit repeat containing 2, PTAR2), but differ in their β-subunits—FNTB and PGGTB, respectively—that manifest 25% sequence identity in mammalian homologs.[93] Both farnesylation and geranylgeranylation type I prefer an ordered sequential kinetic mechanism.[94–96] The isoprenoid substrate initially binds to the enzyme, followed by the Ca_1a_2X-containg protein substrate binding and thioether bond formation.[94] A second isoprenoid binds to the ternary complex that triggers product release either prior to or simultaneously with the binding of a second Ca_1a_2X protein substrate (rate determining step). In the case of geranylgeranylation, the GGPP in the GGTase-I active site adopts a bent conformation and the terminal isoprene unit is accommodated in a deeper pocket, which is not present in the corresponding region in the FTase active site.[97] This serves as the critical determinant for the isoprenoid specificity of each enzyme. On the other hand, RabGGTase is comprised of RabGGTA (or PTAR3 in some organisms) and RabGGTB as its α and β subunits, respectively. It sequentially adds geranylgeranyl groups to the Rab protein substrate in the Rab:REP complex with the second isoprenoid addition and product release being slow steps.[89,98] Although the substrate specificity features of REPs and RabGGTase towards the Rab substrates are not clear, variations in the extent of *S*-prenylation across these proteins are apparent.[99] These observed differences in the extent of *S*-prenylation should be interpreted with caution as these were conducted under

physiologically perturbed conditions, *i.e.* in the presence of statins. Regardless, further studies are needed to define the substrate specificity of Rab prenylation under native conditions and across cellular systems. These differences are of particular interest as altered levels of *S*-prenylation of a few key Rab proteins may contribute to diseases such as choroideremia as discussed in later sections.

Being a ubiquitous post-translation modification, protein *S*-prenylation modulates protein localization and a plethora of protein functions, which can be targeted for therapeutic interventions in diseases and infections where it is implicated.[11,100] In particular, inhibition of the farnesylation of oncogenic Ras proteins was initially the main motivation for the development of prenyltransferase inhibitors (PTIs).[101] However, candidate PTIs often failed in clinical trials partially owing to the ability of these protein targets to be alternatively prenylated typically by geranylgeranylation in lieu of farnesylation, and none of these potential drugs has been approved for clinical use to date in treating cancer. Despite these limitations, several lines of evidence show that targeting protein *S*-prenylation remains a promising strategy in treating neurogenerative diseases and progeria, as well as bacterial, protozoal, and viral infections.[100,102–104] For example, the farnesyltransferase inhibitor (FTI) lonafarnib has been recently approved by the FDA as the first drug to treat Hutchinson-Gilford progeria syndrome (HGPS).[105] Specifically, it inhibits the farnesylation of a genetic variant of nuclear Lamin A that is incapable of the normal Lamin A processing—a mechanism that involves cleavage of a portion of the protein containing the farnesyl modification. Clinical studies showed that patients with HGPS treated with lonafarnib, manifested improved vascular function and bone

structure.[106] In addition, oral administration of lonafarnib demonstrated success in a Phase II clinical trial of chronic hepatitis D infected patients by suppressing the prenylation of large hepatitis delta antigen (LHDAg) in human delta virus (HDV).[107] These results clearly emphasize that targeting specific prenylated proteins offers an avenue for the development of therapeutic agents but requires a clearer understanding of both the specificity and dynamics between PTIs and protein *S*-prenylation in an actual biological milieu.

Clickable analogues of isoprenoids paved the way for profiling the *S*-prenylated proteomes in different species and delineating the effects of potential therapeutic agents that target protein *S*-prenylation. Click chemistry also aided the discovery of a fourth class of prenyltransferase enzyme GGTase-III, which consists of an orphaned protein PTAR1 (α-subunit) and RabGGTB (β-subunit).[108] Additionally, the short Ca_1a_2X sequence has found significant applications in *in vitro* C-terminal modification of proteins of interest that can be further functionalized with fluorescent reporters or drug cargos. Details on the utility of click chemistry in uncovering the biological significance of *S*-prenylated proteins, as well as its application in enzymatic protein C-terminal modification are described in this chapter.

1.3. Click chemistry in studying the biological significance of protein lipidation

Studies of protein lipid modifications have faced significant challenges. Classical methods to detect and identify lipidated proteins involve radioactive techniques using isotopic analogues including [^{3}H]palmitic acid, [^{3}H]myristate and [I^{125}]myristate.[63,109,110] However, these techniques are expensive, labor-intensive, generate radioactive waste and require

special permitting, and suffer from low sensitivity that often entails lengthy film exposures to acquire sufficient and quantifiable signals. Proteins bearing canonical sequences for lipidation motifs determined by available prediction tools such as MyrBase[111] or PrenBase[81] may be validated using this approach. For those with new or undefined motifs or those for proteins with inherently low expression levels, such methods may not be suitable. Mass spectrometry-based approaches for intact and fragmented lipidated proteins may also be exploited to confirm and map the modification sites in individual proteins. Although useful, the hydrophobic character of these lipid PTMs hampers the separation and isolation of proteins and peptides, which often results in lower signal-to-noise intensities and false identification of PTM sites.[112]

In the past decade, the development of a repertoire of bio-orthogonal, clickable analogues of these hydrophobic molecules has made a major impact in the arena of lipidation science. This chemical toolbox consists primarily of alkyne- and azide-modified lipids that allow conjugation of fluorescent reporters, affinity handles, and drug cargos.[3,13,14,18,113,114] For most biological investigations, these chemical probes are typically metabolically incorporated into proteins using cells of interest—from here on referred to as click chemistry-based metabolic labeling (CCML) in this review (Fig. 1.3A). Within cells, the host machinery converts these probes into bonafide substrates that can be incorporated by host enzymes into the lipid-modified proteins, in lieu of the native lipid substrates. The convenient introduction of the small alkyne or azide tags causes minimal interference on protein processing, subcellular localization, and crucial protein-protein interactions. After a certain period of probe incubation, the labeled cells are fixed and

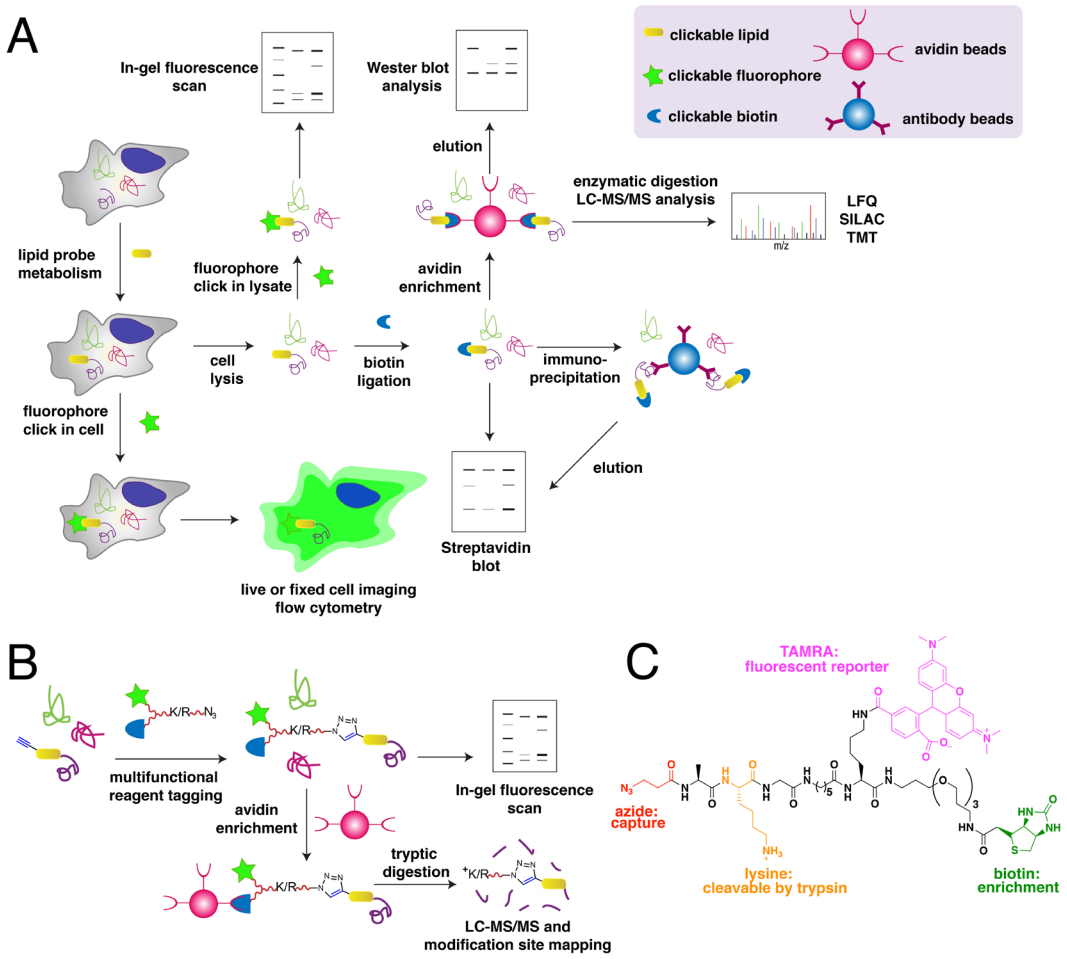

Figure 1.3. Click chemistry-based metabolic labeling (CCML) for the analysis of protein lipid modifications.

(A) A general scheme for metabolic labeling of cells with clickable analogues of small lipid molecules and subsequent detection and identification. Lysates from cells metabolically labeled with clickable probes are subjected to click reaction with their cognate bio-orthogonal tag linked to a fluorophore for fluorescence imaging or biotin for enrichment and/or streptavidin blotting. Enriched proteins from biotinylated samples can be detected through western blot or identified through label-free or isotopic tag-based quantitative LC-MS/MS proteomic analysis. Metabolic probe labeling and subsequent fluorophore tagging also allows for imaging of whole live or fixed cells and flow cytometric analysis.**(B)** The use of cleavable multifunctional reagents allows inclusion of the lipid-modified peptide for mapping of the site of lipid modification. Tryptic digestion cleaves the lysine or arginine in the linker and releases the lipidated peptide in solution. **(C)** An example of a cleavable multifunctional reagent containing a reactive group, fluorescent reporter, biotin handle, and cleavable linker.

reacted with fluorophores for cellular imaging and flow cytometric analysis, or harvested and lysed, followed by ligation in lysates with the corresponding click reagent partner of the probes used. Conjugation via click reaction with fluorescent dyes allows visualization of tagged proteins typically separated via gel electrophoresis. Immunoprecipitation and antibody-based detection such as western and streptavidin blots can be combined with CCML to verify the PTMs on proteins of interest.

More importantly, the use of affinity reagents for click reaction with the labeled lysates enables enrichment of the probe-modified proteins. The ability to enrich these labeled proteins is a pivotal step in chemical proteomics, a powerful tool that affords a catalogue of multiple PTM-proteins in a single experiment (Fig. 1.3A).[14,18] In this scheme, the probe-labeled lysates are often ligated with biotin and subjected to protein enrichment using avidin-functionalized resins, which serve to isolate the labeled proteins. The lipid-modified proteins immobilized on the solid support are digested either on-bead or eluted for subsequent enzymatic digestion in solution. The resulting peptides are then chromatographically separated and introduced into a mass spectrometer (MS) for qualitative or label-free quantitative (LFQ) analysis. Alternatively, improved quantitation can be achieved using more sophisticated approaches including Stable Isotope Labeling with Amino acids in Cell culture (SILAC) or Tandem Mass Tag (TMT) labeling.[115,116] In SILAC, isotopically labeled amino acids (typically Lys and Arg) are incorporated into all proteins via prolonged cell culture prior to metabolic labeling. These isotopic tags provide distinct mass signatures that permit calculation of fold-changes by computing the ratios of modified peptides from enriched proteins across samples. This approach ensures consistent

downstream processing of proteins but is typically performed with two or three samples at a time. In contrast, TMT introduces isotopic tags on the digested peptides after enrichment which offers a rapid labeling strategy, as well as an improved multiplexing scheme (up to 16 samples per experiment). However, inconsistencies in the upstream processes can introduce additional variability among samples and may diminish the accuracy of the results.

Tremendous efforts have been put forth in attempts to develop bio-orthogonal chemistries but only a few have been found to be viable in real biological systems. Application of a particular bio-orthogonal reaction also needs to be matched with specific requirements demanded by the system under study.[117] The classical Staudinger reaction was repurposed into a bio-orthogonal tool, in which an azide analogue of the chemical reporter is subsequently tagged with a phosphine-based reagent, resulting in intramolecular trapping with an electrophilic ester to form a stable amide bond (Fig. 1.4).[118] However, this strategy presents crucial drawbacks, such as the sensitivity of azides to reduction to amines and the propensity of phosphine reagents to undergo oxidation under physiological conditions.

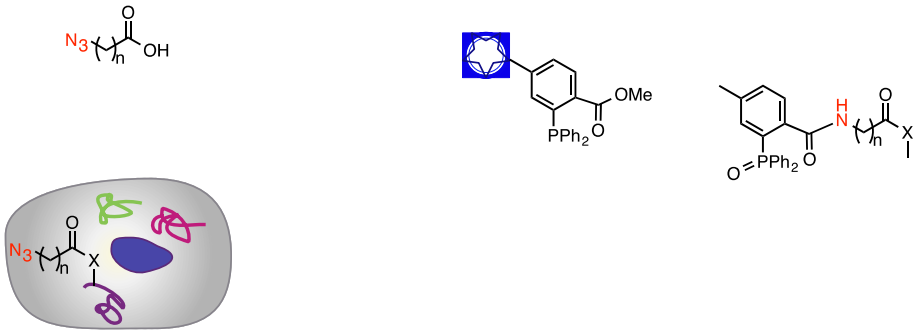

Figure 1.4. Bio-orthogonal ligation strategies with azide-modified lipid analogues.

Cycloaddition reactions have recently emerged in the search for biocompatible bio-orthogonal reactions. These so-called "click reactions" are more convenient, faster, and yield a less obtrusive linkage between a pair of functional groups under mild, aqueous conditions.[119] The copper-catalyzed azide-alkyne cycloaddition (CuAAC) is the most widely used reaction, in which an azide and a terminal alkyne form a 1,3-cycloaddition product mediated by a copper catalyst (Fig. 1.4).[120] Owing to the total absence of azides and alkynes in biological systems, this reaction has proven to be efficient and versatile in probing targets and mechanisms within cells.[121] Furthermore, azides and alkynes are one of the smallest bio-orthogonal designs among the existing click chemistries to date, and thus have lesser propensity to perturb the natural biological chemistries.[117] However, CuAAC has been limited to cell-surface labeling and imaging of fixed cells, as the copper (I) induces toxicity by generating radical species when introduced intracellularly into living cells.[122] With a need to avoid the use of copper (I) in the click reaction, Bertozzi *et al.*

pioneered the use of ring strain in the alkyne moiety to drive the reaction.[123] In this strain-promoted azide-alkyne cycloaddition (SPAAC), the transition state energy for the reaction is lowered sufficiently for it to proceed without a metal catalyst (Fig. 1.4).

Early efforts to identify the site of lipid modifications were impeded by the low ionization of these hydrophobic peptides during MS analysis. For this reason, cleavable multifunctional reagents were designed to contain a fluorescent reporter, a biotin handle, and a cleavable linker (typically basic residues Arg or Lys for trypsin digestion).[124,125] This allows fluorescent detection, enrichment, and site identification using a single reagent (Fig. 1.3B and 1.3C). The cleavage of the linker releases the modified peptides for inclusion in the LC-MS/MS analysis, with an additional positive charge from Arg or Lys that enhances peptide ionization.

Indeed, the development of an array of chemical probes with small clickable tags has permitted the detection, validation, and large-scale chemical proteomic analysis of lipidated proteins. Accounts in the literature where click chemistry has aided in the discovery of novel regulation of protein function and localization through protein lipidation are reviewed in this section. The technologies based on these clickable lipid probes that provided platforms for rapid evaluation of enzymatic lipidation activities are also included.

1.4. Biological applications in *S*-acylation (*S*-palmitoylation)

Nonradioactive click chemistry-based labeling of fatty acylated proteins generally employs alkyne- or azide-modified analogues of the fatty acid. Although the azido analogues were first developed,[126] the alkyne-modified versions are typically preferred owing to enhanced

sensitivity and lower background signal compared to azide-modified fatty acids.[127,128] Several analogues with various chain lengths have been synthesized for metabolic or *in vitro* labeling of fatty acylation substrates (Fig. 1.5).[15] These fatty acid probes are converted into their acyl-CoA forms for *in vitro* experiments. For metabolic labeling studies, the free or saponified forms of the fatty acid analogues are metabolically converted inside cells by acyl-CoA synthetases into the bonafide fatty acyl-CoA substrates.[129] Among the fatty acid analogues developed, Alk-C16 (15-HDYA) and Alk-C18 (17-ODYA) are preferentially incorporated by palmitoyl acyl transferases (PATs) onto the *S*-palmitoylation sites within protein substrates.[113,128,130] Similar to their native counterparts, these probes can also undergo β-oxidation at the C2 and C3 positions to yield α,β-unsaturated esters that may result in aberrant palmitoyl-protein adducts via Michael addition. To address this issue, a different version of the probe modified at C3 (15-HDYOA, Fig. 1.5) was explored and found to largely label the same proteins (70%) identified with Alk-C18.[131] The disparity in the sets of proteins identified between treatments suggests that a fraction of the Alk-C18-labeled proteins may be a result of adduct formation with the oxidized probe. Regardless, Alk-C16 and Alk-C18 have been widely used in click chemistry-based *S*-acylation studies reported up to the present. While Alk-C16 better mimics a palmitoyl moiety and Alk-C18 more likely resembles a stearoyl group in terms of chain length, both of these probes have been interchangeably used in investigations of protein *S*-palmitoylation. The preference for the incorporation of each analogue is dictated by the specific protein substrates and/or fatty acyltransferase.[132,133] Furthermore, these probes are not only metabolized to label fatty acylated proteins, but they can also be incorporated into biosynthetically more complex phospholipids and neutral lipids.[134,135]

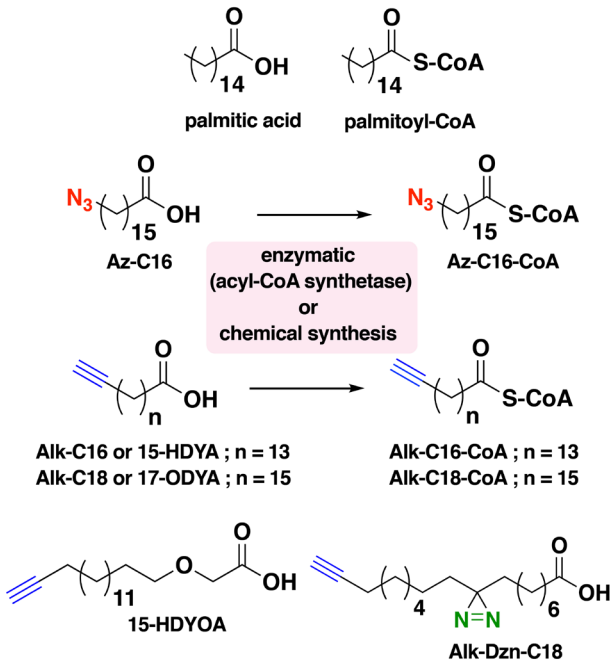

Figure 1.5. Structures of clickable probes for protein S-palmitoylation.

The native structures of palmitic acid and palmitoyl-CoA along with their azide- and alkyne-modified analogues are shown. Varying chain lengths can serve as surrogate for this lipid modification and hence can be generalized as *S*-acylation. The presence of a diazirine moiety in Alk-Dzn-C18 allows for a photocrosslinking strategy that enables identification of proteins that interact with fatty acylated proteins through the lipid modification.

The use of bio-orthogonal analogues of fatty acids for click chemistry tremendously impacted and revolutionized the field of protein *S*-palmitoylation.[15,17,114,136] These tools permitted rapid and robust fluorescence-based detection and large-scale proteomic analysis of fatty acylated proteins, thereby facilitating the discovery of novel *S*-acylated proteins and contributing to the understanding of *S*-palmitoylation dynamics. The development of a bifunctional fatty acid reporter with both clickable and photoaffinity tags (Alk-Dzn-C16) enabled the discovery of new membrane protein-protein interactions as well.[137–139] In this section, several strategies using clickable fatty acid analogues for proteomic profiling of *S*-palmitoylated proteins, as well as their utility in biochemical assays and enabling platforms to validate such lipid modification and screen for potent PAT inhibitors are described. It is

important to note that in this review, the term *S*-palmitoylated proteins is used according to the claims made by the following studies in the literature, although this type of modification is more precisely described as protein *S*-acylation.

1.4.1. Proteomic studies for profiling S-palmitoylated proteins

Advances in proteomics strategies to identify *S*-acylated proteins have contributed to unveiling regulatory mechanisms and critical functions of protein *S*-palmitoylation. Early proteomic methods to detect and identify *S*-acylated proteins took advantage of the lability of thioesters, via procedures described as acyl-biotin exchange (ABE) or acyl-resin-assisted capture (acyl-RAC).[140,141] In these multistep procedures, free cysteines in protein lysates are blocked with N-ethylmaleimide (NEM) and subsequently treated with hydroxylamine to selectively cleave the thioesters (Fig. 1.6A). *S*-acylated proteins are enriched by either biotinylation with a thiol-reactive biotin (biotin-HPDP) and streptavidin pulldown for ABE or immobilization using a thiol-reactive resin for acyl-RAC. Although these typically provide extensive lists of identified proteins, both methods are prone to false positives since neither are exclusive to *S*-acylated proteins and are not suitable for dynamic profiling studies. CCML with fatty acid analogues incorporating small azide or alkyne tags allows for more specific labeling and enrichment of *S*-acylated proteins (Fig. 1.3A). Employing such a strategy afforded several lists of *S*-acylated proteins from multiple research groups obtained from different cellular systems and provided insights into the dynamic nature of protein *S*-palmitoylation. These catalogues of *S*-acylated proteins have

been consolidated into a comprehensive database, SwissPalm©, which is accessible online for free.[142]

1.4.1.1. S-acylated (S-palmitoylated) proteins in mammals

The tagging strategy for *S*-palmitoylated proteins using biorthogonal analogues combined with mass spectrometric analysis facilitated the identification of multiple *S*-palmitoylated proteins in a single experiment. The first report using bio-orthogonal labeling for proteomic identification of *S*-palmitoylated proteins *in vitro* used Az-C16-CoA (Fig. 1.5), an azide analogue of palmitate-CoA, ligated with a phosphine-biotin reagent via Staudinger ligation.[143] A total of 21 putative *S*-palmitoylation substrates were identified from lysates of rat liver mitochondria matrix, which included 19 novel *S*-palmitoylated proteins. Following this chemical proteomic approach, large-scale proteomic profiling of *S*-palmitoylated proteins relied on metabolic labeling with palmitic acid analogues introduced into cultured cells of interest. The commercially available Alk-C18 or 17-ODYA (Fig. 1.5) has been the probe of choice owing to its better specificity and minimal background in tagging *S*-acylated proteins amenable to labeling with shorter fatty acyl chains.[127] This CCML strategy combined with proteomic analysis affords identification of hundreds of *S*-palmitoylated proteins involved in multiple cellular mechanisms and processes. Cravatt and coworkers first reported the metabolic labeling of Alk-C18 in

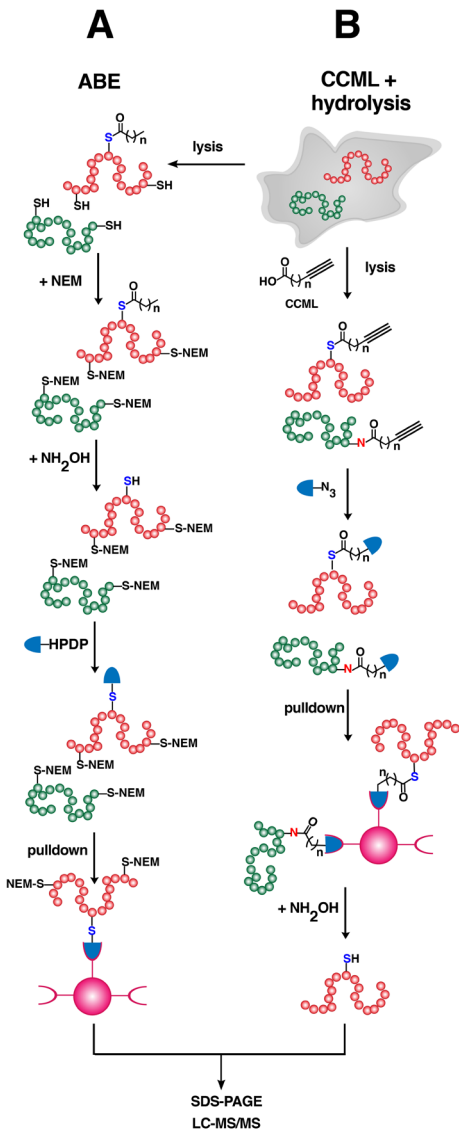

Figure 1.6. Strategies for profiling of S-acylated proteins.

(A) An acyl-biotin exchange (ABE) method that does not require metabolic labeling with clickable analogues. Lysates are treated with *N*-ethyl maleimide to block free cysteines followed by hydrolysis using NH_2OH to expose the thiols of *S*-acylated proteins. The newly unmasked free cysteines are reacted with thiol-reactive reagents such as biotin-HPDPand enriched. Immobilized proteins are eluted for SDS-PAGE or processed for proteomic analysis. **(B)** Cells can be metabolically labeled with clickable fatty acid analogues followed by click reaction with biotin-based reagents for enrichment of labeled proteins. Immobilized proteins that are probe-labeled are selectively released from the beads through hydrolysis with NH_2OH, improving the confidence of the identities of the profiled *S*-acylated proteins.

mammalian cells followed by click reaction with biotin-azide for CuAAC and subsequent enrichment.[144] A total of 125 candidate *S*-palmitoylated proteins were identified at high

confidence including G proteins, receptors, and Fam108 serine hydrolases.

Similarly, Hang and coworkers identified 178 *S*-acylated proteins at high confidence from Jurkat cells using alkyne-modified fatty acyl probes of various chain lengths (myristic, palmitic and stearic acid analogues).[145] This list of proteins contained less than 30% overlap with a previous study performed by Cravatt and coworkers. The differences in the identities of profiled *S*-acylated proteins may be attributed to variations in identity of the probes and their incubation periods, proteomic strategies (gel-based vs MudPIT) and subtle differences in MS analysis.[145] Moreover, other proteomic studies reported by the Hang and coworkers in dendritic cell lines profiled more than 150 *S*-palmitoylated proteins, which included those involved in innate immunity.[130,146] Another group analyzed the differential *S*-palmitoylation of proteins in macrophages upon treatment with bacterial surface lipopolysaccharides (LPS), a recapitulation of the initial engagement of bacteria that activates a cascade of cellular events inside the host.[147] A total of 154 and 186 upregulated and downregulated *S*-palmitoylated proteins, respectively, responded throughout the immune stimulation. In particular, LPS activates *S*-palmitoylation on phosphatidylinositol kinase II (PI4KII) that results in increased levels of the phosphorylated forms of phosphatidylinositol, leading to enhanced production of cytokines that support inflammatory responses.

S-palmitoylated proteome profiling has also provided a tool to hunt for biomarkers of diseases. For example, androgen-dependent malignant tumors in prostate cancer were investigated for potential *S*-palmitoylated protein biomarkers using CCML with Alk-C18

in a human prostate adenocarcinoma cell line.[148] By comparing the set of *S*-palmitoylated proteins in the presence or absence of androgen, the eIF3L subunit of the initiation factor eIF3 exhibited a remarkable extent of enrichment. Further assays confirmed the androgen-induced *S*-palmitoylation of eIF3L that may be implicated in cancer progression and may also serve as a novel prostate cancer biomarker.

1.4.1.2. S-acylated proteins in lower class organisms and viruses

Protein *S*-palmitoylation is a ubiquitous PTM across kingdoms and can be a key regulator for the pathogenicity of lower organisms. Bacterial lipoproteins (LPPs) are tethered to membranes often by diacylglyceryl moieties modified with fatty acids.[149] This modification is essential for proper LPP localization and function for the virulence of pathogenic bacteria, as well as for the recognition of host cell receptors. Large-scale profiling in the Gram-negative *Escherichia coli* using Alk-C16 identified more than 90 high- and medium-confidence LPPs involved in diverse biological processes.[150] However, half of these proteins are not annotated and therefore these studies should stimulate further investigation into the role of lipidation in the biological functions of these LPPs.

S-palmitoylation also plays key roles in the development and virulence of protozoans and fungi. Using Alk-C18 for labeling *S*-palmitoylated proteins and identification in the asexual stage of the causal agent of malaria, *Plasmodium falciparum*, resulted in 176 statistically enriched *S*-palmitoylated proteins essential for cytoadherence, drug resistance, and host-cell invasion mechanisms, among others.[151] Analysis of the *S*-palmitoylated proteome in a related parasite, *Toxoplasma gondii*, identified 501 proteins,

revealing the essential role of *S*-palmitoylation in all stages of its life cycle.[152] Furthermore, it was shown that blocking the *S*-palmitoylation of apical membrane antigen 1 (TgAMA1) can trigger its release along with other proteins implicated in host-cell invasion. This also highlights the parasite-specific nature of *S*-palmitoylation; TgAMA1 is *S*-palmitoylated while the *P. falciparum* homolog PfAMA1 is not.[151] In *Cryptococcus neoformans*, an opportunistic fungus that causes lethal meningitis, Alk-C18 labeling identified 72 *S*-palmitoylation substrates essential for fungal integrity and virulence.[153] *S*-palmitoylation in this pathogen is catalyzed by a single PAT, Pfa4, and its deletion causes morphological defects and virulence attenuation. Developing an inhibitor of *S*-palmitoylation in *C. neoformans* could be of great advantage since specificity can be better achieved for a single PAT compared to mammalian zDHHCs, which have functional redundancies and broader substrate scope to which the current inhibitors developed lack specificity.

Viral proteins may also require palmitoylation for their function. In epithelial cells infected with herpes simplex virus (HSV), click chemistry-based *S*-palmitoylated proteome analysis using Alk-C17 afforded a novel set of virus-encoded proteins *S*-palmitoylated by the host machinery.[154] Selective repression of the global fatty acylation of host proteins was also observed, suggesting that the virus hijacks the *S*-palmitoylation pathway to promote its virulence. HIV-1 infection was also found to alter cellular acyltransferase activity.[155] As a consequence, differential modification of proteins such as phosphatases lead to altered cellular phosphorylation levels, potentially favoring viral pathogenicity. Identifying the key zDHHCs implicated in the virulence of these viruses is essential to

delineating which of these enzymes could serve as potential therapeutic targets to treat infections caused by these viral pathogens.

1.4.2. Quantitative proteomics unravels S-palmitoylation dynamics

Combining CCML with palmitic acid analogues and quantitative proteomic approaches such as SILAC and TMT not only provides robust and accurate quantitation of *S*-palmitoylated protein levels but also enables *S*-palmitoylated proteome-wide analysis of dynamic *S*-palmitoylation events.[151,154] In a study reported by Cravatt and coworkers, a pulse-chase technique combined with SILAC in mouse hybridoma T-cells was employed to uncover the role of dynamic cycling controlled by depalmitoylases.[156] Alk-C18 was added to the cells (pulse) and subsequently competed by the addition of natural palmitic acid at different time points (chase), showing a decrease in total *S*-palmitoylation with time. Through the addition of a serine lipase (depalmitoylase) inhibitor hexadecylfluorophosphonate (HDFP), stably *S*-palmitoylated proteins were distinguished from those that undergo rapid cycling, allowing the important regulatory mechanism of depalmitoylation in dynamic *S*-palmitoylation to be examined. The phosphonofluoridate warhead is particularly reactive towards the hydroxyl group of the catalytic serine in serine hydrolases as evidenced by other proteomic studies.[157,158] A recent study combining CCML with TMT in mouse endothelial cells with an APT1 (depalmitoylase) deletion identified proteins involved in focal adhesion potentially regulated by depalmitoylation.[159] Pulse-chase analysis on the candidate RRas revealed the importance of dynamic regulation by

APT1 on its role in vascular function. Despite its utility in profiling a number of dynamically modified proteins, the pulse-chase technique is often compromised by low sensitivity since membrane-localized labeled proteins are often stable with slow turnover rates[45] and the methods employed may require additional optimization (*e.g.*, appropriate detergents) for improved detection. Furthermore, fatty acyl analogues are widely incorporated across various phospholipid species and may result in reduced labeling of the actual fatty acylation substrates.[134]

As an alternative to the pulse-chase method, a temporal profiling strategy of CCML combined with TMT-based multiplexing was used to streamline the evaluation of *S*-palmitoylation kinetics.[45] Cells were treated with Alk-C18 or natural palmitic acid at various time points, multiplexed using TMT tags, and analyzed as a single experiment in a highly accurate multinotch SPS-MS3 LC-MS approach. This revealed conserved *S*-palmitoylation kinetic profiles in different cell lines and that the previously observed effect of HDFP only represents a small fraction of the bulk *S*-palmitoylated form of various proteins. An orthogonal proteomic analysis using acyl-RAC revealed that inhibition of depalmitoylation with HDFP affects the rate of *S*-palmitoylation but steady-state *S*-palmitoylation levels remain unchanged.

1.4.3. Combining CCML with hydrolysis-based methods for robust profiling

Results from CCML labeling for *S*-palmitoylated proteome analysis have similarities and differences when compared with biotin-switch approaches (ABE and acyl-RAC). Initial

reports on the direct quantitative comparison between Alk-C18 labeling and ABE showed large complementarity in the identities of the *S*-palmitoylated proteins profiled.[151] In *Trypanosoma brucei*, analysis of the *S*-palmitoylated proteins using CCML identified more than 100 potentially *S*-palmitoylated proteins, 70 of which were not found in a previous report that employed the ABE method.[160,161] While both approaches may be useful, the differences in the life stages of the parasite studied in each method may contribute to the observed variations in the *S*-palmitoylated proteome. ABE was also used to validate proteins with altered *S*-palmitoylation levels identified through Alk-C18 labeling in breast cancer cells after Snail-induction, an event associated with chemoresistance and metastasis.[162] While some proteins showed consistent enrichment levels with metabolic labeling, other candidate proteins were not detected using ABE potentially due to their lack of a hydroxylamine-dependent linkage (such as an amide or ester modifications) or high background enrichment. While it was thought that these methods should give similar results, a more recent study found that hydroxylamine-based switch methods are significantly more sensitive than metabolic labeling, with only 10% overlap of profiled *S*-palmitoylated proteomes.[45] One of the disadvantages of using CCML is that stably *S*-palmitoylated proteins containing endogenously produced palmitate are unresponsive, and therefore clickable analogues only label those proteins that reveal free cysteines available for labeling during the course of probe treatment. It was therefore suggested that this disparity between methods warrants reevaluation of mass spectrometry-based *S*-palmitoylated proteome analyses reported in the literature.

Selective release of labeled proteins is desirable for robust identification of *S*-palmitoylated proteins. Improved detection of lipidated proteins labeled with alkyne-modified analogues of fatty acids can be achieved using a biotin-azide reagent containing a linker such as azobenzene cleavable by sodium dithionite.[145,150] However, this may not discriminate *S*-palmitoylated proteins from those that are irreversibly *N*- or *O*-palmitoylated with the bio-orthogonal probes.[132,163] Combining the principles of CCML and acyl-switch methods provides a robust method for the delineation of *S*- versus *O*- and *N*-palmitoylated proteins. In this method, cells are metabolically labeled with Alk-C18 (or Alk-C16), clicked with biotin-N_3 and enriched on beads (Fig. 1.6B). Treatment with NH_2OH cleaves thioester linkages and selectively releases *S*-palmitoylated proteins from the resin. Employing such method afforded a robust list of 282 NH_2OH-sensitive *S*-palmitoylated proteins out of the total 501 labeled with Alk-C18 in *T. gondii*.[152] Extending this approach to Raw264.7 murine macrophages identified <150 NH_2OH-sensitive proteins out of > 400 total Alk-C18-labeled proteins.[164] Furthermore, this provides a more accurate determination of *S*-palmitoylated sites. Comparison with the acyl-RAC approach revealed overlapping but distinct sets of protein substrates.[164] Since acyl-RAC captures other thioester-linked proteins including ubiquitin processing enzymes, the Alk-C18 labeling combined with NH_2OH treatment is more specific for *S*-palmitoylated proteins.

Indeed, chemical proteomics presents a powerful tool not only to rapidly identify multiple fatty acylated proteins in a single experiment but also to delineate dynamics of protein *S*-palmitoylation. It is noteworthy that optimization of click chemistry conditions is critical to maximize the labeling and number of identified *S*-palmitoylated proteins in

these types of proteomic approaches.[164–166] The choice of buffer and the amount of detergent for solubilization may significantly impact the extent of labeling particularly for proteome-wide analyses. In gel-based analyses, sample preparation must be carefully designed since these reporter tags are labile to hydrolysis. Inhibitors of depalmitoylases may be included in the lysis buffer to block depalmitoylation activities and retain the incorporated probes onto proteins.[156,162] The use of dithiothreitol (DTT) and sample heating may hydrolyze thioester linkages, leading to decreased detection of labeled proteins.[167] Furthermore, MS-compatible detergents are recommended to avoid *S*- to *N*-palmitoyl transfer, which may complicate the MS data analysis in discriminating *S*- vs *N*-palmitoylated proteins or peptides.[168]

1.4.4. Discovery of S-palmitoylation-regulated proteins

Proteomic studies using palmitic acid analogues containing bio-orthogonal functionality has indeed led to the discovery of several novel *S*-palmitoylation substrates. Click-chemistry based analysis can also be exploited to explore and validate the *S*-palmitoylation status of individual proteins of interest. This subsection describes the use of several strategies to detect and validate the *S*-acylation or *S*-palmitoylation of a given protein of interest.

1.4.4.1. Direct fluorescence-based detection

Assessment of successful labeling of proteins treated with clickable probes can be conveniently performed through click reaction with a fluorophore and visualization through in-gel fluorescence analysis. Using this method, Hang and coworkers first discovered the *S*-palmitoylation of interferon-induced transmembrane protein 3 (IFITM3) in murine models using a chemical proteomic approach, which was later confirmed to have three *S*-palmitoylation sites on membrane-proximal cysteines (Cys 71, 72, and 105) essential for its antiviral activity.[130,169] The palmitate modification was validated by immunoprecipitating the metabolically labeled IFITM3 and subjecting it to click reaction with rhodamine-azide.[170] More than half of the known zDHHC-PATs can *S*-palmitoylate IFITM3, with a preference for zDHHC20 that uniquely increases its antiviral activity upon co-expression.[171] Later studies employing transfection of wild-type and mutant forms of human and bat IFITM3 followed by CCML revealed discrepancies and contradictions in the *S*-palmitoylation of the three conserved cysteine residues.[172,173] Thus, the regulatory mechanism of *S*-palmitoylation might differ among these homologs. Furthermore, IFITM3 also requires an amphipathic helix that impacts its antiviral activity upon mutation that does not influence *S*-palmitoylation as shown through a CCML assay.[174] After the discovery of IFITM3 *S*-palmitoylation, other members of the IFITM family were also examined for potential *S*-palmitoylation. This includes IFITM5 whose *S*-palmitoylation was validated using Alk-C18 and found to mediate its interaction with FKBP11 that is essential for bone formation.[175] In the same vein, *S*-palmitoylation was also confirmed at a non-conserved position as well as on three conserved cysteine residues in IFITM1, which

are crucial for its protection from proteasomal degradation and antiviral activity against influenza A.[176]

Non-mammalian *S*-palmitoylated proteins were also validated through CCML and fluorescence labeling. In bacteria, *S*-palmitoylation on the two bacterial effector proteins SspH2 and SseI is indispensable for their localization in the host-cell plasma membrane, highlighting a mechanism for how pathogens exploit the host-cell PTM machinery.[177] Interestingly, mycobacterial IFITM is *S*-palmitoylated when expressed in human cells and confers antiviral activity against influenza.[178] This demonstrates that a plausible IFITM gene transfer between bacteria and eukaryotes may be beneficial to eukaryotic cells to combat viral infections. In yeast cells undergoing cell division, differential *S*-palmitoylation on Rho3 GTPase was visualized, implicating its role during meiosis under the control of Erf2 palmitoylase.[179] Beyond validation, CCML is also useful for mapping essential residues that influence *S*-palmitoylation such as in yeast protein Yck2.[180] Through site-directed mutagenesis, a dipeptide Phe-Phe near the C-terminus of Yck2 was found to be essential for its *S*-palmitoylation and surmised to be involved in enzyme recognition.

Labeling with the shorter fatty acid analogues Alk-C16 and Alk-C17 combined with fluorescent detection further illuminated the role of *S*-palmitoylation on novel and known *S*-palmitoylated proteins. Dual *S*-palmitoylation drives the amyloid precursor protein (APP) to concentrate in lipid rafts where it undergoes amyloidogenic processing, thereby enhancing the production of Aβ peptides, a hallmark of Alzheimer's disease pathology.[181] Along the same lines, zDHHC7-catalyzed dual *S*-palmitoylation on junction

adhesion molecule C (JAM-C) mediates its localization in the tight junction regions in cells, which may serve as a target to attenuate cancer metastasis.[182] Alk-C17 was used to confirm that knockout of hedgehog acyltransferase (Hhat) results in diminished sonic hedgehog (Shh) *S*-palmitoylation, leading to attenuation of the proliferation and invasiveness of human carcinoma cells.[183]

In vitro fluorescence labeling may also provide a platform for quantitative assessment of the levels of *S*-palmitoylation of specific proteins within cells. For example, GFP-fused STX-19 was co-transfected with the 23 mammalian zDHHCs and labeled with Alk-C18, followed by click reaction with an azide-dye, IR-800.[184] Ratiometric quantitation of the IR-800/GFP fluorescence after electrophoretic separation in gels provided information on the extent of labeling promoted by each zDHHC of STX-19, revealing zDHHCs 2,3,7, 11, and 12 as efficient enzymes that modify STX-19. *S*-palmitoylation of this Q-SNARE protein by these zDHHCs is essential for its targeting to tubular recycling and may also mediate Rab8 trafficking to the plasma membrane.

1.4.4.2. Antibody-based methods and streptavidin blotting

Detection methods based on CCML and fluorescent-azide or -alkyne conjugation combined with antibody-based recognition or immunoprecipitation approaches were carried out to validate the *S*-palmitoylation of proteins. The click reaction can be carried out in solution after elution of immunoprecipitated proteins or directly on proteins immobilized on beads. Pulse-chase labeling with Alk-C18 on the tyrosine kinase Lck demonstrated its highly dynamic *S*-palmitoylation kinetics that plays key roles in

transduction downstream of Fas receptor activation, a process that mediates T-cell responses during inflammation .[185–187] Novel *S*-palmitoylation on another kinase, dual leucine-zipper kinase (DLK), was found to control its localization and activity that is critical in axonal injury signaling.[188] Another example is the zDHHC6-catalyzed *S*-palmitoylation on MYD88 that was found to influence toll-like receptor inflammatory signaling *via* regulation by fatty acid synthase (FASN).[189]

Alk-C18 labeling also demonstrated that *S*-palmitoylation reduces the depalmitoylase activity of PPT1, an enzyme linked to the neurodegenerative disease neuronal ceroid lipofuscinosis (NCL).[190] PPT1-deficient mouse models displayed higher levels of *S*-palmitoylated proteins as well as mislocalization of *S*-palmitoylated proteins that regulate neuronal ciliogenesis including Rab3IP.[191] Results of these studies implicated PPT1 *S*-palmitoylation as a key player in the progression of NCL and that this disease is a form of ciliopathy. Similarly, Alk-C18 labeling in cardiac myocytes showed that *S*-palmitoylation of the voltage-gated sodium channel Nav1.5 can markedly modulate cardiac sodium currents, leading to alterations in cardiac excitability.[192]

Although in-gel fluorescence scans can be used to directly visualize labeled proteins, indirect approaches by means of click reaction with biotin have been widely applied. The labeled proteins in these lysates can be probed for biotin-modification *via* streptavidin blotting. Through this strategy, the novel *S*-palmitoylation of peripheral myelin protein 22 (PMP22) was discovered and shown to be critical for its role in cell shape and motility.[193] Likewise, the *S*-palmitoylation site near the N-terminus of the

transframe (TF) protein of Sindbis virus was mapped and its role in trafficking TF to the host plasma membrane to promote virus budding was established.[194]

S-palmitoylation on proteins of interest from biotinylated samples can be more specifically probed or validated by isolating the protein *via* immunoprecipitation prior to streptavidin blot detection. For example, probing the *S*-palmitoylation state of calnexin showed that ER stress promotes its depalmitoylation.[195] This approach validated the autopalmitoylation on a conserved residue in TEA domain (TEAD) transcription factors that is required for their proper folding, stability, and interaction with coactivators.[196,197] Novel *S*-palmitoylation on plakophilin was discovered and found to be indispensable for the assembly of desmosomes that are specialized structures that serve a key role in cell-cell adhesion of epithelial and cardiac tissues.[198] Similarly, SOD1 was confirmed to be *S*-palmitoylated and the enhanced *S*-palmitoylation of its disease-relevant mutants may contribute to the pathogenesis of familial amyotrophic lateral sclerosis (FALS).[199] *S*-palmitoylation was also discovered for junctophilin-2 (JPH-2), a modification essential for its function in tethering the sarcoplasmic reticulum to the plasma membrane.[200] Moreover, *S*-palmitoylation of the tumor suppressor Scribble (SCRIB) by zDHHC7 was evaluated to be essential for its plasma membrane targeting, and impairment of this modification activates pathways that promote tumorigenesis.[201] A follow up study combining CCML and fluorescent labeling revealed that Snail overexpression, implicated in cancer, stimulates depalmitoylation of SCRIB, resulting in enhanced growth signaling and malignancy.[202]

1.4.4.3. Enrichment approaches

Alternatively, metabolically labeled samples can be reacted with biotin-azide or -alkyne, enriched using avidin beads, eluted and detected via western blot using an antibody against the protein of interest or fused tags such as FLAG or GFP. Using this method, the *S*-palmitoylation by the host-cell machinery on the effector protein LpdA in the pneumonia-causing bacteria *Legionella pneumophilia* was validated, a mechanism that allows spatial control of LpdA's activity inside the host.[203] The novel *S*-palmitoylation on Glut4 and IRAP was confirmed and altered levels of their *S*-palmitoylation may play a role in obesity.[204] Similarly, *S*-palmitoylation was validated and found to modulate the function of the apical sodium-dependent bile acid transporter (ASBT) crucial for the circulation of bile acids in human cells.[205] Moreover, the *S*-palmitoylation on the C-terminal region of mucolipin 3 whose activation induces autophagy in a *S*-palmitoylation-dependent manner was verified.[206] This approach also aided in the discovery of the regulatory function of dickkopf1 (DKK1) in the dynamic *S*-palmitoylation of its receptors CKAP4 and LRP6, which may play pivotal roles in cancer proliferation.[207] Recently, both the programmed cell death ligand 1 (PD-L1) and its cognate receptor PD-1—two interacting proteins that are key therapeutic targets in cancer treatment—were discovered to be *S*-palmitoylated.[208,209] Inhibition of *S*-palmitoylation in PD-L1 enhances the immune response against tumors while blocking PD-1 *S*-palmitoylation manifested anti-tumor effects. Therefore, designing selective inhibitors capable of suppressing the *S*-palmitoylation of both cancer targets should yield new weapons in the battle against cancer.

1.4.4.4. Validating S-palmitoylated receptors

The methods described above were useful to validate or identify sites of modification on protein receptors and provided insights into the regulatory role of *S*-palmitoylation for proteins including the D2 dopamine receptor (D2R), c-Met receptor tyrosine kinase (RTK) epidermal growth factor receptor (EGFR), bone morphogenic protein receptor 1a (BMPR1a), and tumor necrosis factor alpha receptor 1 (TNF-R1).[210–214] Multiple PATs were found to mediate *S*-palmitoylation of the μ-opioid receptor D2R on Cys433 that is essential for its stability and membrane trafficking.[210] The localization of the frequently overexpressed or mutated protein c-Met RTK in cancer was found to be controlled by *S*-palmitoylation by modulating transport from the Golgi to the plasma membrane.[211] zDHHC20 was discovered to *S*-palmitoylate EGFR and disruption of its *S*-palmitoylation combined with inhibition of EGFR phosphorylation may serve as an effective therapeutic strategy to treat EGFR-driven cancers.[212] *S*-palmitoylation on Cys173/175/180 of BMPR1a may affect BMP signal transduction and proper embryonic development in neural stem cells (NSC), therefore regulating the fate of NSC.[213]An earlier study using azido palmitate to investigate *S*-palmitoylation on the ligand TNF-α provided the first evidence for the role of *S*-palmitoylation in TNF-R1 signaling.[215] This most recent study of the *S*-palmitoylation of the TNF-R1 receptor itself exemplifies how *S*-palmitoylation may regulate multiple aspects of a single signaling pathway.

1.4.4.5. Validating depalmitoylation substrates

Validation and mapping of *S*-palmitoylation sites in proteins using CCML has also served to unveil information regarding their regulation through depalmitoylation as well as well

as contributed to the discovery of novel depalmitoylases. For example, Wnt5a signaling was shown to drive the APT1-mediated depalmitoylation of melanoma cell adhesion molecule (MCAM), a protein upregulated in melanoma, that influences it localization and ability to promote cell invasion—a mechanism often linked to metastasis.[216] CCML with Az-C16 in melanoma cells treated with Wnt5a displayed reduced MCAM *S*-palmitoylation. Wnt5a was speculated to control depalmitoylation through the Wnt adaptor protein Dvl2, which interacts with APT1. Moreover, oncogenic mutants of zDHHC20 in melanoma were also assessed for their inability to *S*-palmitoylate MCAM through CCML, which delineates the importance of these mutations to support the dominance of unpalmitoylated MCAM for melanoma cell invasion. In another study, APT1 was found to regulate the differential localization of Numb and β-catenin—two proteins that determine cell fate.[217] The *S*-palmitoylation status of these proteins, probed through CCML with Az-C16, including the three conserved residues in Numb predicted to be *S*-palmitoylation sites was verified through site-directed mutagenesis. The tight control of protein localization conferred by APT1 on Numb and β-catenin affects the downstream transcriptional activity of Notch and Wnt signaling during cell division.

Both palmitoylation and depalmitoylation can proceed simultaneously to promote protein function.[218] For example, Alk-C16 labeling showed that the T helper 17 (T_H17) cell differentiation stimulator, STAT3, undergoes a cooperative palmitoylation and depalmitoylation by zDHHC7 and APT2, respectively. zDHHC7 palmitoylates STAT3 at Cys108 for membrane recruitment and subsequent phosphorylation. APT2 then selectively depalmitoylates phosphorylated STAT3 (p-STAT3) over unphosphorylated species, which

is a critical step for the translocation of p-STAT3 in nuclear membranes and its delivery to the nucleus to promote cell differentiation. However, overactivation of p-STAT3 leads to accelerated differentiation that is often associated with inflammatory diseases such as inflammatory bowel disease (IBD). Impairing the function of zDHHC7 or APT2 through knockout or chemical inhibition relieved symptoms in mouse models of colitis—a form of IBD characterized by colon inflammation. Moreover, zDHHC7 and APT2 were also found to be upregulated in IBD patients. Therefore, designing strategies to specifically inhibit zDHHC7- or APT2-catalyzed palmitoylation/depalmitoylation of STAT3 offers a novel mechanism for therapeutic intervention to treat IBD.[218]

CCML also facilitated the discovery of α/β-hydrolase domain-containing thioesterases (ABHDs) as novel classes of depalmitoylases. These enzymes are directed to the plasma membrane through *S*-palmitoylation on their N-termini.[43,144] Pulse-chase labeling using Alk-C18 revealed the role of ABHD17 proteins in controlling palmitate turnover on PSD95 and NRAS. All three ABHD17 isoforms (ABHD17A, ABHD17B, and ABHD17C) are required for dynamic cycling of NRAS *in vivo*.[43] Similarly, ABHD10 governs the anti-oxidant activity of PRDX5 (an *S*-palmitoylated protein validated *via* Alk-C18 labeling) in mitochondria through the depalmitoylation of a nucleophilic cysteine in its active site.[219]

In summary, these various approaches for validating the lipid modification on proteins offer a range of options for researchers to achieve their goals. Although fluorescence-based methods offer direct confirmation of the PTM on the protein, several

other labeled proteins in the lysate that co-migrate with the protein may overwhelm the signal and therefore complementary validation through western blotting may be required. The use of streptavidin enrichment of biotinylated samples may enhance the confidence on the labeling of proteins, although it generally suffers with issues of high background. Efforts to improve this background problem through optimizing the blocking step have been reported.[220]

1.4.5. Imaging methods to visualize dynamic PAT activity and localization

Earlier methods to tag *S*-acylated proteins using isotopically labeled fatty acyl analogues were limited to detection in gels. The advent of chemical probes to tag *S*-palmitoylated proteins enabled the visualization and monitoring of changes in *S*-palmitoylation events in fixed cells.[221] Cellular imaging of *S*-acylated proteins using clickable fatty analogues allows for global visualization of the modified proteins, as well as the detection of a specific protein of interest using antibodies.

1.4.5.1. Global *S*-acylated proteins

The first data that provided a cellular view of global fatty acylation was conducted on PC3 cells, which were metabolically labeled with various alkyne-modified fatty acyl analogues and clicked with rhodamine-azide after cell fixation.[128] Fatty-acylated proteins were distributed as punctate patterns across the cytoplasm and plasma membrane, with subtle variations observed among varying fatty acyl analogues employed. Changes in *S*-

palmitoylation events were also monitored at different stages of cell division, revealing that *S*-palmitoylation is spatiotemporally regulated during the cell cycle.

Imaging of protein *S*-acylation in protozoans illuminated its multiple roles in the invasion mechanism of these parasites. Flow cytometric analysis and cellular imaging on *Leishmania donovani* cells labeled with Alk-C16 and treated with 2-BP showed a drastic decrease in global *S*-palmitoylation with concomitant morphological defects.[222] Inhibition of *S*-palmitoylation further led to a severe loss of cell movement and disconcerted invasion pattern. Cellular imaging using Alk-C18 allowed for quantification of the total *S*-palmitoylated proteome in multiple life stages of *P. falciparum*.[223] The PAT activity in free merozoites were imaged for the first time, with the schizont stage showing the highest number of *S*-palmitoylation events compared to the ring and trophozoite stages. *S*-palmitoylation in merozoites was found to be dynamic and regulated in response to natural signals that trigger microneme secretion, an important mechanism for red blood cell (RBC) invasion. Similarly, visualization of the *S*-palmitoylated proteome shed some light on the relationship between *S*-palmitoylation and other regulatory mechanisms involving cysteine residues. A recent study employing Alk-C18 observed similar results, showing that the schizont stage harbors the most *S*-acylated proteins followed by trophozoite and ring stages, respectively.[224] Higher resolution images were acquired by using single-molecule switching super-resolution microscopy (SMS) on samples directly labeled with a fluorophore-azide, or through electron microscopy on biotinylated samples tagged with streptavidin-gold nanoparticles. These methods provide rapid and high-throughput strategies for microscopic examination of protein *S*-acylation without the need for

transfection, which is a difficult endeavor to achieve in many cellular systems such as *P. falciparum.*

CCML and fluorescent labeling with primary mouse cortical neurons revealed that alterations in *S*-nitrosylation result in decreased global *S*-palmitoylation.[225] Perturbations of *S*-nitrosylation/*S*-palmitoylation crosstalk of proteins associated with synaptic transmission and plasticity might lead to the destabilization of synaptic systems implicated in chronic stress-related diseases. In dorsal root ganglion (DRG) neurons, cellular labeling and imaging revealed that cGKI, a kinase involved in axon branching, co-localizes in the DRG growth cone along with the bulk *S*-palmitoylated proteome.[226] This evidence, together with other biochemical data, suggests a potential role for cGKI-mediated transduction in modulating *S*-palmitoylation, which contributes to cone enlargement and neurite extension of DRG neurons.

The dynamic feature of *S*-palmitoylation is central to its regulatory role in protein function, stability, and localization. Pulse labeling techniques in imaging PAT activity may provide insights into the rate of turnover in cells similar to chemical proteomics. CCML using palmitate analogues as a pulse can be a valuable tool to determine protein turnover. Pulse-washout experiments using Alk-C16 revealed rapid turnover of global *S*-palmitoylation in PC3 cells.[128] Pulsing with Alk-C16 and subsequent chasing with palmitic acid enabled tracking of dynamic *S*-palmitoylation of specific proteins.[132] The *O*-palmitoylated Wnt3a appeared to have the slowest turnover rate compared to the *S*-palmitoylated proteins investigated. Pulse-chase experiments in cellular imaging also allowed for monitoring of protein transport. Anterograde transport proteins were found to

be *S*-palmitoylated by zDHHC3 and zDHHC7 in the *cis*-golgi and this modification accelerates their intragolgi (*cis* to *trans*) transport.[227] The intrinsic physical properties of the fatty acyl side chain promotes localization in the highly curved regions of the *cis*-golgi, resulting in the observed enhanced rate of transport.

1.4.5.2. Specific S-acylated protein

Another strategy to assess the localization of specific *S*-acylated/*S*-palmitoylated proteins is through subcellular fractionation of labeled protein lysates, followed by immunoprecipitation, click reaction and western blot detection.[228] However, imperfections in the cell lysis may affect the integrity of the generated fractions and could complicate subsequent interpretation concerning the true localization of *S*-acylated/*S*-palmitoylated proteins of interest.[15] To this end, Hannoush and coworkers developed a robust fluorescence imaging platform by combining CCML using Alk-C16 with proximity-ligation assay (Palm-PLA) to track specific *S*-acylated/*S*-palmitoylated proteins in intact cells (Fig. 1.7A).[229,230] In this method, cells expressing the protein of interest are metabolically labeled with Alk-C16 (or Alk-C18), fixed and permeabilized, then clicked with an azide-modified tag. Two primary antibodies that recognize the protein and the tag are introduced, followed by treatment with two secondary antibodies specifically binding to each primary antibody. These secondary antibodies are conjugated to complementary oligonucleotides, which hybridize to form a closed circle when both are in close proximity. A rolling-circle amplification is then carried out with a fluorophore-labeled oligonucleotide complementary to the closed circle, generating a fluorescence signal to visualize localization of the tagged protein. This approach enabled the visualization of various

proteins in multiple intact cell lines,[229] as well as successful tracking of Wnt3a through the secretion pathway.[132]

Palm-PLA was also used with Alk-C18 to examine the distribution pattern of *S*-palmitoylated JPH2 (palm-JPH2) in rat ventricular myocytes, while the total JPH2 was concurrently visualized by immunofluorescence (IF-JPH2).[200] In order to authenticate the observed palm-PLA signals, unpalmitoylated forms were also imaged by reaction with a maleimide derivative of biotin in lieu of the palmitate-alkyne/biotin-azide tag (Unpalm-PLA, Fig. 1.7B). Through the complementary methods Palm-PLA, Unpalm-PLA and IF, palm-JPH2 was found to exhibit slow turnover rates of *S*-palmitoylation along the z-axis of the cell periphery. Using structured illumination microscopy on the myocyte surface, palm-JPH2 and IF-JPH2 were observed to localize at distinctly different plasma membrane subdomains with little overlap. These results indicated that JPH2 *S*-palmitoylation is stable in the cell periphery while dynamic along the lateral cell surface.

Indeed, imaging *S*-acylated/*S*-palmitoylated proteins in intact cells has been made possible through the use of CCML. In labeling with azide-modified probes, significant background arises from non-specific reaction of the alkyne reagent with free thiols. Activation of terminal alkynes by copper (I) can result in reactions with other nucleophiles (beyond azides), leading to strong background labeling when the alkyne reagent is present in excess. In fact, this copper (I)-catalyzed reaction between terminal alkynes and thiols has been repurposed for the construction of alkylsulfides in the presence of molecular

oxygen.[231] Blocking these functional groups via alkylation with iodoacetamide may improve visualization[232] and excluding the complexing ligands (*e.g.* TBTA and THPTA) may also provide enhanced quality of cellular imaging of cells treated with clickable analogues.[132,223,225] Furthermore, these methods have generally been limited to fixed cells since the requirement for toxic Cu(I) in CuAAC restricts its application to live-cells. Imaging of *S*-palmitoylation activity in living cells and *in vivo* may provide real-time monitoring of *S*-palmitoylation dynamics and should be of great interest in future studies.

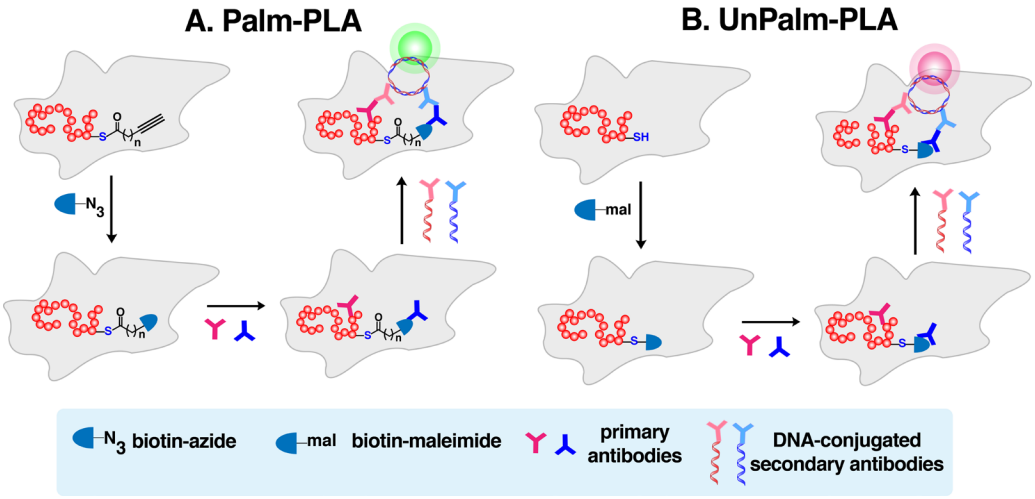

Figure 1.7. Imaging of proteins inspired by proximity ligation assay (PLA).

(A) Palm-PLA visualizes localization of specific palmitoylated proteins. Intact cells metabolically labeled with clickable fatty acids are tagged with a biotinylated click reaction partner. Two primary antibodies that recognize the target protein and biotin tag are added, followed by treatment with a pair of oligonucleotide-labeled secondary antibodies that bind to the primary antibodies separately. When they are in close proximity, the oligonucleotides complement and form a closed circle that is required for rolling-circle amplification (RCA). **(B)** UnPalm-PLA detects the unpalmitoylated species of the protein of interest (POI). Cells are treated with biotin-maleimide to directly tag the free form of the POI followed by treatment with antibodies as described in Palm-PLA. An orthogonal fluorophore is used to distinguish localization of the unpalmitoylated POI from the palmitoylated species.

1.4.6. Evaluation of fatty acyltransferase activity and inhibition

Inhibitors of PATs are essential to study protein *S*-palmitoylation and have potential to serve as therapeutic agents for relevant diseases. Inhibition of PATs can be evaluated through examining the *S*-palmitoylation states of proteins of interest metabolically labeled with Alk-C16, Alk-C17, or Alk-C18 and detected *via* western blotting. Inhibition of zDHHC3-mediated *S*-palmitoylation of integrin β4 (ITG β4) by curcumin occluded autoacylation of zDHHC3 and effectively reduced levels of *S*-palmitoylated ITG β4 in invasive breast cancer cells.[233] Inhibition of *N*-palmitoylation of Shh by Ruski-201 was visualized via a gel mobility shift assay by using Alk-C17 labeling followed by click reaction with a multifunctional reagent.[234] Likewise, several small molecules including IWPs, C59, and ETC-159 were shown to effectively inhibit the *O*-palmitoylation of Wnt proteins by blocking the acyltransferase activity of porcupine (PORCN) using Alk-C16 labeling experiments.[228,235–237] Alterations in Wnt signaling including overexpression of Wnts and their receptors are implicated in various human cancers.[238] Using these inhibitors may offer an effective strategy to prevent such Wnt-driven diseases.

Cell-based *in vitro* assays were developed to evaluate PAT inhibition on *S*-palmitoylation of specific proteins through qualitative or quantitative analysis using fluorescence microscopy as previously described.[132,184,229,230] These techniques can be extended to high-throughput analysis in a 96-well format that may facilitate rapid screening of PAT inhibitors.[132,230] Recently, a cell-based approach was reported utilizing bacterial expression systems to visualize PAT inhibition by 2-BP.[239] *P. falciparum* PATs ectopically expressed in an engineered PTM-null *E. coli* expression system can incorporate Alk-C18

into bacterial proteins. Effects on the global *S*-palmitoylation enforced by PfDHHCs can be evaluated to screen for effective inhibitors of specific zDHHCs. This technique provides potential for chemotherapeutic targeting of pathogenic zDHHCs via a high-throughput screening platform.

The identification of PAT inhibitor targets using CCML can also be accomplished via mass spectrometry activity-based protein profiling (ABPP) and fluorescence-based assays. For example, the palmitic acid analogue 2-bromopalmitatic acid (2-BP, Fig. 1.8) has been commonly used as an irreversible inhibitor and thought to be selective for the *S*-palmitoylation activities of PATs.[240] However, profiling for its protein targets using its corresponding azide (Az-2-BP) and alkyne (Alk-2-BP) analogues (Fig. 1.8) revealed its poor selectivity, reacting with many targets beyond PATs such as transporters and chaperones.[241,242] Therefore, studies employing 2-BP to validate *S*-acylated proteins should be interpreted carefully and take into account any phenotypic changes or off-target effects this reagent induces.[151,222] The natural product cerulenin (Fig. 1.8), a known PAT inhibitor, was derivatized into an alkyne-containing clickable form (Alk-cer, Fig. 1.8) to evaluate its protein targets.[243] Metabolic labeling of zDHHC4-expressing HEK293 cells with Alk-C16 or Alk-cer followed by biotinylation and western blot detection showed that Alk-C16 adducts are sensitive to hydroxylamine while Alk-cer derived modifications are resistant. This confirms that cerulenin directly and irreversibly alkylates zDHHCs similar to 2-BP. While Alk-cer displayed improved potency and could label all zDHHCs tested in this study, it also reacts with some zDHHCs bearing mutant active sites, suggesting it is not truly on-target and "activity-based". This may be attributed to the design of the probe which

contains a linear 12-carbon chain and differs from the native cerulenin structure. The loss of the double bonds may affect the conformation of this probe and may explain its difference in target specificity with the native cerulenin.

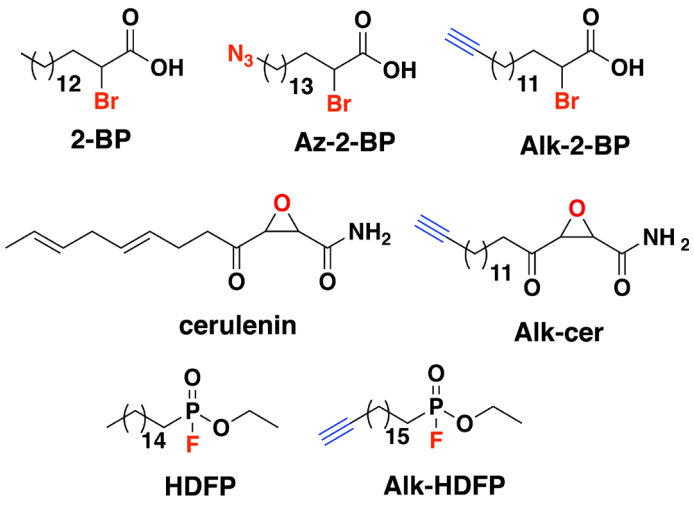

Figure 1.8. Structures of PAT and APT inhibitors and their clickable analogues for activity-based protein profiling (ABPP).

2-bromopalmitic acid and the natural product cerulenin are pan inhibitors of zDHHCs. Hexadecyl fluorophosphonate (HFDP) is a serine lipase inhibitor that targets many hydrolase enzymes.

As mentioned earlier, fatty acyl modification of proteins can be reversed by acylthioesterases such as APT1/2, which are known to be targets of the serine lipase inhibitor HDFP (Fig. 1.8). Activity-based protein profiling of depalmitoylases/deacylases using Alk-HDFP showed reactivity with a specific subset of serine hydrolases with a strong preference for lipid substrates, particularly lipases.[156] HDFP-inhibition of depalmitoylases increases Alk-C18 probe incorporation but only represents a small fraction of the bulk *S*-palmitoylated form of the proteins.[45] The targets of selective inhibitors for specific fatty acyl transferases can be also identified through the use of Alk-C18 labeling. A SILAC-based quantitative proteomic approach was employed to demonstrate that the inhibitor

RUSKI-201 can selectively reduce the palmitoylation levels of Hhat palmitoylation substrates at submicromolar concentrations.[234]

The development of cell-based *in vitro* assays and the use of clickable analogues of PAT inhibitors can indeed allow for evaluation of their inhibition capacity. More importantly, employing chemical proteomics with inhibitor analogues can help delineate side reactions with proteins and may offer information on how to improve their design to avoid reactivity with these off-target proteins. These current inhibitors for zDHHCs are largely based on fatty acid structures and other scaffolds may be required to achieve greater target specificity. With the recent success in obtaining crystal structures for zDHHC20, the development of inhibitors tailored to be specific to this enzyme should be possible. It is likely that additional crystal structures for other zDHHCs will be acquired in the future, which should aid in the rational design of inhibitors specific to a particular zDHHC of interest.

1.4.7. Enabling technologies based on clickable palmitic acid

Although cell-based and chemical proteomic approaches presented above may be useful in evaluating inhibition of fatty acyltransferase activity, more rapid and higher throughput methods are desirable. In an effort to innovate non-radioactive detection methods for acyltransferase activity suitable for high-throughput screening of inhibitors, click chemistry-based screening platforms were developed. A high-throughput method designed for screening inhibitors of zDHHC9-catalyzed N-Ras *S*-palmitoylation employed

immobilized N-Ras peptide and Alk-C18-CoA adaptable with a 384-well format (Fig. 1.9A).[244] Through a turn-on fluorescence assay conferred by successful N-Ras modification, the inhibition efficiency of inhibitors were quantified and IC_{50} values were calculated from dose-response curves. Counter-screening with an unrelated *S*-palmitoylated protein such as Fyn aided in the validation of the specificity of candidate antagonists. Such a method is suitable for pursuing potent inhibitors with high specificity for the protein substrates of interest.

Tate and coworkers established ELISA-inspired methods for high-throughput analysis of fatty acylation. They initially introduced click chemistry ELISA (click-ELISA) to detect and measure PAT activity of Hhat on Shh (Fig. 1.9B).[245,246] In this approach, an immobilized Shh peptide is acylated by Hhat with Alk-C17-CoA and functionalized with azido-FLAG peptide, followed by probing with anti-FLAG fused to horseradish peroxidase (anti-FLAG-HRP) to evaluate levels of Hhat labeling. Such a method was able to quantify the potencies of inhibitors and calculate kinetic parameters for the Hhat-catalyzed Shh *N*-palmitoylation. The same group developed a fluorescence-based microfluidic mobility shift and acylation-coupled lipophilic induction of polarization (acyl-cLIP) assays that obviate the need for the multiple handling steps involved in click-ELISA.[247,248] In acyl-cLIP, a fluorescently labeled Shh peptide is *N*-palmitoylated and the resulting hydrophobicity increase drives binding to BSA, providing fluorescence polarization readouts. Alk-C18-CoA was used to counter-screen candidate inhibitors for Hhat. On the basis of lipid binding to BSA, this assay is broadly applicable to other protein lipid transferases and hydrolase enzymes.

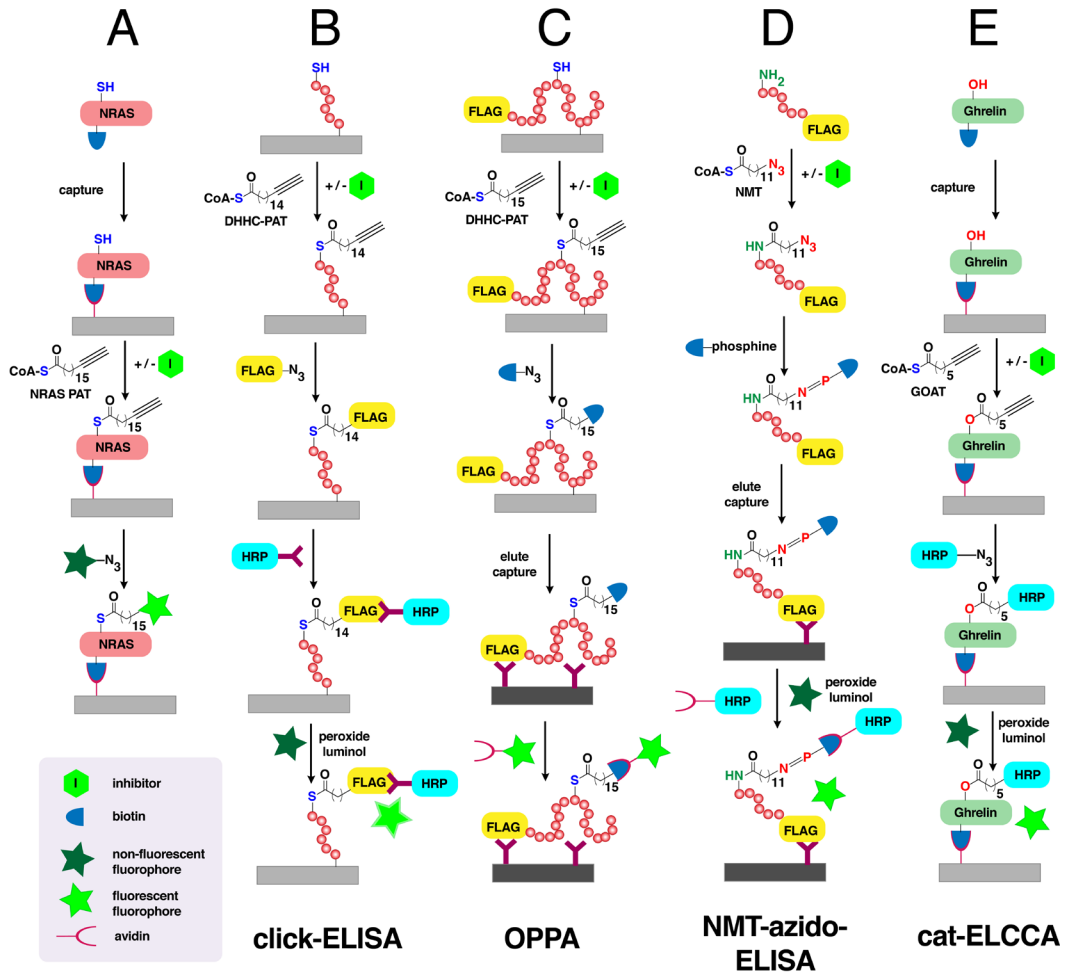

Figure 1.9. Enabling technologies based on click chemistry.

(A) A high-throughput method for screening inhibitors of NRAS palmitoylation. **(B)** An ELISA-inspired click chemistry-based technology (click-ELISA) for inhibitor screening. Immobilized substrates are labeled with a clickable fatty acyl-CoA analogue and tagged with FLAG-N_3. Addition of anti-FLAG conjugated to HRP in the presence of luminol and peroxide gives of chemiluminescence. **(C)** On-plate palmitoylation assay (OPPA) that involves labeling of a FLAG-tagged substrate with a fatty acid analogue and biotin and subsequent immobilization on plates coated with anti-FLAG. **(D)** NMT-azido-ELISA especially designed for evaluating NMT activity. FLAG-tagged substrates modified with azide are ligated with phosphine-biotin through Staudinger ligation. Labeled-substrates are then trapped on anti-FLAG-coated plates and NMT activity is quantified through chemiluminescence. **(E)** Catalytic enzyme-linked click chemistry assay (cat-ELCCA) to detect GOAT activity. Ghrelin substrate captured on a plate is labeled with a clickable octanoyl-CoA analogue and clicked with HRP.

Albeit high-throughput, the aforementioned assays are limited to truncated peptides of *S*-palmitoylation substrates. A rapid click chemistry-based On-Plate Palmitoylation Assay (OPPA) was demonstrated to be efficient for quantifying time-dependent *S*-palmitoylation on intact proteins (Fig. 1.9C).[249] His- and FLAG-tagged protein substrates were bound to Ni-NTA plates, *S*-palmitoylated with Alk-C16-CoA and clicked with azido-biotin. Products were then eluted and captured onto anti-FLAG coated plates and detected using fluorescently labeled streptavidin. *S*-palmitoylation on VAMP7 and LAT by full-length and truncated zDHHC18 was confirmed using this method. Transforming this method into a high-throughput scheme has yet to be accomplished.

While well-suited for determining the *S*-palmitoylation state of proteins of interest or evaluating PAT inhibition, none of the methods described above directly provide details regarding the number of fatty acylated sites nor the differential *S*-palmitoylation on multiple sites in a given protein. PEG-switch or acyl-PEG exchange (APE) assays based on thioester hydrolysis strategy were initially developed (Fig. 1.10A). [40,169] These methods use maleimide-functionalized heavy PEG groups reactive with putative *S*-palmitoylation sites on free cysteines that can be used to delineate several *S*-palmitoylated species of a protein based on mass shifts in electrophoretic gels. An orthogonal approach based on click chemistry was recently innovated by the Chamberlain group referred to as mPEG-click (Fig. 1.10B).[250] In this strategy, cells expressing the proteins of interest were treated with a clickable probe, *e.g.* Az-C16, followed by click reaction with a heavy PEG linker and detected *via* western blot. Similar to PEG-switch assays, the number of *S*-acylated sites can

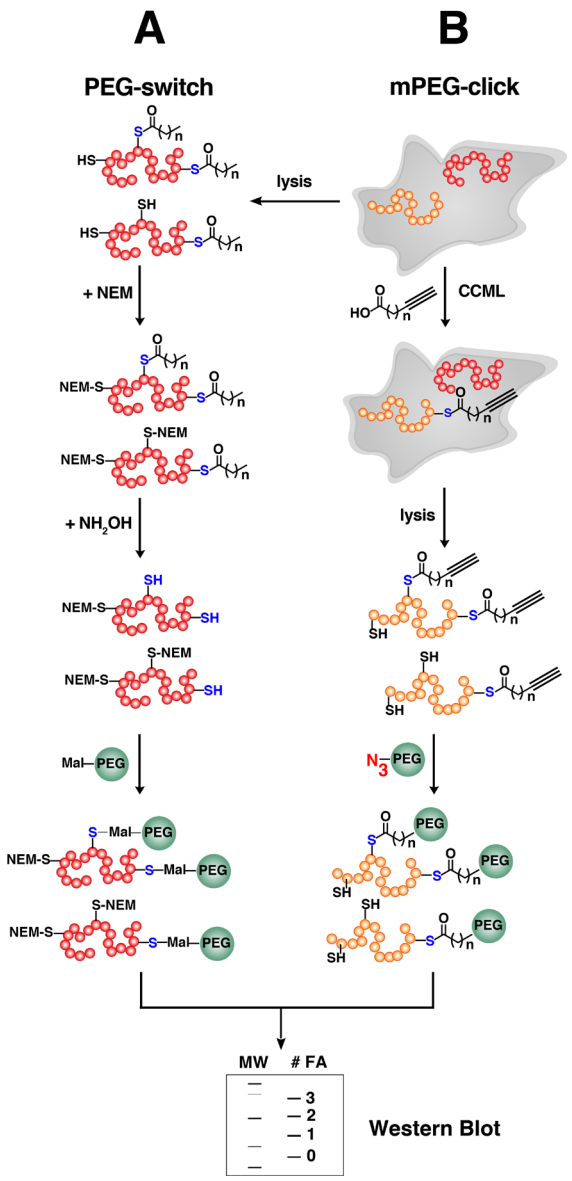

Figure 1.10. Methods to determine number of fatty acyl modifications in a protein.

(A) PEG-switch assay similar to ABE where free cysteines are blocked with NEM and the thiols of modified residues are liberated through hydrolysis. These free residues are subsequently reacted with maleimide-functionalized heavy PEG reagents and resolved in gels for western blot analysis. PEG-switch assay is suitable for non-active samples (*e.g.* tissues) but may not be specific to detect fatty *S*-acylated proteins. **(B)** mPEG-click assay involves metabolic labeling of clickable fatty acids in cultured cells and lysates are subsequently reacted with a heavy PEG linker *via* click reaction. Samples are resolved in an SDS-PAGE and proteins of interest are detected through western blotting. The number of fatty acyl modifications reflect the number of PEG conjugates displayed as protein bands with retarded migration.

be visualized as the number of differentially migrated bands, as well as used to distinguish between mutations that abrogate either site-specific or global protein *S*-acylation. It also facilitates the study of dynamic acylation cycling within a single protein when combined with pulse-chase and time-course labeling techniques. Using this strategy, the extents of modification of multiple *S*-palmitoylated cysteine residues in SNAP25 were determined, as influenced by mutations in its linker region that alters its interaction with zDHHCs. Indeed, mPEG-click complements PEG-switch assays in that it provides a broader scope for investigating *S*-acylation dynamics in active living cells, while the latter is suitable for analyzing the extent of *S*-acylation in samples not amenable to metabolic labeling such as tissues.[250]

In summary, these enabling methods developed for detecting fatty acyltransferase activity have indeed expanded the utility of the clickable analogues of palmitic acid. However, technologies based on *in vitro* enzymatic activities of zDHHCs have been limited to the screening platforms noted above and not generally for selective modification and bioconjugation of proteins. Unlike *N*-myristoylation and *S*-prenylation where the site modification and substrate recognition is well-defined, *S*-acylation lacks these features and hence may not be useful for site-specific protein labeling applications.

1.5. Biological applications in *N*-Myristoylation

The recent efforts in defining the N-terminal canonical sequence, as well as the development of bioinformatic tools has aided our ability to predict *N*-myristoylated proteins.[54,251] Although these tools are useful, their less than perfect predictive power

necessitates experimental validation of putative *N*-myristoylated proteins of interest. Click chemistry-based analogues of myristic acid including Az-12 and Alk-C14 (Fig. 1.11) have been used to simplify the validation of *N*-myristoylated proteins, assessment of NMT inhibitor efficacy, and proteome-wide profiling of *N*-myristoylated proteins.[18,127,252–254] Although selective, these probes can also be recognized as substrates that modify *S*-palmitoylated and GPI-anchored proteins.[125,128] Owing to the stability of the amide bond in *N*-acylation versus *S*-acylation (*S*-palmitoylation) and ester (GPI anchor) bonds, selective monitoring of *N*-myristoylated proteins can be achieved through releasing *S*-palmitoylated and GPI-APs aided by basic hydrolysis prior to detection (Fig. 1.6B).[140]

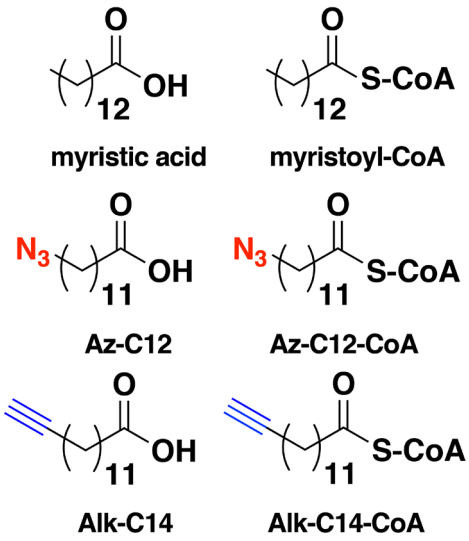

Figure 1.11. Clickable analogues of myristic acid and myristate-S-CoA for metabolic and *in vitro* labeling of myristoylated proteins.

The use of clickable myristic acid analogues has also facilitated cellular imaging,[232] when used in concert with additional technologies involving transfection vectors,[255,256] cell-free expression systems,[257] and ELISA-based techniques.[258] These methods have allowed the characterization of *N*-myristoylation substrates and probing for NMT activity. Furthermore, methods complementary to bio-orthogonal labeling such as photo-

crosslinking, and Sort-A and Phospho tagging strategies have expanded the available tools to study *N*-myristoylation.[259–261] Although *N*-myristoylation plays major roles in cancer and immunity,[262] significant efforts have been invested into understanding and targeting this lipidation process in pathogens via CCML-based methods. This section focuses on those studies enabled by CCML with clickable myristic acid probes that highlight the importance of *N*-myristoylation in regulating protein functions.

1.5.1. Proteome-wide analysis on N-myristoylation and defatty-acylation

Although the probes developed for fatty acylation of proteins are often amenable for incorporation into both *N*-myristoylated and *S*-acylated proteins, the analogues Az-C12 or Alk-C14 more efficiently label *N*-myristoylated proteins.[253] The preference for these probes corroborates observations made regarding the substrate specificity of NMTs which include the importance of chain length over hydrophobicity and the polarity of functional groups present in the fatty acyl-CoA analogue.[52] Their active site architecture also allows for bending of the fatty acyl substrate with exquisite control of acceptable chain length and steric bulk in the chain end. Moreover, comparison of the extent of labeling of biorthogonal fatty acid probes with varying chain lengths revealed that metabolic labeling with Az-C12 or Alk-C14 provides robust and irreversible labeling compared to analogues 2-4 carbons longer.[126,127] Their observed resistance to base hydrolysis in streptavidin blots and in-gel fluorescence analysis is a strong indication of amide bond formation, a characteristic feature of *N*-myristoylated proteins. Their labeling profiles also exhibit distinct labeled proteins compared to the longer probes across varying cell lines, suggesting that the

substrate scope of Az-C12 or Alk-C14 differs from the longer probes that are potentially *S*-palmitoylation substrates. More importantly, Alk-C14 is preferentially and effectively blocked by inclusion of the native myristic acid or the weak NMT inhibitor 2-hydromyristic acid, further validating this probe as a suitable surrogate for labeling *N*-myristoylated proteins.

1.5.1.1. Profiling N-terminal myristoylation

Tate and coworkers first described the use of Alk-C14 combined with CCML and quantitative proteomics in *P. falciparum*.[125] In this protozoan, both *N*-myristoylated proteins and GPI anchors were identified. To distinguish NMT substrates from GPI-anchored proteins, basic hydrolysis before enrichment enabled identification of more than 30 *N*-myristoylated proteins, with some showing evidence of intact modification on their N-terminal peptide determined through the use of a trypsin-cleavable reagent, AzKTB. These proteins participate in a diverse range of functions including motility, transport, development and phosphorylation pathways.

When quantitative mass spectrometric methods described above were applied to mammalian cells, more than 100 co- and post-translationally *N*-glycine myristoylated proteins were detected in HeLa cells.[263] To validate those candidates, both NMT knockdown and inhibition experiments using a small molecule were conducted, revealing 70 proteins responsive to inhibition at high confidence. This NMT inhibition perturbs the function of myristoylated proteins, leading to ER stress, cell cycle arrest, and induced apoptotic cancer cell death.[264] Furthermore, 87 candidate *N*-myristoylated proteins were

identified across HeLa, MCF7, and HEK293 cells, with 36 found in common among these cancer cell lines.[265] This suggests that the levels of NMTs and expression of their substrates are cell-type specific. The same group also presented the first quantitative analysis of the dynamic changes in *N*-myristoylation in a developing organism through pulse-chase labeling with Alk-C14.[124] *N*-myristoylation events were found to be more prominent during the early development of zebrafish, particularly with those involved in maturation, melanogenesis, meiosis, and hedgehog and Wnt pathways.

1.5.1.2. Lysine fatty and defatty-acylation

As discussed previously, fatty acylation on the N^{ε}-side chain of lysine was previously thought to occur on a limited number of proteins with TNFα described as the first N^{ε}-lysine myristoylated protein.[63] There is burgeoning evidence that this modification is regulated by members of the histone deacetylase (HDAC) and sirtuin families of hydrolases.[71,266] Although early studies suggested that this lysine modification occurs through *N*-myristoylation, metabolic labeling with the palmitate analogue Alk-C16 results in better incorporation compared with Alk-C14.[127,267] In contrast, recent findings suggest that N^{ε}-lysine fatty acylation is catalyzed by NMTs in mammalian cells, at least for the potentially N^{ε}-lysine myristoylation of ARF6 GTPase.[67] Due to this ambiguity, this modification is more rigorously referred to as N^{ε}-lysine fatty/defatty-acylation. Proteome-wide analysis of probe-labeled N^{ε}-lysine fatty acylated proteins can be accomplished through combining CCML and quantitative proteomics with genetic manipulation, chemical inhibition of the hydrolases, or selective hydrolysis of *N*-glycine myristoylated proteins. Lin and coworkers utilized both Alk-C14 and Alk-C16 in a SILAC-based quantitative proteomic analysis to

profile the targets of the defatty-acylase SIRT6 in mouse embryonic fibroblasts (MEFs) with wild-type and SIRT-6 knockout phenotypes.[65] Out of 865 and 1285 proteins enriched from Alk-C14 and Alk-C16 labeling, respectively, the list was narrowed down to 5 proteins as targets of SIRT6 after strict data filtering. One of those proteins was RRas2, where N^{ε}-lysine fatty acylation is essential for the activation of P13K/Akt pathway and promotion of cell proliferation. Owing to the stringent criteria used in this study, the data should be interpreted with caution as many actual protein targets may have not qualified to be included in this extremely reduced list of SIRT6 substrates. Following the same approach using Alk-C16, a proteome-wide analysis of MCF-7 cells identified SHMT2 as an HDAC11-mediated defatty-acylated protein.[71] The N^{ε}-lysine fatty/defatty-acylation of SHMT2 was shown to play a key role in regulating the type I interferon (IFN) signaling during immune response.

Several other hydrolases including SIRT1, SIRT2, and SIRT3 and HDAC8 display appreciable lysine defatty-acylation activity *in vitro*.[68,268] SIRT2 efficiently hydrolyzes Alk-C16 in metabolically labeled KRas-4a, RalB, and ARF6, but no validated fatty acyl-modified substrates were identified for the other hydrolases.[64,66,67,269] Proteins with fatty acylation regulated by these hydrolases are anticipated and their discovery should be facilitated by the established CCML and chemical proteomic approaches described here. Importantly, while these relatively recent studies presented strongly suggest that lysine fatty/defatty-acylation is plausible based on clickable probe labeling, they have been conducted through exogenous treatment with fatty acid analogues. It is possible that this approach may result in induced hypermodification of proteins that may not necessarily

reflect physiological conditions. In order to further hone in on the role this type of modification and its potential biological implications, direct evidence of N^{ε}-lysine modification under more native (unperturbed) conditions may be required. Future investigations should strive towards providing concrete evidence for the existence of this type of modification and deconstruct the precise molecular mechanisms that rationalize its occurrence. It is noteworthy that while NMTs can facilitate N^{ε}-fatty acylation in Gly1Lys2-containing substrates, the enzymes responsible and mechanisms involved in this type of modification on Lys residues near the C-terminus of a protein such as in KRas-4a and RalB remain unknown. It is possible that an *S*-to-*N* type of lipid transfer may occur from initially formed *S*-acylated proteins but further studies are needed to investigate this possibility.

1.5.2. Mammalian N-myristoylated proteins

The use of Az-C12 was pioneered by Hang and co-workers for detecting the *N*-myristoylation of the kinase Lck at endogenous levels *via* Staudinger ligation.[126] This marked the birth of using clickable myristic acid probes to validate *N*-myristoylation substrates. While intact proteins are viable for post-translational labeling *in vitro*,[270] the co-translational nature of *N*-myristoylation on nascent proteins can be examined by tagging proteins in one pot using cell-free transcription/translation systems (Fig. 1.12A).[257] In this strategy, genes for proteins of interest are inserted in plasmids and transcribed and translated in lysates obtained from rabbit reticulocytes or insects. These lysates contain the essential elements to express proteins and in the presence of a clickable myristic acid

analogue, co-translational labeling takes place. Importantly, the free acid form of the lipid analogues can be used since they are converted to their -CoA forms *in situ.*

Prior to the development of Alk-C14, the complementarity between azides and phosphines for Staudinger ligation enabled the use of Az-C12 to rapidly detect and identify post-translationally *N*-myristoylated proteins during apoptosis.[252] The Staudinger reaction was also useful in confirming the *N*-myristoylation and *S*-palmitoylation of DCNL3 in cells treated with Az-C12 and Az-C14, respectively.[271] While related proteins DCNL1 and DCNL2 share the same function by mediating Cul neddylation, only DCNL3 is directed to the plasma membrane through a myristoyl anchor, facilitating neddylation of the membrane-localized Cul protein. This exemplifies the role of lipid modification in modulating localization and subsequent substrate specificity of related proteins sharing the same function. Likewise, this method aids in understanding how species-specific function is regulated by *N*-myristoylation. Human LMCD1 activates transcription factors that stimulate cell proliferation and migration while the mouse homolog conversely represses this pathway. The NMT2-mediated *N*-myristoylation of mouse LMCD1, as evidenced by Az-C12 labeling, reversed its repressor activity, underscoring the differential roles of LMCD1 transactivation activity in humans versus mice.[272] Furthermore, *N*-myristoylation regulates the cell type-specific sorting of proteins such as the spermatozoan variant Hexokinase 1 (HK1S).[273] Cell-free translation combined with co-translational labeling with Az-C12 and subsequent Staudinger detection confirmed HK1S *N*-myristoylation; and the presence of myristate directs it to the plasma membrane, which is not the case in other cell-types.

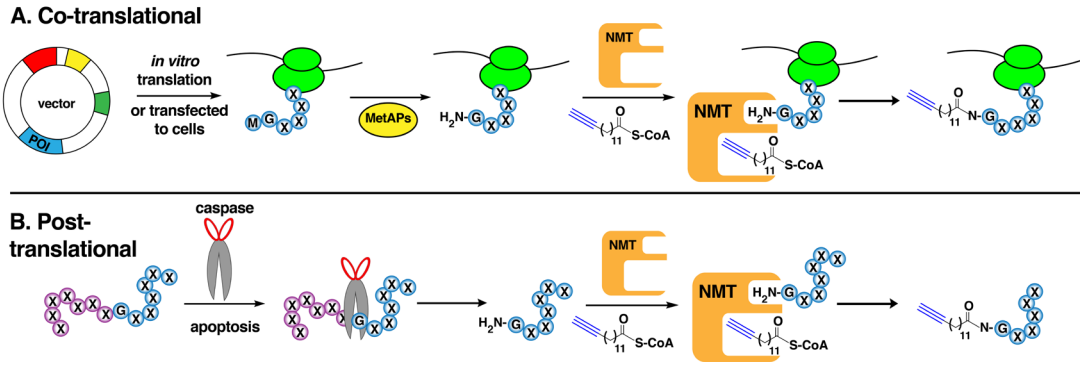

Figure 1.12. Mechanisms for labeling the N-myristoylated proteins.

(A) Co-translational modification where probes are added to either cultured cells or *in vitro* in lysates containing plasmids that express proteins of interest (POI) for cell-free expression. The N-terminal methionine is cleaved off by MetAPs and the clickable myristoyl analogue is appended by NMTs to the N-terminal amine on the exposed glycine of the nascent protein. **(B)** Post-translational *N*-myristoylation during apoptosis on protein substrates generated through cleavage by caspases that expose a new N-terminal glycine.

Labeling with Az-C12 was also the basis for the development of an ELISA-based method called NMT-azido-ELISA (Fig. 1.9D).[258] This approach differs from those designed for palmitoylation in that it does not involve immobilization in the first step. Instead, peptide substrates bearing a FLAG tag are enzymatically labeled with Az-C12-CoA in solution followed by Staudinger coupling with a biotin-phosphine reagent. The biotinylated substrates are then captured with immobilized anti-FLAG antibodies and detected through peroxidation-driven chemiluminescence. This versatile technology offers the ability to measure enzymatic activities of wild-type and mutant NMTs, as well as measure the efficacy of candidate NMT inhibitors. Using this method, the loss of NMT activity in NMT-deficient knockouts was confirmed, serving as a framework for the succeeding biochemical assays that pinpointed that NMT deficiency results in aberrant T

cell development; this was later ascribed to changes in calcineurin activity during IFN signaling.[274,275] Although this method uses Staudinger reaction in its current form, it could be adapted to function with other bio-orthogonal reactions that manifest faster kinetics and use more stable reagents.

The Alk-C14 probe has found wider applications in discovering and characterizing *N*-myristoylated proteins owing to its lower background, similar to the clickable palmitic acid probes.[127,128] CCML with Alk-C14 aided the discovery of regulatory mechanisms of proteins or their binding partners through their subcellular localization dictated by *N*-myristoylation. The *N*-myristoylation on Fragile X-related protein 2 (FXR2P) was shown to control its distribution in neuronal axons and its interaction with Fragile X mental retardation protein (FMRP).[276] Since FMRP plays important roles in axonal and presynaptic functions and relies on FXR2P for proper localization, *N*-myristoylation on FXR2P may be implicated in Fragile X syndrome linked to intellectual disability and autism. *N*-myristoylation also influences the subcellular localization of proteins associated with mitochondrial morphology and degradation (mitophagy). Myristate modification directs the autophagy receptor mouse Stbd1 to ER-mitochondria junctions, and impairment of this process induced significant mitochondrial fragmentation and clustering, possibly associated with autophagy.[277] Similarly, the *N*-myristoylation-dependent localization of AMP-activated proteins kinase (AMPK) to damaged mitochondria was also found to mediate mitophagy.[278] Treatment with a 2-hydroxymyristic acid, a weak inhibitor of NMTs,[279] validated its *N*-myristoylation through mislocalization upon treatment with effective concentrations of this inhibitor. Furthermore, *N*-myristoylation can be controlled

by proteins that modulate the interaction between NMTs and their substrates. The CSIG protein facilitates *N*-myristoylation of PPM1A by mediating the NMT-PPM1A interaction.[280] Evidence for a CSIG-PPM1A-NMT complex was obtained by co-immunoprecipitation and reduced Alk-C14 labeling of PPM1A was observed upon CSIG knockdown. Indeed, the use of clickable analogues of myristic acid not only directly validates the myristoyl modification on proteins but also can indirectly confirm the role of this lipid modification in the assembly of protein complexes.

Although most *N*-myristoylated proteins are co-translationally modified, a number of substrates are post-translationally modified during apoptosis.[263] Apoptotic caspase activation leads to *N*-myristoylation of a newly exposed N-terminal glycine (Fig. 1.12B).[281] Thus, CCML with Az-C12 or Alk-C14 was used to show the upregulation and post-translational *N*-myristoylation of protein kinases A and C during chemically induced apoptosis.[186,255] Alk-C14 labeling readily detected drastic changes in the *N*-myristoylated proteome during apoptosis, with concomitant caspase-mediated cleavage of NMTs resulting in impaired NMT activity.[55] The interplay between NMTs and caspases may explain the high expression levels of NMTs in cancer cells subverting apoptosis. Moreover, the caspase-cleaved huntingtin protein (HTT) liberates a myristoylated C-terminal product detected using Alk-C14.[282] The lipidated product localizes to the ER and promotes accumulation of autophagosomes, suggesting a connection between HTT and autophagy with possible implications in Huntingtin's disease (HD). A later study showed that an HTT variant with G533E mutation blocked caspase cleavage and subsequent *N*-myristoylation,

leading to cytotoxicity.[283] It was noted that this HTT variant was an important disease marker that may lead to earlier onset of HD.

Several proteins associated with oncogenesis such as Src and various kinases are dependent on *N*-myristoylation for their proper cellular function.[284] Alk-C14 labeling revealed that excessive exogenous levels of myristic acid elevates levels of *N*-myristoylated Src, implicating high-fat diets as drivers of prostate cancer tumorigenesis.[285] In a separate study, Az-C12 labeling illustrated that NMT1 regulates cancer cell proliferation through Src *N*-myristoylation and blocking the lipid-modification suppresses Src kinase activity.[286] A recent study has shown that treatment with the NMT pan-inhibitor PCLX-001 along with Alk-C14 labeling in B-cell lymphoma induced global impacts on the *N*-myristoylated proteome and particularly abrogated Src *N*-myristoylation.[287] This protein along with non-myristoylated proteins involved in B-cell receptor signaling were degraded upon NMT inhibition, leading to cancer cell death both *in vitro* and *in vivo*. In addition to Src, the *N*-myristoylated protein fibroblast growth factor receptor substrate 2 (FRS2) also contributes to carcinogenesis through FGF/FGFR-mediated oncogenic signaling and FGF10-induced tumorigenesis.[288] Pharmacologically targeting its *N*-myristoylation, as verified through diminished Az-C12 incorporation, inhibits cancer cell proliferation and migration as well. These studies provide evidence that designing effective NMT inhibitors can lead to promising drug candidates for cancer treatment. Clinical applications for such compounds including PCLX-001 are anticipated. However, exploring their on-target selectivity through enzymology and crystallographic studies will

be required to validate these inhibitors, especially in the case with PCLX-001 treatment where many non-myristoylated proteins were also degraded.

1.5.3. Parasitic protozoans and fungi

Targeting NMTs is a viable strategy for the development of therapeutic agents owing to the requirement of *N*-myristoylation for the survival of human pathogens.[52,289–291] Integrated chemical biology methods combining CCML and quantitative proteomics with selective NMT inhibition allowed for the robust identification of the parasite *N*-myristoylated proteome in *P. falciparum.*[125] From that proteome-wide analysis, the proteins ISP1 and ISP3 required for RBC invasion emerged as attractive targets; additionally, their *N*-myristoylation status was previously validated using Alk-C14 in a related malaria parasite, *P. berghei*.[292] Increasing resistance of these parasites to current antimalarial drugs underscores the need to generate new classes of parasite-specific chemotherapeutics. In an effort to preempt potential resistance to lead candidate inhibitors of *P. falciparum* NMTs, a mutant PfNMT with a single amino acid substitution (G386E) was generated that exhibited resistance to current known parasitic NMT inhibitors.[293] Such an approach enabled the generation of a new class of NMT inhibitors capable of inhibiting the growth of predicted resistant strains. IMP-1002 emerged as a lead candidate with on-target inhibition of NMT as shown by decreased labeling by Alk-C14 of myristoylated proteins. Future studies can be directed towards designing pharmacological inhibitors against G386E-mediated resistance without compromising target selectivity.

Trypanosomes are the causative agents for fatal diseases including African sleeping sickness and Chagas disease caused by *Trypanosoma brucei* and *Trypanosoma cruzi*, respectively. *N*-myristoylation is essential for the cell viability and development of these parasites and therefore offers an attractive target for treating those diseases. For example, *N*-myristoylation of ARL6 was demonstrated using CCML with Alk-C14 and is important for its membrane localization to promote flagellum extension in *T. brucei.*[294] Global profiling robustly identified 101 enriched proteins with 46 possessing the N-terminal glycine motif and 53 responded to TbNMT inhibition.[160] On the other hand, the azide analogue Az-C12 was employed to validate NMT inhibition as a potential therapeutic strategy to target *T. cruzi*.[295,296] Subsequent CCML with Az-C12 and quantitative proteomic analysis profiled more than 50 *N*-myristoylated proteins sensitive to NMT inhibition.[297] Only half of that list of proteins overlaps with those identified from *T. brucei*.[160] This observed disparity in the sets of myristoylated proteins between two species could be attributed to the type of myristic acid analogues used or differences in metabolism such as the rate of plasma turnover, as evidenced by their differential responses to NMT inhibition.[160]

Other neglected tropical diseases such as leishmaniasis and toxoplasmosis are caused by protozoans that also require *N*-myristoylation for proper protein functions.[291] Label-free quantitative analysis with Alk-C14 labeling in *L. donovani* revealed 67% overlap between the parasite and host *N*-myristoylated proteomes, of which 30 parasitic *N*-myristoylated proteins displayed sensitivity to LdNMT inhibition.[298] Although this indicates that LdNMT is a druggable target, some bonafide *N*-myristoylated proteins

including CAP5.5 and phosphatase PPEF did not respond to chemical inhibition. This prompted the development of more potent pharmacological inhibitors based on benzothiophene and pyrazolyl scaffolds that exhibit high selectivity for LdNMT.[299,300] However, these effective inhibitors suffer from problems of chemical stability and display poor cellular uptake. A recent study reported a comprehensive development of a series of thienopyrimidine-based small molecules that showed high selectivity towards LdNMT versus human NMT.[301] Through the use of Alk-C14 labeling, a dose-dependent decrease in signals from *N*-myristoylated proteins was observed, signifying the on-target intracellular activity of this novel set of LdNMT inhibitors. Furthermore, these promising therapeutic agents are effective against the amastigote form of *L. donovani*, which is an excellent model to study owing to its clinical relevance.

Global profiling of *N*-myristoylation in *T. gondii* identified 76 myristoylated proteins including 31 *N*-myristoylated peptides using azide-modified, trypsin- and TEV-cleavable multifunctional reagents.[302] Validation of *N*-myristoylation through Alk-C14 labeling on two proteins, CDPK1 and MIC7, was accomplished, followed by biochemical assays resulting in defining their key roles in egress and host-cell invasion, respectively. Interestingly, a recent study validated the *N*-myristoylation of the previously uncharacterized active serine hydrolase 4 (ASH4) in *T. gondii* through Alk-C14 labeling.[303] *N*-myristoylation on ASH4 does not influence membrane localization but is involved in a mechanism important for parasite organization in the parasitorous vacuole. Prior evidence suggested that this enzyme is a protein depalmitoylase.[304] However,

biochemical and cell-based assays in this more recent work demonstrated its esterase activity on small molecules with short chain acyl esters.

N-myristoylation is also of functional importance in opportunistic fungal pathogenic genera including *Candida, Cryptococcus*, and *Aspergillus*, indicating that NMTs could serve as attractive targets for antifungal agents.[305–308] Despite the fact that this lipid modification has been established in these pathogens for decades, information on their NMT substrates is limited. Advances in chemical proteomic strategies should pave the way for defining their sets of *N*-myristoylated proteins. Recently, Tate and coworkers profiled the *N*-myristoylated proteome using Alk-C14 in the fungal pathogen of wheat, *Zymoseptoria tritici.*[309] Out of the 25 predicted *N*-myristoylated proteins from the fungal proteome, 20 were detected through LC-MS analysis, providing a robust list *of N*-myristoylated proteins in *Z. tritici*. Furthermore, a ZtNMT-selective inhibitor IMP-1088 showed an NMT-dependent mode-of-action, in contrast to a previously reported NMT inhibitor IMP-162 that displayed off-target effects.

It is noteworthy that there are no N^{ε}-lysine fatty/defatty-acylation substrates amongst these protozoan and fungal pathogens reported to date. However, the previously characterized *P. falciparum* SIRT2 can catalyze hydrolysis of medium and long chain fatty acyl groups on model peptides *in vitro*.[310] Hence, lipid modifications on the N^{ε}-side-chain may yet be discovered in protozoans and chemical biology tools such as CCML should aid in the characterization of its potential functional importance in these parasites. Similar to those experiments conducted in mammalian cells, detection of this type of modification under native conditions is necessary to demonstrate its true existence in lower eukaryotes.

1.5.4. Bacteria and viruses

As mentioned above, bacterial LPPs can be modified with diacylglyceryl bearing fatty acids on an exposed N-terminal cysteine (Fig. 1.13A). Compared with *S*-palmitoylation, only a modest number of myristoyl-containing LPPs are present in Gram-negative *E. coli*.[150] However, clickable fatty acid labeling in the Gram-positive *Clostridium difficile*, a bacteria associated with severe gastrointestinal diseases, revealed that Alk-C14 can efficiently label its LPPs.[311] Inactivation of lipoprotein diacylglyceryltransferase (Lgt) led to almost complete loss of probe labeling, validating the observed *N*-myristoyl modification that occurs on LPPs. Quantitative proteomic analysis then yielded 65 candidate LPPs with 56 responsive to competition with the native myristate, comprising 74% of the predicted LPP proteome in *C. difficile*. The transcription factor Spo0A which regulates sporulation, a self-preservation mechanism of bacteria, was further shown to be modulated by LPP expression. These results highlight the involvement of LPPs in *C. difficile* sporulation and lays the groundwork for future studies on LPP lipidation in other Gram-positive bacteria.[311]

Bacteria also leverage protein *N*-myristoylation to direct their secreted effector proteins to appropriate subcellular locations critical for their virulence.[60,312,313] Concurrently, these pathogens may also alter PTMs on host proteins to redirect host pathways that promote their replication and escape from the host immune system.[314] A bacterial T3SS effector protein IpaJ peptidase, a cysteine protease from *Shigella flexneri,*

was discovered to efficiently cleave the *N*-myristoylated glycine of host proteins (Fig. 1.13B).[315] Lysates from mammalian cells metabolically labeled with Alk-C14 showed diminished global *N*-myristoylation after infection with *S. flexneri*.[316] Global *N*-myristoylated proteome profiling revealed a number of substrates cleaved by IpaJ with high specificity to *N*-myristoylated ARF/ARL GTPases. The myristoyl group on these proteins serve as the binding site of IpaJ, leading to hydrolysis of the substrate glycine peptide bond catalyzed by its active site cysteine. Interestingly, ARF6 was the only protein in ARF family found to be an unsuitable substrate for IpaJ. It is possible that the observed regulation on ARF6 dimyristoylation by NMTs for its localization in the plasma membrane is implicated in the poor cleavage by IpaJ.[67] In a subsequent study, BT3 from *Vibrio vulnificus,* which belongs to a family of multifunctional auto-processing repeats-in-toxin (MARTX) effector proteins, was observed to bind myristoylated ARF1.[317] Its domain X (DmX) is structurally homologous to a cysteine protease AvrPphB and it was therefore speculated to hydrolyze *N*-myristoylated glycine. However, Alk-C14 labeling experiments did not reveal diminished *N*-myristoylation of ARF1 upon incubation with DmX unlike IpaJ.

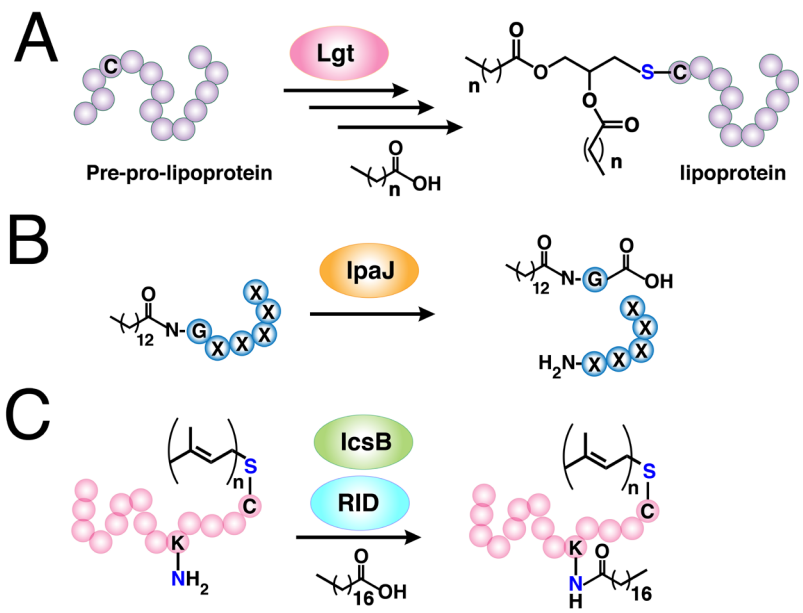

Figure 1.13. Bacteria-mediated lipidation/delipidation.

(A) Incorporation of saturated fatty acids into the S-linked diacylglycerol unit on bacterial lipoproteins (LPPs). The pre-pro-lipoprotein undergoes processing steps that exposes a new N-terminal cysteine and its thiol side-chain is modified by lipoprotein diacylglyceryltransferase (Lgt) with a glyceryl group containing two fatty acyl moieties. **(B)** Demyristoylation on host proteins catalyzed by the bacterial effector protein IpaJ. The *N*-myristoylated N-terminal glycine is cleaved by this peptidase. **(C)** *N*-fatty acylation on prenylated small GTPases by bacterial effector proteins IcsB or RID. The prenyl modification on their substrates appears to be essential for their recognition.

N-myristoylation of viral proteins is critical for their host cell entry, replication, assembly, and infectivity.[318–320] Due to the small proteomes of viruses, *N*-myristoylated proteins can be conveniently assigned based on predicted N-terminal glycine motifs unlike *S*-palmitoylation. However, viruses not only require lipid-modification of their proteins but also modulate host-cell PTM machinery.[314] Therefore, CCML allows the detection and identification of not only *N*-myristoylated viral proteins, but also host proteins impacted due to infection. Az-C12 labeling in infected cells validated the *N*-myristoylation of $Pr55^{gag}$ HIV-1 protein, and that NMT1 promotes HIV-1 replication by modulating the expression of viral proteins.[321] In HSV, quantitative profiling of *N*-myristoylated proteins using Alk-

C14 in HSV-infected cells afforded 5 putative myristoylated viral proteins and revealed a dramatic reduction in host global *N*-myristoylation.[154] Although novel myristoylated viral proteins were identified, known *N*-myristoylated viral proteins were not enriched, potentially owing to the small number of tryptic peptides from these short proteins.

Among the diverse roles of *N*-myristoylation in promoting viral virulence, the co-translational *N*-myristoylation of viral structural capsid proteins (VPs) is critical for viral capsid assembly.[322] Therefore, inhibiting their *N*-myristoylation may attenuate viral infectivity. Effective inhibition by a non-selective human NMT inhibitor DDD85646 on the capsid protein VP0 was verified using Alk-C14 and in-gel fluorescence assays.[323] Cells infected with the picornavirus CVB3 and treated with DDD85646 diminished viral RNA encapsidation and viral genome transfer, rendering the virus less infectious. At the same time, Tate and coworkers screened a series of HsNMT inhibitors on cells infected with the common cold virus, rhinovirus (RV).[324] The most potent and HsNMT-selective inhibitor IMP-1088 reduced *N*-myristoylation of host proteins and capsid protein VP0 in a chemical proteomic profiling experiment. This picomolar inhibitor is a derivative of the *P. vivax* NMT-specific IMP-72,[325] refined through a fragment reconstruction and linking approach. Moreover, it displayed effective inhibition of replication of poliovirus and foot-and-mouth disease virus with no observed toxicity to host cells.

Given the key role of *N*-myristoylation in oncogenesis and infections, designing human and parasitic NMT-selective inhibitors as potential chemotherapeutic agents against cancer and infectious diseases remains an active area of research.[284,291] Several inhibitors

have emerged and been claimed to be selective for targeting HsNMT. However, a recent study investigated the potency of five commonly used inhibitors against HsNMT through a series of biochemical assays including metabolic labeling with Az-C12.[279] Three of those compounds failed to arrest NMT activity while two high-affinity inhibitors displayed on-target NMT inhibition with low cytotoxicity. Transforming these potent inhibitors into formulations viable for clinical trials is therefore anticipated.

1.6. Biological applications in *S*-Prenylation

The existing paradigm for protein *S*-prenylation is that it occurs on proteins that terminate with Ca_1a_2X box motifs for farnesylation and geranylgeranylation, and CCXX, XXCC, XCXC motifs for dual geranylgeranylation of the Rab family of proteins.[326–328] Basing on those criteria, previously validated prenylated proteins have been used as models to generate computational tools that allow *in silico* screening for protein *S*-prenylation substrates.[81,329] However, despite the existence of canonical *S*-prenylation motifs and prediction tools, several approaches have been put forth to experimentally validate the true *S*-prenylation status of proteins. These methods involve *in vitro* reactions on Ca_1a_2X box-containing substrates in peptide libraries or genetic screening in yeast thermotolerance assays.[79,80,330,331] Although these methods are generally high throughput, they are often limited to Ca_1a_2X box peptide substrates mimicking the C-termini of proteins. The sequences upstream of the Ca_1a_2X box on proteins contribute to substrate reactivity and therefore these peptides may not completely reflect substrate recognition on intact proteins.[82]

Bio-orthogonal labeling of prenylated proteins rapidly emerged and a number of isoprenoid analogues were reported. [16] The promiscuity of prenyltransferase enzymes offers the advantage of introducing a variety of functional groups onto the isoprenoid probe.[332,333] For example, light-activatable and antigenic groups enabled photoaffinity labeling and prenyl-targeted antibody-based detection of prenylated proteins.[334–338] A biotin-conjugated geranyldiphosphate analogue (BGPP, Fig. 1.14) was also utilized to directly detect and enrich prenylated proteins in both metabolic labeling and *in vitro S*-prenylation experiments, obviating the need of secondary tagging unlike click reaction-based approaches.[99,339–341] Although that probe is an efficient substrate for RabGGTase owing to this enzyme's larger binding site, it however requires an engineered FTase and GGTase-I to effectively label singly prenylated proteins.[339] Therefore, the scope of BGPP in probing prenylated proteins is restricted.

Clickable analogues of isoprenoids containing azides and alkynes were developed in different versions of alcohol and diphosphate forms (Fig. 1.14).[342–345] Although isoprenoid diphosphates are the bonafide substrates for prenyltransferases, the alcohol versions of the probes have been extensively used in metabolic labeling experiments since they are readily incorporated into proteins through intracellular conversion by host-cell kinases.[346,347] This additional pathway (distinct from the well characterized mevalonate pathway) for converting the alcohol forms to their diphosphate counterparts is not well

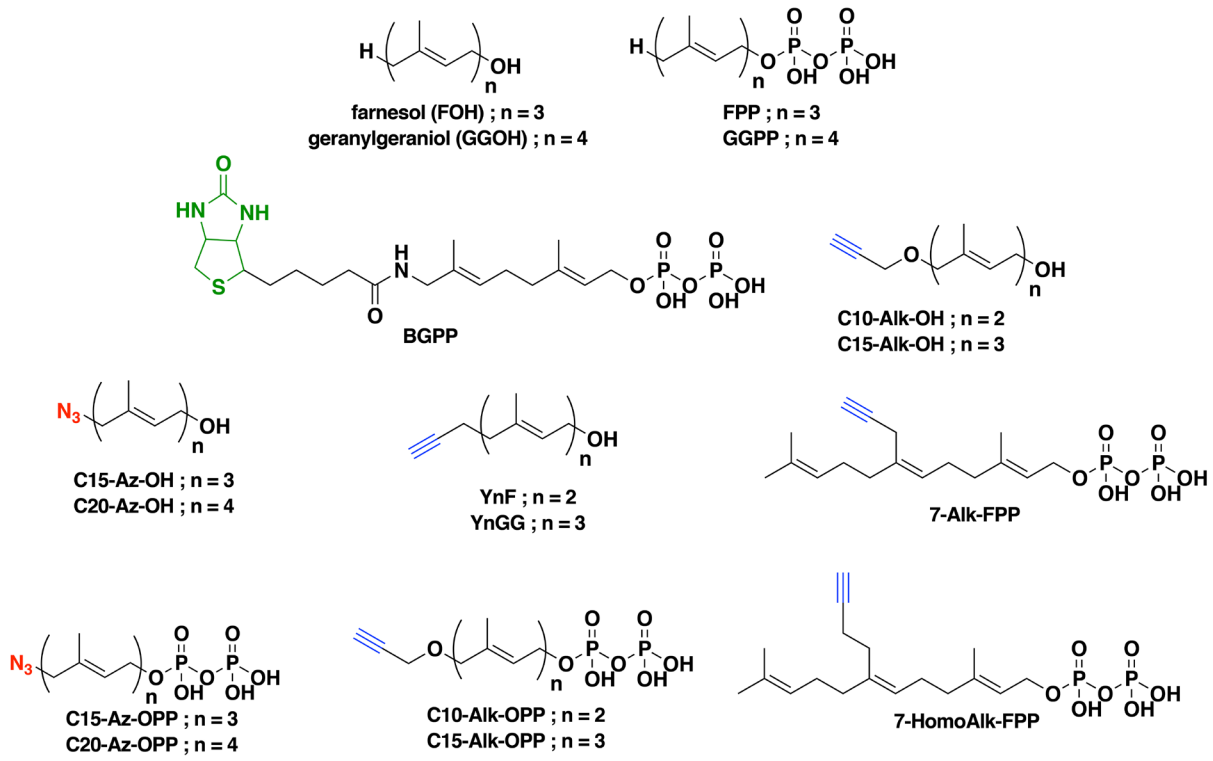

Figure 1.14. Bio-orthogonal isoprenoid analogues for probing protein prenylation.

understood and warrants further investigation concerning what enzymes are involved and how this process occurs. However, it is important to note that the exogenous treatment of isoprenols (*e.g.* farnesol) induces potential toxicity that may impact cell physiology. This may complicate the biological interpretation of experiments using alcohol analogues of isoprenoid probes.[348,349] The azide functionalized farnesol (C15-Az-OH) and the corresponding diphosphate form, C15-Az-OPP, were first reported by two independent groups to detect prenylated proteins *via* Staudinger ligation.[342,343,350] Later studies demonstrated that the longer C20-Az-OH and C20-Az-OPP are more suitable for detecting geranylgeranylated proteins.[351,352] However, employing alkyne-modified isoprenoids results in lower noise signal compared to the azide versions, consistent with the

observations in using fatty acylation probes.[127,128,353] Therefore, alkyne-modified isoprenoids were exploited to identify and characterize prenylated proteins. The position of the alkyne was also varied along the isoprenoid chain such as in the second isoprene unit of FPP (7-Alk-FPP and 7-HomoAlk-FPP, Fig. 1.14).[354] Kinetic analysis comparing C15-Alk-OPP and 7-substituted FPP indicates that alkyne-modification at the terminus of FPP presents the best mimic for the native FPP.[355] In this section, studies that utilized these isoprenoid analogues to profile and validate known and novel prenylated proteins are reviewed.

1.6.1. S-prenylated proteome profiling

Proteomic profiling of prenylated proteins has been reported using various isoprenoid analogues *via* metabolic labeling in a number of studies. These methods often involve the use of statins that impede isoprenoid biosynthesis by inhibiting HMG-CoA reductase in the mevalonate pathway.[356] This reduction of the pool of endogenously occurring isoprenoids generally improves labeling efficiency by forcing the prenyltransferase enzymes to incorporate the analogues in lieu of the native isoprenoids. Methods to profile a set of *S*-prenylated proteins from cells of interest can be performed through metabolic labeling or *in vitro S*-prenylation approaches as described below.

1.6.1.1. Metabolic labeling with isoprenoid analogues

Early pioneering work utilized the alcohol probe C15-az-OH to metabolically label farnesylated proteins in statin-treated cells.[342] Tagging *via* Staudinger ligation with biotin-phosphine for affinity enrichment, followed by proteomic analysis resulted in the

identification of 17 enriched proteins containing Ca_1a_2X motifs. A longer analogue C20-az-OH was used in a subsequent study to tag geranylgeranylated proteins, which were detected using an alkyne-containing fluorophore.[351] Separation of the labeled proteins via two-dimensional SDS-PAGE and excision of the labeled spots subjected to LC-MS/MS afforded a list of 10 geranylgeranylated proteins dominated by Rabs.

The alkyne containing analogues C10-Alk-OH and C15-Alk-OH along with their diphosphate counterparts C10-Alk-OPP and C15-Alk-OPP, respectively, were evaluated for their labeling efficiencies in HeLa cells.[353] Replacing the alcohol probes with the diphosphate analogues enabled effective labeling although no direct comparison was performed. However, other cell lines may have behave differently such as COS-7, which displayed intense labeling of prenylated proteins using the diphosphate analogue versus the alcohol form. Treatment with lovastatin displayed modest enhancement of labeling in HeLa, indicating that this cell line maybe less responsive to statin treatment, or isoprenoid labeling in this cell line is less efficient such that small differences cannot be observed. Following a two-dimensional SDS-PAGE approach for proteomic analysis, only 6 Ca_1a_2X -containing proteins were identified, reflecting a low efficiency of labeling in HeLa cells treated with C10-Alk-OH. Optimal concentrations of lovastatin may have not been attained to furnish enhanced probe labeling.[357] Furthermore, HeLa cells may not respond to isoprenoid labeling as efficiently as other cell lines do such as COS-7, which displayed excellent labeling with C15-Alk-OPP but not with C15-Alk-OH.[358] This disparity in labeling between cell lines using different forms of the isoprenoid probe can be rationalized with the observation that different cell-types respond with varying degrees of probe

labeling with C15-Alk-OH.[359] Profiling of *S*-prenylated proteome in the macrophage cell line RAW264.7 yielded 23 Ca_1a_2X-containing and 12 Rab proteins using C15-Alk-OH.[360] Furthermore, a novel prenylated zinc antiviral protein (ZAP) was discovered and further characterized to show that its farnesylation enhances its membrane-targeting and inhibitory activity against Sindbis virus.[360]

Like other protein lipid-modifications, *S*-prenylation mediates diverse pathways across organisms and is therefore implicated in numerous human diseases, as well as viral, bacterial, and protozoal infections.[11,361] For example, prenyltransferase inhibitors (PTIs) directed towards the development of antimalarial drugs indicate that protein *S*-prenylation is indispensable for parasite development.[362] Two independent studies sought to define the *S*-prenylated proteome in that organism. First, Distefano and co-workers employed bioinformatic analysis and proteomic profiling using C15-Alk-OPP in blood-stage *P. falciparum*.[363] A total of 15 putative *S*-prenylated proteins were identified comprising 78% of the bioinformatically predicted protein *S*-prenylation substrates in the parasite. One of the proteins identified, heat shock protein 40 (Hsp40), was later shown to require farnesylation to promote parasite thermotolerance and facilitate vesicular trafficking.[364] A subsequent study provided a similar list of *S*-prenylated proteins in the parasite using C15-Alk-OH.[365] It was shown that farnesylation of the protein FCP directs it to the parasitorous vacuole and treatment with an antimalarial farnesyltransferase inhibitor (FTI) disrupts its localization. Furthermore, an unusual *S*-prenylation on PfFRab5b was observed, which does not contain the canonical *S*-prenylation motifs. These studies demonstrated that the malaria parasite possesses a restricted set of *S*-prenylated proteins, making prenyltransferases attractive targets to develop antimalarial drugs.

More than 200 proteins bearing *S*-prenylation motifs in mammalian cells are predicted to be *S*-prenylation substrates based on genomic, structural, biochemical, and functional analyses.[2] Although the C15-Alk-OH and C15-Alk-OPP can be incorporated into the three classes of *S*-prenylation substrates, early reports on profiling of *S*-prenylated proteins in diverse mammalian cell lines provided less than a quarter of the predicted number.[345,353,360] Recently, Tate and coworkers applied a dual chemical probe labeling strategy for CCML, where both alkyne-modified farnesyl (YnF) and geranylgeranyl (YnGG) isoprenoid analogues were used in tandem to identify protein substrates of the three classes of *S*-prenylation in a human endothelial cell line.[366] These probes are shorter by one atom compared to the previously reported *S*-prenylation probes C10-Alk-OH and C15-Alk-OH. A total of 80 known and novel *S*-prenylated proteins were identified with 64 detected at endogenous levels in the absence of statins. The assignment of the *S*-prenylation status of proteins (farnesylated or geranylgeranylated) were deduced through their ability to be prenylated by YnF or YnGG and their corresponding response to FTI or GGTI treatment, as well as to competition with FPP or GGPP. In addition, a cleavable multifunctional reagent, originally developed for the detection of *N*-myristoylated proteins, was used in the enrichment step,[124] which allowed for the detection of prenylated peptides in the LC-MS/MS analysis. A total of 26 intact *S*-prenylated peptides from 18 distinct proteins were successfully detected. Furthermore, a choroideremia disease model with knocked out Rep-1, the escort protein that recruits Rabs for *S*-prenylation, showed 10 out of 29 quantified Rab proteins as having a significant reduction in *S*-prenylation. In particular, Rab12 and Rab27b displayed the most significant reduction in prenylation in

this model. Previous *in vitro* *S*-prenylation studies indicated that Rab27b along with Rab27a, Rab38, and Rab42 are the least efficient substrates of RabGGTase, suggesting that these proteins are the key contributors to the disease.[99] The latter three Rab proteins were not quantified nor identified in the MEFs with Rep-1 knockouts, perhaps owing to the limitations in the detectability of these proteins in the chemical proteomics workflow. It is also worth noting that these results in Rep-1 knockout models indicate that under conditions where Rep-1 is dysfunctional, rescue by the other escort protein Rep-2 is not efficient. This further supports the previous findings that suppression of Rab *S*-prenylation occurs in retinal degeneration in the choroideremia disease.[367]

While the study above demonstrates that the use of more than one isoprenoid probe widened the scope of *S*-prenylated proteins profiled through quantitative chemical proteomics, a recent report revealed that C15AlkOPP acts as a surrogate for both FPP and GGPP, leading to the identification of a comparable number of prenylated proteins in COS-7.[368] Using this single isoprenoid analogue also led to the identification of novel prenylated proteins that were not reported in the dual isoprenoid probe labeling strategy (although the converse of this was also true). In an effort to rationalize what factors affect the detectability of *S*-prenylated proteins in this chemical proteomics scheme, predicted scores and reported *in vitro* activity assays for *S*-prenylation substrates were investigated but none appeared to correlate with the degree of enrichment of each substrate. Rather, the best correlation was observed when the fold-enhancement from the proteomic analysis was compared with the native abundances of the *S*-prenylation substrates. Furthermore, COS-7 displayed superior labeling compared with HeLa and the brain-derived cell lines for

neurons, microglia, and astrocytes, with variations in the extent of labeling across cell lines. This indicates that the cell line of choice also greatly affects the number of detectable prenylated proteins that can be identified. These differences may be attributed to the innate expression levels of the prenylation substrates in each cell line, their levels of the prenyltransferases, and their respective efficiencies for probe uptake.[368] It is noteworthy that these experiments were performed using both stable cell lines and primary cells suggesting that these isoprenoid analogues should be useful for a broad range of experiments with other primary cells and perhaps even tissue samples or whole animals, thereby greatly increasing their utility.

1.6.1.2. *In vitro* labeling

The chemical proteomic approaches discussed so far for profiling of *S*-prenylated proteins involve metabolic labeling with isoprenoid probes. In some instances, samples of interest may not be metabolically active and hence not suitable for metabolic labeling. These experiments may require labeling of prenylated proteins outside of the biological matrix. *In vitro S*-prenylation on protein substrates was pioneered by Alexandrov and co-workers using the biotinylated isoprenoid analogue BGPP (Fig. 1.14).[339] Lysates from cultured COS-7 cells treated with statin were prenylated with BGPP in the presence of the prenyltransferases *in vitro* and subjected to streptavidin blot detection and enrichment for proteomic analysis. Chemical proteomic analysis was only performed for Rab *S*-prenylation substrates, leading to a total of 42 Rab proteins identified. Although this method is excellent for detecting Rab proteins—perhaps owing to the flexibility of RabGGTase active site to accommodate the bulky analogue—engineered mutants of FTase and GGTase-I are required to label Ca_1a_2X box-containing protein models. These mutants

were only shown to modify lysates in conjunction with Rab *S*-prenylation through streptavidin blotting and no proteomic analysis were performed. Following the same approach, lysates from a macrophage cell line identified 18 Rabs and 3 GGTase-I substrates, supporting the previous observation of the sensitivity of this method to Rab proteins.[341] Treatment with zoledronic acid (ZOL), an N-bisphosphonate inhibitor of RabGGTase, allowed for the identification of a few Rab proteins responsive to inhibition by this inhibitor.

While previous attempts for *in vitro* labeling of FTase and GGTase-I substrates showed limited detectability, a recent study combined *in vitro S*-prenylation and click chemistry to identify compromised prenylated proteins in mouse brain tissues .[369] Previous studies have shown that genetic deletion of FTase and GGTase-I mitigates neuropathology in mouse models, suggesting a possible role of *S*-prenylation in Alzheimer's disease.[104] Neuron-specific deletion of FTase in mouse forebrain can result in diminished synaptic plasticity and memory retention while haplodeficient GGTase-I knockout is sufficient for synaptic and cognitive impairment.[369] In order to identify these compromised proteins upon prenyltransferase deletion, lysates from mouse brain with wild-type and FTase or GGTase-I knockout phenotypes were subjected to *in vitro* labeling with C15AlkOPP followed by biotinylation, enrichment and proteomic analysis. Putative *S*-prenylated proteins remain unprenylated in knockout models and therefore achieve higher levels of C15AlkOPP incorporation upon *in vitro* labeling compared to the wild-type controls. A total of 11 FTase and 5 GGTase-I substrates were enriched compared to their wild-type controls. Among these farnesylated proteins, Rheb was identified which is known to regulate synaptic

plasticity, neuronal morphology, and memory functions. FTase deletion may have impaired Rheb function and contributed to the observed reduction of synaptic and cognitive functions in FTase knockout mice. A geranylgeranylated protein RhoA was also identified which is involved in regulating the structure and function of dendritic spine in the brain. This novel *in vitro* labeling strategy offers significant improvements from the previous approaches using BGPP since it allows the detection of FTase and GGTase-I substrates. This method should also be suitable in future studies that involve samples less amenable to metabolic labeling techniques such as tissues.

Collectively, the above metabolic and *in vitro* labeling techniques using isoprenoid analogues that aimed to define the set of *S*-prenylated proteins indeed provided the scope of prenylated proteomes detectable in various systems. However, it should be noted that while isoprenoids modified at the terminal isoprene unit are the best substrates for farnesylation, no single analogue recapitulates the reactivity and specificity of FPP *in vitro* and *in vivo*.[355] Different alkyne-containing isoprenoid analogues manifest intrinsic bias concerning which substrates are efficiently modified. Therefore, in order to broaden the list of farnesylated proteins identified from proteomic profiling strategies, a variety of these isoprenoid analogues may be used to overcome analogue bias.[355] Additionally, the development of new biorthogonal approaches may be necessary to improve the detection and to validate the substrate scopes of the prenylated proteomes in various systems.

1.6.2. Profiling proteins responsive to perturbations

Proteomic strategies enable quantitation of the differential responses of modified proteins upon small molecule-induced disruption of the normal lipidation process.[45] Since a large number of PTIs have been developed, efforts to understand their selectivity and impact on individual proteins have been undertaken using clickable isoprenoid probes. The effects of the FTI L-744,832 on *S*-prenylated proteins labeled with C15-Alk-OH were visualized using a dual color approach in a two-dimensional gel electrophoresis analysis.[370] Proteomic analysis of these labeled proteins not only revealed that known farnesylated proteins displayed reduction in labeling but also that GGTase-I and RabGGTase substrates showed increased *S*-prenylation levels. Furthermore, FTI treatment facilitated the discovery of potentially novel farnesylated proteins GNAI-1 and GNAI-2. Enzymatic farnesylation on their C-terminal Ca_1a_2X box confirmed that these proteins are farnesylated *in vitro*.[370] CCML and quantitative proteomics employing YnF and YnGG also enabled proteome-wide quantification of individual *S*-prenylated proteins in response to PTIs, revealing a wide range of estimated individual IC_{50}.[366] The identified novel *S*-prenylated proteins also displayed significant sensitivity to PTI treatment, further validating their true *S*-prenylation status inside the cell.

Inhibition of protein *S*-prenylation using PTIs offers pharmacological benefits, especially as anticancer agents targeting oncogenic isoforms of proteins involved in signal transduction.[101] However, the potency of FTIs are sometimes offset by the ability of some targets to switch to geranylgeranylation catalyzed by GGTase-I. To identify these proteins capable of this "rescue prenylation", the proteome-wide YnF/YnGG incorporation was compared to inhibition of YnF labeling in response to FTI treatment.[366] The small GTPase

proteins KRAS, NRAS, and RRAS2 exhibited robust dose-dependent increases in labeling, confirming switch-like behavior for these proteins; this effect is partially responsible for the failure of FTIs in clinical trials. FTI treatment in primary astrocytes labeled with C15AlkOPP also revealed that RRAS2 can switch from farnesylation to geranylgeranylation.[368] Being a surrogate for both FPP and GGPP, C15AlkOPP is able to label RRAS2 even in the presence of an FTI. This further supports the switch-like behavior of RRAS2, potentially making it an interesting target for developing inhibitors that block both farnesylation and geranylgeranylation.

While extensive efforts were focused on targeting the *S*-prenylation of oncogenic small GTPases through inhibition of FTase using FTIs, a more specific strategy directed towards this subset of *S*-prenylation substrates could be conceived. Some small GTPases are regulated and trafficked through GGTase-I-catalyzed *S*-prenylation by the splice variants SmgGDS607 and SmgGDS558 chaperone proteins, with SmgGDS607 bearing an extra exon (Ex5).[371,372] SmgGDS607 delivers the protein substrate to the prenyltransferase

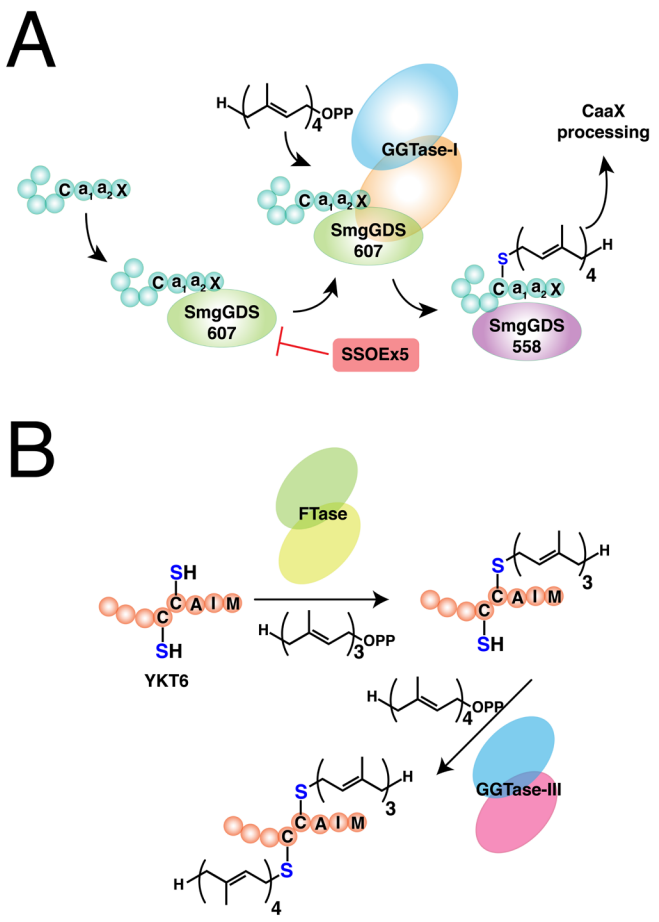

Figure 1.15. Other mechanisms for regulating protein prenylation.

(A) Trafficking of prenylation substrates mediated by SmgGDS chaperone proteins. SmgGDS607 recruits the substrate for prenylation by GGTase-I and the prenylated protein is sequestered and delivered by SmgGDS558 the endoplasmic reticulum for subsequent processing steps. Splice-switch oligo (SSOEx5) can reduce the ratio of SmgGDS607:SmgGDS558 for potential treatment of cancer. **(B)** Dual prenylation on Ykt6 catalyzed by FTase and GGTase-III. Ykt6 is first farnesylated by FTase on the Ca_1a_2X box cysteine followed by geranylgeranylation by GGTase-III on the adjacent cysteine upstream from the farnesylated residue.

while SmgGDS shuttles the prenylated protein to the ER for maturation (Fig. 1.15A). Since a high SmgGDS607:SmgGDS558 ratio is implicated in some cancers, a splice-switch oligonucleotide (SSO) therapeutic strategy was developed to reprogram the ratio of the SmgGDS isoforms.[373] A small oligonucleotide SSOEx5 site-specifically targets Ex5, which reduces and increases the levels of SmgGDS607 and SmgGDS558, respectively,

resulting in a reduced SmgGDS607:SmgGDS558 ratio. Through the use of C15-Alk-OPP labeling, the SSO was found to suppress global protein *S*-prenylation, inducing apoptotic cell death in cancer cell lines and diminishing tumorigenesis *in vivo*. Since all three classes of *S*-prenylation substrates respond to alterations in SmgGDS607:SmgGDS558, there may be unexplored interactions between SmgGDS proteins and the other prenyltransferases FTase and RabGGTase.

1.6.3. *S*-Prenylation of Rho GTPases

S-prenylation of small GTPases is essential for their membrane localization and interaction with effector proteins that regulate their activity.[374] The Rho family of small GTPases are implicated in tumor growth and metastasis, as well as in regulating phagocytosis and signaling in inflammatory cells. Protein *S*-prenylation was found to control innate immunity by restricting the interaction between the Rho protein Rac1 with its effector proteins.[375] Through C20-Az-OH labeling, Rac1 was shown to be unprenylated in GGTase-I-deficient mouse macrophages, stimulating proinflammatory signaling and severe rheumatoid arthritis. The inflammation in the GGTase-I-deficient model was reversed upon Rac1 deletion, but not when other geranylgeranylated Rho proteins RhoA and Cdc42 were knocked down. The reduction in *S*-prenylation of Rac1 enhanced its affinity with its interacting partner proteins Tiam1 and Iqgap1, resulting in enhanced GTP-loading and its ubiquitin-mediated degradation, respectively. Inhibition of these interactions is a key component for understanding the molecular basis of how protein *S*-prenylation normally restrains innate immunity.[375]

The brain specific splice variant of the Cdc42 (bCdc42) which contains a C-terminal Ca_1a_2X box ^{188}CCIF^{191} was initially shown to be *S*-palmitoylated rather than exclusively *S*-prenylated, in contrast to its canonical splice variant with a C-terminal CVLL sequence.[376] However, a subsequent study showed that bCdc42 is sequentially geranylgeranylated and *S*-palmitoylated using C20-Az-OH and Alk-C18 labeling at C188 and C189, respectively.[377] Thus, bCdc42 may not undergo the typical Ca_1a_2X processing (Fig. 1.2A) and instead become *S*-palmitoylated, which stabilizes the association of this protein bearing two different lipid modifications with membranes. CCML with isoprenoid and palmitoyl probes on a few other proteins terminating in CCa_2X demonstrated that some may mature through the normal Ca_1a_2X processing pathway while others can be dually lipidated with prenyl and palmitoyl modifications.[377] The dual lipidation in bCdc42 prevents its binding with RhoGDI which usually facilitates the trafficking of Rho proteins including the canonical archetype Cdc42. Approximately 80-95% of the total bCdc42 population is left singly prenylated which is subsequently processed in Ca_1a_2X maturation steps. A recent study conducted on mouse brain tissues identified the post-prenylation processed C-terminal geranylgeranylated peptide of the canonical splice variant of Cdc42 but not the brain specific isoform.[378] Therefore, modifications on their analysis should have been applied to discern the concurrent geranylgeranylation and *S*-palmitoylation on the brain-specific variant bCdc42 since their targeted database only contained only singly lipidated peptides. Moreover, the archetype Cdc42 is responsive to both competition by farnesol or geranylgeraniol, suggesting that it may be both farnesylated and geranylgeranylated.[366] The bCdc42 protein may also be a substrate of farnesylation and

therefore warrants further investigation. Regardless, this aberrant CCa_2X *S*-palmitoylation exemplifies the complexity of lipidation and may not be limited only to bCdc42.

1.6.4. Imaging S-prenylated proteins

The versatility engendered by clickable isoprenoid probes allows conjugation with fluorophores and subsequent quantitative flow cytometric analysis and cellular imaging on fixed cells.[379] C15-Alk-OH labeling on various cell types analyzed via flow cytometry revealed variations in the levels of expressed *S*-prenylated proteins, consistent with in-gel fluorescence analysis from other studies.[359,366] In cellular models of autophagy and aging, significantly higher levels of labeled proteins were observed compared to normal cells, highlighting the potential involvement of protein *S*-prenylation in compromised autophagy.[379] In addition, CCML enabled cellular imaging of fixed cells to visualize the *S*-prenylated proteins localizing in the ER. Despite their established localization in plasma membrane, *S*-prenylated proteins were not detected on cell surfaces. It should be noted that a limited number of proteins modified with alkyne-functionalized isoprenoids were shown to proceed through Ca_1a_2X processing and should therefore be directed to the plasma membrane.[366,380] It is possible that the alkyne moiety on plasma membrane-localized *S*-prenylated proteins may be buried in the lipid bilayer, making it inaccessible by the bulky azide-fluorophores for effective visualization.[381]

Confocal imaging of labeled *S*-prenylated proteins also provides insights into changes in protein *S*-prenylation in response to stimuli. Nerve growth factor (NGF) was

discovered to trigger *S*-prenylation of proteins in neuronal axons with a dependence on axonal protein synthesis.[382] C15-Alk-OH labeling revealed that *S*-prenylation does not take place throughout the cytoplasm but rather appeared as puncta in subcellular sites after NGF stimulation. Among several *S*-prenylated proteins, Rac1 was shown to be geranylgeranylated in axons and serve as a key effector of NGF signaling. The overall results of this study imply that aberrant localization, activity, or stability of *S*-prenylated proteins may contribute to the pathology of neurodegenerative diseases.[382]

1.6.5. Discovery of both a novel prenyltransferase and new S-prenylation substrates

Since its discovery over the past decades, the mechanism of protein *S*-prenylation by the three types of prenyltransferases have been extensively studied in efforts to develop selective and specific PTIs.[11] Recently, a novel prenyltransferase has emerged whose discovery was facilitated through the use of bio-orthogonal isoprenoid analogues. A previously unknown human prenyltransferase consisting of PTAR1 and the β-subunit of RabGGTase was recently reported as GGTase-III (Fig. 1.2C).[108] CCML with C20-Az-OH and streptavidin blotting showed that FBXL2 is specifically geranylgeranylated by GGTase-III. The leucine-rich repeat domain of FBXL2 interacts with PTAR1, serving as the structural basis for GGTase-III specificity.[108] Shortly after, another group discovered the same enzyme but presented contradicting results, indicating that GGTase-III could not prenylate FBXL2 under conditions where GGTase-I robustly prenylated the substrate.[383] Instead, they showed through BGPP-labeling that the SNARE protein Ykt6 is dually *S*-

prenylated; it is first farnesylated by FTase and subsequently geranylgeranylated by GGTase-III on the upstream cysteine adjacent to the farnesylated residue (Fig. 1.15B). The use of BGPP in this study was suitable as previous reports showed excellent incorporation of this probe into Rab proteins by RabGGTase,[339] which shares the same catalytic β-subunit with GGTase-III. It was suggested that since FBXL2 also bears an adjacent cysteine upstream of its Ca_1a_2X box, it is possible that GGTase-III appends a second geranylgeranyl moiety to this substrate after initial geranylgeranylation by GGTase-I.

The current paradigm for protein *S*-prenylation has been restricted to the Ca_1a_2X box motif on singly modified proteins. Recent efforts to probe for a broader substrate scope for *S*-prenylation demonstrated that extended CXXXX sequences including CVAGP and CMIIM can be farnesylated.[83] CCML with C15-Alk-OPP on model proteins terminating in such motifs were found to be prenylated *in vitro* and within cells, as detected through fluorescence labeling and chemical proteomic approaches. In addition, the same group reported that peptide models with shortened CXX sequences can also be recognized as *S*-prenylation substrates *in vitro*.[84] These studies highlight the promiscuity of prenyltransferase enzymes, and may expand our current understanding of their substrate recognition and potentially enlarge the scope of *S*-prenylation substrates. However, it has been noted that no endogenous proteins terminating in such unconventional prenylation motifs have been identified. If some of these sequences are indeed recognized as substrates under native conditions, several factors may hamper their detectability in click-chemistry based approaches including low expression levels. [368]

Beyond identification, clickable isoprenoid probes can be utilized to validate the *S*-prenylation status of novel *S*-prenylated proteins. For example, farnesylation of the human mitotic check point protein Spindly was found to be essential for its targeting to kinetochores.[384] Disruption of its farnesylation abrogates its localization, resulting in prolonged prometaphase and delayed anaphase with concurrent defects in chromosome alignment. FTI treatment, however, does not affect other farnesylated proteins including CENP-E and CENP-F that are also involved in mitosis. These results indicate that HsSpindly is a novel mitotic FTI target in specific cancers that manifest high levels of its expression such as in oral cancer.[385]

Bacterial effector proteins not only rely on fatty acylation, as previously described, but also on *S*-prenylation. Several *Legionella pneumophila* effector proteins that modulate host functions in host cell membrane compartments depend on prenylation.[386] By individually validating the *S*-prenylation of proteins using C15-Alk-OH labeling with subsequent immunoprecipitation and fluorescence detection, at least eight *L. pneumophila* effector proteins were shown to require *S*-prenylation for proper localization. Farnesylation does not seem to direct localization of two *S*-prenylated bacterial proteins but may play key roles in regulating their function. Similarly, the *Salmonella* T3SS effector protein SifA was shown to be prenylated with C15-Alk-OH.[359] It was previously reported that GGTase-I modifies its C-terminal sequence, ^{331}CLCCFL^{336}, possibly at C333.[387] However, mutational studies on the C-terminal cysteines and C15-Alk-OH labeling suggest that SifA may be heterogeneously prenylated.[359] With the recent discovery of GGTase-III adding a

second prenyl moiety on proteins, it is tempting to speculate that SifA maybe a substrate of GGTase-III.

As a final comment, it is important to note that in the studies described above, the use of isoprenoids bearing small clickable handles in metabolic labeling studies does not appear to compromise the function of prenylated proteins or cause toxicity. Studies with a-factor, a farnesylated pheromone involved in yeast mating indicate that azide and alkyne substitutions have minimal effects on the activity of the mature pheromone; additionally, no significant effects on the subsequent proteolysis or methylation steps were observed either.[380] While high concentrations of the alcohol forms of the analogues may exhibit some level of toxicity as was observed in the malaria parasite,[365] the use of the diphosphate analogues may circumvent this issue, particularly when working with sensitive cell lines.[358]

1.7. Biological applications in other lipids

The applications of click chemistry in the major classes of protein lipid modifications have been discussed above. Other types of lipidation do exist albeit in a smaller set of proteins. Although protein fatty acylation occurs mainly through *S*-palmitoylation and *N*-myristoylation, shorter, longer, and unsaturated fatty acylation adducts have also been observed. Shorter saturated fatty acids such as octanoic (C8) or butyric (C4) acids, as well as longer saturated fatty acids such as stearic (C18) acid can be covalently attached to proteins via enzymatic or non-enzymatic mechanisms. Unsaturated fatty acids (UFA), on the other hand, can compete for palmitoylation sites, as well as generate oxidation products capable of forming adducts with proteins. Moreover, cholesterylation and GPI modification take place in the lumen of secretory organelles as mentioned previously.

While cholesterylation proceeds through esterification of the C-terminus of a few known substrates, its precursors in the biosynthetic pathway generate intermediates that form protein adducts similar to UFA. The click chemistry toolbox has also been used to investigate the occurrence and biology of these relatively rarer lipid modifications.

1.7.1. Longer chain fatty acylation

The widespread *S*-acylation by fatty acids on proteins is often attributed to *S*-palmitoylation. However, other lipid-modified cysteines with longer fatty acyl chains such as stearate were observed in bovine heart and liver tissues.[388] The ability to incorporate different lengths of fatty acyl chains into protein substrates varies across the known zDHHCs.[133,240] In particular, zDHHC7 efficiently catalyzes stearoylation of SNAP25, indicating that zDHHCs facilitate lipid modifications beyond *S*-palmitoylation.[133] Only a handful of human and viral *S*-stearoylated proteins are known.[389–392] The S-stearoylation on viral spike proteins is essential for host-membrane fusion but is not mechanistically well-understood.[393] The functional role of protein stearoylation in humans is not clearly defined as well. Here we discuss potentially stearoylated mammalian substrates and the discovery of a bacterial enzyme capable of removing this longer fatty acid modification. Modifications with very long-chain fatty acids (VLCFA) is described as well.

1.7.1.1. Stearoylation in mammals

Previously thought to be an *S*-palmitoylation substrate, stearoylation of the human transferrin receptor 1 (TFR1) was the first reported evidence for a regulatory function of

stearoylation in humans.[394,395] Treatment with an azide analogue of stearic acid (az-C17, Fig. 1.16) in HeLa cells for enrichment and proteomic analysis revealed TFR1 as the most abundant protein identified. In cultured cells, TFR1 stearoylation promotes mitochondrial fusion and function, while the loss of TFR1 stearoylation leads to mitochondrial fragmentation. CCML with az-C17 and streptavidin blotting identified zDHHC6 as a candidate enzyme that catalyzes TFR1 stearoylation. Furthermore, mitochondrial dysfunction in *Drosophila* lacking Parkinson disease genes Pink or Parkin can be rescued upon exogenous supplementation of stearic acid.[395] In a follow up study, stearic acid was shown to regulate mitochondrial function *in vivo*, resulting in mitigation of fat accumulation and therefore reduces the risk for cancer and cardiovascular diseases.[396]

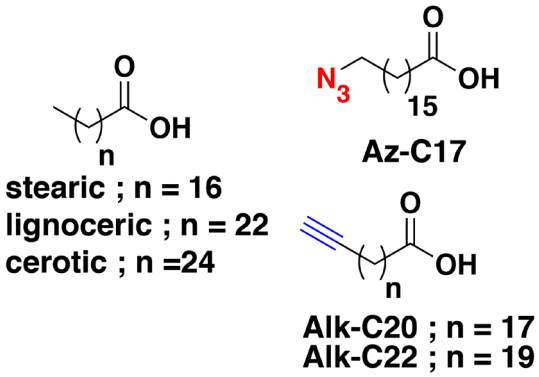

Figure 1.16. Chemical structures of fatty acylation probes with chain lengths longer than palmitic acid.

Another protein found to potentially incorporate stearic acid is the regulatory factor X 3 (RFX3), a transcription factor associated with ciliopathy.[397] Fatty acylation on this protein appears to be a zDHHC-independent process since CCML with RFX3 co-expressed with each of the 23 known zDHHCs does not result in enhanced labeling. Furthermore, incubation of recombinant RFX3 with clickable fatty acyl-CoA analogues in an APE assay

resulted in fatty acyl modification, with Alk-C18 and Alk-C18:1 exhibited a slightly more intense signal compared with Alk-C16. Therefore, RFX3 prefers the 18-carbon stearoyl and oleyl (C18:1) modifications that potentially proceeds through an autoacylation mechanism. Loss of this modification abolishes RFX3 transcriptional activity and suppresses ciliogenesis and Hh signaling, emphasizing that stearoylation is essential for RFX3 function. The dearth of studies investigating protein stearoylation in humans has hampered understanding of its functional and regulatory role, which stems from the ambiguous and interchangeable use of Alk-C16 and Alk-C18 in *S*-palmitoylation-centric studies. Regardless, the studies described above provide insights into the biological role and clinical relevance of protein stearoylation and suggest that this will be a fruitful area for future study.

1.7.1.2. Bacteria-mediated destearoylation

As previously discussed, bacterial effector proteins can alter lipid modifications on host proteins exemplified by the demyristoylation activity of *S. flexneri* IpaJ.[316] In addition to this mechanism, *S. flexneri* was also discovered to release a T3SS effector protein IcsB that *N*-stearoylates lysine residues on host proteins (Fig. 1.13C).[398] Stearoylated proteome profiling using Alk-C18 in infected cells identified 60 host proteins modified by SfIcsB which includes families of *S*-prenylated proteins such as Ras, Rho, Rab, and Rap proteins. Rho GTPases are inactivated by stearoylation at their C-termini, resulting in the disruption of the actin cytoskeleton in mammalian cells by increasing their hydrophobicity or interfering with their protein-protein interactions. *S*-prenylation of these Rho proteins appears to be required for recognition by SfIcsB, at least in the case of RhoA. Moreover,

N-stearoylation of the host autophagy protein CHMP5 inactivates its function and hampers autophagy of the infected host. This mechanism is apparently unique to *S. flexneri* since CHMP5-deficient host cells infected with other bacteria such as *S. typhimurium* and *Y. pseudotuberculosis* were capable of inducing cell death. Therefore, CHMP5 in this context specifically functions in directing *S. flexneri* to antibacterial autophagy and this pathogen circumvents this mechanism by disarming CHMP5 function through fatty acylation by SfIcsB and escape autophagy. Concurrently, a MARTX effector protein Rho GTPase inactivation domain (RID) in *Vibrio cholerae* was shown to possess *N*-stearoylation activity.[399] RID shares the same mechanism with IcsB in that it also modifies the polybasic C-terminal region of Rho GTPases but has a strong substrate preference for Rac1. Immunoprecipitation and streptavidin blot detection of Rac1 from RID-expressing mammalian cells treated with Alk-C18 validated its stearoylation. Both the core domain and the prenylated C-terminal end of Rac1 are recognized by RID. This aberrant modification of Rac1 disrupts its cytosol-membrane cycling and inhibits its function. These studies highlight a novel mechanism for how bacterial pathogens alter host cellular processes and may not only be limited to *S. flexneri* and *V. cholerae.* More efforts should be conducted in exploring other pathogens that may share similar molecular mechanisms for impairing cellular functions inside their infected hosts.

1.7.1.3. Very long-chain fatty acids (VLCFA)

In lipid biosynthesis, palmitic acid is the major *de novo* product over myristic and stearic acids, which can be further extended by elongases to generate VLCFA. Accumulation of saturated VLCFAs such as lignoceric (C24:0) and cerotic (C26:0) acids (Fig. 1.16) was

observed during necroptosis in cells, a form of programmed cell death associated with various human diseases.[400] Knockdown of the elongase ELOVL7 reduces VLCFA accumulation and necroptosis, while exogenous addition of VLCFA promotes cell death.[401] Metabolic labeling with Alk-C20 and Alk-C22 with subsequent in-gel fluorescence scanning revealed a wide range of VLCFA-modified proteins. Pre-treatment with a pan inhibitor of zDHHCs resulted in only a modest increase in the cell viability of necroptotic cells. This suggests that the metabolism of VLCFA may involve other mechanisms or fatty acylation routes other than zDHHC-catalyzed processes during necroptosis.[401]

1.7.2. Shorter chain fatty acylation

Fatty acyl modification with chains longer than acetyl and propionyl but shorter than myristoyl and palmitoyl functional groups have been reported in the literature, although they occur at rarer occasions with smaller substrate scope. Octanoylation has only been described for one substrate and butyrylation may potentially occur in many bacterial and mammalian substrates through enzymatic and non-enzymatic mechanisms.

1.7.2.1. Butyrylation

Short-chain fatty acids (SCFAs) such as butyric acid (Fig. 1.17) can modulate signaling pathways and have been found to mitigate infections caused by enteric pathogens.[402] Although its beneficial effect on suppressing the transcription of bacterial virulence factors is known, the molecular mechanisms by which this occurs are unclear. In order to explore the potential of butyrylation of proteins, the alkyne analogue Alk-C5 (Fig. 1.17) was

recently synthesized and used to profile SCFA-acylated proteins in *Salmonella enterica* serovar Typhimurium.[403] Alk-C5 labeling indicated that many proteins are acylated by this probe. Proteomic analysis identified an array of SPI-1 virulence proteins are potentially butyrylated with the transcription regulator HilA displaying the most significant enrichment. Unnatural amino acid substitution of several lysine residues indicates that site-specific acylation of HilA affects bacterial transcriptional activity and invasion *in vitro,* and acylation on the particular site Lys90 disarms virulence *in vivo*. However, gene deletion of known bacterial acyltransferase reveal that none of these enzymes catalyze butyrylation of HilA and this modification may proceed non-enzymatically. Further investigations should be carried out to either support the chemical acylation of these butyrylated proteins or characterize the acyltransferases that may catalyze this process. Regardless, this novel discovery of protein butyrylation on specific sites of a bacterial protein should prompt optimization of existing covalent inhibitors that are effective in treating infections caused by SCFA-sensitive pathogens.[403]

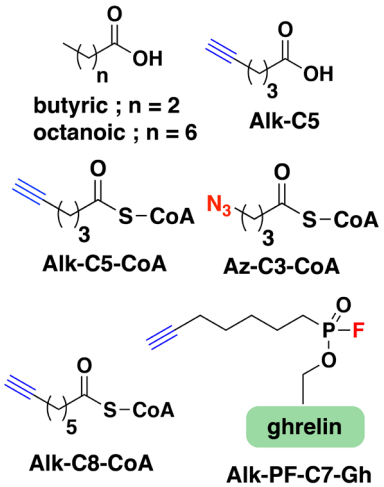

Figure 1.17. Chemical structures of fatty acylation probes with chain lengths shorter than myristic acid.

In mammals, lysine acetyltransferases (KATs) such as p300 and GCN5 were found to catalyze not only acetylation but also propionylation and butyrylation of histone proteins as part of epigenetic regulation of transcription.[404] Dysregulation in the activity and expression of these enzymes has been implicated in diseases in which potentially compromised pathways is not well-understood. In order to identify these protein substrates potentially acylated on lysine by these enzymes, alkyne and azide analogues of short fatty acyl-CoAs were synthesized.[405] In particular, Alk-C5-CoA and Az-C3-CoA (Fig. 1.17) were used to profile these protein substrates *in vitro*.[406,407] Incubation of Hela nuclear extracts with Alk-C5-CoA in the presence of p300 identified 23 known and novel substrates of this enzyme.[406] In HEK293 whole lysates, treatment with Az-C3-CoA resulted in protein labeling in the presence of p300 or the mutant GCN5-T612G as shown through in-gel fluorescence imaging. Chemical proteomic analysis of lysates in the presence of the probe and either p300 or the GCN5 mutant identified 379 substrates common to both enzymes with approximately 90 protein substrates unique to each. As expected, histone proteins were highly enriched and many known acetylated proteins were identified in the analysis, The previous study performed in the nuclear extracts of HeLa identified significantly less protein substrates for p300 compared to the HEK293 whole lysate, indicating that this enzyme may function in modifying proteins outside of the nucleus. Functional annotation and pathway analysis of the p300 and GCN5 substrates reveal that these proteins are associated with diverse biological processes including gene expression, cell cycle, and cellular metabolism. While these studies have identified hundreds of potentially lysine acylated substrates with short fatty acids, they have been conducted *in vitro* and may not quite recapitulate the actual acylation substrates in a cellular

context or *in vivo*. Furthermore, the probes used may ambiguously modify substrates of propionylation and butyrylation. Therefore, these data should be interpreted with caution and future studies should validate the type of modification (*e. g.* propionylation vs butyrylation) catalyzed by these KATs on specific proteins of interest.

1.7.2.2. Octanoylation

Another fatty acyl modification shorter than myristoyl and palmitoyl moieties is the octanoylation of ghrelin, an appetite-stimulating stomach hormone involved in glucose metabolism.[408] Its precursor form undergoes processing steps allowing it to mature into a 28-residue peptide that is esterified with an octanoyl group on Ser3 by ghrelin *O*-acyltransferase (GOAT).[409] To date, ghrelin is the only known and predicted octanoylated peptide substrate of GOAT. Owing to its regulatory role in metabolic processes and implications in diseases such as diabetes and obesity, effective GOAT inhibitors are constantly being sought after.[410] A catalytic enzyme-linked click chemistry assay (cat-ELCCA) was developed to probe the fatty acyltransferase activity of GOAT and is amenable to inhibitor screening (Fig. 1.9E).[411,412] In this strategy, biotinylated ghrelin substrates are immobilized on streptavidin-coated plates and incubated with GOAT and Alk-C8-CoA. Subsequent click reaction with azide-modified HRP confers signal amplification through an HRP-sensitive fluorogenic substrate. Using this method, non-peptidic small molecule antagonists of GOAT were discovered that could serve as promising drugs to treat obesity and diabetes.[412]

While the octanoylation of ghrelin is essential for its binding to its cognate receptor GHSR1a, the deacylated form of ghrelin also participates in metabolic processes, thereby rendering both fatty and defatty-acylation as regulators of ghrelin function.[413] Several hydrolases in serum were found to display deacylase activity on octanoylated ghrelin.[410] In order to identify enzymes with esterolytic activity against octanoylated ghrelin in rat serum, an activity-based ghrelin probe octanoyl containing a phosphonofluoridate warhead and alkyne handle was designed (Alk-PF-C7-Gh, Fig. 1.17) similar to Alk-HDFP.[414] In this study, two prominent bands were observed in an in-gel fluorescence scan and identified through gel-based proteomics. One of the proteins was α_2 macroglobulin (α_2M), a large heterotetrameric protein with no previously known esterase activity. An HPLC-based assay validated its ability to deacylate lipidated ghrelin and inhibitor titration experiments revealed four active sites in the heterotetrameric protein. Further analysis of α_2M levels in the serum suggests that it is present in sufficient amounts to be an important deacylase for ghrelin.[414]

In summary, ghrelin octanoylation plays an essential role in metabolic diseases and obesity. Being the only known substrate of GOAT, inhibiting GOAT activity is an attractive strategy to target diseases associated with ghrelin signaling and methods have been developed to streamline that process as discussed above. While this is true, there have been no reports on using clickable analogues of octanoic acid or those with comparable chain lengths in profiling their potential targets using any CCML strategy. Employing such methods may allow for the discovery of potential new substrates of GOAT or other proteins modified by mid-sized fatty acids through enzymatic or non-enzymatic mechanisms.

1.7.3. Unsaturated fatty acylation

Covalent modification of proteins with mono- (MUFAs) or polyunsaturated fatty acids (PUFAs) has also been reported for a few mammalian proteins including Src kinases, G-proteins, and Wnts.[415,416] While saturated fatty acids (SFA) promote insertion of lipidated proteins into lipid rafts, MUFAs and PUFAs diminish their localization in those sites, which can partially be attributed to the distortions conferred by *cis* double bonds.[4] This difference in saturated versus unsaturated modification of proteins represents one of the modulatory mechanisms for protein localization through fatty acylation. Furthermore, excess dietary SFAs often present risks for certain diseases while replacing with UFAs provide beneficial effects.[417] Therefore, understanding the role of protein modification with SFAs vs UFAs is essential and may provide insights into these observed phenomena.

1.7.3.1. Monounsaturated fatty acids (MUFAs)

Wnts are a family of secreted signaling proteins that mediate communication between cells, thereby controlling cell fate and influencing developmental processes and the maintenance of adult homeostasis.[418] These proteins are *O*-palmitoyleated (C16:1) on a serine residue by Porcupine (PORCN), a member of the membrane-bound *O*-acyltransferases (MBOAT) family of enzymes.[419] Metabolic labeling using various alkyne-modified SFAs in PORCN- and Wnt3a-expressing cells revealed that PORCN efficiently transfers a range of fatty acid chain lengths onto Wnt3a, particularly Alk-C16.[132,420] However, the potent ability of palmitoleic acid to compete with the Alk-C16 (palmitoyl probe) labeling indicates that

PORCN prefers this MUFA. A recent study reported that the PORCN active site topology enforces *cis*-C16:1 fatty acylation on Wnts.[421] Pulse labeling with either *cis*-Alk-C16:1 or *trans*-Alk-C16:1 (Fig. 1.18) showed that the *trans* isomer resulted in detrimental effects to Wnt cellular release, possibly indicating that the *trans*-fatty acylated Wnt is trapped in a complex with PORCN. The kink in *cis*-C16:1 may facilitate the release of Wnts from PORCN by lowering the energy required for sequestration by the Wnt-carrier protein. This may also explain the protracted turnover of Wnt3a in metabolic labeling studies using the saturated analogue Alk-C16.[132] Therefore, in a biological milieu, Wnts are lipidated with *cis*-palmitoleic acid, and excess sources of SFAs and *trans* fats from diet may dysregulate Wnt signaling by impeding their release to the secretory pathway.[421]

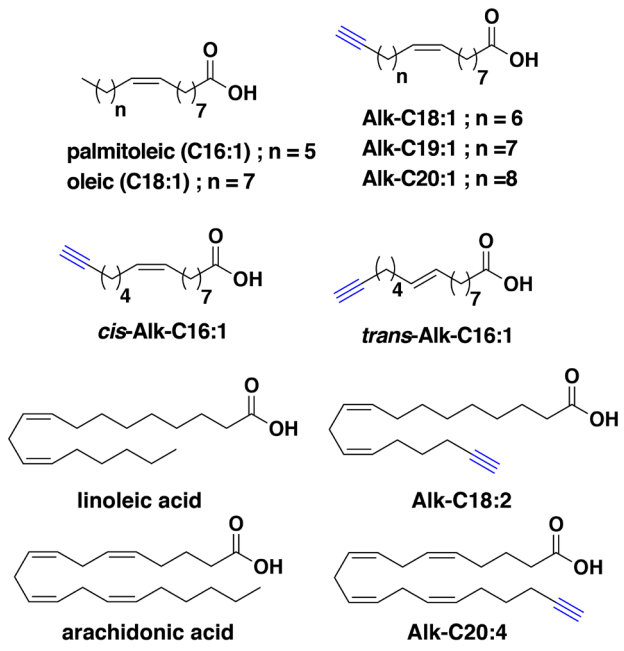

Figure 1.18. Chemical structures of unsaturated fatty acylation probes.

Some proteins were found to be modified by MUFAs longer than palmitoleic acid such as oleic acid (Fig. 1.18).[422,423] The alkyne-modified analogue of oleic acid (Alk-

C18:1) was employed to trace fatty acid metabolism, as well as to develop click chemistry-based platforms for *in vitro* enzymatic assays.[134,135,424] With the interest of identifying proteins that can be covalently modified with oleic acid, Hang and coworkers synthesized Alk-C18:1 along with the longer MUFA probes Alk-C19:1 and Alk-C20:1 (Fig. 1.18).[425] Metabolic labeling and fluorescence detection using these probes indicated that many protein targets are modified by these MUFAs with varying chain lengths. HRAS and IFITM3 were validated to be substrates for C18:1 modification. Furthermore, comparative proteomic analysis revealed that Alk-C18:1 and Alk-C18 labeling share a large number of modified proteins, with only 13 proteins preferentially labeled by Alk-C18. These results point to the possibility of a prevalent protein modification with MUFAs. Since the levels of palmitic and oleic acids are comparable in mammalian cells,[133] this suggests that the investigation of palmitic vs oleic acid modification in a physiological context is important.

1.7.3.2. Polyunsaturated fatty acids (PUFAs)

Fatty acylation on proteins with PUFAs such as arachidonate (C20:4) and eicosopentaenoate (C20:5) has been described earlier with human platelets.[426,427] It is not currently established whether zDHHCs catalyze these PUFA modifications but arachidonic acid was shown to effectively block zDHHC17-catalyzed Az-C16 labeling.[133] While MUFAs are generally resistant to peroxidation,[428] PUFAs can generate electrophiles and yield protein adducts.[429] Alkyne-modified versions of linoleic acid (Alk-C18:2, Fig. 1.18) and arachidonic acid (Alk-C20:4, Fig. 1.18) were shown to undergo autooxidation processes *in vitro* analogous to their native counterparts.[430] Quantitative proteomic analysis using these probes in a macrophage cell line identified membrane and mitochondrial

proteins, which included those associated with inflammatory signaling oxidant defense.[431] Interestingly, the extent of adduction correlated with the expression levels of proteins. Since 12/15-lipoxygenase (12/15-LOX) catalyzes the peroxidation of these PUFAs, the extent of protein adduction by Alk-C20:4 was investigated in peritoneal macrophages known to express high levels of 12/15-LOX.[432] It is important to note that the use of Alk-C20:4 as a surrogate for C20:4 is not suitable for investigating all metabolic processes that involves this lipid.[433] For example, elongation of Alk-C20:4 to Alk-C22:4 by elongases is less efficient in Jurkat cells and platelets are less able to generate LOX-dependent products of Alk-C20:4 metabolism than C20:4. Fatty acid tracing of Alk-C20:4 in mouse peritoneal macrophages in this study showed it is metabolized by LOX enzymes similarly to the native C20:4, making it a suitable C20:4 analogue for investigating the 12/15-LOX-dependent metabolism in this cell type. Proteomic analysis revealed over 200 proteins labeled by Alk-C20:4. ACADL and GAPDH were validated, which are involved in mitochondrial fatty acid β-oxidation and glycolysis, respectively. Indeed, 12/15-LOX-deficient mouse peritoneal macrophages displayed diminished glycolytic rate and mitochondrial respiration. These results aided by Alk-C20:4 labeling highlight the role of PUFAs in energy metabolism mediated by 12/15-LOX.

Under oxidative stress, PUFAs are also prone to generating shorter lipid-derived electrophiles (LDEs) such as 4-hydroxy-2-nonenal (4-HNE) and 4-oxo-2-nonenal (4-ONE) that may directly modify DNA and proteins through non-enzymatic mechanisms.[434] These lipids contain an α,β-unsaturated aldehyde functionality that acts as a Michael acceptor and reacts with nucleophiles particularly thiols. Several studies have used clickable analogues

of 4-HNE and 4-ONE in order to profile their cellular targets,[435–437] as well as to validate and monitor their biological consequences in protein function.[438,439] Moreover, these types of modification may be reversed by the lysine fatty deacylase SIRT2,[440] although evidence of this phenomenon under unperturbed and physiologically relevant conditions will be necessary to ascertain its biological significance. This growing topic, however, is outside the scope of this review and will not be discussed in detail. The reader is therefore directed to other excellent reviews that cover the use of click chemistry in studying this type of non-enzymatic protein modification.[441,442]

1.7.4. Cholesterylation

The lipidation processes discussed thus far are catalyzed by transferases that are localized in the cytoplasm or cytoplasmic face of the plasma membrane. In contrast, protein cholesterylation occurs in the lumen of secretory vessels on members of the Hedgehog (Hh) family of proteins in a self-processing manner.[443] These secreted morphogens play major physiological roles in embryonic development, tissue repair, and regeneration; dysregulation in the Hh pathway leads to severe abnormalities in embryonic and tissue development.[444,445] Hyperactivation of Hh signaling has also been linked to certain types of cancer.[446] Hh proteins are synthesized as precursors that are truncated, and subsequently *N*-palmitoylated on their N-terminus and auto-*O*-cholesterylated on their C-terminus forming an ester bond.[447] The cholesterol modification on Hh is crucial for membrane tethering, receptor binding, secretion, and transport.[5]

1.7.4.1. Hh proteins and Smoothened

Given its essential role in pathways with disease relevance, clickable analogues of cholesterol were synthesized in order to characterize cholesterylated proteins. An azide-modified cholesterol (Az-Chol, Fig. 1.19A) was first reported by Tate and coworkers to successfully label Shh overexpressed in cultured cells.[448] However, this analogue presented several drawbacks including low incorporation efficiency, non-specific labeling, and cytotoxicity. A series of alkyne-modified cholesterol analogues were designed in an effort to address the issues encountered with Az-Chol (Fig. 1.19A).[449] The optimized form of the alkyne probes, Alk-Chol-2, successfully labeled Shh with intense signals and low cellular toxicity. The localization of cholesterylated Hh proteins were visualized in cultured cells and in developing zebrafish, the first successful imaging of lipidated proteins *in vivo*. Quantitative proteomic analysis on Alk-Chol-2-treated cellular models revealed subtle variations in the levels of cholesterylated Shh across multiple pancreatic cancer cell lines. Since Hh signaling is an important factor in clinical pancreatic ductal adenocarcinoma, these observed differences warrant further investigations into the potential role of cholesterylation in pancreatic cancer.[449]

For a long time, covalent cholesteryl modification was found only in Hh proteins, although its occurrence on proteins beyond this family was proposed.[450] Recent studies have shown that the Hh signal transducer and oncoprotein Smoothened (SMO) binds cholesterol within its cysteine-rich domain (CRD).[451] Cholesterol immobilized on agarose resin through click chemistry efficiently isolated SMO in binding assays. Shortly thereafter, compelling evidence for the covalent cholesterol esterification of SMO emerged

through metabolic labeling with Az-Chol-2.[452] Proteomic analysis on Az-Chol-treated cells yielded 20 protein candidates, which were then each validated through Az-Chol labeling and immunoprecipitation. Among these proteins, SMO retained Az-Chol modification under denaturing conditions indicating covalent modification. A robust mass spectrometric analysis showed Asp95 as the site of cholesterylation, a residue situated in the vicinity of the CRD. Since protein cholesterylation is not known to be catalyzed by any cognate

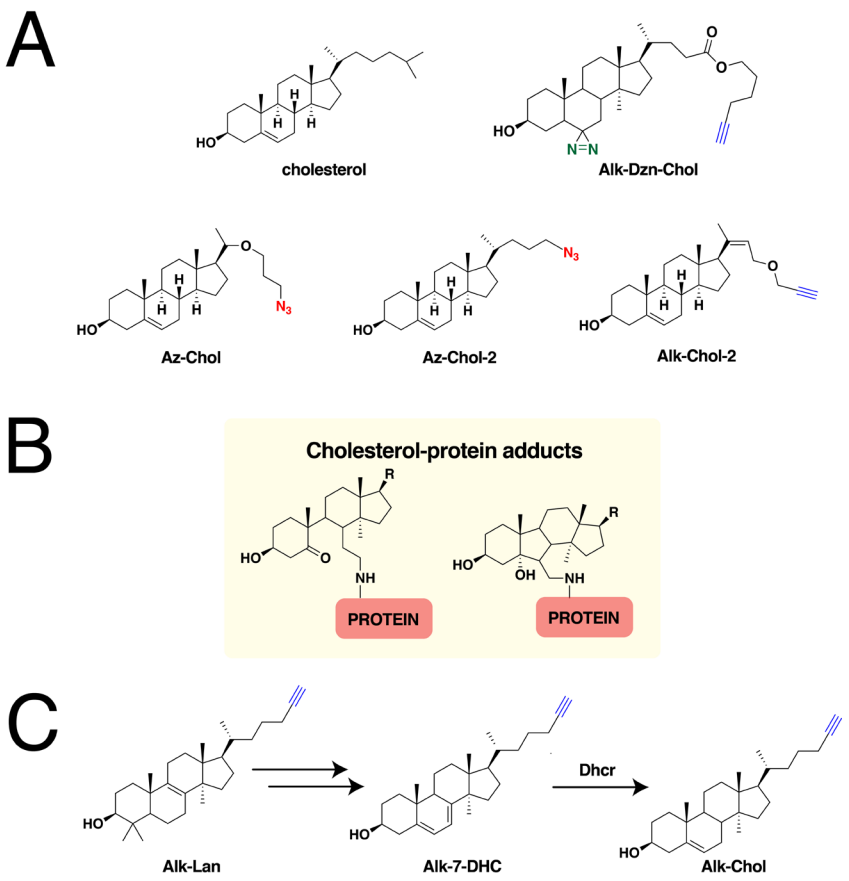

Figure 1.19. Probes for O-cholesterylated proteins.

(A) The bio-orthogonal analogues of cholesterol contain azide and alkyne functionalities and may vary in length of their linkers. **(B)** The electrophilic species of cholesterol form adducts with proteins through their amine side chains. **(C)** The alkyne-modified versions of the cholesterol precursors can be efficiently metabolized to form cholesterol inside cells.

enzymes, it was hypothesized that cholesterol binds first to the CRD followed by auto-esterification at Asp95. Furthermore, this novel SMO cholesterylation was found to be regulated by SMO-interacting proteins Patched-1 (suppressor) and Shh (enhancer). Such lipidation is required for SMO-driven gene transcription and modulation, and loss of this modification resulted in severe developmental defects *in vivo*. These results open new doors for possible therapeutic interventions on treating Hh-pathway-related cancers by targeting SMO cholesterylation.[452]

1.7.4.2. Non-covalent interactors

Beyond covalent modification by cholesterol, a wide range of membrane proteins are also regulated through non-covalent interactions with this lipid. Probing these cholesterol-interacting proteins can be accomplished using cholesterol probes with photoaffinity crosslinking capabilities.[453] In order to globally profile these proteins, the Cravatt group employed a diazirine- and alkyne-containing cholesterol analogue (Alk-Dzn-Chol, Fig. 1.19A), which confer both photoaffinity and clickable handles, respectively.[454] Probe-treated cells were UV-irradiated and cell lysates were biotinylated with biotin-azide, enriched, and subjected to a SILAC-based quantitative proteomic analysis. Out of >800 proteins enriched, more than 250 cholesterol-interacting proteins displayed high selectivity and sensitivity to cholesterol—the majority of which were integral membrane proteins as expected. These results highlight the key cellular pathways that may depend on cholesterol concentration to modulate protein localization and modification. Interestingly, known sterol-interacting proteins and covalently cholesterylated Hh were not enriched in this approach; the authors noted that the introduction of these unnatural modifications may

impair sterol-protein interactions and the inevitable hydrolysis of esters may impede the enrichment of covalently modified proteins.[454] Indeed, this study exemplifies the use of a combination of both affinity and photocrosslinking tags in a single probe can identify interacting proteins mediated by lipid PTMs in a single experiment. Such a strategy could be useful for studying many other types of protein-lipid modifications as well.

1.7.4.3. Adducts of oxidized cholesterol intermediates

The biosynthesis of cholesterol also yields intermediates that can be oxidized and generate reactive electrophiles that react with amines forming protein adducts (Fig. 1.19B).[455] High levels of 7-dehydrocholesterol (7-DHC), the immediate precursor of cholesterol, is a hallmark of the genetic neurodegenerative and developmental disease Smith-Lemli-Opitz Syndrome (SLOS).[455] This is attributed to the impairment of 7-DHC reductase (DHCR7), the enzyme responsible for converting 7-DHC to cholesterol. Metabolic labeling experiments using an alkyne-modified 7-DHC (Alk-7-DHC, Fig. 1.19C) exhibited high levels of protein adduction in an SLOS cellular model deficient in DHCR7.[456] In a follow-up study, the protein adducts of lanosterol, the precursor of sterols from squalene, were also profiled using its alkyne-modified analogue (Alk-Lan, Fig. 1.19C).[457] Alk-Lan efficiently undergoes multistep conversion to Alk-7-DHC and Alk-Chol within neuronal cells, indicating that the alkyne moiety remains intact during Alk-Lan metabolism and that the biosynthetic enzymes can tolerate such modification of the sterol precursor. The identified Alk-Lan-modified proteins were a subset of those labeled with Alk-7-DHC in a neuronal cell line. This provides evidence that both Lan and 7-DHC form protein adducts through the same mechanism and that 7-DHC is the major source of reactive sterol

electrophiles. Further efforts into characterizing the members of the sterol adductome should shed more light into the implications of this protein modification during oxidative stress and in diseases such as SLOS.

1.7.5. Glycosylphosphatidylinositol anchor

Glycosylphosphatidylinositol-anchored proteins (GPI-APs) are involved in secretory and endocytic pathways and are tethered to lipid membranes through a GPI glycolipid.[458] The GPIs are assembled in the ER and transferred by GPI transamidases to the exposed C-termini of cleaved proprotein substrates. The structure of GPI anchors consists of a core phosphatidylinositol modified with fatty acyl groups and a conserved glycan linked to the protein through phosphoethanolamine (Fig. 1.20A).[459] An estimate of more than 250 GPI-APs being present in eukaryotes is derived from annotations and prediction tools, making up less than 2% of the eukaryotic proteome.[460,461] GPI-APs display a myriad of biological functions such as signal transduction, cell recognition and adhesion, and cell surface enzymatic reactions.[459] They are also implicated in parasitic and bacterial infections, as well as in genetic blood diseases and prion pathogenesis.[462]

CCML-based methods to study the biology of GPI-APs have been limited owing to the complicated structure of GPIs. There are three strategies that have been reported to generate clickable GPI probes: i.) the use of clickable fatty acid probes to tag the fatty acyl portion of GPI anchors; ii.) azide-functionalized sugar analogues to label the glycan core which is suitable live-cell copper-free click reaction; and iii.) clickable versions of the

complete GPI assembly. In the first approach, the fatty acyl portion of GPIs can incorporate medium-chain saturated fatty acids in bacteria and protozoans.[463] Chemical proteomic analysis of *P. falciparum* using Alk-C14 identified both *N*-myristoylated NMT substrates and GPI-anchored proteins.[125] Since the myristoyl groups in GPIs are linked through an ester bond, GPI-APs can be distinguished from the *N*-myristoylated proteins through hydroxylamine cleavage prior to protein pulldown. This strategy yielded a list of potentially novel and previously known GPI-APs in the malaria parasite. Employing a similar strategy in *T. gondii* identified 52 known and predicted GPI-APs.[302] Alk-C18 for *S*-palmitoylated proteome labeling in a macrophage cell line also enriched both *S*-palmitoylated proteins and GPI-APs.[147] Seven predicted and annotated GPI-APs were identified in this profiling experiment and one of these proteins, CD14, was validated through CCML with Alk-C18 combined with immunoblotting. Removal of the C-terminal site of GPI attachment results in loss of Alk-C18 labeling, indicating that the lipid modification is located in the GPI-anchor. This membrane-anchored protein is critical in initiating signaling cascades that trigger immune response. Interfering with its GPI modification may therefore offer therapeutic benefits in the onset of infection.

The conserved glycan scaffold in GPIs in mammalian GPI-APs is often modified with N-acetylgalactosamine (GalNAc) as a side chain of the first mannose proximal to the phosphatidylinositol core (Man1).[464] Thus, the second strategy for probe construction involves incorporation of sugar analogues into this site such as an azide analogue of GalNAc (GalNAz, Fig. 1.20B). Metabolic incorporation of GalNAz in GPI-APs in mammalian cells and subsequent Staudinger ligation with phosphine-biotin enabled the

detection of both endogenous and recombinantly expressed GPI-APs.[465] Another strategy of labeling the sugar moieties in GPI-APs is through the introduction of bio-orthogonal functional groups into the inositol portion of the glycan scaffold. An array of azide-modified inositols were also synthesized where the azide moiety was placed in various positions in the sugar molecule (*e.g.* InoAz, Fig. 1.20B), along with their peracylated analogues, *i.e.* all the hydroxyl groups are acylated (per-InoAz, Fig. 1.20B).[466] Through conjugation with alkyne-biotin and subsequent streptavidin-fluorophore tagging, cell surface-localized GPI-APs on fixed cells were successfully visualized and quantified using confocal microscopy and flow cytometry, respectively. It is noteworthy that the peracylated forms of the probes (Fig. 1.20B) are more efficiently metabolized to label GPI-APs and exhibit lower cytotoxicity. Moreover, GPI-APs are often exposed to the exterior surface of the plasma membrane and are amenable to click reactions outside the cell. This enables the use of SPAAC chemistry with bulky reagents and overcomes the need for Cu(I) known to be toxic to cells. Indeed, super-resolution imaging was made possible on live cells that were treated with peracylated GalNAz and tagged with a DBCO-modified fluorophore in a copper-free approach.[467]

While a high number of GPI-APs have been identified through predictions, a more limited set of these proteins has been experimentally validated. The lower abundance of GPI-APs relative to other membrane proteins and contamination with non-GPI-APs suppress their detectability in LC-MS/MS proteomic analysis, even after membrane fractionation and selective release into the solution using phospholipases.[468] In an attempt to provide an improved strategy, GalNAz was used to enrich and identify GPI-APs in

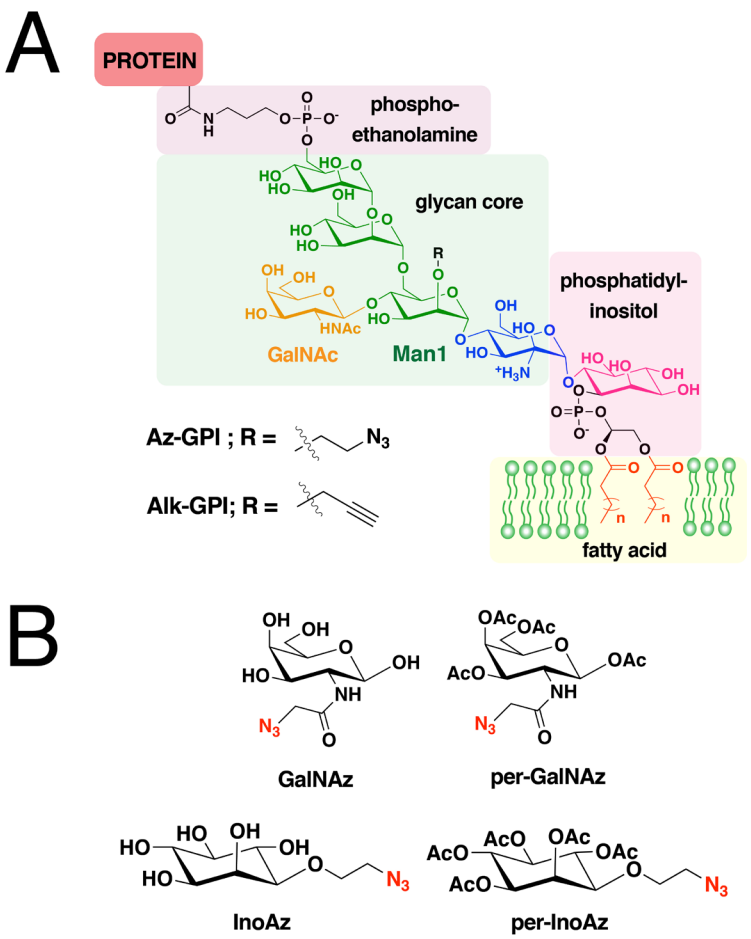

Figure 1.20. Chemical probes for labeling GPI-APs and structure of the GPI scaffold.

(A) Structure of the GPI assembly comprised of a glycan core linked to fatty acids through a phosphatidyl-inositol, which is also attached to the C-terminal of a protein through a phospho-ethanolamine that forms an amide bond. The lipid portion of the GPI anchors the protein to membranes. Whole GPI probes were synthesized with bio-orthogonal modifications in the glycan scaffold. **(B)** Structures of the azide-modified monosaccharides that can be metabolically incorporated to the glycan core of the GPI anchor.

mammalian cell lines.[469] The intact, GalNAz-labeled cells were treated with phosphatidylinositol-specific phospholipase C (PI-PLC) to release GPI-APs and enriched using alkyne-functionalized agarose beads. A complementary method to pulldown GPI-APs using immobilized lectins was also conducted in cells that were not treated with GalNAz. Out of more than 250 predicted GPI-APs, only 33 were identified and almost

50% were shared by both methods. Polarized epithelial cells also displayed differential populations of GPI-APs in the apical and basolateral regions of the cell, with more proteins localized at the apical surface. Although fewer proteins were profiled than expected, this method employed on intact cells preserves the cell integrity and hence opens up opportunities for spatiotemporal analysis of GPI-AP expression and dynamics in cells.[469]

Clickable probes that are considerably more specific for GPI-APs are those that encompass the complete GPI structure similar to that synthesized *in vivo*. However, the reductive nature of standard hydroxyl protection strategies for the sugar molecules are not compatible with azides and alkynes during the course of their synthesis. Through the use of *para*-methoxybenzyl (PMB) protection, complete GPI-anchor probes functionalized with azide (Az-GPI) or alkyne (Alk-GPI) on Man1 in the glycan core were successfully generated (Fig. 1.20A).[470] The same strategy was used to append an alkyne to the phosphate moiety in a GP anchor specific to *L. donovani*.[471] Although efficient conjugation could be achieved with their partner click reagents, there have been no studies in the literature that used these probes in labeling GPI-APs in cells. Perhaps the arduous nature of glycan chemical synthesis and challenges in the scale up of these probes limit their accessibility. Moreover, their relatively large structures may result in poor cellular uptake. Hence, employing these clickable GPIs in biological studies of GPI-APs has yet to be reported.

Chapter 2: Global proteomic analysis of prenylated proteins in *Plasmodium falciparum* using an alkyne-modified isoprenoid analogue

2.1. Introduction

Over the past 15 years, improved efforts at controlling malaria, caused by infection with the protozoan parasite *Plasmodium falciparum*, have significantly decreased the overall number of cases and childhood deaths attributable to severe malaria.[472] However, there remain over 200 million infections and over half a million deaths due to malaria each year.[473] Access to highly effective antimalarial therapies remains a cornerstone of malaria control efforts. Unfortunately, widespread resistance to former first-line agents, such as chloroquine, and emerging resistance to newer treatments, such as the artemisinin-combination therapies, endangers control of malaria worldwide.[474,475]

Target-based antimalarial drug development depends on identification of essential biological processes in *P. falciparum* that are amenable to small molecule inhibition. Development of therapeutics for the developing world is hampered by a relative lack of commercial pharmaceutical interest. Therefore, one strategy has been to identify potential antimalarial target proteins whose human homologs have themselves been explored as

pharmaceutical targets. These kinds of repurposing approaches thus harness the power of previous large-scale small molecule screening and development pipelines, in hopes of reducing the effort and expense of developing novel antiparasitics for resource-limited settings.

Protein prenyltransferases have emerged as one such "piggybacking" target for antimalarial drug development.[476,477] Protein prenylation is the C-terminal modification of cellular proteins with either a farnesyl (15-carbon) or geranylgeranyl (20-carbon) isoprenyl group. Prenyl modification of proteins is catalyzed by several classes of cellular prenyltransferase enzymes, including farnesyl transferase (FT) and geranylgeranyltransferase type I and type II (GGT-1 and GGT-2).[11,77] Prenylation is typically required for the membrane association and therefore the cellular activity of prenyltransferase substrates. For example, farnesylation of the small G-protein oncogene, K-Ras, is required for the transformation of many human cancers, including lung and colon cancer.[478] For this reason, protein farnesyltransferase inhibitors have been extensively explored by the pharmaceutical industry as potential human chemotherapeutics.[101,361] Like most eukaryotic organisms, *P. falciparum* malaria parasites also possess protein prenyltransferase activity and have been found to incorporate both farnesyl and geranylgeranyl modifications into protein substrates.[479,480] Chemical inhibition of isoprenoid precursor biosynthesis in malaria parasites blocks protein prenylation and is lethal to cultured *P. falciparum*, suggesting that production of isoprenyl substrates for protein prenylation is an essential function of isoprenoid biosynthesis in the parasite.[481] In addition, inhibition of parasite prenyltransferase activity halts parasite replication,[362,482–484]

providing compelling evidence that protein prenylation is indispensable for malaria parasite growth.

Since protein prenyltransferase activity is required by *P. falciparum*, identification of prenyltransferase substrates will likely reveal additional antimalarial targets. Bioinformatic approaches have been previously used to predict a limited number of potential prenylated proteins in the malaria genome.[485] However, since *Plasmodium* spp. are evolutionarily divergent from organisms used to generate these models, and few prenylated proteins have been experimentally confirmed in malaria parasites, it is not clear how well bioinformatics algorithms perform in predicting prenyltransferase substrates for *Plasmodium* spp.

2.2. Research Objectives

In this work, we use a chemical labeling approach to metabolically tag, potentially, the full complement of prenylated proteins in asexual *P. falciparum* parasites. Our approach was to metabolically incorporate an alkyne-modified isoprenoid analogue into the pool of prenyltransferase protein substrates. This additional alkyne functional group permits selective binding of prenylated proteins to streptavidin beads, via click chemistry with biotin-azide. The resulting prenylated proteins were identified by subsequent tryptic digestion and LC-MS analysis, coupled with bioinformatics analysis.

2.3. Results

2.3.1. An alkyne-functionalized isoprenoid analogue is metabolically incorporated into malaria parasites

To identify the prenylated proteins in *P. falciparum* using an alkyne-containing isoprenoid analogue, we first tested for metabolic incorporation of the compound C15AlkOPP (Fig. 2.1A), which was previously employed to identify prenylated proteins in mammalian cells.[353,486] This probe structurally resembles the native isoprenoid substrates farnesyl pyrophosphate (FPP) and geranylgeranyl pyrophosphate (GGPP) used for prenylation of proteins, and is a substrate for both mammalian FT and GGT-1.[345] Red blood cells infected with *P. falciparum* were exposed to the probe in the presence or absence of fosmidomycin (FSM), an established inhibitor of isoprenoid biosynthesis in *P. falciparum,*[487,488] followed by release of the intact parasites via mild detergent treatment. The free parasites were then lysed and the resulting lysates subjected to copper-catalyzed click reaction with TAMRA-N_3, which generates a stable cycloaddition product between the alkyne-tagged prenylated proteins and TAMRA-N_3 to allow visualization of labeled proteins (Fig. 2.1B). The samples were then fractionated via SDS-PAGE and subjected to in-gel fluorescence imaging (Fig. 2.1C, top panel).

Fluorescent protein bands were observed at approximately 25 and 50 kDa in samples obtained from parasites treated with C15AlkOPP (lane 3); a number of weaker bands, including species near 37 and 150 kDa, were also observed. A substantial enhancement of labeling ensued upon co-administration of FSM (lane 4), suggesting that

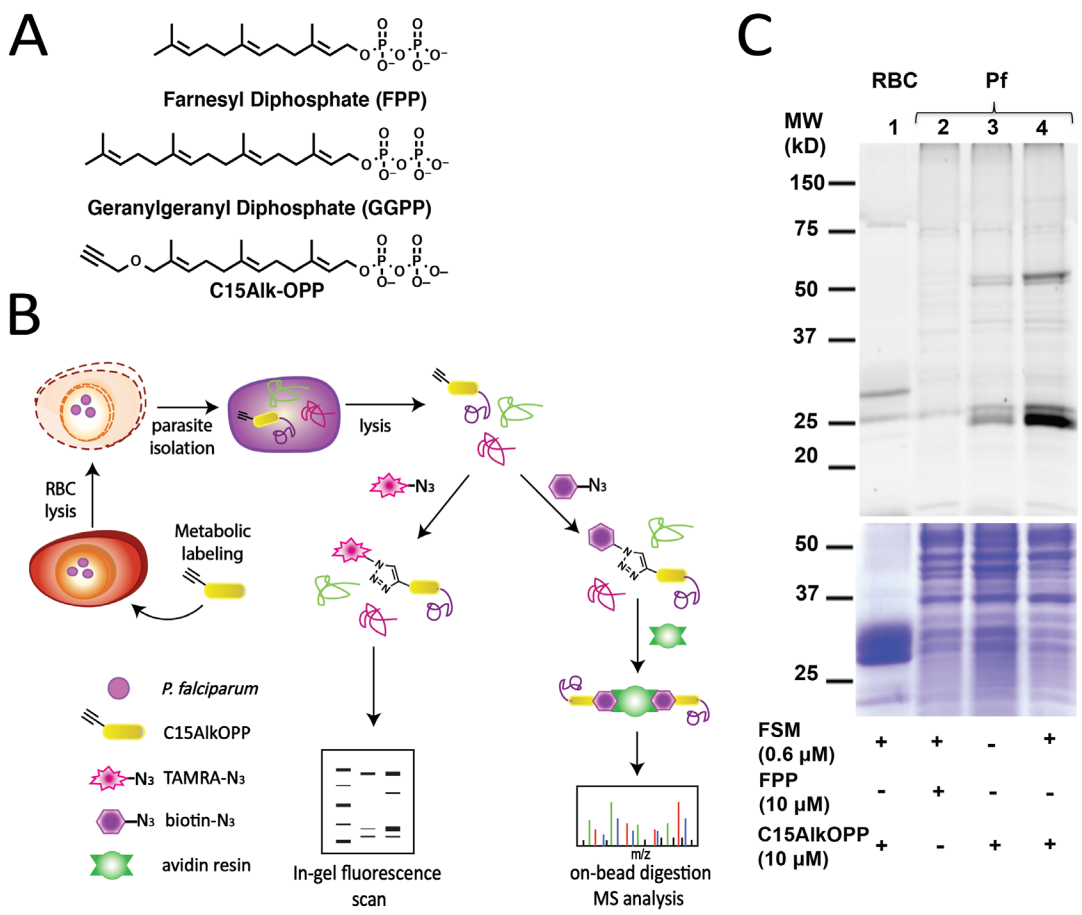

Figure 2.1. The C15AlkOPP probe allows tagging of prenylated proteins for in-gel fluorescence labeling and pulldown for proteomic analysis.

(A) Structures of native isoprenoid substrates of prenylation, farnesyl pyrophosphate (FPP) and geranylgeranyl pyrophosphate (GGPP), and the probe analog C15AlkOPP. **(B)** Scheme for metabolic labeling using the C15AlkOPP probe followed by selective labeling or enrichment using click chemistry. In-gel fluorescence and proteomic analysis of prenylated proteins were facilitated through click reactions with fluorescent reporter TAMRA-N_3 and affinity handle biotin-N_3, respectively. **(C)** Labeling of prenylated proteins visualized through in-gel fluorescence (top panel) in *P. falciparum* lysates. Lane 1: C15AlkOPP + FSM in red blood cells; lane 2: FPP + FSM in Pf; lane 3: C15AlkOPP in Pf; lane 4: C15AlkOPP + FSM in Pf. Total protein loading by Coomassie blue stain is shown in purple (bottom panel).

depletion of the endogenous FPP pool results in increased incorporation of the analogue; similar results with C15AlkOPP have been observed in mammalian cells treated with lovastatin.[353] Replacing the probe with FPP showed only limited labeling in these regions

(lane 2), indicating that the alkyne analogue is a viable tool to tag cellular prenylated proteins.

It should be noted that *P. falciparum* parasites develop within human erythrocytes. Although human prenyltransferases have not been identified in the mature erythrocyte proteome,[489] we evaluated for the possibility that erythrocyte proteins could incorporate C15AlkOPP probe in the absence of parasite infection. Human red blood cells were thus also treated with C15AlkOPP and FSM, and did not demonstrate significant labeling (lane 1). The band observed above 25 kDa is almost certainly an artifact due to a highly abundant protein band in this region as shown in the Coomassie stained gel (Fig. 2.1C, bottom panel); given its size, that protein may represent a hemoglobin dimer.[490] Overall, these results indicate that the C15AlkOPP probe successfully labels prenylated proteins in the malaria parasite with minimal interference from human proteins.

2.3.2. The C15AlkOPP probe is elongated by *P. falciparum* FPPS/GGPPS

As noted above, C15AlkOPP is a substrate for the mammalian FT and GGT-1 enzymes. Previously reported metabolic labeling data suggests that C15AlkOPP can also be used to label substrates of GGT-2. However, those results do not preclude elongation of C15AlkOPP to C20AlkOPP prior to prenyltransferase-catalyzed incorporation. Hence, we next sought to investigate whether C15AlkOPP can be elongated to C20AlkOPP in malaria parasites. Unlike other organisms that express a series of prenyl synthases, *P. falciparum* produces a single multi-functional enzyme (*Pf*FPPS/GGPPS, hereafter *Pf*FPPS) that is responsible for synthesis of geranyl pyrophosphate, farnesyl pyrophosphate, and

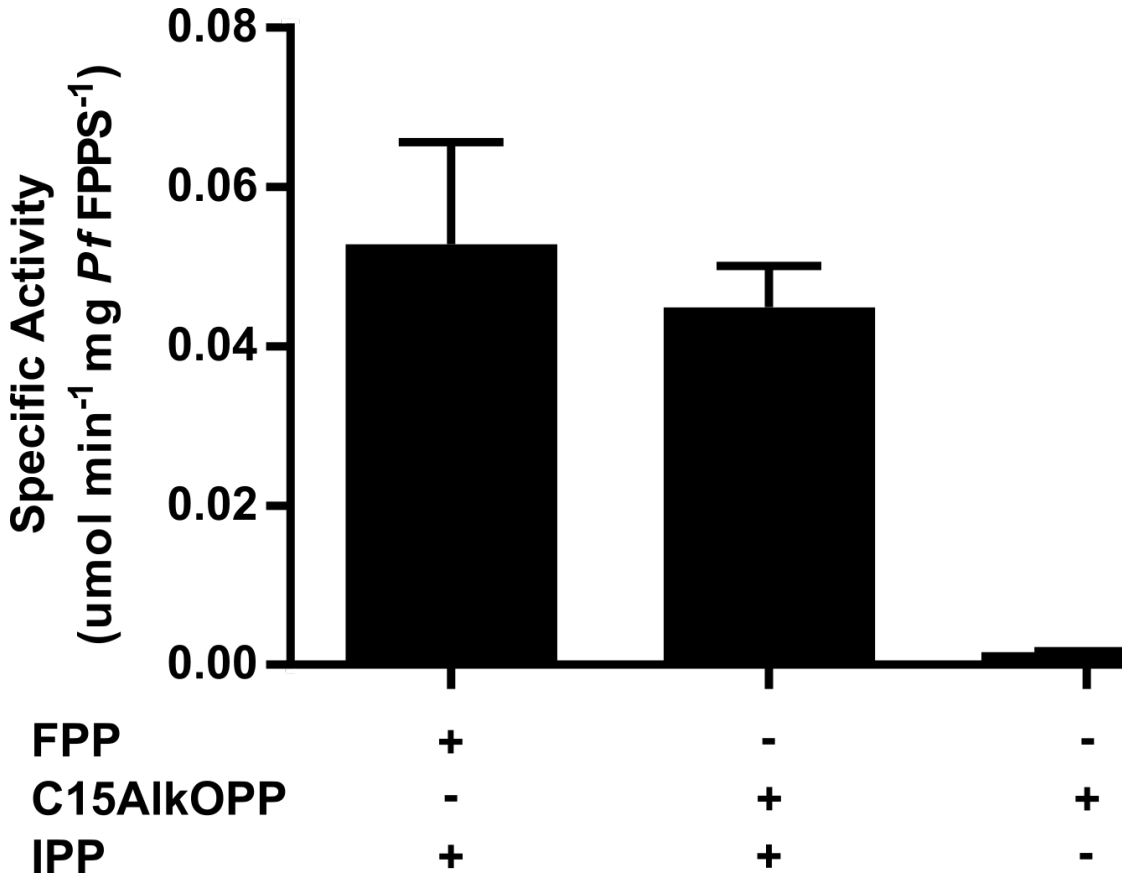

Figure 2.2. P. falciparum farnesyl pyrophosphate synthase (PfFPPS) accepts C15AlkOPP as a substrate.

Specific activity (mean ± S.E.M.) of *Pf*FPPS, measured using an absorbance-based phosphate release assay. Left to right, enzyme activity in the presence of FPP and IPP, C15AlkOPP probe and IPP, or C15AlkOPP alone. No activity was seen in absence of *Pf*FPPS. Three replicates were performed for each condition.

geranylgeranyl pyrophosphate.[491,492] To evaluate whether the parasite enzyme may utilize the C15AlkOPP probe as a substrate, we assayed purified recombinant *Pf*FPPS protein. As expected, *Pf*FPPS uses IPP to elongate its natural substrate, FPP, thus generating GGPP. Similarly, we found that *Pf*FPPS also effectively uses C15AlkOPP as a substrate (Fig. 2.2). Thus, while it is not clear whether the elongated analogue is a substrate for the malarial GGTs, the production of that species maximizes the likelihood that our single probe

strategy using C15AlkOPP will function to tag both farnesylated and geranylgeranylated proteins in the parasite.

2.3.3. Bioinformatic analysis of the *P. falciparum* proteome affords a list of putative prenylated proteins

To date, only a limited number of proteins with canonical C-terminal prenylation motifs have been demonstrated to be bona fide substrates in *P. falciparum*.[481,493–495] Prior to proteomic analysis, we performed a bioinformatic investigation to create a list of all possible prenyltransferase substrates present in the *P. falciparum* proteome. FASTA sequences of proteins from the *Plasmodium falciparum* genome reference isolate 3D7 proteome (UniProt ID UP000001450) with possible C-terminal –CaaX, –CXC, and –CC prenylation motifs were analyzed using Prenylation Prediction Suite (PrePS).[81] Out of 90 protein sequences with Cys at the 4th position from the C-terminus (–CaaX), a total of 8 proteins were predicted to be prenylated (Table 2.1). This group contains 5 proteins whose molecular masses are close to 25, 37, 50, and 150 kDa, similar to what we observed experimentally via in-gel fluorescence labeling (Fig. 2.1C). Furthermore, five of these proteins contain basic residues upstream of the putatively prenylated Cys, a typical pattern observed for most prenylated proteins. In addition to these predicted proteins, we examined those that were not recognized by PrePS but met additional criteria for prenylation: basic residues upstream of Cys at the -1 to -5 positions and a hydrophobic or aromatic residue at the +2 position. Seven proteins that satisfy these additional parameters were thus identified

FASTA sequence of Methionyl-tRNA formyltransferase from isolate 3D7 proteome database.
The Cys is at the 5th position from the C-terminus.

MYVKCFFYVIQILFIIFLKCHCYKIKCFNILDLNKKKYYSFREHINCEHIRNSVNRNNLS
NVLLRRRTKNALVKELYVSKLKDNYKTHTNFIRTNNIFLEEDKKIQECNINNIINNNVDI
QENVEKYNILYKNQLDDINILYILLFNTLMIYKKKYDFFMNENYIRSYYYIYKNNLGRDK
KIYNTKNYFINTFSITWYNTIKPYMNNIFLEILNIIENTLGNKIFYIDIKQELNKNRDEI
INTLYNIYKGNFRKRDKKPIKLLFIGSNEYSNLCFKIILLIIKRLRNDIILDNVITKSPR
RKGRNLILKKSNVEDEAIKNNINVFYYDKLKNNIHMLQNKKMDLCISISFGEIFNCNFFK
TIKSNIFSLHPSLLPFYKGASPIQRSLLNNEILYGYSVFLTTLNIDSGNVIMKKPFWFNS
NYNFNDIITILFTQGTLSLLKNISYLANYNKDIPHKNIYNNNICEETKNNLNQNHVQNKY
DSEINIHNSNLENKNNSRNNILPLNINNVLNNYNNKMYIQNDYNINNNYAPKIKNDEKYV
CFFCSTSLFIHNKIRSFINWPKAECTLFLLQNEVIKPLEIKIIKSSYDLNNNYKFIKYDG
LINTHDQHTCFDNIPRNFVYIQNDSLNILCKNNTLLKIYKLQQKNKKIVDAMSFINSINK
CSLLY

FASTA sequence of DEAD/DEAH box helicase from isolate 3D7 proteome database.
There is no putative prenylation motif at the C-terminus.

MNDAQIKDMMNDEEEKEEIEIKENINDKINEIDDNDDNDDGDDDGDDDDEDEDEDSDDND
DEDNDEDEDNDDNDDNDDSDNNDDDHNDVKKSSKNKKKNNEEMFDRSNHFDNFDNIMLDV
RLRKALLYLFKYQHPTIIQKMSICKILNGHDVIISSKTGSGKTMAYLIPVVHNLIKFNLN
EKDHLKFFYKCIIICPTEELCLQIYDVTKKLCTYLKDIITVNHNVNNTFYEHPTILISTP
KDLCTHIIEKKKKNNLDILMNLKILILDEADVLHTQEFQSYLKTLTSYLPKKFNKKYQIV
MASATLKRNILEKTKLFLHNPIYVSHEQKNESSFEKKKNKTNNTNSVIMKREEAGKNNIH
DEGNEGKTKYQKFTGKAFYYVYKEELIKYIYLYNLIKIKIIPYKSIIFTTTIHDAYKIKI
FLTYLNVSSSILNPNHPILIRQNIISAFNNSKFHFLICPQYEKNNMKHVKGVLGSNKMDN
VDGGDDNDDDEDDGDYNDDDDNDDDDNDDDNDDDNDNDDDEDNDEDEDNDDDDGDDNDDD
NDDNNDDDNDNDDQTLNEPLSDNNSCRTYNSDDENEKTDDTTKLNEEKDFLYSRGLDFYD
VKCVVNFDMPSDSETFIHRIGRTCRLNNKGKCISFVNELNYGEKEFLQKLIEDKNICTMI
KKNIQYNIVEKYRYRVESTLNKCTNKKIKLFIQKEILYQSLKSKELKDFFNTNINEKRKI
NKIIKHFNKAVIPQKLIKDRNQSIFLNKSKVKNKIIQKNNTNNKNKNNNNNIKPFALKNN
NGLVITEQGYESQLTKEPEREVADPSKLPPLCGQRLRNYMYLKYIKGKKNKNGSNMNKSY
NSNNKKRKNNNKYNNRYNKYNKKGINKNHNKRNTNFNR

FASTA sequence of DEAD/DEAH box helicase from isolate HB3 proteome database.
The putative prenylation motif CMLQ is present.

MNDAQIKDMMNDEEEKEEIEIKENINDKINEIDDVDGGDDNDDNDDGDDDGDDDDEDEDE
DNDDNDDEDNDNDEDNDDDEDNDDDEDNDEDEDNDDNDDNDDSDNNDDDHNDVKKSSKNK
KKNNEEMFDRSNHFDNFDNIMLDVRLRKALLYLFKYQHPTIIQKMSICKILNGHDVIISS
KTGSGKTMAYLIPVVHNLIKFNLNEKDHLKFFYKCIIICPTEELCLQIYDVTKKLCTYLK
DIITVNHNVNNTFYEHPTILISTPKDLCTHIIEKKKKNNLDILMNLKILILDEADVLHTQ
EFQSYLKTLTSYLPKKFNKKYQIVMASATLKRNILEKTKLFLHNPIYVSHEQKNESSFEK
KKNKTNNTNSVIMKREEAGKNNIHDEGNEGKTKYQKFTGKAFYYVYKEELIKYIYLYNLI
KIKIIPYKSIIFTTTIHDAYKIKIFLTYLNVSSSILNPNHPILIRQNIISAFNNSKFHFL
ICPQYEKNNMKHVKGVLGSNKMDNVDGGDDNDDDEDDGDYNDDDDNDDDNDDDNDDDDN
DDDEDNDEDEDNDEDEDNDDDDGDDNDDNNDDQTLNEPLSDNNSCRTYNSDDENEKTDDT
TKLNEEKDFLYSRGLDFYDVKCVVNFDMPSDSETFIHRIGRTCRLNNKGKCISFVNELNY
GEKEFLQKLIEDKNICTMIKKNIQYNIVEKYRYRVESTLNKCTNKKIKLFIQKEILYQSL
KSKELKDFFNTNINEKRKINKIIKHFNKAVIPQKLIKDRNQSIFLNKSKVKNKIIQKNNT
NNKNKNNNNNIKPFALKNNNGLVITEQGYESQLTKEPEREVADPSKLPPLCGQRLRNYMY
LKYIKGKKNKNGSNMNNSYNSNNKKRKNNNKYNNRYNKYNKKGINKNHNKRNTNFNRIQK
KIIFLLSLFCMLQ

Figure 2.3. FASTA sequences of DEAD/DEAH box Helicase and Methionyl-tRNA formyltransferase in isolate 3D7 and other proteome databases from

from the proteome database (Table 2.2). A previous study reported 8 proteins that satisfied these criteria based on the *P. falciparum* genome, which included a DEAD/DEAH box Helicase and Methionyl-tRNA formyltransferase (along with six predicted in our analysis).[494] However, neither of these two proteins contains a C-terminal CaaX sequence in the reference *Plasmodium falciparum* isolate 3D7 proteome database (although one of them does in another database, see Fig. 2.3). Interestingly, the remaining protein listed in

Table 2.1. Candidate prenyl transferase substrates from the P. falciparum 3D7 proteome, which contain canonical CaaX motifs and were identified by PrePS.

PrePS was used to predict the likelihood of prenylation of the proteins identified: *low, **intermediate, ***high

Accession No.	Name	C-term	Mol. wt. (kDa)	PrePS
Q8I346	SNARE protein (putative)	KKQCCSIM	23	FT*** GGT-1***
Q8I583	Ulp1 protease (putative)	ISQGCLVF	123	FT* GGT-1*
Q8IKN0	Uncharacterized protein	QRRMCNIM	38	FT* GGT-1**
Q8IEC5	Uncharacterized protein	KKKKCTIM	95	FT*** GGT-1***
Q8IL88	Hsp40 subfamily A (putative)	GRVACAQQ	48	FT**
C0H5D3	SNARE protein (putative)	NNQCCSLY	26	FT*
Q8IE80	Uncharacterized protein	NIAACKQC	34	FT*
Q8IEK2	Uncharacterized protein	NRLKCNIM	73	GGT-1**

Table 2.2. Candidate prenyl transferase substrates from the P. falciparum 3D7 proteome, which were not identified by PrePS but possess additional, promising CaaX features.

PrePS was used to predict the likelihood of prenylation of the proteins identified: *low, **intermediate, ***high

Accession No.	Name	C-term	Mol. wt. (kDa)	Basic residue at -1 to -5	Hydrophobic residue at +2	Aromatic residue at +2
Q8IIN1	Protein tyrosine phosphatase	NCLRKCHFM	25	+	+	+
Q8ILH7	Uncharacterized protein	KKRNKCNFM	51	+	+	+
Q8I3K7	Membrane skeletal protein IMC1-related	QRNLYCSYA	34	+	+	+
Q8I0W8	Deoxyribodipyrimidine photolyase	KREKKCVAS	129	+	+	-
O77306	Ser/Thr protein kinase	NKKNSCAYT	157	+	+	-
Q9NLB7	Uncharacterized protein	NYNFLCLYI	10	-	+	+
O77380	CPSF	DLENMCSFL	339	-	+	+

Table 2.2 (but not identified in the aforementioned genomic analysis), PRL protein tyrosine phosphatase, does appear to be a real prenylated protein. Recent computational docking

studies[496] suggested that it is a substrate and this has been confirmed through additional in vitro assays.[494]

Proteins with C-terminal –CXC and –CC motifs were also extracted from the proteome and analyzed in PrePS. As expected, Rab proteins were predicted to be substrates of geranylgeranyl transferase type II (GGT-2) with high degrees of probability (Table 2.3).

Table 2.3. Candidate prenyl transferase substrates from the P. falciparum 3D7 proteome, which possess –CXC and –CC C-terminal motifs.
PrePS was used to predict the likelihood of prenylation of the proteins identified: *low, **intermediate, ***high.

Accession No.	Name	C-term	Mol. wt. (kDa)	PrePS
Q8IL79	Copper transporter putative	ADPAC*C*G*C*	27	No
Q8IM51	Secreted ookinete adhesive protein	ECSCS*C*S*C*	23	No
Q8IHR8	Rab6	NMLSKCLC	24	GGT-2**
Q7K6B0	Rab18	ESRSNCAC	23	GGT-2***
Q8I3W9	Rab1a	SPQSFCSC	24	GGT-2***
Q8IHW0	Myosin heavy chain subunit, putative	ELNMFK*CC*	208	No
C6KST4	Uncharacterized protein	IKKKKMR*CC*	33	No
Q8II49	Conserved Plasmodium protein	TKKFFP*CC*	30	No
Q8IHW1	Conserved Plasmodium protein	KTKKCY*CC*	19	No
Q8IAL1	Uncharacterized protein	GKRFLG*CC*	9	No
Q7K6A8	Rab1b	KDTKKKCC	23	GGT-2***
O96193	Rab5a	TLSKKGCC	27	GGT-2***
Q8I274	Rab5c	EETKKKCC	24	GGT-2***
Q76NM4	Rab11a	TKKKNKCC	25	GGT-2***
Q8I5A9	Rab2	SRSGFSCC	24	GGT-2***
C0H516	Rab7	KMYKSRCC	24	GGT-2***
C0H5G2	Rab11b	NMNKVKCC	24	GGT-2**

The molecular weights of these small GTPases are consistent with the bands observed near 25 kDa via in-gel fluorescence labeling (Fig. 2.1C). No proteins other than those belonging to the Rab family were identified as potential substrates, suggesting that there are no known proteins with these – CXC and –CC sequences that have the specific neighboring residues upstream of Cys necessary to render them substrates for GGT-2. In aggregate, our bioinformatics analysis suggests that the *P. falciparum* proteome contains 8 –CaaX, 3 – CXC, and 7 –CC proteins (18 total) that may be prenyltransferase substrates.

2.3.4. Proteomic analysis of the prenylated proteins in *P. falciparum*

After validating the use of C15AlkOPP as a prenylation probe in *P. falciparum*, we next sought to determine the molecular identity of prenylated proteins in the parasite. To reduce cellular production of FPP, which would compete with probe incorporation, cultured asexual *P. falciparum* were treated with sub-lethal (50% of the half-maximal inhibitory concentration) concentrations FSM. Fosmidomycin-treated parasites were grown in the presence of either C15AlkOPP probe or FPP as a negative control. Following labeling, parasites were freed from host erythrocytes, and parasite protein lysates were subjected to click reaction with biotin-N3; the affinity handle conferred by biotin permits the selective enrichment and isolation of labeled prenylated proteins upon pull-down through the strong biotin-avidin interaction (Fig. 2.1B). Proteins were washed under stringent conditions (1% SDS and 8 M urea) followed by on-bead trypsin digestion. Equal amounts of peptides from C15AlkOPP- and FPP-treated samples, were pre-fractionated and analyzed by nano-flow liquid chromatography and tandem mass spectrometry (MS/MS), followed by database searching against *Plasmodium falciparum* (UniProt ID UP000001450) and *Homo sapiens*

proteomes (UniProt ID UP000005640). After data processing, 445 proteins were identified at 99.0% minimum probability with at least 2 identified peptides from 9073 spectra, and 98.0% minimum peptide confidence within a 1% false discovery rate, for both C15AlkOPP- and FPP-treated samples.

Our labeling strategy was designed to enrich for prenyltransferase substrates labeled with C15AlkOPP and/or C20AlkOPP using a biotin pull-down approach. Proteomic studies that use such enrichment methods are sometimes complicated due to nonspecific adsorption of proteins onto the avidin-coated beads used in these experiments. To address that issue, our approach employed a quantitative comparison based on spectral counting between the samples treated with C15AlkOPP and those treated with FPP. We used the average total spectral counts for each identified protein to calculate the enrichment of proteins (fold-change) across three replicates of samples treated with C15AlkOPP probe versus FPP. Proteins with potential prenylation motifs (–CaaX, –CC, –CXC on their C-terminus) were extracted from that data and summarized in Table 2.4. A total of 15 prenylated proteins are listed, including 14 of the 18 predicted in our bioinformatics analysis. One additional protein (Q81LH7) bearing the –CaaX sequence CNFM, which was not predicted by PrePS, was also identified. Conversely, four of the –CaaX sequences predicted by PrePS were not observed (Q81583, Q81EC5, Q81E80 and Q81EK2 with –CaaX sequences CLVF, CTIM, CKQC and CNIM, respectively). All Rab proteins predicted to be prenylated by PrepPS were identified.

The list of all proteins identified in our analysis is ordered based on the fold change between the C15AlkOPP- and FPP-treated samples. The top 12 proteins in that list correspond to the first 12 entries in Table 4 (9 to 33-fold change). For each of these top 12 hits, very few spectral counts were observed in the absence of probe, giving high confidence that these represent bona fide prenylated proteins. In contrast, numerous proteins were found below the 6-fold threshold. In those cases, substantial spectral counts were observed in the absence of probe; we attribute those proteins to nonspecific adsorption. However, the last 3 entries in Table 2.4, while manifesting low levels of spectral counts in the C15AlkOPP-treated samples, gave no spectral counts in the FPP-treated samples, suggesting that they may represent true, low abundance hits; one of those three, SNARE Ykt6.1, has been confirmed as a prenyltransferase substrate.[495] It is worth noting that the aforementioned DEAD/DEAH box Helicase and Methionyl-tRNA formyltransferase suggested by previous investigators as possible prenylated proteins based on bioinformatics analysis[494] were not identified in our analysis.

Finally, it should be noted that human Rab homologs were also identified and grouped into clusters with the parent proteins from *P. falciparum* (Fig. 2.4), since the data analysis was conducted using both the *H. sapiens* and *P. falciparum* databases. However, for each identified Rab, the change in spectral counts in the presence of probe was always higher for the candidate malarial proteins than their human homologs. Additionally, we found, in each case, that protein probabilities for parasite sequences were higher than those for the cognate human orthologs. Together, these characteristics indicate that the Rab proteins identified upon metabolic labeling of *P. falciparum* are indeed malarial in origin and that the human candidates are artifacts of sequence similarities.

Table 2.4. Proteins bearing prenylation motifs identified in *P. falciparum* using C15AlkOPP labeling. For each protein, fold-change indicates the ratio of the average total spectral counts obtained following C15AlkOPP- versus FPP-labeling, across three experimental replicates. An imputation of 1 was employed to calculate fold changes. Spectral counts and percent coverage for each replicate are shown. Two uncharacterized proteins (italicized) containing predicted prenylation motifs were identified with low spectral counts. [a]Protein accession numbers including theoretical molecular weights and [b]gene IDs were obtained from UniProt and PlasmoDB, respectively. [C]Unless otherwise referenced from previous reports, biological processes and cellular component of identified proteins were obtained from UniProt.[d] PrePS was used to predict the likelihood of prenylation of the proteins identified: *low, **intermediate, ***high.

Protein Name	Accession No.[a]/Gene ID[b]	Mol. wt. (kDa)[a]	Biological Process[c]	Cellular Component[c]	Spectral Count		Fold Change	Percent coverage (%)		C-term sequence[c]	Confirmed prenylation	PrePS[d]
					C15Alk-OPP	FPP		C15Alk-OPP	FPP			
Rab6	Q8IHR8 PF3D7_1144900	24	vesicular transport (putative)	trans Golgi, cytosolic	33,32,33	0,0,0	33	70,70,59	0,0,0	NMLSKCLC	Yes[29]	GGT-2**
HSP40 subfamily A	Q8IL88 PF3D7_1437900	48	protein folding, protein translocation (putative)[54]	cytosolic, RBC membrane[43]	39,34,37	1,2,0	28	41,35,33	2,5,0	GRVACAQQ	No	FT**
Rab7	C0H516 PF3D7_0903200	24	retrograde transport[55]	endosomes[55]	25,27,25	0,0,0	26	59,66,66	0,0,0	KMYKSRCC	No	GGT-2***
Rab1b	Q7K6A8 PF3D7_0512600	23	ER to Golgi transport (putative)[40]	ER, Golgi (putative)[40]	19,12,17	0,0,0	16	37,35,31	0,0,0	PDTKKKCC	No	GGT-2***
Rab1a	Q8I3W9 PF3D7_0513800	24	ER to Golgi transport[40]	ER, Golgi[40]	11,10,12	0,0,0	11	17,21,22	0,0,0	SPQSFCSC	No	GGT-2***
Rab2	Q8I5A9 PF3D7_1231100	24	ER to Golgi transport (putative)[40]	ER, Golgi (putative)[40]	25,21,28	2,0,0	18	58,56,57	11,0,0	SRSGFSCC	No	GGT-2***
Rab5c	Q8I274 PF3D7_0106800	24	retrograde transport[14]	endosomes[14]	18,15,14	0,0,0	16	43,35,33	0,0,0	EETKKKCC	Yes[14]	GGT-2***
Rab11a	Q76NM4 PF3D7_1320600	25	formation of inner membrane complex[56], recycling endosome transport (putative)	vesicles[56]	12,17,12	0,0,0	14	41,42,41	0,0,0	TKKKNKCC	No	GGT-2***
Rab5a	O96193 PF3D7_0211200	27	retrograde transport[14]	endosomes[14]	9,9,11	0,0,0	9.7	25,29,29	0,0,0	TLSKKGCC	Yes[14]	GGT-2***
Rab18	Q7K6B0 PF3D7_0807300	23	mobilization of lipid droplets (putative)[57]	Parasitophorous vacuole membrane (putative)[57]	9,7,11	1,1,1	9	28,24,28	6,6,6	ESRSNCAC	No	GGT-2***
Rab11b	C0H5G2 PF3D7_1340700	24	transport (putative)	membrane (putative)	8,10,9	0,0,0	9	30,25,31	0,0,0	NMNKVKCC	No	GGT-2**
SNARE Ykt6.2	C0H5D3 PF3D7_1324700	26	vesicular fusion, transport (putative)[58]	membrane (putative)	5,6,7	0,0,0	6	14,18,24	0,0,0	KNNQCCSLY	No	FT*
SNARE Ykt6.1	Q8I346 PF3D7_0910600	23	vesicular fusion, transport (putative)[58]	Golgi, cytosolic, vacuolar[31]	3,2,2	0,0,0	2.3	17,13,11	0,0,0	LKQCCSIM	Yes[58]	FT*** GGT-1***
Uncharacterized	*Q8IKN0 PF3D7_1460100*	*38*	*PI3P binding, trafficking to the food vacuole[59]*	*food vacuole lumen[59]*	*0,2,1*	*0,0,0*	*1.3*	*0,8,5*	*0,0,0*	*QRRMCNIM*	*No*	*FT* GGT-1***
Uncharacterized	*Q8ILH7 PF3D7_1428700*	*51*			*0,1,3*	*0,0,0*	*1.7*	*0,3,5*	*0,0,0*	*KRNKCNFM*	*No*	-

Comparison of peptide sequences identified between Pf Rab7 and human Rab7a.

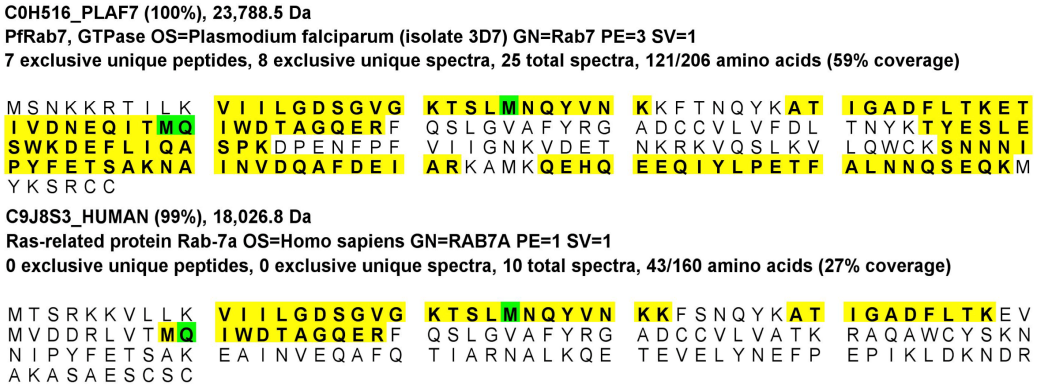

Comparison of peptide sequences identified between Pf and human Rab1B.

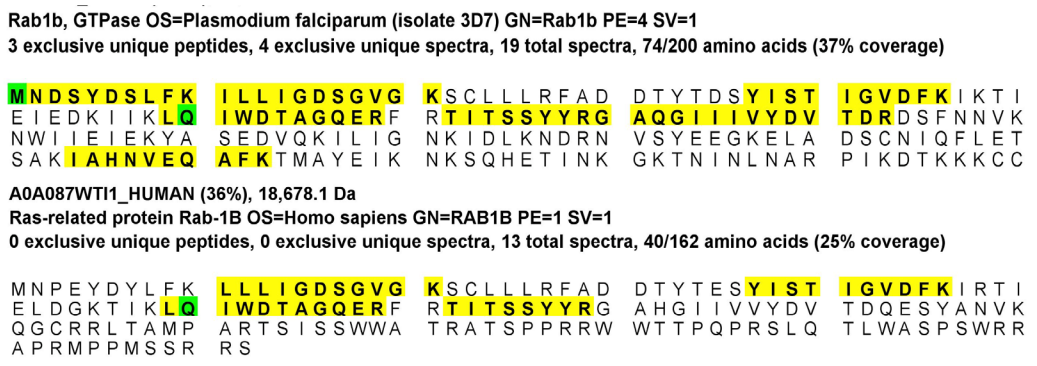

Comparison of peptide sequences identified between Pf and human Rab1A.

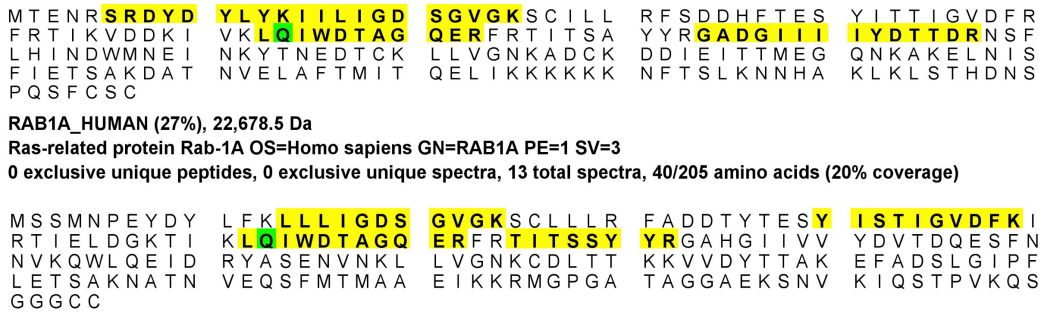

Figure 2.4. Comparison of peptide sequences identified between P. falciparum and human Rab protein homologs.

P. falciparum proteins contain peptides present in human homologs but with statistically higher probabilities, spectral counts, and percent coverages.

2.4. Discussion

Due to the ongoing spread of drug resistance, there is a pressing need for new therapies to treat malaria. Evidence strongly suggests that protein prenylation is required for asexual development of the *P. falciparum* malaria parasite; several distinct chemotypes of prenyltransferase inhibitors exhibit potent antimalarial activity.[362,482,484,497–499] Given the essential nature of protein prenylation, it follows that the functions of prenyltransferase substrates themselves are necessary for parasite replication. Thus, identification of prenylated proteins in *P. falciparum* may reveal new, essential, and highly valuable targets for antimalarial drug development. Such targeting could be accomplished either indirectly by interfering with prenylation or directly via inhibition of their cognate functions.

Here we present the first experimentally determined catalog of prenylated proteins (the "prenylome") of blood stage *P. falciparum*. We have identified prenyltransferase substrates through the use of metabolic labeling with a novel, alkyne-containing isoprenoid analogue. We find that the *P. falciparum* farnesyl pyrophosphate synthase (FPPS) successfully elongates the probe (which is a derivative of FPP) to generate the cognate 20-carbon (GGPP derivative) probe. Therefore, we believe our in vivo metabolic labeling approach has likely captured the full complement of both farnesylated and geranylgeranylated proteins in *P. falciparum*, with the exception of prenylated proteins with very low levels of expression during blood-stage development that may not react in our derivatization strategy.

Eukaryotic systems possess three different protein prenyltransferases: farnesyltransferase (FT) and geranylgeranyltransferase type I (GGT-1) commonly recognize the same motif (the CaaX box) that includes the cysteine of their substrates they modify, and are thus referred to as CaaX prenyltransferases, whereas geranylgeranyltransferase type II (GGT-2, also called Rab geranylgeranyltransferase) recognizes an alternative motif.[500] Active prenyltransferases consist of two polypeptide subunits, α and β; FT and GGT-1 typically share an α subunit. As has previously been suggested,[485] we find that experimentally confirmed prenyltransferase substrates of *P. falciparum* parasites possess canonical motifs that indicate the presence of both CaaX prenyltransferases and Rab geranylgeranyltransferases. *P. falciparum* lysate has previously been shown to possess both FT and GGT-1 activity.[479] The current annotation of the *P. falciparum* genome indicates a full complement of genes encoding the candidate prenyltransferases, as follows: *Pf*FT [PF3D7_1242600 (α subunit) and PF3D7_1147500 (β subunit)], *Pf*GGT-1 [PF3D7_1242600 (α subunit; shared with *Pf*FT) and PF3D7_0602500 (β subunit)], and *Pf*GGT-2 [PF3D7_1442500 (α subunit) and PF3D7_1214300 (β subunit)].

Our work experimentally confirms that protein prenylation in *P. falciparum* reflects a more modest set of prenylated proteins than is observed in fungi or higher eukaryotes, including humans. According to PRENbase (http://mendel.imp.ac.at/PrePS/PRENbase/), a curated online database of protein prenylation across sequenced genomes, prenylated proteins in the human genome are spread into 43 clusters of paralogous proteins.[501] Biological functions of prenylated proteins are well conserved, even amongst unicellular

eukaryotes, as 42 similarly defined clusters are present across fungal genomes. In stark contrast, we find robust experimental evidence for a total of only thirteen prenylated proteins in *P. falciparum*, with suggestive evidence for an additional two probable prenyltransferase substrates. While a restricted prenylome has been suggested bioinformatically for malaria parasites, our study provides important evidence that there are not unrecognized, non-canonical motifs used by the *P. falciparum* prenyltransferases.

During asexual replication, *P. falciparum* is an obligate parasite of human erythrocytes, and relies on vesicle-mediated trafficking of erythrocyte cytoplasm and hemoglobin, as well as export of essential proteins for remodeling of the erythrocyte membrane and cytoplasm. The importance of membrane trafficking to *P. falciparum* development is underscored by the restricted biological functions of the malaria prenylome. Interestingly, we find that the majority of proteins in the *P. falciparum* prenylome belong to a single cluster of paralogous proteins, the Rab family of small GTPases, classic regulators of endomembrane trafficking. These proteins likely make up the broad band at 25 kDa found in our in-gel fluorescence images upon C15OPP labeling (Fig. 1C), as well as in studies using radiolabeling of parasites with [^{3}H]-geranylgeranyl pyrophosphate.[502] Unsurprisingly, of the eleven Rabs annotated in *P. falciparum*, we found all ten predicted to be geranylgeranylated by GGT-2.[503]

In addition, three more prenyltransferase substrates in *P. falciparum* (two SNARE proteins and a phosphatidylinositol 3-phosphate binding protein) are also likely to function in membrane trafficking. Notably absent from the *P. falciparum* prenylome are a number

of GTPase superfamilies, including Ras and Rho, typical of other unicellular eukaryotes and metazoans. This restricted use of protein prenylation for a single biological function reflects the complement of small GTPases that has been suggested to have been present in the last common eukaryotic ancestor, prior to the dramatic expansions of paralogous GTPase gene families.[504,505] The limited collection of GTPases and prenylated proteins that we find in *P. falciparum* is therefore not unique to this parasite, but is shared with other Alveolates in this lineage, including several other important mammalian parasitic pathogens, such as *Cryptosporidium*, *Toxoplasma*, and *Eimeria*.

We identified only four confirmed prenylated proteins in *P. falciparum* that possess a canonical CaaX motif, which should serve for recognition and modification by either FT or GGT-1. Bioinformatic analyses are insufficient to indicate whether a given CaaX-containing protein is farnesylated or geranylgeranylated. However, experimental evidence suggests that at least one of these proteins, PF14_0359, a Hsp40 analog, is specifically farnesylated. In *P. falciparum*, metabolic labeling with [^{3}H]-farnesyl pyrophosphate, but not [^{3}H]-geranylgeranyl pyrophosphate, identifies a dominant band at approximately 50 kDa.[502] As the remaining proteins in the malaria prenylome are between 23-38 kDa, this finding most likely represents farnesyl modification of *Pf*Hsp40 (48 kDa).[506]

P. falciparum expresses an expanded repertoire of molecular chaperones, comprising 2% of the overall genome, and including 49 Hsp40 superfamily members in total.[507] However, while other eukaryotes typically express up to five type I Hsp40s, *Pf*Hsp40 is the sole, cytosolic type I Hsp40 homolog in the malaria parasite. In other organisms,

farnesylation of orthologous type I Hsp40s has been well described, and is required for the biological functions of these chaperones in mediating protein stability.[508,509] The cellular function of *Pf*Hsp40 in *P. falciparum* has yet to be explored, although immunofluorescence microscopy indicates that this protein is cytosolic.[506] However, data from proteomics and yeast two-hybrid studies indicate it may play a role in trafficking to the RBC membrane.[510] The extent to which farnesylation plays a role in the localization or functions of *Pf*Hsp40 remains to be explored.

2.5. Conclusion

Our work contributes to an increasingly complete picture of post-translational hydrophobic modifications in blood-stage *P. falciparum*. The identification of a limited set of CaaX proteins has important implications for understanding the evolution of this modification process, as well as the active work developing novel antimalarial therapies targeted to isoprenoid synthesis and prenyltransferases.

2.6. Methods

2.6.1. *P. falciparum* tissue culture

All culturing was done with *Plasmodium falciparum* genome reference strain 3D7. 3D7 was obtained from the Malaria Research and Reference Reagent Resource Center (strain MRA-102, contributed by D. J. Carucci, ATCC, Manassas, Virginia). Parasites were grown in RPMI-1640 media (Sigma-Aldrich, SKU R4130) supplemented with 27 mM sodium bicarbonate, 11 mM glucose, 5 mM HEPES, 1 mM sodium pyruvate, 0.37 mM hypoxanthine, 0.01 mM thymidine, 10 μg ml^{-1} gentamycin (Sigma-Aldrich) and 0.5%

Albumax (Life Technologies) with a 2% suspension of human erythrocytes under an atmosphere of 5% CO_2, 5% O_2, balance N_2 and incubated at 37°C, as previously described.[488,511] For in-gel fluorescence, 40 mL of culture was used per replicate. Samples destined for mass spectroscopy analysis were derived from 200 mL of culture per replicate. For all experiments, cultures were adjusted to 4% of red blood cells infected (4% parasitemia) at experiment start. Cultures were treated with fosmidomycin (Life Technologies) to a final concentration of 600 nM (approximately half IC_{50}). Pyrophosphate probes or prenyl pyrophosphates (Echelon Biosciences) were added to a final concentration of 10 μM. After compounds were added, cultures were mixed thoroughly and incubated for 24 hours.

After 24 hours, cultures were saponin lysed as previously described,[488] with modifications. In brief, cells were pelleted and washed with PBS before being lysed with 1% saponin in PBS. Saponin lyses red blood cell (RBC) membranes but not parasite cell membranes, thus freeing the parasites from the RBCs. The lysed mixture was pelleted, and the loose RBC membrane layer and supernatant removed, leaving a parasite pellet. This pellet was washed with PBS, centrifuged again, the supernatant removed, and stored at -80°C.

RBC controls were performed with 5 mL per replicate of 2% hematocrit in supplemented RPMI media with no parasites. RBCs were pelleted without saponin since internal RBC proteins are released with lysis. This volume corresponds to the volume of saponin-freed parasites from 200mL total culture at 4% parasitemia.

2.6.2. In-gel fluorescence labeling

RBC controls and saponin-lysed pellets of *P. falciparum*, treated with or without FSM and FPP or C15AlkOPP, were suspended in 300 µL lysis buffer (10 mM PO_4^{3-}, 137 mM NaCl, 2.7 mM KCl, 2.4 µM PMSF, benzonase nuclease, protease inhibitor cocktail and 1% SDS) and sonicated 6 to 8 times for 2 seconds in 10-second intervals. Click reactions were performed on 100 µg samples of protein lysate (1 µg/µL) with 25 µM TAMRA-N_3, 1 mM TCEP, 0.1 mM TBTA, and 1 mM $CuSO_4$ at room temperature for one hour. Proteins were precipitated using a ProteoExtract precipitation kit (Calbiochem) to remove excess click chemistry reagents. Protein pellets were dissolved in 1X Laemlli loading buffer and heated at 95 ^oC for 5 minutes. Samples were fractionated using 12% SDS PAGE gels and imaged via in-gel fluorescence using a BioRad FX Molecular Imager with 542/568 nm excitation/emission wavelengths. Gels were stained with 1X Coomasie blue stain followed by destaining to visualize protein loading.

2.6.3. Cloning and expression of *Pf*FPPS

The gene *PfFPPS* (PF3D7_1128400) was PCR amplified from *P. falciparum* 3D7 cDNA (primers *Pf*FPPS Fwd 5'-CTCACCACCACCACCACCATGCUGAGAACGAGCAGAA TAACCAAGATTC-3'; *Pf*FPPS Rev 5'-ATCCTATCTTACTCACTCAAGCGCCTGTAA ACAAAATGTCC-3') and cloned into pBG1861 using ligation independent cloning as previously described.[512] The cloned *PfFPPS* sequence was verified by Sanger sequencing. The primers used add coding for a six histidine tag at the N-terminus of the gene to allow for nickel affinity purification.

Subsequently, pBG1861 was transformed into ArticExpress (DE3) RIL *E. coli* (Agilent Technologies). Cultures were grown in LB media with 100 µg/mL ampicillin at 37°C and 200 rpm until mid-log phase, at which point they were cooled to 8°C. Expression was induced with 0.5 mM isopropyl β-D-1-thiogalactopyranoside (IPTG), 5 µM geraniol and 5 µM farnesol overnight at 8°C and 200 rpm. Following induction, cells were pelleted and then lysed by sonication in a solution of 25 mM Tris pH 7.5, 250 mM NaCl, 1 mM $MgCl_2$, 10% v/v glycerol, 20 mM imidazole, 1 mM dithiothreitol (DTT), 1 mg/mL lysozyme, 200 µM phenylmethylsulfonyl fluoride (PMSF) 0.3 U/mL benzonase nuclease (Novagen), and EDTA-free protease inhibitor (Roche). 6-histidine tagged protein was purified from soluble lysate over Ni-NTA resin (Goldbio). The resin with bound protein was washed with 25 mM Tris pH 7.5, 250 mM NaCl, 1 mM $MgCl_2$, 10% v/v glycerol, 20 mM imidazole, 1 mM dithiothreitol (DTT). Bound protein was then eluted with 25 mM Tris pH 7.5, 250 mM NaCl, 1 mM MgCl2, 10% v/v glycerol, 300 mM imidazole, 1 mM dithiothreitol (DTT).

Next, the elutant was further purified over a HiLoad 16/60 Superdex 200 gel filtration column (GE Healthcare) using an AKTAExplorer 100 FPLC (GE Healthcare). The FPLC buffer was 250 mM NaCl, 25 mM Tris pH 7.5, and 1 mM $MgCl_2$, 10% glycerol v/v. Fractions enriched with *Pf*FPPS, as seen by a strong band at ~ 44 kDa on a Coomassie-stained SDS-PAGE gel, were pooled and concentrated by centrifugation using Amicon Ultra-15 centrifugal filter units (EMD Millipore). Concentrated protein was supplemented with 1mM DTT, was flash-frozen in liquid N_2, and was then stored at -80°C prior to use. Protein concentration was measured by a BCA protein assay kit (Thermo Scientific).

2.6.4. Isoprenyl pyrophosphate synthase assay

Following purification, release of pyrophosphate during GGPP/C20AlkOPP synthesis from FPP/C15AlkOPP by *Pf*FPPS was monitored using the EnzChek phosphate assay kit (Life Technologies), as previously described.[513] Reactions were performed in a 50 µL volume, with final reagent concentrations as follows: 250 mM NaCl, 50 mM Tris pH 7.5, 1mM $MgCl_2$, 1 U/mL purine nucleoside phosphorylase (PNP), 0.2 mM 2-Amino-6-mercapto-7-methylpurine riboside (MESG), 0.1 U/mL yeast inorganic pyrophosphatase (New England Biolabs), and 2 µM purified *Pf*FPPS, and, where indicated, 100 µM IPP, FPP (Echelon Biosciences) and/or C15AlkOPP. All reagents save *Pf*FPPS were pre-warmed to 37°C. Reactions were initiated by the addition of *Pf*FPPS, after which absorbance at 360 nm was recorded over a 30 min period with a BMG POLARStar plate reader preheated to 37 °C. Absorbance monitoring was performed in clear 96-well flat-bottomed plates. Enzyme reactions were linear with respect to time and enzyme concentration. Absorbance units were converted to µM phosphate using a phosphate standard curve.

2.6.5. Pull-down of labeled proteins

Protein lysates (1.5 mg/mL) from parasites treated with FSM and FPP or C15AlkOPP were subjected to click reactions with 100 µM biotin-N_3, 50 mM TCEP, 10 mM TBTA, and 50 mM $CuSO_4$ for 90 minutes at room temperature. Excess reagents were removed by protein

precipitation using 1 volume of chloroform, 4 volumes of CH_3OH, and 3 volumes of PBS. Proteins were precipitated in between two immiscible phases by centrifugation at 4,500 x *g* for 5 minutes. The aqueous layer was discarded and 4 volumes of CH_3OH was added, followed by centrifugation at 4,500 x *g* for 3 minutes to pellet the proteins. Proteins were dissolved in 1% SDS in PBS buffer (1.5 mg/mL) and incubated with 300 µL of NeutrAvidin® agarose resin (Thermo Scientific) for 90 minutes. Resin samples were washed to remove unbound proteins with 3-mL volumes of 3 × 1% SDS in PBS, 1 × PBS, 3 × 8 M urea, and 3 × 50 mM NH_4HCO_3. Resin was suspended in 300 µL of 50 mM NH_4HCO_3 and combined with 5 µg trypsin (sequencing grade, Promega Corp.) for overnight digestion at 37 ºC. Supernatants were collected by washing the resin with 200 µL x 4 of 50 mM NH_4HCO_3 and samples were lyophilized.

2.6.6. Sample preparation for MS/MS analysis

Lyophilized peptides were dissolved in 200 mM NH_4COO. Aliquots from resulting peptide solutions (20 µg) were obtained to prepare 0.25 µg/µL solutions. Each sample was loaded in SDB-XC extraction disk (3M, USA) packed in stage tips conditioned with 80% acetonitrile (ACN) and equilibrated with 200 mM NH_4HCO_2. Samples were washed with 200 mM NH_4HCO_2 and eluted into three fractions using 40 µL of 6%, 11%, and 17% ACN in H_2O. Each sample was dissolved in 100 µL of 5% ACN and 0.1% TFA in H_2O and loaded onto packed extraction disks in stage tips that were conditioned (80% ACN and

0.1% TFA in H_2O) and equilibrated (5% ACN and 0.1% TFA in H_2O). Peptides were eluted with 80% ACN with 0.1% TFA in H_2O, lyophilized, and dissolved in 0.1% formic acid.

2.6.7. LC-MS/MS analysis of tryptic digested peptides

LC-MS/MS analyses were carried out using an RSLCnano System (Dionex, UK) and an Orbitrap Fusion Tribrid mass spectrometer (Thermo Scientific). Samples were directly loaded and eluted at a flow rate of 300 nL/min onto a reverse-phase column (75 μm i.d., 450 mm) packed with ProntoSIL C18AQ 3 μm media (Bischoff, Germany) that was prepared in-house. The peptides were eluted with buffer A (0.1% formic acid in H_2O) and buffer B (0.1% formic acid in CH_3CN) in the following gradient segments of buffer B: 17 mins, 0-2%; 60 mins, 2-25%; 2 mins, 25-44%; 2 mins, 44-76%; 3 mins, 76%; and 2 mins, 76-2%. The eluted peptides from the column were sprayed into a nanospray ion source on an Orbitrap Fusion Tribrid mass spectrometer set to record single microscan FTMS scan events at a resolution of 30000 over the m/z range 300-1500 Da in positive ion mode, with charge states of 2-7 included. The top 15 data-dependent CID MS/MS were triggered from the FTMS scan and introduced into the Orbitrap- Fusion ion trap. The collision energy was set to 35% and activation Q to 0.25 with the scan range and ion trap scan rate both set to normal. The automatic gain control (AGC) target values were set to optimal conditions using 500,000 for MS1 and 5,000 for MS2.[514] Dynamic exclusion was allowed once for a 90-second duration.

2.6.8. Proteomic data processing

The .raw files were searched using Sequest embedded in Proteome Discoverer (version 1.4.0.288, Thermo Scientific) against the *Plasmodium falciparum* 3D7 isolate (ID UP000001450) appended with *Homo sapiens* (ID UP000005640) from UnipProtKB/SwissProt.[515] The precursor mass tolerance was set to 10 ppm and the fragment mass tolerance was set to 0.6 Da. A variable modification was set as oxidized methionine. The enzyme was set to Trypsin (Full) and up to 4 missed cleavages were allowed. A decoy search was also performed.

The resulting .msf files were processed in Scaffold (version 4.4.1, Proteome Software Inc., Portland, OR) through searching with X! Tandem (version 2010.12.01.1, GPM Organization). Glu → pyro-Glu of the N-terminus, ammonia-loss of the N-terminus, Gln → pyro-Glu of the N-terminus and oxidation of methionine were specified in X! Tandem. Peptide identifications were accepted if they could be established at greater than 95% by the Scaffold Local FDR algorithm. Protein identifications were accepted if they could be established at greater than 99.0% probability and contained at least 2 identified peptides. Protein probabilities were assigned by the Protein Prophet algorithm.[516] Proteins that contained similar peptides and could not be differentiated based on MS/MS alone were grouped to satisfy the principles of parsimony. Proteins sharing significant peptide evidence were grouped into clusters. Fold changes in enrichment between probe-treated and control samples were calculated using total weighted spectra; in cases where no spectral counts were observed (zero), those were imputated to a value of 1 in the Scaffold software for subsequent analysis.

Acknowledgements

This work is supported by the Children's Discovery Institute of Washington University and St. Louis Children's Hospital [MD-LI-2011-171], the National Institute of Allergy and Infectious Diseases at the National Institutes of Health [R01AI103280 and R21AI123808], the National Science Foundation [CHE-1308655], the March of Dimes [Basil O'Connor Starter Scholar Research Award], the Washington University Monsanto Excellence Fund and the Mass Spectrometry Core Facility of the Masonic Cancer Center, a comprehensive cancer center designated by the National Cancer Institute, supported by P30 CA77598. Kiall Suazo was supported by the Newman and Lillian Bortnick Excellence Fellowship in Chemistry from UMN Chemistry department. Kiall Suazo performed the bioinformatic analysis and proteomic experiments, as well as prepared table and figures. Chad Schaber performed the culture and metabolic labeling of the isoprenoid analogue in live *P. falciparum* as well as the kinetic assays. Charuta Palsuledesai, Audrey Odom-John, and Mark Distefano provided guidance in the design of the experiments. I would like to thank Shaoren Yuan for the probe synthesis and David Goldfeld for assistance in the bioinformatic analysis.

Chapter 3:Evaluation of alkyne-modified isoprenoid phosphate analogues and optimization of lovastatin treatment

3.1. Introduction

Protein lipid modifications, including prenylation, myristoylation and palmitoylation, are important for directing and stably anchoring proteins to cellular membranes as well as for protein trafficking and the facilitation of protein-protein interactions involved in cell signaling. In particular, protein prenylation involves the attachment of an isoprenoid onto a cysteine residue located near the C-terminus of a protein, recognized *via* a specific prenylation motif and results in the formation of a thioether bond.[77] Following prenylation, the protein undergoes further processing namely proteolysis of the C-terminal peptide and carboxymethylation to afford the mature protein (Fig. 3.1A). Many protein substrates for

prenylation have a tetrapeptide CaaX box

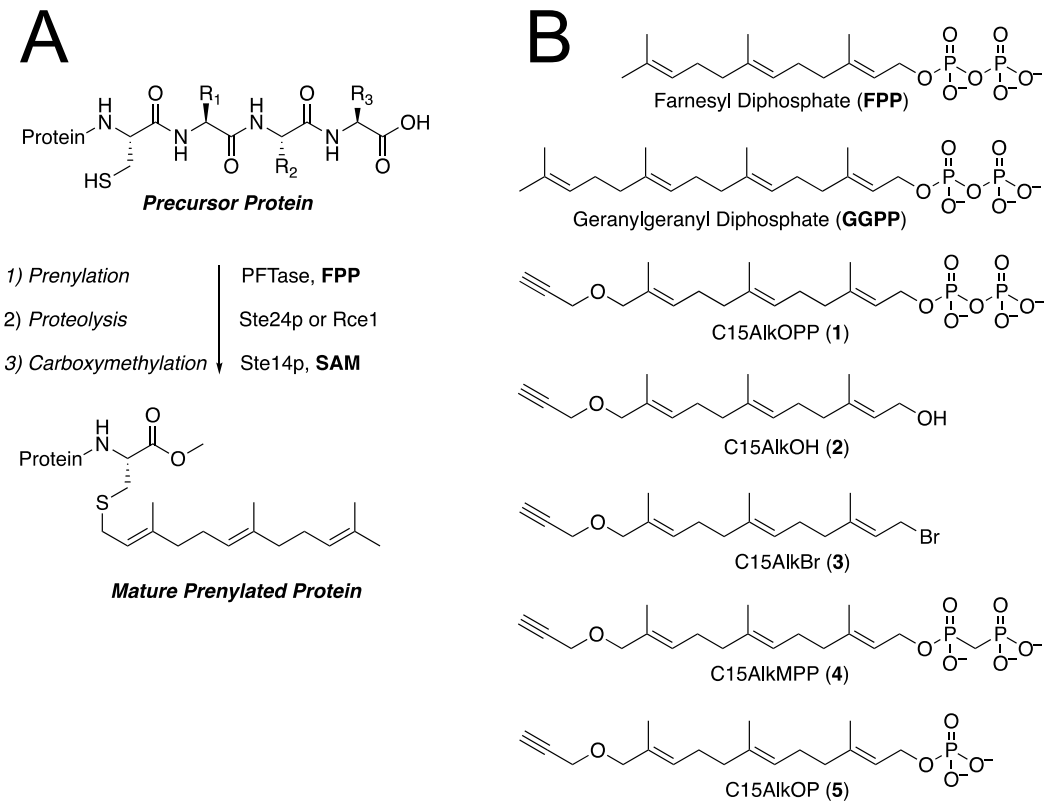

Figure 3.1. Schematic representation of the maturation of a farnesylated protein from a substrate with a CaaX box (A) and parent and analogue forms of isoprenoids (B).

motif that is either modified with a farnesyl or geranylgeranyl group from farnesyl- (FPP) and geranylgeranyl diphosphate (GGPP), catalyzed by farnesyltransferase (FTase) and geranylgeranyltransferase type I (GGTase-I), respectively.[326,327] Dual geranylgeranylation on two proximal cysteine residues near the C-terminus also occurs for some proteins with –CCXX, -CXC, or –CC motifs. [328] This process is catalyzed by geranylgeranyltransferase type II (GGTase-II) also known as Rab GGTase, in a process facilitated by rab escort protein (REP). Protein prenylation has been a target of interest for developing anti-tumor drugs, particularly in inhibiting the prenylation of Ras which is one of the most commonly

mutated proteins observed in cancer.[517] Changes in protein prenylation have also been implicated in a number of diseases including neurodegenerative disorders and progeria, and has served as an attractive drug target against microbial and viral infections.[11]

Several biochemical strategies have been developed to study prenylation. A number of these approaches rely on the use of chemically modified isoprenoid analogues that introduce bioorthogonal groups suitable for both *in vitro* and *in vivo* investigations.[16] Reports on functional groups used to modify isoprenoids include azides[350] and alkynes[345] for copper-catalyzed cycloaddition (click) reactions, aldehydes for oxime ligation[518] and photoactivatable benzophenones[519] and diazirines[336] for labeling of enzyme active sites. Some of these isoprenoid analogues have proved to be useful for biotechnology applications including enzymatic labeling for bioconjugation of proteins, DNA and nanostructures.[333,520,521] Aldehyde-functionalized isoprenoids not only allow site-specific labeling of proteins but also facilitate protein purification via capture and release strategies.[522,523]

To identify putative prenylated proteins and investigate changes in their levels of expression, metabolic labeling and subsequent bioorthogonal labeling has become one of the methods of choice.[118] In that strategy, synthetic analogues of biosynthetic precursors for post-translational modification bearing bioorthogonal functionality are added to the growth media from which they enter cells and become incorporated into proteins. Subsequently, the cells may be lysed and proteins bearing the analogues are then covalently modified using selective chemical reagents that react *via* bioorthogonal processes allowing

a variety of probes for visualization or enrichment to be attached for subsequent analysis.[524] Early work on the metabolic labeling of prenylated proteins employed azide-containing analogues.[342] However, due to the lower level of background labeling typically obtained with alkynes, more recent studies have used alkyne-containing isoprenoids.[525] The synthesis of C15AlkOPP (Fig. 3.1B) and its incorporation *in vitro* by protein farnesyltransferase was reported in 2007[345] followed by reports of its use in metabolic labeling in 2010.[353] Since that time, it has been employed for a variety of experiments including differential electrophoresis to study prenylation inhibitors[370], labeling of proteins sensitive to human pathogens[360] and the delineation of the prenylome of *Plasmodium falciparum*, the causative agent of malaria.[363,365] It has been demonstrated that a-factor, a farnesylated pheromone from yeast retains full activity when the farnesyl group is substituted with several chemically modified isoprenoids used for metabolic labeling. Those results suggest that such probes can be used without concern that they will cause undesired interference in normal cell physiology.[526]

The alkyne-modified farnesol analogue C15AlkOH (Fig. 3.1B) has been commonly used for probing prenylated proteins through metabolic labeling since it is commercially available.[353,360,527] The cellular machinery converts this analogue into the bonafide diphosphate analogue recognized by the prenyltransferase for prenylating protein substrates. The use of the diphosphate form has been gaining popularity in recent metabolic labeling experiments. However, it is believed that the diphosphate form intuitively exhibits lesser penetrability into the cells owing to the negative charges inherent to the diphosphate moiety, which may be electrostatically repelled by the negatively charged outer surface of

the cell membrane. While this is plausible, there has been no direct comparison of the labeling efficiency of these probes. The synthesis of the diphosphate form presents a number of challenges such as low yields, formation of monophosphate side product C15AlkOP (Fig. 3.1B) and instability to hydrolysis. It is not clear whether the alcohol form is first converted to a monophosphate form C15AlkOP or directly to the diphosphate form, and thereby poses the question whether C15AlkOP can serve as a substrate. Furthermore, a stable analogue of the diphosphate such as methylenebisphopsphonate C15AlkMPP (**4**) (Fig. 3.1B) may be suitable for metabolic labeling studies to label prenylated proteins

Statin treatment has been commonly used in metabolic labeling experiments with isoprenoid probe analogues.[353,360,379] Statins are a class of drugs that selectively inhibit the rate-limiting enzyme, HMG-CoA reductase, in the mevalonate-isoprenoid-cholesterol pathway.[356] Thus, these drugs reduce the biosynthesis of isoprenoid intermediates as well as the final product cholesterol. Statins have been successfully used to control plasma cholesterol levels and prevent cardiovascular disease.[528–530] The first statin, ML-236B (later known as compactin or mevastatin), was discovered by Akira Endo in 1976 from work with a penicillium mold.[531] This discovery stimulated the worldwide development of natural and synthetic HMG-CoA reductase inhibitors.[532] At present, the US Food and Drug Administration (FDA) have approved the use of seven statins: lovastatin, pravastatin, simvastatin, fluvastatin, atorvastatin, rosuvastatin, and pitavastatin.[533] Each of the statins has a characteristic structure that competes with HMG-CoA binding to HMG-CoA reductase (Fig. 3.2).[534] As a result, the enzyme activity of HMG-CoA reductase is inhibited and the biosynthesis of downstream molecules, including isoprenoids and sterols, is

blocked. Importantly, probe incorporation can also be enhanced by inhibition of the synthesis of the endogenous isoprenoid substrates farnesyl and geranylgeranyl diphosphate. Like fosmidomycin that enhanced probed incorporation by inhibiting the MEP pathway in the malaria parasite,[535] statins can be used to inhibit HMG-CoA reductase upstream in the FPP biosynthetic pathway in mammalian cells.[356]

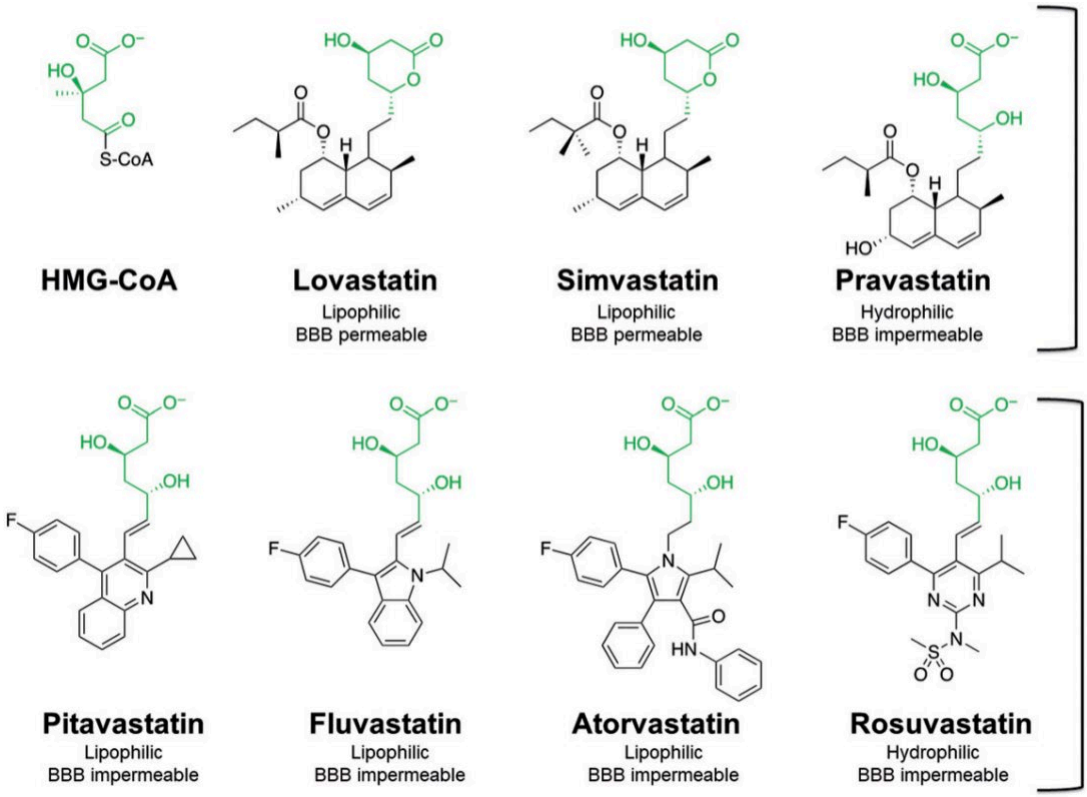

Figure 3.2. Structure of statins. The structure in green indicates the HMG-CoA like unit that binds to the enzyme HMG-CoA reductase.

3.2. Research Objectives

In this chapter, the labeling efficiency of the different phosphate forms of the alkyne-modified isoprenoid analogue were evaluated. These isoprenoid analogues were introduced

metabolically into COS-7 cells followed by in-lysate fluorophore conjugation *via* click chemistry and subsequent in-gel fluorescence analysis. Probes were added at different doses as well as at different incubation times. The optimal concentration of statins to enhance probe incorporation were also determined.

3.3. Results

3.3.1. Synthesis of isoprenoid probes

In synthesizing the phosphorylated analogues, C15AlkOH is first converted to the brominated form, C15AlkBr using tetrabromomethane (CBr_4) and triphenylphosphine via the Appel reaction. This compound, which has a limited shelf life, is then immediately transformed into the phosphate analogue using a specific phosphorylating reagent (Fig. 3.3). The synthesis of the diphosphate analogue C15AlkOPP is accomplished using the diphosphorylating reagent tris(tetra-*n*-butylammonium) hydrogen pyrophosphate [536]. However, it is commonly contaminated with the corresponding monophosphate form, C15AlkOP (**5**), due to the susceptibility of C15AlkOPP to hydrolysis. C15AlkOP is produced in significant amounts and is challenging to separate from C15AlkOPP as both products coelute in several fractions during HPLC purification. Since a substantial amount of the C15AlkOPP is contaminated with C15AlkOP, this analogues was also evaluated whether it could potentially serve as a probe in metabolic labeling experiments. If C15AlkOP can be used, the purification of C15AlkOPP will be greatly simplified and yields will be higher, as no separation of the two probes will be required. However, isolation of the pure fractions of monophosphate from diphosphate-monophosphate

mixture does not yield sufficient amounts for metabolic experiments. C15AlkOP was synthesized from C15AlkBr with no contamination with C15AlkOPP. The monophosphate reagent is first generated from phosphoric acid and tetra-*n*-butyl- ammonium hydroxide and subsequently reacted with C15AlkBr.[537]

An analogue of C15AlkOPP stable to hydrolysis was also desirable. Replacing the bridging oxygen between the two phosphorus atoms with a carbon may afford such stable isoprenoid analogue. Therefore, a hydrolytically resistant analogue C15AlkMPP containing a methylenebisphosphonate moiety was synthesized, guided by related procedures.[536,538] C15AlkMPP was synthesized using a methylenebisphosphonate reagent, which was first generated by combining methane diphosphonic acid and tetra-*n*-butyl-ammonium hydroxide and subsequently used to phosphorylate C15AlkBr.

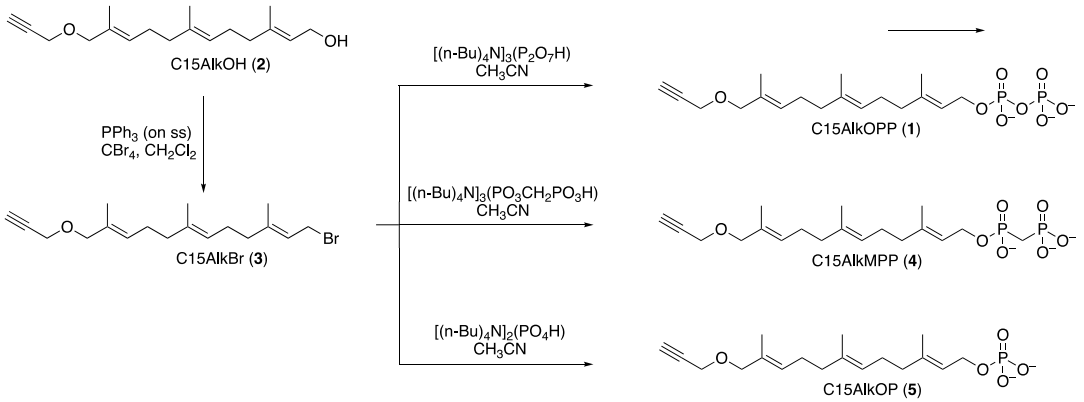

Figure 3.3. Schematic representation of the synthesis of the isoprenoid phosphate analogues starting from C15AlkOH (2) and the common precursor C15AlkBr (3).

3.3.2. Evaluation of labeling efficiency of isoprenoid analogues

The success of using alkyne-modified isoprenoid probes in metabolic labeling experiments was initially evaluated *via* click reaction with an azide-modified fluorophore followed by

in-gel fluorescence analysis. Labeled proteins appear as bands in the fluorescence scan due to the conjugated fluorophore. Additionally, treatment with inhibitors of the isoprenoid biosynthesis such as lovastatin [379] and fosmidomycin [363] are employed to reduce the pool of endogenous FPP and GGPP, thereby enhancing the incorporation of the isoprenoid probe to the prenylated proteins. Metabolic labeling was performed using the isoprenoid analogues C15AlkOH, C15AlkOPP, C15AlkMPP, and C15AlkOP in COS-7 cells in the presence or absence of lovastatin. In each case, the lysates obtained were subjected to click reaction with TAMRA-N_3 and proteins resolved using an SDS-PAGE gel and subjected to in-gel fluorescence analysis.

Using 10 μM probe and cell incubation for 24 hours (Fig. 3.4), protein labeling is apparent with all probes. These proteins may include Ras and Rab proteins near 25 kDa and DnaJ's and lamins near 50 and 75 kDa, respectively, as profiled from a mammalian macrophage using the C15AlkOH probe [360]. Although C15AlkOH was able to label these regions in COS-7 cells (lane 2) with dramatic improvement in the presence of 20 μM lovastatin (lane 3), improved labeling is achieved with the isoprenoid analogues C15AlkOP and C15AlkOPP (lanes 4 and 6), which is further enhanced by the addition of lovastatin (lanes 5 and 7). In contrast, the C15AlkMPP manifests minimal incorporation (lane 8) and requires lovastatin to induce more effective labeling. Some level of toxicity was also observed in cells treated with C15AlkOH and C15AlkMPP in the presence of lovastatin, manifested by the presence of dead cells, slower cell growth and lower yield of cell mass. Since lovastatin depletes the supply of native isoprenoids, the cell machinery relies on the

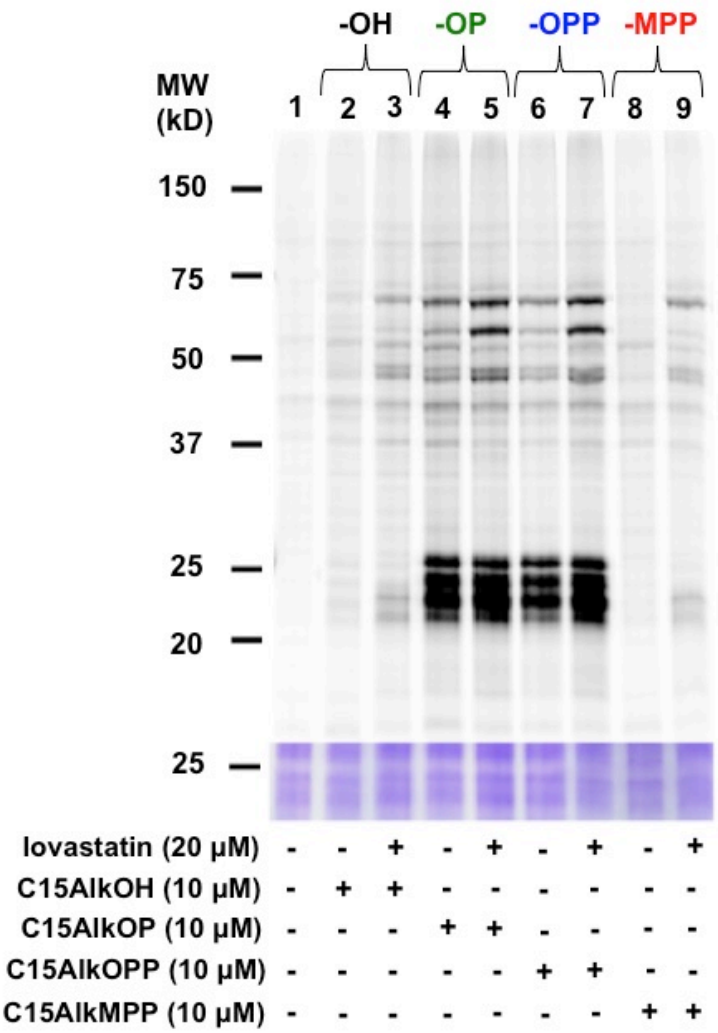

Figure 3.4. In-gel fluorescence analysis of prenylated proteins from COS-7 cells metabolically labeled with C15AlkOH, C15AlkOP, C15AlkOPP, and C15AlkMPP.

analogues being supplied to retain cellular processes unperturbed. Both C15AlkOPP and C15AlkOP may better mimic the natural substrates.

A dose-dependent experiment with varying concentrations of the probes at 0.1, 1, 10, and 25 μM was performed to evaluate to optimal concentrations needed to achieve sufficient labeling by each probe. In general, 10 μM probe treatment in the presence of lovastatin is optimal for sufficient labeling to be observed across all probes (Fig. 3.5 lanes

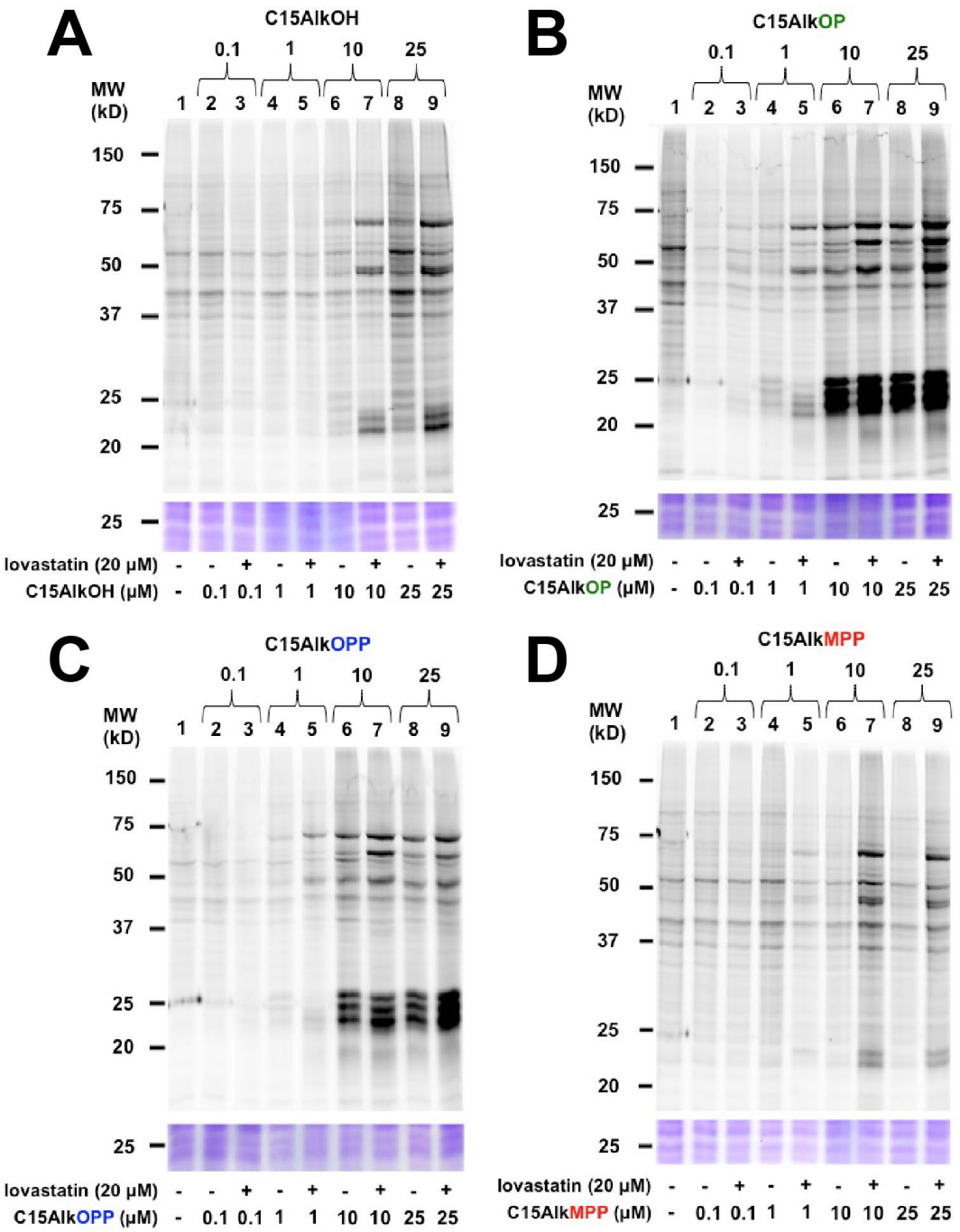

Figure 3.5. In-gel fluorescence analysis on the dose-dependent metabolic labeling of COS-7 cells with probes C15AlkOH (A), C15AlkOP (B), C15AlkOPP (C), and C15AlkMPP (D) at concentrations of 0.1, 1, 10, and 25 μM.

Probes were incubated with cells for 24 h after the cells are first pre-incubated in the presence or absence of 20 μM of lovastatin for 6 h.

A7, B7, C7, and D7). Labeling with C15AlkOH and C15AlkMPP shows lower efficiency compared to C15AlkOP and C15AlkOPP as evidenced by the intensity of the bands observed near 25, 50, and 75 kDa regions. Although not optimal, labeling can already be observed with 1 μM of C15AlkOP and C15AlkOPP in the presence of lovastatin (lanes B5 and C5) but not in C15AlkOH and C15AlkMPP (lanes A5 and D5). Both C15AlkOP and C15AlkOPP at 10 μM (lanes B6 and B7, and C6 and C7) did not necessarily require lovastatin to achieve excellent labeling. Interestingly, C15AlkMPP requires lovastatin for sufficient labeling to be observed. While it is a stable form of the diphosphate, removal of the methylenebisphosphonate group during the catalytic process might be challenging as the presence of carbon instead of oxygen alters the lability of the phosphate group carry the negative charges as it leaves the isoprenyl moiety. Therefore, competition with the endogenous isoprenoids is less feasible. The presence of statin may help in enforcing the prenyltransferase enzymes to utilize C15AlkMPP as the sole source of isoprenoid.

For the time-course experiments, labeling of proteins is already observable after 6 hours across all probes (Fig. 3.6). The C15AlkOH already achieved its maximum labeling capacity (Fig. 3.6A) while both C15AlkOP (Fig. 3.6B) and C15AlkOPP (Fig. 3.6C) require 12 hours to maximize protein labeling. The C15AlkMPP appears to perform best after a 24-hour incubation (Fig. 3.6D). These results suggest that both C15AlkOP and C15AlkOPP are efficiently metabolize by COS7 cells to tag the prenylated proteins.

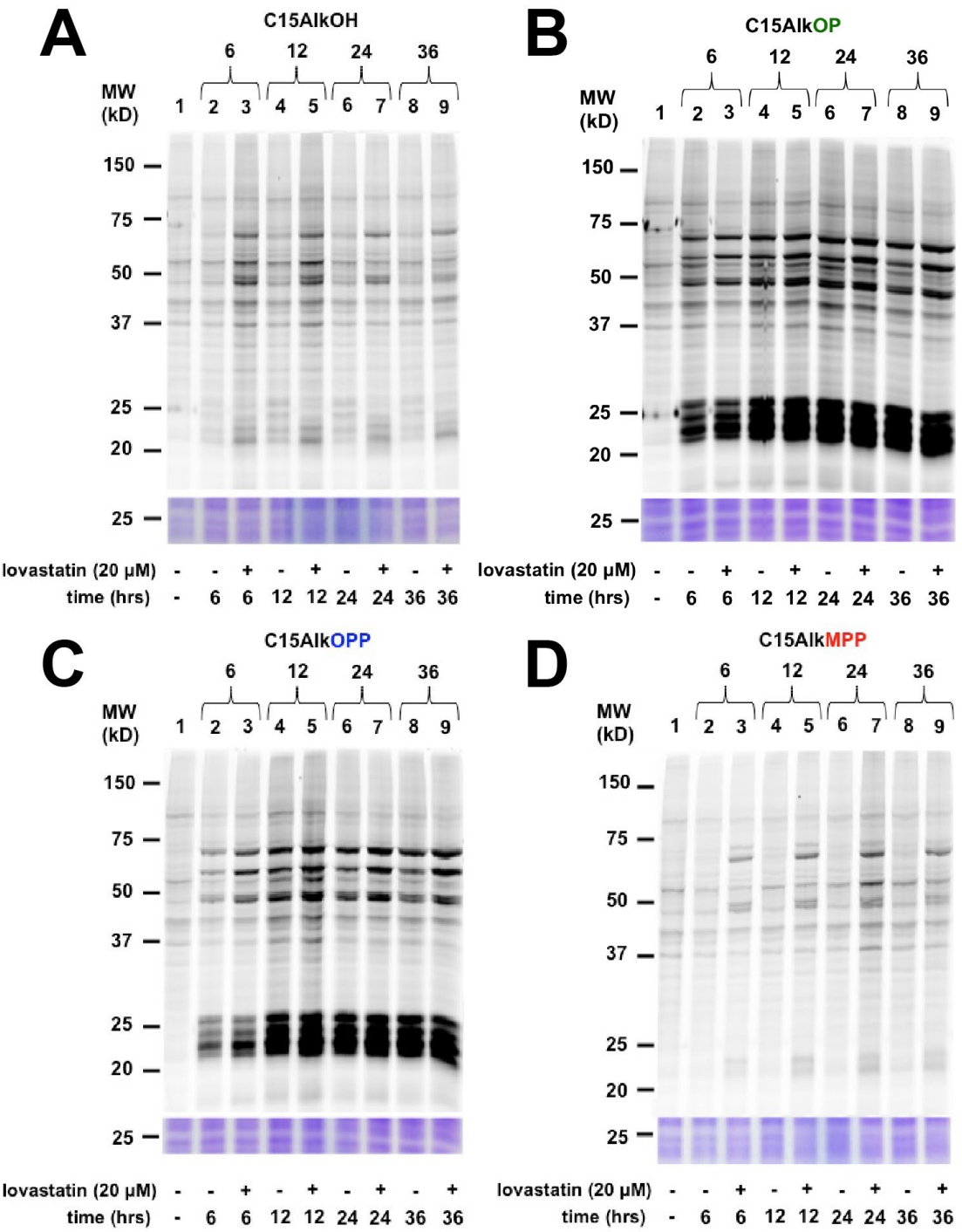

Figure 3.6. In-gel fluorescence analysis of the time-course of metabolic labeling of COS-7 cells with probes C15AlkOH (A), C15AlkOP (B), C15AlkOPP (C), and C15AlkMPP (D) incubated for 6, 12, 24, or 36 h.

Probes were added at 10 µM final concentrations for the times indicated in the presence or absence of 10 µM of lovastatin pre-treated for 6 h.

3.3.3. Optimization of lovastatin treatment to achieve maximum labeling efficiency

As observed in the previous section, the presence of lovastatin statin can significantly enhanced the labeling of the prenylated proteins. However, since inhibition of the mevalonate pathway not only depletes FPP and GGPP but also other compounds of biological significance such as squalene and cholesterol, multiple cellular processes may be perturbed. The pleiotropic effects (affecting multiple genes) of statins have beneficial effects in clinical trials such as lowering cholesterol levels in the blood.[539] However, in the context metabolic labeling experiments with the purpose of suppressing the pool of native isoprenoids, high concentrations of lovastatin is undesirable as it induces toxicity to cells under study.[540] The sensitivity of individual cell lines also vary[541], and thus optimal concentrations to be used in a specific cell line might require evaluation. An ideal concentration of the statin should promote significant enhancement of probe incorporation while maintaining low to no toxicity. Therefore, optimal statin treatment needs to be evaluated.

The probes C15AlkOH, C15AlkOP, and C15AlkOPP were evaluated for their labeling efficiency at constant 10 μM concentrations in COS-7 cells in the presence of varying lovastatin concentrations: 0.1, 1, 10, and 25 μM. C15AlkMPP was excluded from this analysis since it does not appear to achieve labeling substantial for downstream applications such as for proteomic profiling of prenylated proteins. Cells were pre-treated with lovastatin for 6 hours prior to the addition of probes. Pre-treatment is often employed to effectively reduce the pool of native isoprenoids before the probes are introduced, thereby assuring that prenylation substrates are unprenylated and available for probe

incorporation. Furthermore, retaining the lovastatin for longer periods of time may also induce cell death. To reduce potential toxicity by lovastatin, removal after pre-incubation may be beneficial. Therefore, removing lovastatin after pre-treatment was also evaluated.

Treatment with C15AlkOH (Fig. 3.7A) displays observable labeling at 1 μM lovastatin when the statin is retained (lane 5) in the culture media but not when it is removed (lane 4). At higher lovastatin concentrations (lanes 6-9), maximum labeling was achieved whether the statin was removed or not. Cells treated with C15AlkOP (Fig. 3.7B) and C15AlkOPP (Fig 3.7C) do not appear to depend significantly on the presence of lovastatin in enhancing probe incorporation. Cells treated with these probes in the absence of lovastatin (lane 1) display comparable labeling intensities in the 25 kDa region with all the lanes treated with lovastatin. However, the bands observed near 50 and 75 kDa regions, which are putatively farnesyltaed proteins, appear to achieve stronger intensities upon lovastatin treatment that saturates at 10 μM. Comparison of the extent of labeling of all three probes at 10 μM lovastatin (Fig. 3.7D) shows both C15AlkOP (lanes 4-6) and C15AlkOPP (lanes 6-9) attain superior labeling in contrast to C15AlkOH treatment (lanes 1-3). This is consistent with the previous observation that the phosphorylated analogues readily achieve excellent labeling of the prenylated proteins with minor enhancement upon statin treatment.

As mentioned previously, different cell lines may have varying responses to statins. While COS-7 displays superior labeling with C15AlkOP and C15AlkOPP but not with C15AlkOH, other cell lines may not behave similarly. Therefore, HeLa cells were

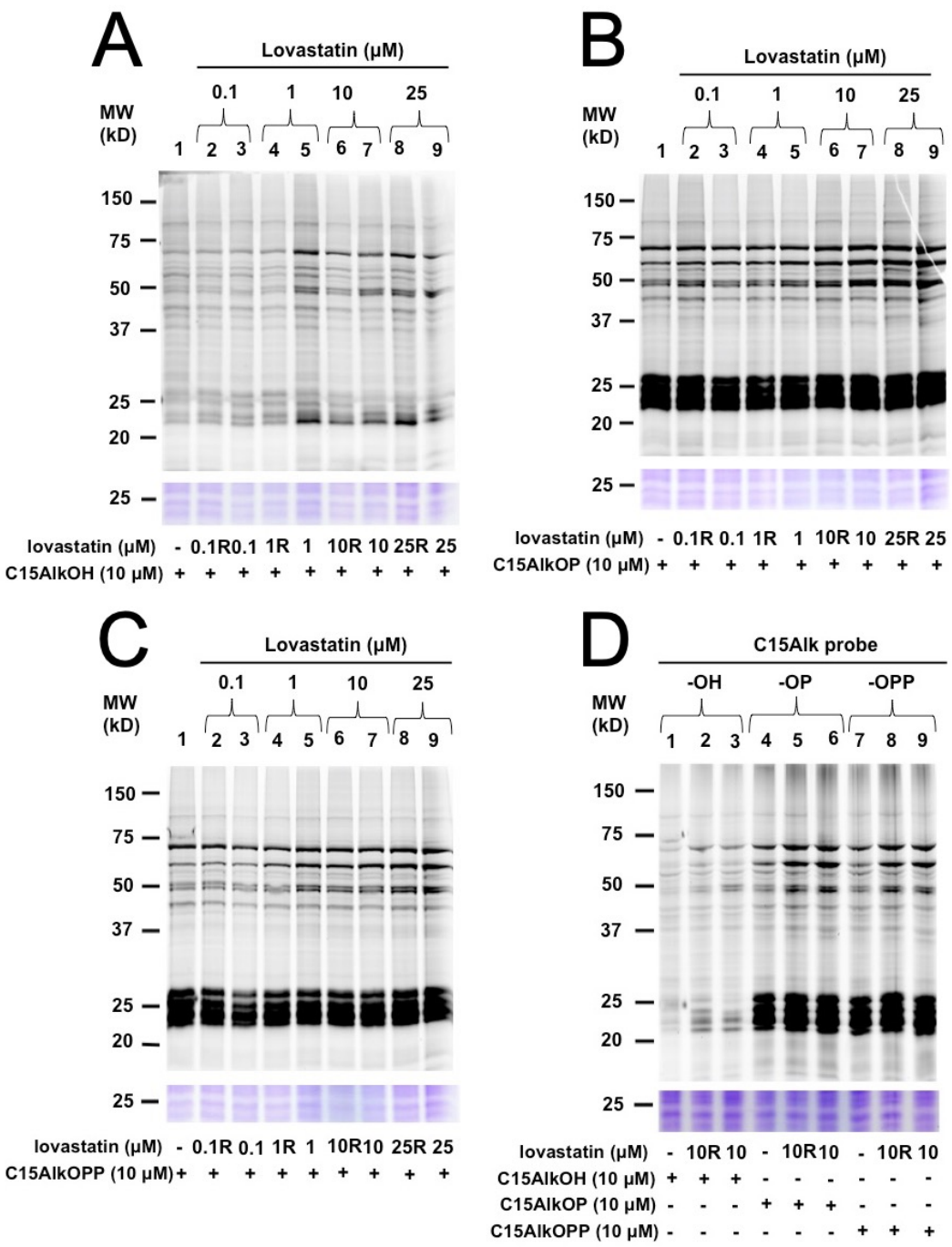

Figure 3.7. In-gel fluorescence of COS-7 cells treated with varying lovastatin concentrations and treated with C15AlkOH (A), C15AlkOP (B), C15AlkOPP (C) and a comparison of probe labeling at 10 μM with lovastatin at 10 μM (D).

The lovastatin was either removed (*e.g.* 10R) or present in the culture medium with the isoprenoid probe.

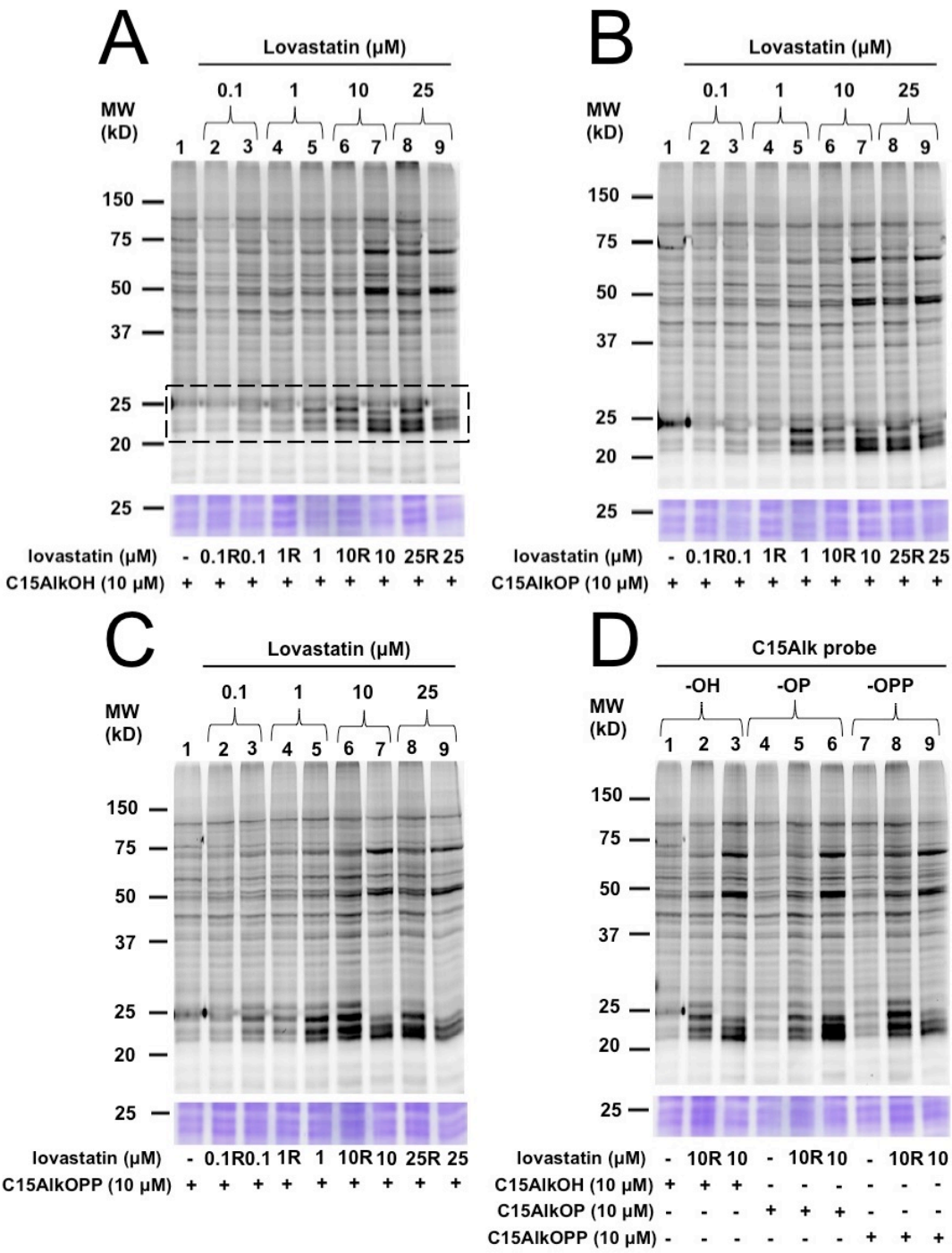

Figure 3.8. In-gel fluorescence of HeLa cells treated with varying lovastatin concentrations and treated with C15AlkOH (A), C15AlkOP (B), C15AlkOPP (C) and a comparison of probe labeling at 10 μM with lovastatin at 10 μM (D).

The lovastatin was either removed (*e.g.* 10R) or present in the culture medium with the isoprenoid probe.

subjected to the same analysis to evaluate the labeling of these probes under varying lovastatin concentrations (Fig. 3.8). Unlike COS-7 cells, HeLa exhibited lower probe incorporation as evidenced by labeling with C15AlkOH (Fig. 3.8A) attaining maximum labeling at 10 μM lovastatin when it was retained (lane 7). COS-7 cells already reached reasonable labeling with this probe at 1 μM. Treatment with C15AlkOP (Fig. 3.8B) and C15AlkOPP (Fig. 3.8C) do not display superior labeling, in contrast to the observations in COS-7 cells. Similar to C15AlkOH, labeling with the phosphorylated analogues saturated at 10 μM lovastatin retained in the culture medium (lane 7). A side-by-side comparison of all probes (Fig. 3.8D) indeed showed that the alcohol versus the phosphorylated analogues equally labeled the prenylated protein. Furthermore, an aberrant banding pattern was observed across all probe treatments. Removal of lovastatin results in enhanced labeling near 25, 50, and 75 kDa regions (lanes 2, 5, and 8). However, retention of the statin (lanes 3, 6, and 9) displays enhanced labeling near 50 and 75 kDa regions but results in more intense yet lesser number of bands near the 25 kDa region. This unexpected result is yet to be explored. The pleiotropic effects of statins have been described in the literature and perhaps these observed changes in the banding pattern may be a result of these effects.

3.4. Discussion

Early metabolic labeling work in the prenylation field used an azide-functionalized isoprenoid for metabolic labeling. Subsequent protein labeling in crude lysate was performed via Staudinger ligation reaction with a biotinylated phosphine reagent.[342] Due to the slow nature of the Staudinger ligation, more recent efforts have focused on using the copper catalyzed alkyne azide cycloaddition; in that case the alkyne group can be present

either on the probe for metabolic labeling or on the reagent used for biotinylation. Interestingly, it has generally been found that protein labeling with an azide-containing probe followed by derivatization with excess alkyne reagent leads to greater nonspecific background labeling than when the converse is performed.[525] Those observations led us to develop alkyne-containing probes including C15AlkOPP (**1**). Not surprisingly, we observed lower background labeling using C15AlkOPP compared with the corresponding azide.[353]

A second issue in the design of probes for metabolic labeling concerns their ability to freely enter cells and become incorporated into target proteins. For lipid modifications such as palmitoylation, probes are introduced as free fatty acids that must be activated within cells to their CoA-esters to be substrates for *N*-myristoyltransferase since the CoA-esters themselves are not cell permeable.[126] In contrast, isoprenoid analogues exhibit different behavior. While the mechanism is unclear, farnesyl diphosphate and related analogues are apparently able to directly enter cells even though they are negatively charged at physiological pH. Despite this fact, most metabolic labeling experiments have been performed using alcohol forms of alkyne analogues based on well established reports that farnesol is readily incorporated into prenylated proteins[346]; in that case, it is believed that such isoprenoid alcohols are converted by microsomal and peroxisomal farnesol kinase and farnesyl diphosphate kinase[347] to the metabolically active diphosphate form. The main reason why the alcohols have been used more often is that the synthesis of the diphosphates is low yielding and inconvenient. The diphosphate products are water-soluble and require reversed-phase HPLC for their purification. In addition, the diphosphates often undergo

some hydrolysis to the corresponding monophosphates, generating mixtures that are difficult to separate. It should be noted that the alcohol forms of isoprenoid analogues appear to exhibit some toxicity that limits the concentrations that they can be employed at and which in turn limits the efficiency of metabolic incorporation.[365]

Results from the dose-dependence study show that 10 μM probe treatment is optimal for sufficient labeling to be observed across all probes. Better labeling was achieved with C15AlkOP and C15AlkOPP. Both C15AlkOH and C15AlkMPP do not exhibit obvious protein labeling at this lower concentration. For the time-course experiments, labeling of proteins is already observable after 6 hours across all probes. The C15AlkOH already achieved its maximum labeling capacity while both C15AlkOP and C15AlkOPP can extend to longer period to maximize protein labeling.

We also explored the optimal concentrations of lovastatin to be used in enhancing probe incorporation. While it is beneficial to suppress the native production of isoprenoids, higher concentrations lead to cell death. The sensitivity of different cell lines to statins also vary and therefore careful selection concentrations of statins to be used in metabolic labeling experiments is essential. Our results provide insights into the appropriate amount of statins to be used. Indeed, using two different cell lines, we demonstrated that the response to lovastatin in improving the labeling of prenylated proteins can significantly differ. The differences in banding pattern observed may reflect the pleiotropic effects of statins that have been observed clinically. This observation may have uncovered an

unknown relationship between the regulation on a set of prenylated proteins and the inhibition of the mevalonate pathway through using statins.

Taken together, these results suggest that the use C15AlkOP and C15AlkOPP function best for metabolic labeling experiments. As both probes label prenylated proteins equally with high efficiency, there is no reason why either C15AlkOP or C15AlkOPP that is contaminated with some C15AlkOP cannot be used for metabolic labeling particularly when the goal of the experiment is simply to identify prenylated proteins (in contrast to experiments where the levels of prenylation are being investigated). Furthermore, treatment with lovastatin may not always be beneficial as maximum labeling efficiency may be readily achieved in some cell lines in the absence of statins.

3.5. Methods

3.5.1. General cell culture and metabolic labeling

Cells were maintained in Dulbecco's Modified Eagle's Medium (DMEM, Gibco) supplemented with 10% of fetal bovine serum (FBS, Gibco) and 1% penicillin-streptomycin (PenStrep, Gibco). A day prior to metabolic labeling, 9 x 10^5 cells were seeded in a 100-mm culture dish and grown overnight at 37 ^{o}C under 5% CO_2 in an incubator. Media was replaced and when indicated, cells were pre-treated with lovastatin for 6 hours and probes (C15AlkOH, C15AlkOP, C15AlkOPP, and C15AlkMPP) at varying concentrations. For samples where lovastatin was removed, the media in cells pre-treated with lovastatin were replaced with fresh DMEM with FBS and PenStrep and subsequently

treated with the probes. The lovastatin and probes were incubated with the cells for 24 hours except for time-course experiments where incubation periods were varied.

3.5.2. Sample preparation for in-gel fluorescence analysis

Treated cells were harvested by first washing with ice cold 1X PBS (8.1 mM Na_2HPO_4, 1.5 mM KH_2PO_4, pH 7.4, 137 mM NaCl, 2.7 mM KCl) and gentle scraping while suspending cells in 1 mL 1X PBS. Cells were pelleted by centrifugation at 180 *x g* for 5 minutes and supernatant was discarded. To each sample, 300 µL of lysis buffer (1x PBS, 1% sodium dodecyl sulfate (SDS), 2.4 µM phenylmethylsulfonyl fluoride (PMSF), 85 kU/mL benzonase nuclease, 1.5% (v/v) protease inhibitor cocktail) was added. Cell lysis was performed while samples were on ice using a stick sonicator pulsed 6 to 8 times for 2 seconds at 10-second intervals. Excess debris were removed by centrifugation at max speed (21,000 *x g*) for 5 minutes at 4 ^{o}C. Clarified lysates were quantified for their protein concentrations using BCA assay following the manufacturer's protocol.

3.5.3. In-gel fluorescence analysis

After the determining the concentration of the protein lysates, an aliquot containing 100 µg of protein were obtained and diluted to 92.5 µL with 1X PBS + 1% SDS. Click reagents were added as follows: 2.5 µL of 1 mM TAMRA PEG_3-N_3 (25 µM final), 2 µL of 50 mM TCEP (1 mM final), 1 µL of 10 mM TBTA (0.1 mM final), and 2 µL of 50 mM $CuSO_4$ (1 mM final). Samples were incubated in the dark with head-to-tail nutation for 1 hour.

Proteins were recovered by precipitation using ProteoExtract® protein precipitation kit by following the manufacturer's protocol. Protein pellets were dissolved in 1X Laemmli buffer and heated at 95 ^{o}C for 5 minutes. Samples were resolved in 12% SDS-PAGE gels (3" x 4" gel) 120 V until the tracking dye runs off. TAMRA fluorescence was detected using a Typhoon FLA 9500 fluorescence scanner (GE) at 542/568 excitation/emission wavelengths. Gels were stained wit Coomassie stain for 20 minutes and destained with destaining solution for 3 hours. Gel images were formatted by adjusting brightness/contrast on ImageJ. Imported images were further formatted on Microsoft Powerpoint.

3.6. Acknowledgements

I would like to thank the following for their contributions to this work: Alexander Hurben, Kevin Liu, and Pa Thao for synthesizing the probes C15AlkMPP, C15AlkOH, and C15AlkOPP; Sudheer Chava and Feng Xu for guiding the undergraduate students in synthesizing the probes; Mina Ahmadi for the assistance in performing the metabolic labeling experiments in HeLa cells particularly in optimizing the lovastatin concentrations; Ling Li and Mark Distefano for their guidance in conducting these evaluation and optimization experiments. This research was supported by the National Institutes of Health (GM084152 and AG056976) and the National Science Foundation (CHE-1308655).

Chapter 4: Metabolic labeling with an alkyne probe reveals similarities and differences in the prenylomes of several brain-derived cell lines and primary cells

4.1. Introduction

Post-translational modifications (PTMs) of proteins are important for regulation of their biological function, as well as in modulating enzymatic activities and cellular localization.[542] Among these modifications, protein prenylation is estimated to occur on 2% of the mammalian proteome, which is essential for stable anchoring of proteins to membranes, mediating protein-protein interactions, and protein trafficking.[543] Protein prenylation is the irreversible attachment of a farnesyl or geranylgeranyl group(s) onto a cysteine residue near the C-terminus of a protein. Farnesyltransferase (FTase) and geranylgeranyltransferase type 1 (GGTase-I) recognize the conventional CaaX-box prenylation motif (C = cysteine, a and X = any amino acid) and append a single isoprenoid from farnesyl diphosphate (FPP) and geranylgeranyl diphosphate (GGPP), respectively (Fig. 1 A).[326,327] Interestingly, recent studies have shown that extended $C(X)_3X$ motifs in model proteins can be farnesylated within cells[83], while shortened Cxx peptides are also acceptable FTase substrates *in vitro*.[84] Dual geranylgeranylation on a family of Rab proteins also occurs on C-terminal CCXX, CXC, or CC motifs catalyzed by rab

geranylgeranyltransferase (GGTase-II or RabGGTase).[328] Recently, a new GGTase (GGTase-III) has been identified with FBXL2 and Ykt6 as its only known substrates identified thus far.[108,383]

Inhibiting protein prenylation using prenyltransferase inhibitors (PTIs) has been of interest in clinical studies for potential anticancer therapies. In particular, inhibition of farnesylation using farnesyltransferase inhibitors (FTIs) of Ras protein and its oncogenic variants that drive tumor growth was initially the main focus of those studies. While these inhibitors failed in early clinical trials, they show great promise in precision medicine applications particularly when cancers can be linked to specific H-Ras mutations. A Phase 2 clinical trial using the FTI Tipifarnib for H-Ras-driven head and neck cancer is currently in progress.[544] The inhibitory effects of FTIs have also been found to be potentially useful for therapeutic applications in other diseases and pathologies where prenylation is required. These include neurodegenerative diseases, progeria, bacterial, viral, and protozoal infections.[11,104] Very recently, the use of the FTI Lonafarnib to inhibit the farnesylation of nuclear lamin was approved by the FDA for the treatment of Hutchinson-Gilford progeria syndrome.[105] Overall, these studies have made it clear that a better understanding of which proteins are actually prenylated is required to develop more effective therapeutic strategies.

Earlier methods to identify prenylated proteins relied on autoradiography techniques where tritiated forms of mevalonic acid, a precursor in isoprenoid biosynthesis, as well as [^{3}H]FPP and [^{3}H]GGPP were used to label prenylated proteins.[545–547] However, these methods are laborious, expensive, less sensitive, and often require longer periods of

exposure time. Immunological methods using isoprenoid-directed antibodies have not proved to be generally useful for prenylated protein identification and have only been used in a limited number of cases.[548,549] Related work with antibodies that target an aniline-containing analogue of FPP successfully identified 22 prenylated proteins.[338] Mass spectrometry-based chemical proteomics has emerged as a powerful tool to identify proteins with specific PTMs. For labeling of prenylated proteins, isoprenoid probes with small biorthogonal functionalities including azides or alkynes are metabolically introduced into cells of interest.[16,18,342,351,352] The cellular machinery incorporates these probes into the prenylated proteins in lieu of the native isoprenoids. Subsequent tagging through click reaction with a fluorophore or a biotin handle allows for selective detection and enrichment, enabling identification and quantitation of the prenylated proteins in a high throughput fashion. Initial efforts employed azide-functionalized isoprenoids[342,350] but in recent years a variety of alkyne-containing analogues have been prepared to capitalize on the lower background obtainable with those types of probes.[127,353]

4.2. Research Objectives

In this work, the use of the probe C15AlkOPP for metabolic labeling and identification of prenylated proteins in a variety of cells and primary cells is explored. First experiments in COS-7 cells were performed to determine how many prenylated proteins could be identified. Efforts to correlate those results with data reflecting substrate efficiency and protein expression levels are described. The result of using either MS2 or MS3 approaches for proteomic analysis is reported. Results from the COS-7 experiments were compared with similar data from HeLa cells to examine how the enrichable prenylated proteins vary

between cell lines. Finally, analysis of the prenylomes from three different brain-derived cell lines and primary astrocytes was performed to obtain a list of prenylated proteins whose levels can be quantified to study dysregulation of protein prenylation in brain-related diseases.

4.3. Results

4.3.1. Incorporation via metabolic labeling of C15AlkOPP varies in different cell lines

The probe C15AlkOPP bearing an alkyne functional group (Fig. 4.1A) has previously been shown to be efficiently incorporated via metabolic labeling into all three classes of prenylated proteins in a number of different individual cell lines.[353,363,550] However, to date, only limited comparisons between different cell lines have been made making it difficult to assess the generality of this approach.[353,366,379] To make that type of comparison here, the success of probe incorporation was first evaluated through in-gel fluorescence analysis. Cells were incubated with the probe, lysed and subjected to click reaction with TAMRA-N_3 through copper-catalyzed cycloaddition (Fig. 4.1B). Labeled proteins were resolved via SDS-PAGE and TAMRA fluorescence resulting from labeling of the prenylated proteins was detected. We have previously shown that using the free alcohol form of the probe (C15AlkOH), which is metabolically converted into its diphosphate form (the bonafide substrate for protein prenylation) results in less efficient labeling compared to incubation with the phosphorylated form (C15AlkOPP) in COS-7 cells based on in-gel fluorescence analysis.[550] Hence, efforts here focused on experiments with the diphosphate form.

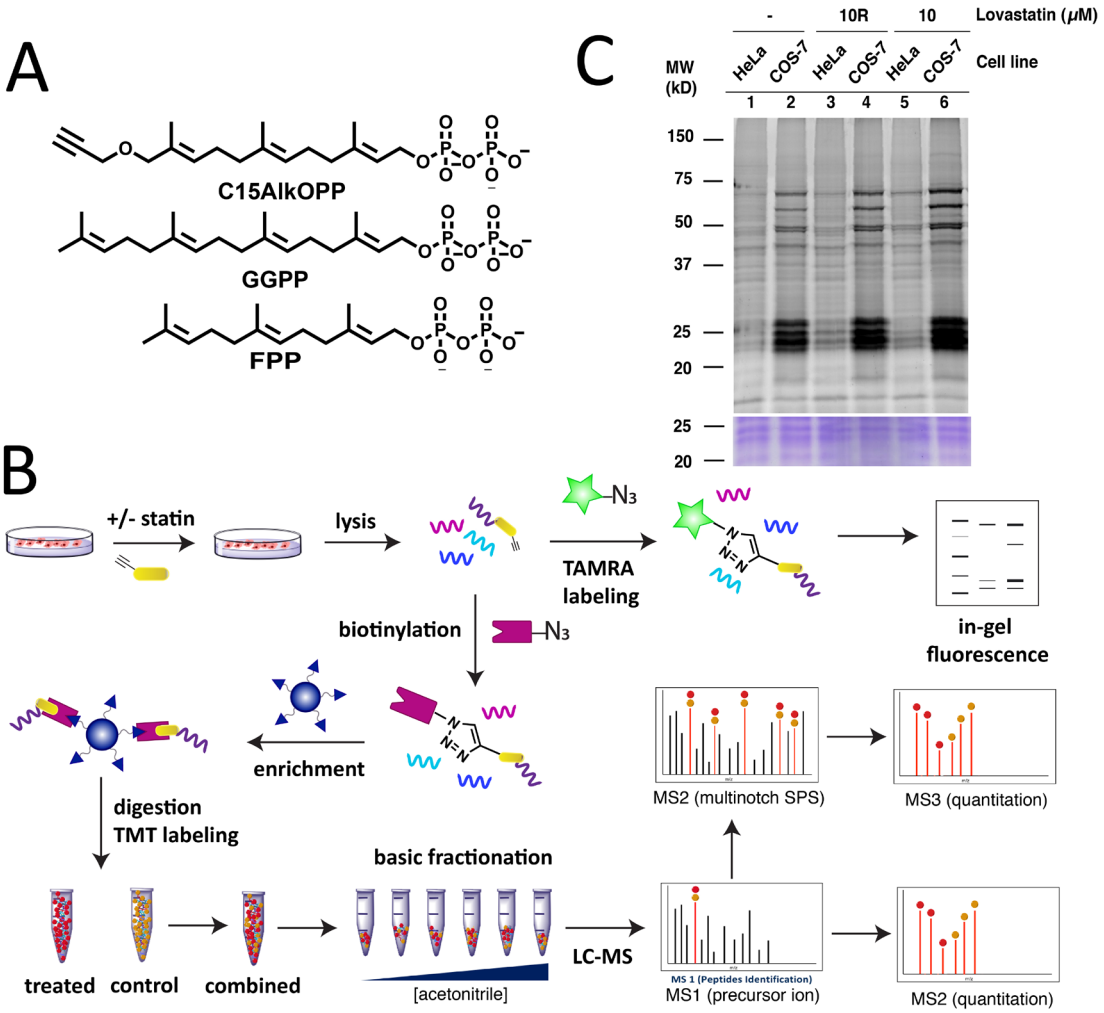

Figure 4.1. The probe C15AlkOPP allows labeling of prenylated proteins for detection and proteomic identification.

(A) Structures of the native isoprenoids FPP and GGPP and the alkyne-modified analogue C15AlkOPP. **(B)** Scheme for metabolic labeling with C15AlkOPP in cultured cells. Labeled prenylated proteins are detected through click reaction with a fluorophore and subsequent in-gel fluorescence analysis. Prenylated proteins are enriched through conjugation with biotin and subsequent pulldown with avidin beads. Isolated proteins are digested and peptides are labeled with TMT reagent for identification and quantitation through LC-MS/MS analysis. Quantitative proteomic analysis can be performed using MS2-based or multinotch SPS-MS3 approaches. **(C)** In-gel fluorescence analysis on COS-7 and HeLa cells treated with 10 μM C15AlkOPP. COS-7 cells display superior labeling compared with HeLa cells. The presence of 10 μM lovastatin enhances probe incorporation whether it is retained (10) or removed (10R) from the culture media during metabolic labeling.

Incubation of cells with 10 μM C15AlkOPP for 24 hours is sufficient to achieve maximum label incorporation; while labeling can be increased using higher probe concentration, that

increase is offset by greater background labeling.

Enhancing the labeling of prenylated proteins can often be achieved through suppression of the native production of FPP and GGPP using various statins or fosmidomycin in organisms that lack the mevalonate pathway.[357,363] In general, it is important to optimize the statin concentration used since there is a balance between improving label incorporation and cellular toxicity due to the statin. Moreover, various cell lines may respond differently to statins[551] and optimization of statin treatment may be required for effective labeling of prenylated proteins in a given cell line. Previous results with COS-7 and HeLa cells showed that 10 μM lovastatin augments label incorporation with no apparent toxicity;[357] hence, that concentration was used throughout the experiments reported here. Using COS-7 cells, some enhancement of labeling was observed in the 25, 50, and 75 kDa regions in cells pre-incubated with 10 μM lovastatin for 6 hours followed by probe treatment (Fig. 4.1C, lane 6) compared to without lovastatin treatment (Fig. 4.1C, lane 2); however, in this cell line, that increase was relatively modest. Interestingly, we have observed that lovastatin induces some level of toxicity in cells when left in the culture media for longer periods of time. Accordingly, we evaluated the effect of removing the lovastatin after pre-incubation prior to probe treatment (Fig. 4.1C, lane 4). This resulted in only a minor decrease in labeling compared with that obtained when lovastatin remained present during metabolic labeling. Overall, the effects of lovastatin on metabolic labeling in COS-7 cells are modest.

In contrast, different results were obtained in HeLa cells. In a side-by-side comparison of metabolic labeling in COS-7 and HeLa cells in the presence (Fig. 4.1C lanes 3 and 5) or absence (Fig. 4.1C, lane 1) of lovastatin, there is clearly less overall labeling in HeLa cells. Regardless of whether the lovastatin is retained or removed in the culture media, it does not increase labeling in HeLa cells to the level observed in COS-7. However, the presence of the statin in HeLa cells does modestly increase the level of probe incorporation relative to that observed in the absence of the statin (compare lane 1 with lanes 3 and 5 particularly in the 25 kDa region). Additionally, statin removal prior to metabolic labeling does appear to alter the pattern of bands observed in the 25 kDa region with fewer labeled bands being seen when the statin remained present during metabolic labeling. This is consistent with previous results reported with HeLa cells and may reflect the effects of statin toxicity or a different pleiotrophic mechanism. Given the goal of identifying a maximal set of prenylated proteins (prenylome) in a mammalian cell line, COS-7 was chosen for subsequent prenylomic analysis due to its superior labeling with C15AlkOPP.

4.3.2. Quantitative prenylomic analysis in COS-7 cells identifies approximately 80 different protein groups

To perform the prenylomic analysis (Fig. 4.1B), COS-7 cells were pre-treated with lovastatin followed by the addition of C15AlkOPP or FPP as a control and incubated for another 24 hours with lovastatin retained in the media. FPP was included in the control (instead of vehicle alone), to offset any potential physiological effect of added isoprenoid

diphosphate and to reverse perturbations caused by the presence of the statin. Labeled protein lysates from triplicate samples were subjected to click reaction with biotin-N_3 to selectively enrich the labeled prenylated proteins through incubation with avidin beads. The beads were washed under stringent conditions to remove non-specifically bound proteins and the resulting immobilized proteins were digested on-bead using trypsin. Equal amounts of the collected tryptic peptides were subjected to TMT-labeling and combined. Samples were fractionated under high pH reversed-phase conditions at different acetonitrile concentrations to decrease the sample complexity. Each fraction was then analyzed via LC-MS followed by database searching and statistical analysis to identify the enriched prenylated proteins. Since the prenylated peptides remain bound to the avidin resin after proteolysis, protein identification was based on the enrichment and identification of other peptides derived from individual proteins. Efforts to identify proteins based on specific prenylated peptides have not been generally successful although several methods to accomplish that are currently being explored.[366,378]

Initially, a multinotch SPS-MS3 approach was employed to limit ion interference and achieve more accurate and precise quantitation of the detected peptides across a two-hour LC gradient.[552] In this approach, the precursor ions from MS1 are fragmented in MS2 and synchronously selected precursors (SPS) from MS2 are further fragmented at the MS3 level where the reporter ions are detected. Using this method, 78 protein groups containing putative prenylation motifs were identified to be statistically enriched from the C15AlkOPP-treated samples (Fig. 4.2A, Appendix Table A1). Most of these proteins are currently annotated or were reported to be prenylated in previous prenylomic

studies.[353,360,366] In enriching prenylated proteins, previous studies using a similar approach identified other proteins that do not bear prenylation motifs.[360,366] These can be proteins that are known to interact with the prenylated proteins that survive the enrichment step after washing. In our analysis, in addition to the 78 protein groups mentioned above, we also enriched five proteins known to interact with prenylated proteins: PIK3C2A, CD9, and UBA52 (interact with Rabs), KRIT1 (interacts with Rho GTPases), and ASPM (interacts with farnesylated proteins CENPF and LMNB1). This indicates that in the approach described, a small number of proteins obtained from the analysis (6%) are not prenylated proteins but are known interacting partners. In the absence of statin, a related set of 59 protein groups of statistically enriched prenylated proteins were identified. The vast majority of the prenylated proteins detected in the absence of statin were also observed in the presence of statin although there were three protein groups (RRAS2, RAB12, RAB43) that were unique to samples that were not pretreated with statin. Given the results from gel-based experiments showing that lovastatin enhances probe incorporation, it was not surprising that the enrichment fold-changes of the prenylated proteins were indeed higher when the cells were pre-incubated with lovastatin (Fig. 4.2B). Interestingly, it was found that enhanced labeling in the presence of statin was more pronounced for farnesylated proteins compared to geranylgeranylated type-I substrates and Rab proteins (Fig. 4.2C).

An important question concerning this experimental approach is what parameters control the enrichment and hence detection of prenylated proteins in metabolic labeling experiments? In an effort to determine the factors that influence the extent of enrichment

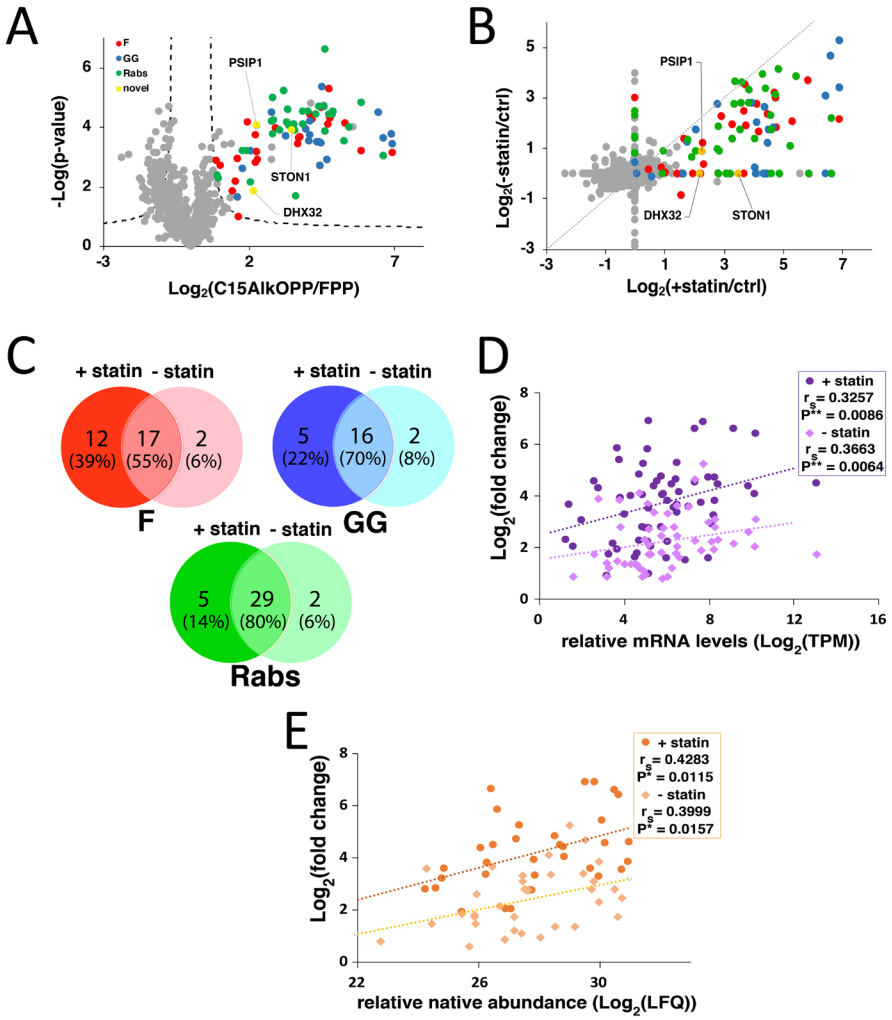

Figure 4.2. A higher number of prenylated proteins were identified when metabolic labeling was performed in the presence of lovastatin.

(A) A volcano plot (FDR = 0.01, s0 = 0.5) showing the statistically enriched prenylated proteins identified in COS-7 cells from triplicate samples (red : farnesylated; blue : geranylgeranylated; green : rab proteins). **(B)** Fold-change correlation plot between the prenylated proteins identified in the presence or absence of lovastatin. **(C)** Venn diagrams displaying the number of proteins from the three classes of prenyltransferase substrates identified in the presence or absence of lovastatin. Protein groups were separated into individual proteins. **(D and E)** Correlation between the enrichment fold-change and relative mRNA levels **(D)** or native abundances **(E)** of GGTase-I substrates and Rab proteins identified in the presence or absence of lovastatin. A significant positive correlation ($p < 0.05$) determined by Spearman's rank-order correlation was observed in the presence or absence of lovastatin.

for individual prenylated proteins, the correlation between the enrichment fold-changes and several parameters reported in the literature were explored. Such factors describe the

propensity of these prenylated proteins to serve as substrates for prenylation. To account for the abundance of each prenylated protein, the mRNA levels of proteins (expressed as transcripts per million reads, TPM) were measured in COS-7 using next-generation sequencing. The values were used to normalize the enrichment fold changes of each prenylated protein and the resulting products were log-transformed. The relationship between enrichment fold-changes of farnesylated proteins and their predicted farnesylation scores (based on their C-terminal CaaX-box motifs) using two different methods was first investigated. In one analysis, the farnesylation scores obtained from Prenylation Prediction Suite (PrePS),[81] an online web-based tool containing a database of prenylated proteins across sequenced genomes, were plotted against the normalized fold changes of the farnesylated proteins identified (Fig. 4.3A). Another set of predicted farnesylation scores derived from a structure-based scheme for prediction of peptide binding (FlexPepBind) developed by Furman and coworkers[329] was used to assess their correlation with the enrichment fold-changes (Fig. 4.3B). In both analyses, no apparent relationship was observed between the extent of enrichment of farnesylated proteins and their predicted probability as efficient substrates for farnesylation, either in the presence or absence of lovastatin. For GGTase-I and Rab substrates, the reported relative efficiency of geranylgeranylation of their C-terminal peptides[553] and the percent Rab prenylation efficiencies[99] determined *in vitro*, respectively, were used (Fig. 4.3C and 4.3D). In the case of Rab proteins, the normalized fold change values of those that contain two prenylatable C-terminal cysteines were divided by 2. Again, no clear correlation between the extent of enrichment of individual prenylated proteins and their measured prenylation efficiencies was observed. Intriguingly, proteins sharing the same C-terminal CaaX-box motifs

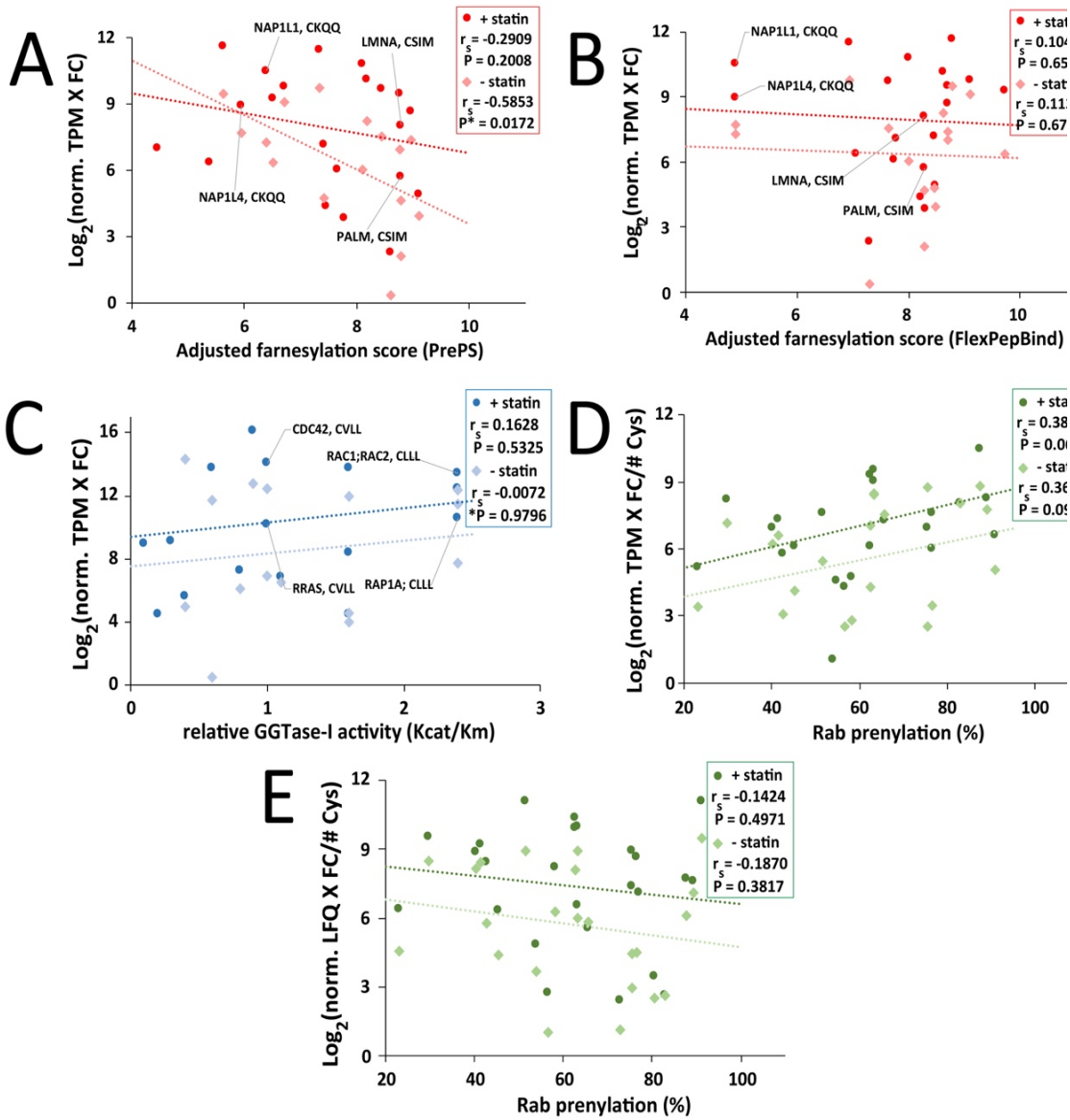

Figure 4.3. Exploring the factors affecting prenylation efficiency.

Dependence of normalized enrichment fold-changes on farnesylation scores from PrePS **(A)** and FlexPepBind **(B)**, GGTase activity using peptide substrates **(C)** and percent prenylation of Rab proteins *in vitro* **(D)** and **(E).** No significant correlation was observed between enrichment fold-changes and these parameters. The mRNA levels (TPM) were used to normalize the enrichment fold changes in A-D while the native abundances (LFQ) were used for E. The number of prenylatable cysteines in Rab proteins were also accounted for in the normalization.

exhibited notable differences in enrichment including PALM and LMNA (CSIM), NAP1L1 and NAP1L4 (CKQQ), CDC42 and RRAS (CVLL), and RAP1A and RAC1 (CLLL) (Fig. 4.3A, 4.3C). Importantly, LMNA is derived from the maturation of prelamin

A, where the farnesylated C-terminal peptide is cleaved off.[554] The loss of the prenylated peptide will impact the native abundance of LMNA available for enrichment, as only the premature LMNA bears the tagged isoprenoid analogue. Such additional processing clearly complicates subsequent analysis.

A large fraction of prenylated proteins belong to the family of small GTPases that have molecular weights of approximately 25 kDa. This is strikingly illustrated by the intense labeling observed in the 25 kDa region of gels analyzed via in-gel fluorescence (Fig. 4.1B). To investigate a possible correlation between the extent of enrichment in a prenylomic metabolic labeling experiment and protein abundance, a quantitative proteomic analysis of the 25 kDa region was performed. Lysates from COS-7 cells cultured in the presence or absence of 10 μM lovastatin were resolved via SDS-PAGE and the proteins in the 20 to 30 kDa region were excised and prepared for label-free quantitative proteomic analysis. The relative native abundances from triplicate samples were measured as label-free quantitation (LFQ) intensities and were used to normalize the enrichment fold-changes. There was no correlation observed between the normalized fold enrichment fold changes and Rab prenylation efficiency (Fig. 4.3E).

We next sought to determine whether protein abundances influence the enrichment fold-changes. Instead of using the mRNA levels or native abundances for normalization, we investigated the direct dependence of the observed enrichment fold-changes on these measures of relative protein abundance. Interestingly, a statistically significant dependence of the enrichment fold-changes with their respective expression levels and native

abundances in the presence or absence of lovastatin was observed (Fig. 4.2D and 4.2E). This observation suggests that the enrichment of prenylated proteins obtained using metabolic labeling may be correlated with their inherent expression levels and native abundances under the conditions the probe labeling is performed. Exogenous treatment with isoprenoids or statins is known to alter expression levels of proteins, including some members of the Ras and Rho proteins that are prenylation substrates.[555,556] We compared the native abundance of the prenylated proteins in the 25 kDa region in COS-7 cells in the presence or absence of lovastatin (Fig. 4.4). The abundances of most of these proteins did not significantly change in the presence of lovastatin except for RhoB. Interestingly, that protein was previously reported to be sensitive to statin treatment, however, exogenous supplementation of isoprenoids can reverse the upregulation of Rhob induced by lovastatin.[555,557] As commented above, it is important to note that the control samples used in the profiling experiments described here were also treated with lovastatin and FPP, and hence dysregulatory effects of statins and isoprenoid diphosphates on expression levels of prenylated proteins are accounted for when the enrichment fold changes are calculated to determine the statistically enriched prenylated proteins in the C15AlkOPP-treated samples.

While the multinotch SPS-MS3 approach employed on isobarically tagged peptide samples provides a more accurate quantitation of the identified proteins, the current instruments equipped with this capability are more expensive and hence often less accessible. Simpler but less sensitive orbitrap mass spectrometers capable of MS2-based identification and quantitation of proteins from TMT-labeled peptides are often more readily available. They should suffice for proteomic profiling studies when quantitative

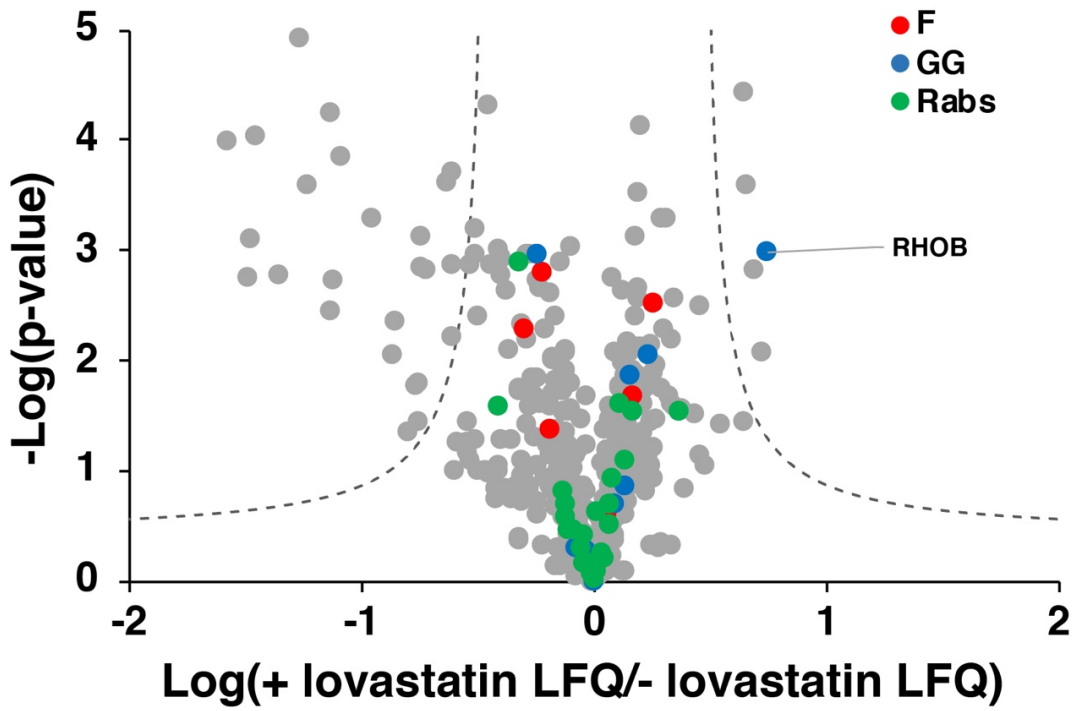

Figure 4.4. Comparison of native abundance of proteins near the 25 kDa region of samples from COS-7 in the presence or absence of lovastatin.

accuracy is not required. Accordingly, the samples described above were analyzed using a less sensitive orbitrap instrument and the reporter ions at the MS2 level were used to quantify the identified prenylated proteins. A total of 79 protein groups of putative prenylated proteins were identified in the presence of lovastatin. For most prenylated proteins identified, the enrichment fold-changes were higher in the multinotch SPS-MS3 approach compared to the MS2-based analysis (Fig. 4.5A). The wider dynamic range of enrichment fold-change values obtained from the SPS-MS3 approach illustrates its superior quantitative accuracy over the MS2 approach. Nevertheless, while differences between the two data sets were observed, 80% of the prenylated proteins were detected using either of the MS approaches (Fig. 4.5B). Such variation is common in proteomic experiments using different LC-MS instruments.[558] We further examined if the enrichment fold-changes of the identified small GTPases and Rabs correlate with their relative native

abundances in COS-7 treated with lovastatin (Fig. 4.5C). In contrast to the SPS-MS3 approach, we did not observe a correlation of the Log_2(fold changes) obtained from our MS2 approach with their relative native abundances. Thus, it appears that the lesser

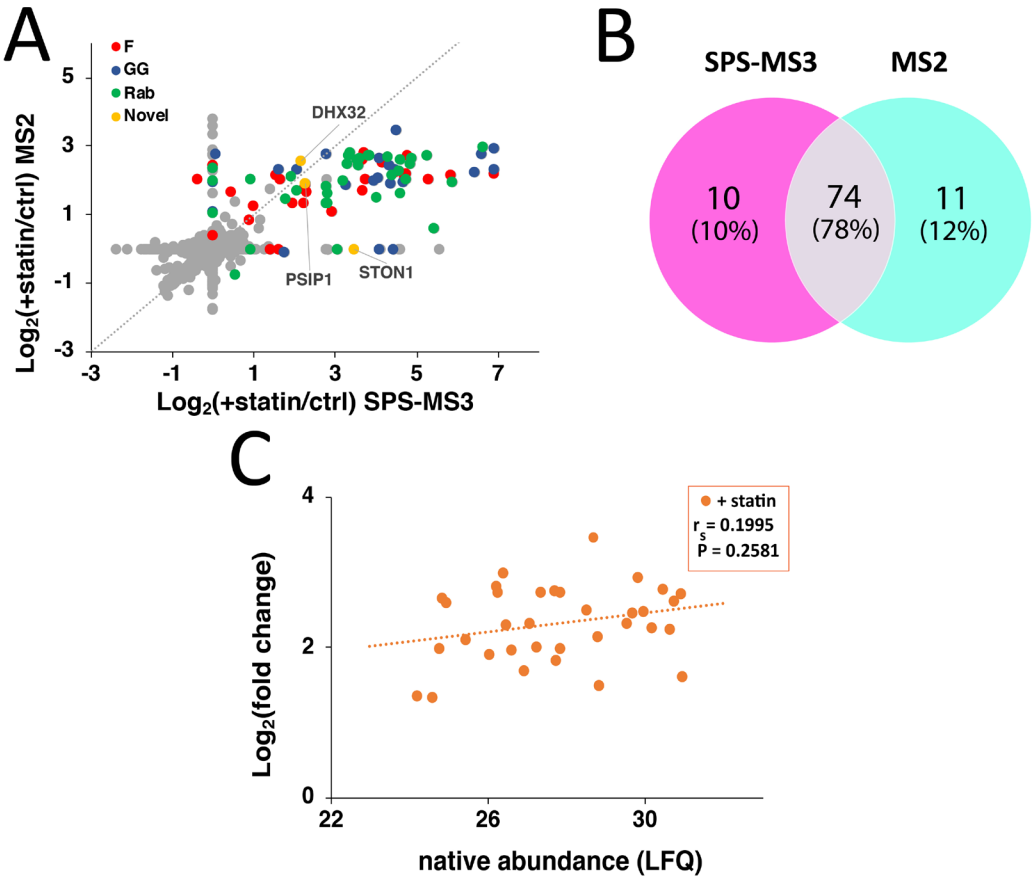

Figure 4.5. Comparison of the prenylated proteins identified from multinotch SPS-MS3 and MS2-based approaches.

(A) Fold-change correlation plot of the prenylated proteins identified from multinotch vs MS2-level quantitative proteomic analyses. A wider dynamic range was observed employing the multinotch approach. **(B)** Summary of the number of individual prenylated proteins identified from the two approaches. Protein groups were separated into individual proteins. A similar number of proteins were identified with good overlap. **(C)** Correlation between the enrichment fold-change and relative native abundances of GGTase-I substrates and Rab proteins from MS2-based analysis on COS-7 in the presence of statin. No statistically significant correlation was observed.

quantitative accuracy of the MS2-based analysis using the less expensive orbitrap instrument may provide less accurate data for the extent of enrichment and therefore complicates efforts to observe a possible correlation between enrichment and native abundance.

4.3.3. The prenylated proteins identified in HeLa cells are a subset of those observed in COS-7 cells

In the fluorescent gel-based experiments described above, the labeling efficiency in HeLa cells using the C15AlkOPP probe was significantly less than that in COS-7 cells (Fig. 4.1B). Albeit less pronounced, the banding pattern observed in the 25, 50, and 75 kDa regions in these two cell lines are similar. We speculated that this less efficient labeling in HeLa cells might only result in lower enrichment fold-changes but would not affect the number of prenylated proteins that could be enriched. Therefore, a proteomic analysis of the prenylated proteins in HeLa cells treated with C15AlkOPP in the presence of lovastatin using a MS2-level approach was performed. Although less accurate, this should suffice for profiling to provide the identities of the prenylated proteins labeled in cells. A total of 28 prenylated protein groups were statistically enriched in HeLa cells (Fig. 4.6A), approximately one-third of those profiled from COS-7 cells using the same LC-MS method and instrument. When the identities of these prenylated proteins categorized into the three classes of prenylation substrates were compared, we found that across all three classes, the set of prenylated proteins identified in HeLa is a subset of those identified in COS-7 cells (Fig. 4.6B). These were equally divided among the three classes and corresponded to less

than 50% of those identified in COS-7. Furthermore, the prenylated proteins in HeLa generally possessed lower enrichment fold-changes compared to those from COS-7 cells (Fig. 4.6C). Therefore, the reduced labeling efficiency in HeLa not only results in diminished enrichment fold-changes but also impacted the number of enriched prenylated proteins detected.

Since a lower number of prenylated proteins were identified in HeLa cells, we speculated that these might correspond to the most efficiently labeled proteins in COS-7. Accordingly, the enrichment fold-changes of the prenylated proteins identified in both HeLa and COS-7 cells in each class of prenylation substrates were determined. Those identified in COS-7 were ranked in decreasing order of enrichment fold-change and plotted along with the corresponding prenylated proteins identified in HeLa. For both GGTase-I substrates and Rabs, the prenylated proteins identified in HeLa were distributed across the range from the most to least enriched prenylated proteins in COS-7 cells, showing no apparent relationship (Fig. 4.7A and 4.73B). Interestingly, the farnesylated proteins identified in HeLa are among the most highly enriched farnesylated proteins in COS-7 (Fig. 4.6D). This set of farnesylated proteins was also readily identified in COS-7 without statin treatment from the prenylomic analysis performed using SPS-MS3, which generally exhibited enhanced enrichment fold-changes in the presence of lovastatin. These proteins are perhaps the most efficiently farnesylated inside cells. To better understand this, we examined whether the C-terminal CaaX-box motifs of these farnesylated proteins in HeLa cells have predicted higher farnesylation scores (Fig. 4.7C). While most of these proteins

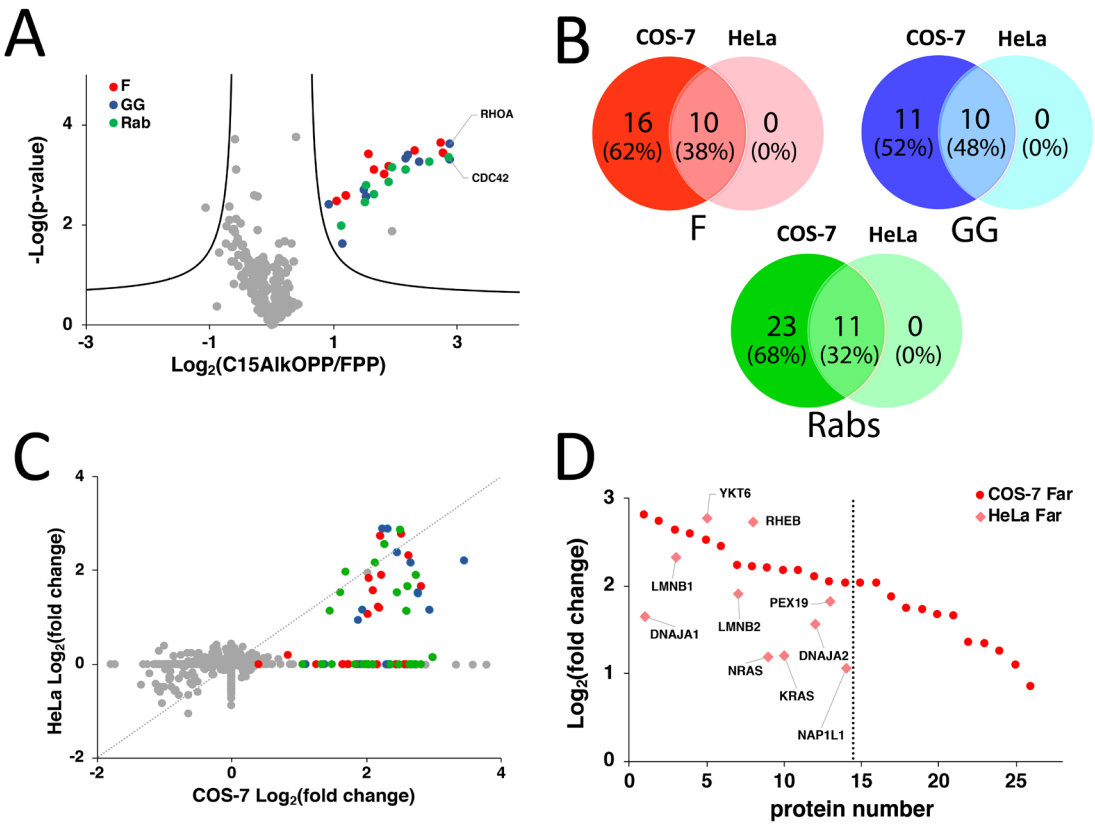

Figure 4.6. The prenylated proteins identified in HeLa is a subset of those in COS-7.

(A) A volcano plot (FDR = 0.01, s0 = 0.5) showing the statistically enriched prenylated proteins identified in HeLa cells from triplicate samples (red : farnesylated; blue : geranylgeranylated; green : rab proteins). **(B)** Venn diagrams displaying the overlap of proteins categorized into the three classes of prenyltransferase substrates identified in COS-7 and HeLa. Proteins groups were separated into individual proteins. **(C)** Fold-change correlation plot between the prenylated proteins identified in COS-7 and HeLa. **(D)** Farnesylated proteins identified in HeLa were the most enriched prenylated proteins in COS-7 identified from the MS2-based analysis.

have scores that predict high or medium propensity for farnesylation, NRas (CVVM) and NAP1L1 (CKQQ) manifesting low farnesylation scores were also identified.

As noted above, an apparent correlation was observed between the enrichment fold-changes and native abundances of GGTase-I substrates and Rabs in COS-7 from the SPS-MS3 approach but not in MS2-based analysis. We examined if the enrichment fold-changes

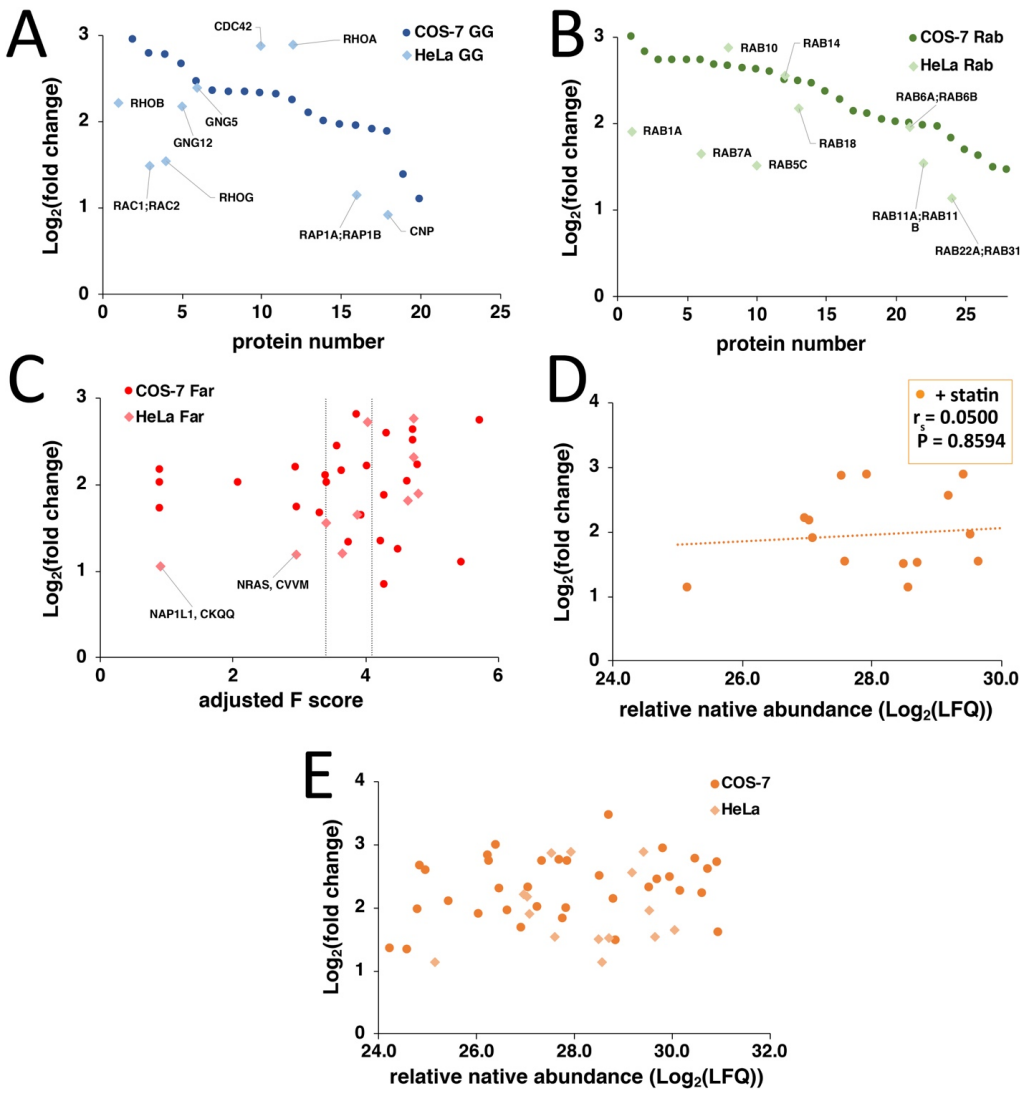

Figure 4.7. The prenylated proteins in HeLa were identified in COS-7.

(A) GGtase-I substrates and **(B)** Rab proteins identified in HeLa were also identified in COS-7 in a wide dynamic range of enrichment fold-changes. **(C)** The farnesylated proteins identified in HeLa were also identified in COS-7 with a wide range of assigned FlexPepBind farnesylation scores. Cut-offs shown in vertical lines for low, medium and highly predicted to be substrates of farnesylation. **(D)** Correlation analysis between the enrichment fold-change and relative native abundances of GGTase-I substrates and Rab proteins identified from MS2-based analysis on HeLa in the presence of statin. No significant Spearman's correlation was observed, **(E)** Most small GTPase and Rab proteins identified in HeLa are those that have relatively higher abundance in both HeLa and COS-7.

of the prenylome identified in HeLa from our MS2-based analysis correlates with their relative native abundances Fig. 4.7D). Unfortunately, no significant correlation was

observed, which may be attributed to the lower quantitative accuracy and dynamic range of MS2-based analysis in the less sophisticated orbitrap instrument. However, we did find that most proteins profiled in HeLa are those that have relatively high abundance in COS-7 (Fig. 4.7E). This comparison suggests that the native abundance of prenylated proteins may contribute significantly to their extent of enrichment and ability to be enriched, rather than their respective catalytic efficiencies.

4.3.4. Prenylomic profiling of brain cell lines

The data presented above demonstrates that approximately 80 prenylated protein groups can be identified using this method in COS-7 cells. Given the aforementioned observations concerning HeLa cells, it is likely that the number and prevalence of prenylated proteins will vary between different cell lines. To study this in more detail, the differences between several closely related cell lines were investigated. In the context of the brain, stable cell lines representing the most common cell types are readily available and therefore suitable for metabolic labeling and *in vitro* analysis. Hence, we hypothesized that it should be possible to identify prenylated proteins that are both common between different cell types as well as reveal others that are differentially expressed or prenylated, which may contribute to the unique function of each cell type. Accordingly, neuronal cells (N2a), immortalized astrocytes, and microglial cells (BV2) were metabolically labeled with the C15AlkOPP probe in the presence or absence of lovastatin. The lysates obtained were subjected to click reaction with TAMRA-N_3 and in-gel fluorescence analysis (Fig. 4.8A). In the absence of lovastatin, appreciable labeling was achieved across all cell lines (lanes

2, 5, and 8). The presence of lovastatin significantly enhanced the labeling of these bands, with some new bands appearing near the 50 and 75 kDa region (lanes 3, 6, and 9). These differential banding patterns observed between cells treated or not treated with lovastatin indicate that there are proteins that can only be detected in the presence of lovastatin. Despite the appearance of new bands in microglia, the labeling enhancement was less compared to those observed in neurons and astrocytes. It is also important to note that in the gel image, the contrast was adjusted in order for the differential banding pattern to be visualized. All brain-derived cell lines have less labeling compared to COS-7 in our in-gel fluorescence experiments.

Next, proteomic analysis of the enriched prenylated proteins within the three brain cell types in the presence of lovastatin was carried out. An MS2-based approach was employed to identify statistically enriched proteins since it suffices for profiling purposes. The total number of statistically enriched prenylated proteins in each cell line was less than that obtained with COS-7 cells, indicating that prenylome labeling was less efficient across all three brain cell lines. There were also no novel prenylated proteins detected. Among the individual prenylated proteins detected, 25 were shared (42%) by all three, with some shared by only two, or uniquely detected in one cell type (Fig. 4.8B). More prenylated proteins were identified from neurons with concurrent stronger background labeling (unprenylated proteins appearing to be enriched, see Fig. 4.9), reflecting the observed differences in labeling from the in-gel fluorescence analysis. Microglia afforded the smallest number of prenylated proteins profiled.

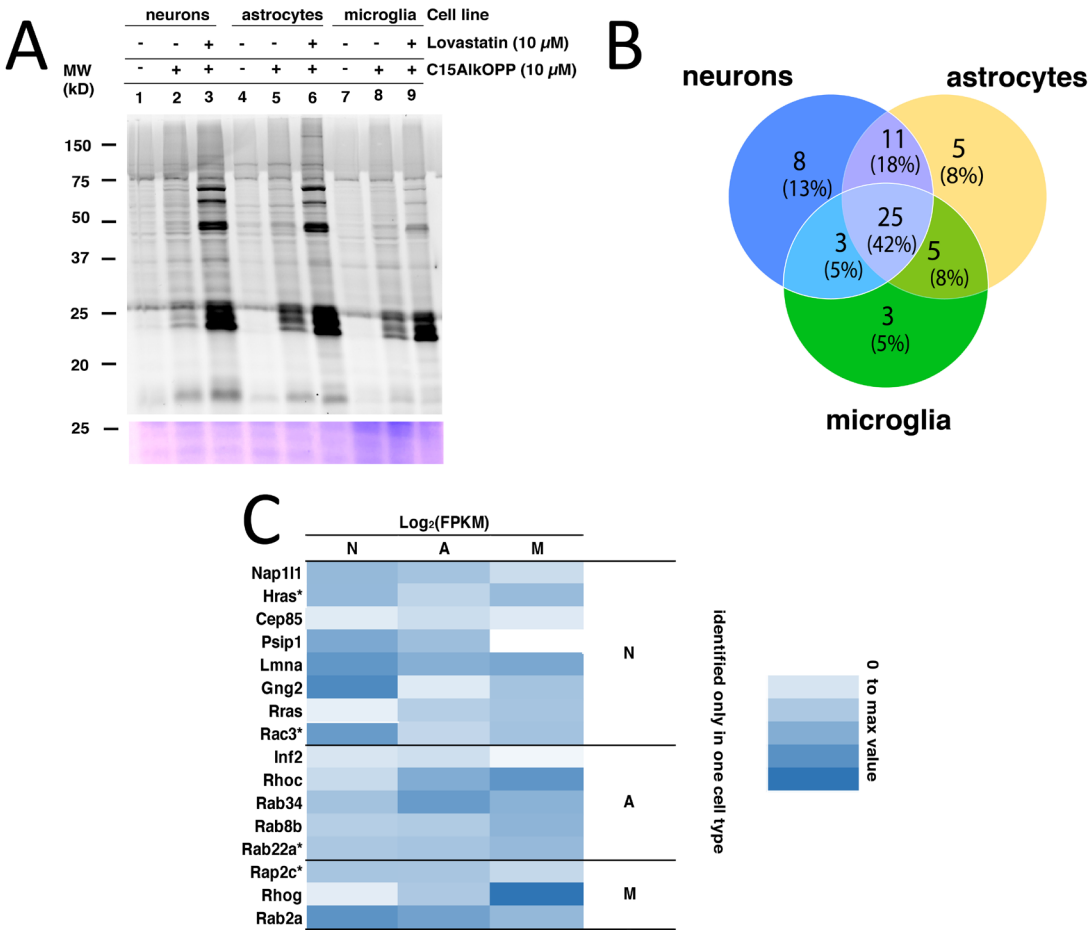

Figure 4.8. Similarities and differences in the sets of prenylated proteins identified from three different brain cell lines and primary astrocytes.

(A) In-gel fluorescence analysis on neurons, microglia, and astrocytes treated with 10 μM C15AlkOPP in the presence or absence of 10 μM lovastatin. **(B)** Summary of the number of identified prenylated proteins that were unique or shared among neuronal cells (N), immortalized astrocytes (A), and microglial cells (M). **(C)** A heat map of the relative mRNA expression levels of the prenylated proteins uniquely identified in each cell type. *proteins that were identified from a protein group.

As discussed above, the resulting similarities and differences in the set of prenylated proteins identified may reflect their endogenous expression levels in each cell type. However, there are no available data on the native abundances of these proteins in each cell line. We therefore turned to published RNA-Seq data reporting on the mRNA expression levels of individual prenylated proteins identified in each cell type using a web-

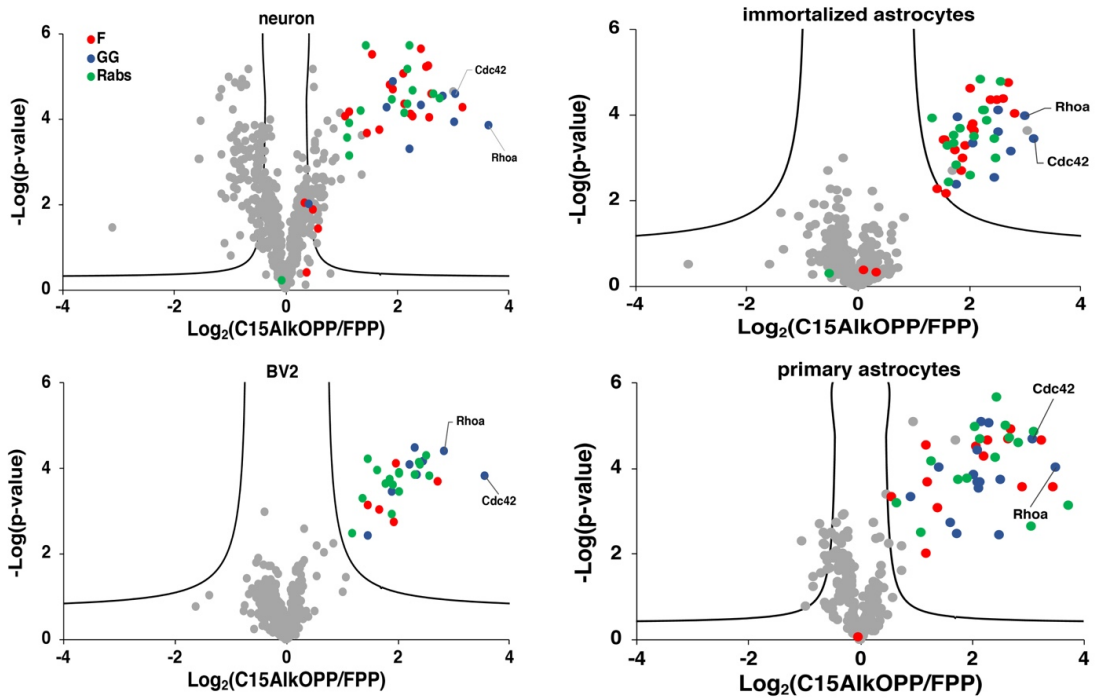

Figure 4.9. Volcano plots generated from the prenylomic analysis in neurons, astrocytes, microglia, and primary astrocytes.

Stronger background labeling was observed in neurons. Statistical parameters: FDR = 0.01, s0 = 0.5.

based tool (www.brainrnaseq.org).[559] The Fragments per Kilobase of transcript per Million mapped reads (FPKM) values of genes corresponding to identified prenylated proteins were extracted from each cell type and log2 transformed. A heat map was generated to compare expression levels of prenylated proteins shared by all three cell types, showing that they were generally expressed at higher levels in microglia (Fig. 4.10A). The proteins identified only in both neurons and astrocytes were dominated by farnesylated proteins (Fig. 4.10B). There were no significant correlations between the enrichment fold-changes and the mRNA levels of the identified prenylated proteins across all cell lines. Nevertheless, CDC42 and RhoA were identified as two of the most enriched prenylated proteins with relatively high mRNA levels in all cell lines (Fig. 4.11).

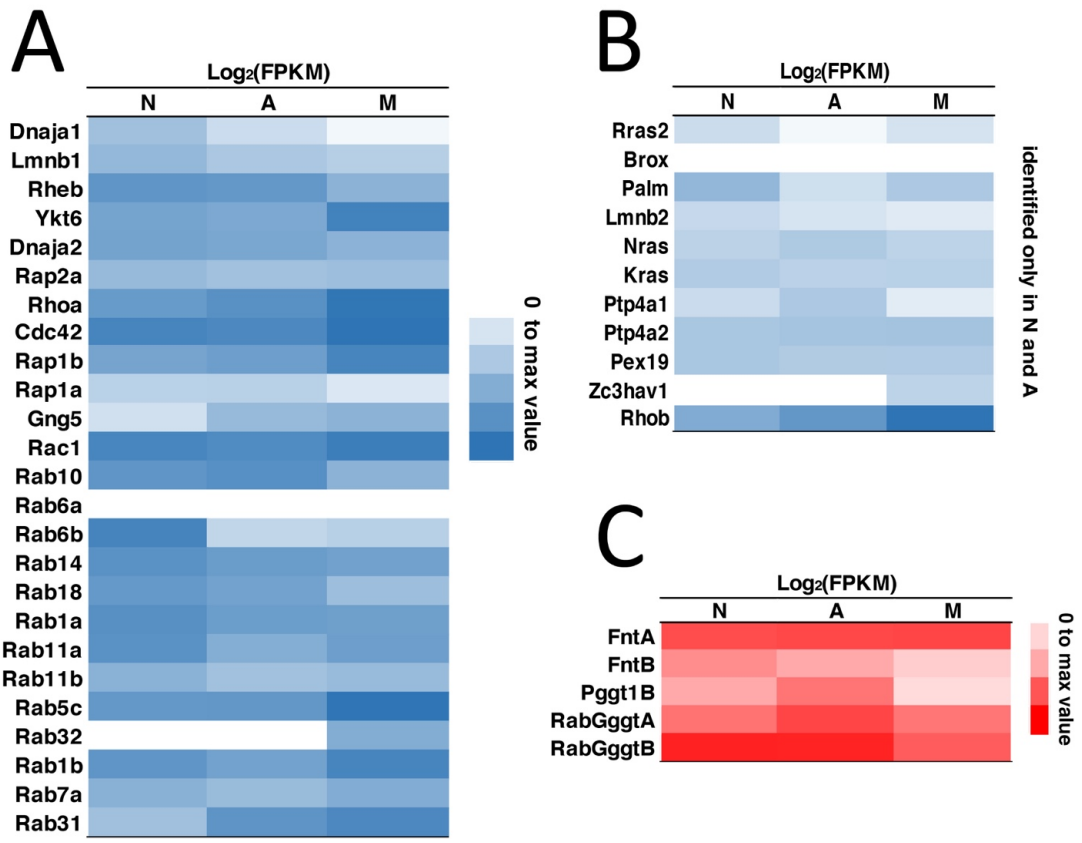

Figure 4.10. Relative mRNA expression levels of prenylated proteins in brain cells.

(A) Relative mRNA expression levels of the identified prenylated proteins shared by neuronal cells (N), astrocytes (A), and microglial cells (M). **(B)** Relative expression levels of prenylated proteins statistically enriched and identified in neurons and astrocytes but not in microglia. **(C)** Relative expression of the prenyltransferase enzymes.

Proteins that were uniquely identified from each cell type were of particular interest (Fig. 4.8C). However, some of these proteins were grouped with proteins that were also identified in other cell lines due to extensive sequence homology and may not be truly uniquely identified. Those that were identified only in neurons were mostly expressed at higher levels in neurons. In contrast, the prenylated proteins uniquely identified in astrocytes or microglia do not generally correlate with their relative expression levels,

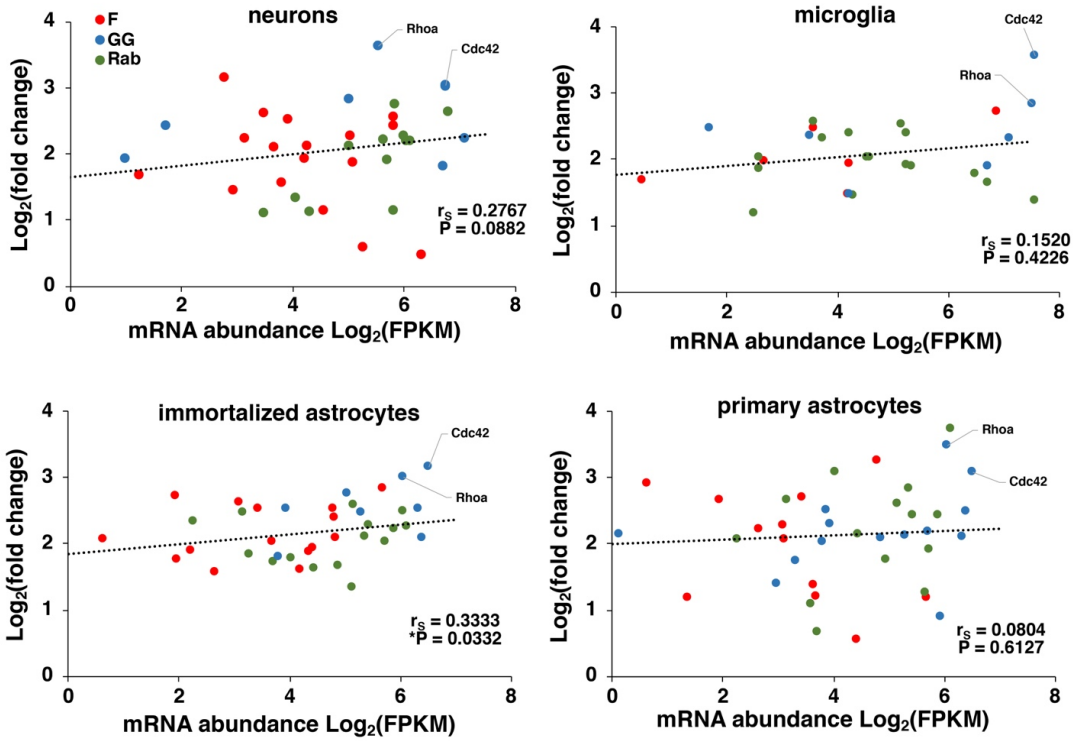

Figure 4.11. Dependence of enrichment fold-changes on mRNA levels of prenylated proteins identified from brain-derived cell lines and primary astrocytes.

Cdc42 and RhoA were consistently identified as two of the most enriched proteins also display high levels of expression.

except for RhoC that is highly expressed and was detected in microglia. Overall, there was no general correlation between the expression levels of individual prenylated proteins (based on the aforementioned RNA-Seq data) and their ability to be enriched in a prenylomic profiling experiment. The relative expression levels among the different prenyltransferase enzymes, which may reflect the innate efficiency of prenylation activity in each cell type (Fig. 4.10C) were also examined. The catalytic subunits FntB (FTase), Pggt1B (GGTase-I), and RabggtB (RabGGTase) are generally expressed at lower levels in microglia. This may explain why fewer proteins were enriched from microglia and why those that were observed were often those with relatively higher expression levels.

4.3.5. Inhibition of prenylation

As mentioned previously, the initial development of PTIs was driven by their potential pharmacological benefits in targeting oncogenic isoforms of proteins that promote tumorigenesis. However, their efficacies maybe negated owing to the ability of the key oncogenic targets to be alternatively geranylgeranylated in lieu of being farnesylated.[366] To determine the proteins displaying the switch-like behavior, a previous report on isoprenoid probe labeling in the presence of farnesyltransferase inhibitors (FTIs) showed that KRAS, NRAS, and RRAS2 can be geranylgeranylated when FTase is inhibited, indicating that these proteins may be responsible for the observed failure of FTIs in clinical trials, a result consistent with previous reports.[366] However, that experiment was performed in a human endothelial cell line.

In order to investigate the differential responses of cell lines to an FTI, COS-7 and HeLa cells were evaluated for their prenylome labeling upon FTI treatment (Fig. 4.12A). In COS-7 cells, the bands near the 50 and 75 kDa regions displayed significant reduction in labeling in the presence of tipifarnib, a validated and commonly used FTI. In HeLa cells, however, the low efficiency of probe incorporation makes it challenging to assess its sensitivity to FTI inhibition. Only one band near the 75 kDa region appears to be inhibited by tipifarnib. The inhibition profiles for the brain-derived cell lines also behaved similarly with that observed in HeLa in the absence of lovastatin (Fig. 4.12B), which can be attributed to the inherently lower probe incorporation in these cell lines compared to COS-7. Since farnesylated proteins are dependent on lovastatin treatment to enhance their probe incorporation as observed in Fig. 4.2C, we included lovastatin treatment to effectively label

farnesylated proteins and assess the effect of FTI-induced inhibition. Indeed, the enhanced labeling induced by lovastatin clearly facilitates the observation of inhibition by tipifarnib. The strongly labeled bands near the 50 and 75 kDa regions were completely abolished in all brain-derived cell lines.

We next sought to identify the farnesylated proteins responsive to inhibition. While immortalized cell lines are convenient for many laboratory experiments because they are easy to grow and can be passaged an unlimited number of times, their transformed nature can alter their physiology and render them less accurate as a disease model compared with primary cells. We first determined the set of prenylated proteins detectable in primary astrocytes using our probe labeling strategy in the presence of lovastatin. A total of 43 protein groups of prenylated proteins were identified, of which 33 individual prenylated proteins overlap (51%) with those identified from the immortalized astrocyte cell line (Fig.

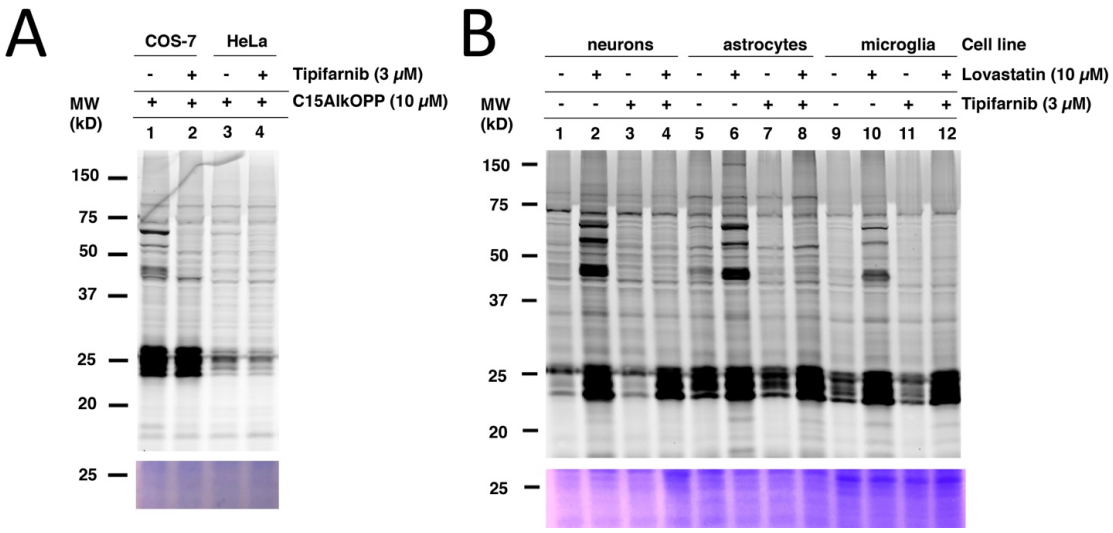

Figure 4.12. Response to FT inhibition using tipifarnib in various cell lines.

(A) Tipifarnib treatment in COS-7 and HeLa cells. **(B)** Tipifarnib treatment in brain-derived cell lines in the presence or absence of lovastatin.

4.13A). In contrast, 13 (20%) prenylated proteins were uniquely identified in the immortalized astrocytes and 19 (29%) were uniquely identified in the primary astrocytes. This suggests that there may be significant differences between the cell line and the primary cells and highlights how prenylomic profiling can be used to hone in on those differences. It is also noteworthy that the immortalized astrocytes used in this study were derived from the human APOE3 targeted replacement mice and thus some of the differences observed might result from the replacement of the APOE gene.

We have recently reported the farnesylated proteins responsive to perturbations in the farnesylation machinery in mouse brain with neuron-specific FTase deletion.[369] A total of 11 farnesylated proteins were identified in that study and are potentially implicated in the memory loss of the FTase-deficient mouse models. In this current study, we first evaluated the chemical inhibition of farnesylation using tipifarnib in the presence or absence of lovastatin through in-gel fluorescence analysis (Fig. 4.13B). Treatment with lovastatin enhanced probe labeling particularly in potentially farnesylated proteins near the 75 and 50 kDa regions (lane 3, indicated by arrows). Consistent with the aforementioned observations with cell lines, tipifarnib effectively suppresses labeling in these upper bands even in the presence of lovastatin (lane 5). Only minor differences in labeling near the 25 kDa region is apparent between tipifarnib treated samples (lanes 3 and 5) and their untreated counterparts (lanes 2 and 4). In order to identify these farnesylated proteins responsive to FTI inhibition, we performed our SPS-MS3 prenylomic approach in statin-treated primary astrocytes in the presence or absence of tipifarnib. We envisaged that since the C15AlkOPP probe can be incorporated by both FTase and GGTase-I, farnesylated

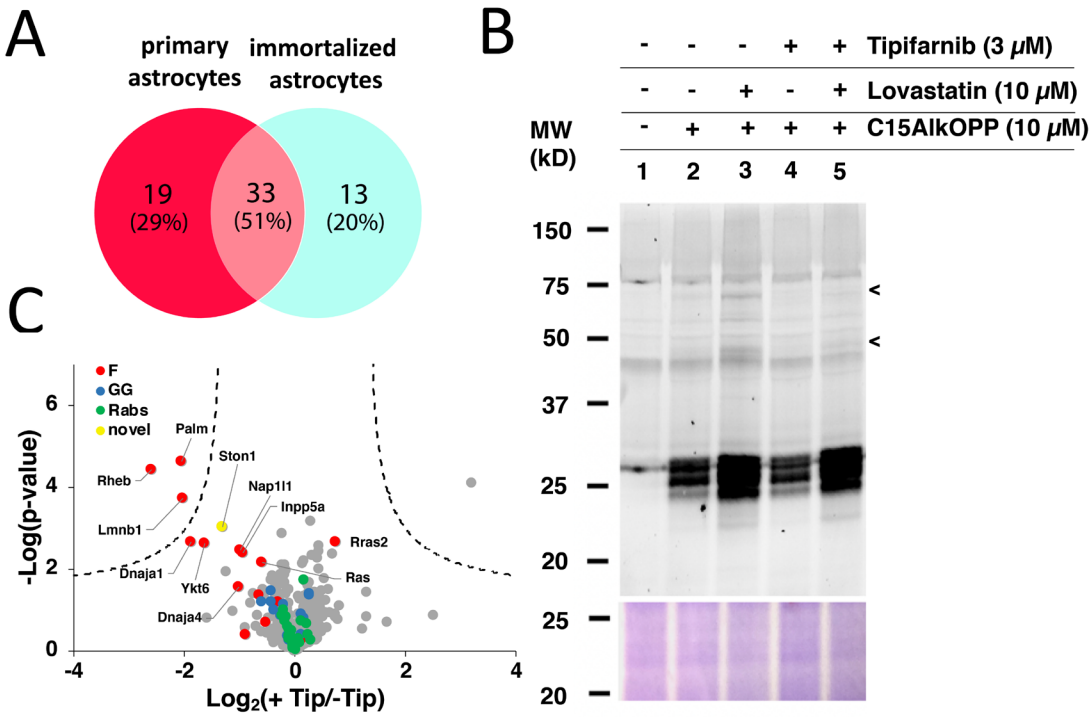

Figure 4.13. Inhibition of farnesylation in primary astrocytes.

(A) Summary of the number of prenylated proteins identified from immortalized and primary astrocytes. **(B)** In-gel fluorescence analysis of primary astrocytes in the presence or absence of lovastatin and tipifarnib. **(C)** A volcano plot (FDR = 0.01, s0 = 0.5) indicating inhibited farnesylated proteins (red) by tipifarnib. Ras is a protein group of HRas, Kras, and NRas.

proteins exhibiting the switch-like behavior would still be labeled under conditions where FTase is inhibited. Prenylomic analysis revealed that farnesylation substrates (15 protein groups, red) are inhibited to varying extents by tipifarnib (Fig. 4.13C). Six of these farnesylated proteins were identified as responsive to neuron-specific genetic deletion of FTase in mouse models.[369] Three of these proteins are above our stringent statistical threshold including Palm, Rheb and Lmnb1 with three more appearing slightly below the statistical threshold (Ston1, Dnaja1 and Ykt6). Ston1, a novel protein we identified in COS-7, displayed an appreciable level of inhibition, suggesting that this protein is truly a bona fide farnesylated protein. The assigned GGTase-I and Rab substrates are unaffected by FTI

treatment. Of the other nine putative farnesylated proteins, statistically significant inhibition was not observed. Since the C15AlkOPP analogue used in these experiments is a substrate for both FTase and GGTase-I, the absence of inhibition is consistent with switch-like behavior suggesting that these proteins including the protein group Nras;Hras;Kras and Rras. can be alternatively geranylgeranylated in the presence of an FTI. A few other proteins including Dnaja4, Nap1l1 and Inpp5a show some limited inhibition that may be due to partial switch behavior or incomplete inhibition. Overall, these inhibition studies on primary astrocytes validate the potential farnesylation of Ston1 and support the switch like behavior of a number of proteins.

4.4. Discussion

In this study, a chemical proteomic approach is described to identify the set of prenylated proteins in a variety of mammalian cells using a single alkyne-modified isoprenoid analogue. In terms of maximizing the number of prenylated proteins that can be identified, it is important to note that probe incorporation via metabolic labeling varies dramatically in different cell lines. Hence, careful selection of a cell line with maximal probe labeling is a prerequisite to maximize the number of prenylated proteins that can be identified. Here, we showed that lower labeling in cells not only impacts the extent of labeling of individual proteins but also reduces the total number of prenylated proteins that are enriched. Although prenylated proteins can be efficiently labeled by the C15AlkOPP probe in the presence of the endogenous isoprenoids, FPP and GGPP, lovastatin significantly enhances the incorporation efficiency as manifested by the increased fold enrichment and number of prenylated proteins identified. The dissociation constants (K_d) across the prenyltransferase

enzymes show tight binding with their corresponding isoprenoid substrates and are of comparable magnitude (FTase:FPP, 2.8 nM; GGTase-I:GGPP, 3 nM: RabGGTase:GGPP, 8 nM).[560–562] However, it has previously been shown that the C15AlkOPP isoprenoid probe is a more efficient substrate for GGTase-I compared with FTase using comparable enzyme concentrations.[333] Therefore, it may functionally mimic GGPP better than FPP. Under physiological conditions, probe incorporation into farnesylated proteins is challenging because of competition with endogenous FPP. Suppression of the pool of native isoprenoids using statins may allow C15AlkOPP to more effectively compete for labeling of those more difficult to farnesylate with potentially lower native abundances. It is also important to note that the use of this probe does not necessarily impact the function of labeled substrates as previously described.[380] Therefore, this isoprenoid tagging approach may operate in viable cells with minimal perturbations in the physiological function of prenylated proteins.

The goal of defining the set of prenylated proteins in a mammalian system through different tagging strategies and proteomic approaches has been pursued for more than a decade.[339,342,353,360] Most early efforts through the use of enrichment strategies led to the identification of less than a few dozen prenylated proteins. Antibody-based detection through the use of aniline-functionalized isoprenoids were also reported but has led to only 22 prenylated proteins.[338] Over time, the number of proteins identified using enrichment methods has steadily risen as technology has improved. A recent report using a dual chemical probe strategy involving two separate isoprenoid analogues (used in their alcohol forms) to tag farnesylated and geranylgeranylated proteins in conjunction with SILAC and

TMT analysis in EA.hy926, a human endothelial cell line, was employed for quantitative proteomic analysis;[366] a total of 80 prenylated proteins were reported, of which 64 were detected in the absence of a statin. Here, a simpler approach using a single analogue in its diphosphate form that is a substrate for all prenylating enzymes[353,363] was employed; the use of the diphosphate form in these experiments may be particularly advantageous for physiological studies since it avoids potential toxicity caused by the presence of prenyl alcohols.[348,349] The resulting analysis yielded 78 and 59 protein groups in the presence and absence of lovastatin, respectively This catalog of prenylated proteins is similar but not identical to the results obtained using the dual probe strategy showing extensive overlap in the identities of proteins profiled as well as identifying unique sets of previously known and novel prenylated proteins. Four out of the seven novel proteins discovered in the earlier work[366] were also identified in the analysis described here: CEP85, DCAF8, DPCD, and NAP1L4. Conversely, three additional novel prenylated proteins were identified here: PC4 and SFRS1-interacting protein PSIP1 (CaaX-box: CNLQ), Stonin-1 (CaaX-box: CITQ), and DHX32 (CaaX-box: CTLQ). Although the C-terminal peptides of these three proteins displayed multiple turnover activity for *in vitro* farnesylation in a previous study,[80] prenylation on their full-length forms has not been reported. Our results validate the farnesylation of these proteins, providing evidence of their prenylation in a cellular context. The differences in the prenylated proteins identified may be attributed to the differences in the cell line employed, labeling conditions, the enzymatic parameters associated with the probe used or the specific MS instrumentation employed for analysis. While extended $C(X)_3X$-box containing proteins and Cxx peptides have been demonstrated to be *in vitro* prenylation substrates,[83,84] none of those proteins were found to be enriched in a

statistically significant manner in our analysis. Several of these polypeptides do exist in mammalian proteomes, however their endogenous levels or efficiency of prenylation may be too low to be detected using the current chemical proteomic strategies. Finally, one cautionary feature related to these prenylomic experiments should be noted. In the strategy employed here, prenylated peptides are not directly observed in the LC-MS/MS analysis since enrichment relies on the alkyne functional group present in the isoprenoid analogue; lipidated peptides linked to biotin via click reaction remain bound to the neutravidin resin following tryptic digestion. Hence the identification of putative prenylated proteins is inferred from the detection of other non-prenylated peptides from the protein. The TMT-based method used here that compares enrichment in the presence and absence of alkyne probe allows most non-prenylated proteins to be excluded. However, this approach does not completely prevent proteins that associate with prenylated proteins from being enriched. There are limits to the stringency of washing conditions that can be employed since they must preserve sufficient protein structure to enable biotin-neutravidin interaction. In the analysis reported here, approximately 6% of the statistically enriched proteins were proteins with no apparent prenylation motif but were known to interact with prenylated proteins. While this number is small, it suggests that caution must be exercised in interpreting data from these experiments and that additional confirmatory experiments and/or data may be necessary to unambiguously identify novel prenylated proteins discovered using this metabolic labeling strategy. This underscores the need for better methods that allow for the enrichment of prenylated peptides that can be used to directly identify prenylated proteins.

Analyses presented here of the factors that influence the extent of enrichment of prenylated proteins in this chemical proteomic approach suggest that the catalytic efficiency of specific substrates for their cognate prenyltransferases does not correlate with their enrichment efficiency. A large number of prenylated proteins having CaaX-boxes with predicted higher farnesylation scores or prenylation efficiencies were not identified. This may be due to the low levels of expression of these proteins or to other regulatory mechanisms that involve chaperones that regulate the delivery of unprenylated proteins to their cognate prenyltransferase.[372] Currently, most of what is known concerning prenylation selectivity relies on data obtained from *in vitro* studies or computational experiments. Instead, it appears that the expression levels and native abundances of protein substrates have a greater impact on their detectability in these chemical proteomic experiments. In particular, CDC42 and RhoA have consistently emerged as two of the most enriched candidates across all cell lines studied here. Both of these contain efficiently prenylated C-terminal CaaX-box sequences[553] and high native abundances or expression levels. Overall, protein levels are determined by a complex interplay of factors including mRNA transcript levels, transcript stability, translation efficiency and rate of protein degradation.[563] Given that metabolic labeling experiments provide a snapshot of the levels of many prenylated proteins in a single experiment, this approach holds great promise for investigating global changes that occur in specific disease states.

For chemical proteomic strategies, quantitative analysis is useful for evaluating the extent of probe incorporation into its cognate protein substrates. The evolution of orbitrap mass spectrometry instrumentation employed in proteomic studies led to improvements in

sensitivity and accuracy of quantitation.[564] Consequently, more accurate quantitation can be achieved through the use of multinotch SPS-MS3 approach, where reporter ion interference that distorts reporter ion signals in MS2-based methods is obviated.[565] From the data reported here, using the multinotch approach with a more sensitive orbitrap instrument afforded a wider dynamic range of fold-change values compared to the MS2-based approach, allowing more accurate quantitation. Although there were some differences in the sets of prenylated proteins that were identified using the two different approaches, overall, the number of profiled prenylated proteins are comparable. Therefore, it appears that an MS2-level analysis of TMT-labeled peptides is generally sufficient to identify prenylated proteins derived from a chemical probe-based enrichment experiment. However, for applications where information regarding changes in the levels of specific prenylated proteins is important, the more accurate quantitation and wider dynamic range of the MS3-level approach make it a better choice.

As a prelude to future work directed at studying protein prenylation in brain-related diseases, we first sought to survey the prenylated proteins in several brain-derived cell lines including neurons, astrocytes, and microglia. Significant overlap (25 proteins, 42%) was found in the prenylated proteins identified in the three cell lines. Given that many of these are involved in cellular processes that are generally essential to cellular function, such as Ras signaling from Ras-related proteins, endocytosis, and chemokine signaling, this is not surprising (Table 4.1). Intriguingly, some prenylated proteins are uniquely enriched in specific cell types. Eight proteins were observed exclusively in neurons, five were observed exclusively in astrocytes and three were observed exclusively in microglia, suggesting their

Table 4.1. Pathway analysis on the prenylated proteins identified shared by all three brain cell lines.

Pathways are ranked based on p-values and sourced from KEGG Mouse 2019 using Enrichr analysis tool.[616] The top ten pathways were selected.

Index	Term	P-value	Adjusted P-value	Odds Ratio	Combined Score
1	Ras signaling pathway	1.07E-08	3.24E-06	24.03	441.10
2	Endocytosis	2.88E-08	4.36E-06	20.82	361.47
3	Chemokine signaling pathway	1.28E-07	1.30E-05	24.37	386.67
4	Pancreatic secretion	1.77E-07	1.34E-05	38.10	592.26
5	Leukocyte transendothelial migration	2.79E-07	1.69E-05	34.78	524.93
6	Neurotrophin signaling pathway	3.60E-07	1.82E-05	33.06	490.52
7	Renal cell carcinoma	1.46E-06	6.34E-05	47.06	632.18
8	Focal adhesion	4.19E-06	1.59E-04	20.10	248.90
9	Rap1 signaling pathway	5.32E-06	1.79E-04	19.14	232.41
10	AMPK signaling pathway	1.71E-05	5.19E-04	25.40	278.70

unique roles in these cells. For example, among the eight proteins identified in neurons, Gng2 (G-protein gamma 2 subunit) is highly expressed there. Gng2 is a specific marker for the forebrain structure claustrum, which integrates multisensory information and promotes cognitive function.[566,567] Rac3, a member of the Rho family GTPases, is also abundantly expressed in neurons. Rac3 plays essential roles in neuronal development and related disorders.[568] The presence of the C-terminal prenylation site of Rac3 is specifically required for the maturation of neurons in culture. Hras, an exclusively farnesylated small GTPase, is modestly expressed in neurons; however, the role of Hras in regulating neuronal synaptic function is well established in vivo.[569] Overexpression or deletion of Hras significantly modulates neuronal function.[570,571] In cultured neurons, the activity and cellular localization of Hras, which depends on its farnesylation state, regulate nascent axonal growth.[572] Notably, another Ras protein, Rras, was also uniquely identified in neurons despite its minimal gene expression. Rras controls axon branching and neuronal polarity in cultured cortical/hippocampal neurons.[573,574] Among the five proteins uniquely

identified in astrocytes, the small GTPase Rab34 is most highly expressed. Rab34 is a member of the secretory pathway and regulates phagolysosome biogenesis and cargo delivery.[575,576] These functions are critical for the normal role of astrocytes in the brain. Dysfunction of Rab34 leads to gliomas.[577] Among the three proteins uniquely identified in microglia, RhoG is most highly expressed. RhoG, a member of the Rho family of small GTPases, regulates neuroinflammation and the clearance of apoptotic cells, key functions of microglial cells in the brain.[578,579] In sum, our findings demonstrated the ability to track the levels of prenylated proteins in different brain cell types, many of which perform key regulatory roles within each cell type. The results will be highly useful in a variety of experiments seeking to explore the dysregulation of protein prenylation.

4.5. Conclusion

The results presented here indicate that metabolic labeling of prenylated proteins in cultured cell lines can be accomplished using a single alkyne-modified isoprenoid analogue. The extent of labeling in each cell line differs, resulting in variations in enrichment and the number of prenylated proteins identified in chemical proteomic profiling. The native abundances of these proteins under steady-state conditions may dictate their ability to be enriched; however, the levels of prenyltransferase enzymes in different cell lines and their capability for probe uptake may also play crucial roles in determining the extent of prenylome labeling. Overall, this study shows that a common core of 19 prenylated proteins identified in 7 different cell types can be monitored using these types of experiments. This should provide important insights into the activity and regulation of signal transduction pathways in cells. In addition, prenylated proteins unique

to specific cell types can also be identified and monitored using this approach. Eight proteins were observed exclusively in neurons, five were observed exclusively in astrocytes and three were observed exclusively in microglia, suggesting their unique roles in these cells. Finally, we report here that this powerful approach can be used to monitor protein prenylation in primary cells. Taken together, this powerful approach should be useful to unravel the role of prenylated proteins in myriad diseases.

4.6. Methods

4.6.1. Metabolic labeling in cultured cell lines and primary astrocytes

COS-7 and HeLa cells were generously provided by Dr. Elizabeth Wattenberg at the University of Minnesota. Mouse N2a neuroblastoma cells (ATCC CCL-131) were purchased from ATCC (Manassas, VA). Mouse BV2 microglial cells were generously provided by Dr. Hongwei Qin at the University of Alabama at Birmingham. The immortalized astrocytes were derived from the human APOE3 targeted replacement mice[580] and were generously provided by Dr. G. William Rebeck at Georgetown University. Primary astrocytes were prepared and cultured from neonatal pups of wild-type C57BL6/J mice as described previously.[581,582] In brief, cortices and hippocampi from neonatal pups were dissected in cold HBSS, and enzymatically digested with 0.05% trypsin/EDTA for 20 min in 37°C. Cells were triturated and passed through a 40 μm cell strainer. The cells were then centrifuged for 7 min at 1,000 rpm, and re-suspended in the culture medium DMEM Glutamax (Gibco, 10569-010) containing 10% FBS (Gibco). After culturing for 2-4 weeks, microglial cells were removed by vigorously tapping the flask on

the bench top and changing media. Remaining astrocytes were passaged and expanded in PDL-coated T75 flasks with DMEM containing 10 % FBS and penicillin/streptomycin/amphotericin B (Antibiotic-Antimycotic, Gibco) and allowed to grow prior to plating into 100-mm dishes for metabolic labeling.

Cells (0.9 to 1.5 x 10^6 seeding density) were grown in a 100-mm dishes containing 10 mL of DMEM (Gibco) media with 10% fetal bovine serum (Gibco) 1% penicillin-streptomycin (Gibco) one day prior to treatment. The media was removed and replaced with 5 mL of fresh media followed by pre-treatment with 10 μM lovastatin (Cayman Chemical) for 6 hours under 5% CO_2 at 37 ºC. After pre-treatment, the media was either removed and replaced to remove the lovastatin or retained, followed by the addition of 10 μM C15AlkOPP or FPP and 3 μM tipifarnib when indicated. After 24 hours of incubation, the cells were collected, pelleted through centrifugation and stored at – 80 ºC until further use.

4.6.2. In-gel fluorescence labeling

In-gel fluorescence analysis of C15AlkOPP-treated cells was performed as previously described.[550] In brief, cell pellets were suspended in lysis buffer (10 mM Na_3PO_4 pH 7.4, 137 mM NaCl, 2.7 mM KCl, 2.4 μM PMSF, 200 units/nL benzonase nuclease (Sigma-Aldrich), protease inhibitor cocktail (1X PBS) and 1% SDS) and lysed by sonication on ice for 6-7 times with 2-sec pulses at 10-sec intervals. Protein concentrations were quantified using a BCA assay (Thermo Fisher Scientific) and 100 ug of the protein samples were subjected to click reaction with TAMRA-N_3 (25 μM TAMRA-N_3 (BroadPharm), 1

mM TCEP, 0.1 mM TBTA (Sigma-Aldrich), and 1 mM $CuSO_4$) for 1 hour at room temperature. Proteins were precipitated out using ProteoExtract precipitation kit (Calbiochem) and resuspended in 1X loading buffer containing 2% SDS, 10% glycerol, 0.02% bromophenol blue in 50 mM Tris-HCl pH 6.8. Labeled protein samples were resolved in 12% SDS-PAGE gels and detection for TAMRA fluorescence was performed using a Typhoon FLA 9500 (GE Healthcare). Gel images were processed in ImageJ.

4.6.3. Enrichment of labeled prenylated proteins

Protein lysates (2 mg in 1 mL) from cells treated with lovastatin and C15AlkOPP or FPP were subjected to click reaction with biotin-N_3 (100 μM biotin-N_3 (BroadPharm), 1 mM TCEP, 0.1 mM TBTA, and 1 mM $CuSO_4$) for 90 minutes at room temperature. Proteins were precipitated out using chloroform-methanol-water (1:4:3) to remove excess reagents and pelleted by centrifugation. Protein pellets were washed with methanol, redissolved in 1 mL of 1X PBS + 1% SDS and quantified using a BCA assay to normalize concentrations across all samples. Biotinylated samples (1 mg in 500 μL) were incubated with 100 μL (settled resin) of pre-washed Neutravidin agarose beads (Thermo Scientific) for 90 minutes. Beads were washed (1X PBS + 1% SDS (3x), 1X PBS (1x), 8 M urea in 50 mM TEAB (3x), and 50 mM TEAB (3x) with 1 mL per wash) and bound proteins were digested on-bead with 1.5 µg of sequencing grade trypsin (Promega Corp.) overnight at 37ºC. Peptides were collected by washing the beads with 100 μL 50 mM TEAB and dried by lyophilization.

4.6.4. TMT-labeled sample preparation

Dried peptides were dissolved in 80 μL of 100 mM TEAB and quantified via BCA assay. Samples (10 μg) were supplemented with 150 fmol of internal standard (yeast ADH1, Waters) and subjected to labeling with TMT 6plex labeling (Thermo Fisher Scientific) following the manufacturer's protocol. TMT-labeled samples were pooled, dried by lyophilization, and redissolved in 200 mM NH_4HCO_2, pH 10. Samples were fractionated under high pH reversed phase conditions on three layers of SDB-XC extraction disks (3M, 1.07 mm x 0.50 mm i.d.) in 200 μL pipette tips into 60 μL volumes of 5,10, 15, 20, 22.5, 27.5, and 80% CH_3CN in 200 mM NH_4HCOO pH 10. The first two fractions were combined. The samples were dried and redissolved in 30 μL of 0.1% HCO_2H in water and stored at -80 ^oC until LC-MS analysis.

4.6.5. Proteomic samples for quantifying native abundances

Lysates from COS-7 cells (40 μg, three biological replicates) were resolved using a 12% SDS-PAGE gel and stained with Coomassie Blue. The 20-30 kDa regions (~1 cm) were excised using a scalpel to evenly cut out bands across the lanes. Coomassie stain was removed by washing the gel pieces with 150 μL of 1:1 100 mM TEAB: CH_3CN twice. Proteins in the gels were reduced with DTT (10 mM) at 56 ^oC for 1 hr. Alkylation with iodoacetamide (55 mM) was performed in the dark for 30 min. Gel pieces were washed twice with the TEAB:CH_3CN mixture and in-gel tryptic digestion was performed overnight at 37 ^oC with 10 ng/µL of trypsin. Tryptic peptides were collected and dried by lyophilization. Dried peptides were dissolved in 2% CH_3CN in H_2O with 0.1% HCO_2H

(Buffer A). Samples were supplemented with internal standard (yeast ADH1, 50 fmol, Waters) and loaded onto a pre-conditioned STAGE Tip (SDB-XC, 3M). Samples were washed with Buffer A and eluted with 40% CH_3CN in H_2O with 0.1% HCO_2H. Desalted peptides were dried and dissolved in 0.1% HCO_2H in H_2O. Proteomic samples were stored at -80 ºC until LC/MS analysis.

4.6.6. LC-MS data acquisition

The TMT-labeled peptides were resolved using a RSLC Ultimate 3000 nano-UHPLC (Dionex) with a reversed-phase column (75 μm i.d., 45 cm) packed in-house with ProntoSIL C18AQ 3 μm media at a flow rate of 300 nL/min. Each fraction from the high pH reversed-phase separation was subjected to a distinct gradient of solvent B (0.1% HCO_2H in CH_3CN) and solvent A (0.1% HCO_2H in H_2O) with amounts ranging between 7-34% for 80 min and sprayed directly into the Orbitrap using a Nanospray Flex source (Thermo Fisher Scientific). For the multinotch SPS-MS3 approach, an Orbitrap Fusion Trihybrid (Thermo Fisher Scientific) mass spectrometer was used. MS1 scans were collected at 120,000 resolution in a 320-2,000 *m/z* range with a max injection time (IT) of 100 ms and an automatic gain control (AGC) target of 200,000. Subsequent data-dependent (top speed at 3s) MS/MS scans were acquired using collision induced dissociation (CID) at a normalized collision energy (NCE) of 35% with a 1.3 *m/z* isolation window, a max IT of 100 ms, and an AGC target of 5,000. Dynamic exclusion was allowed for 60 sec. Acquisition at MS3 was done by synchronously selecting the top 10 precursors for

fragmentation by high-collisional energy dissociation (HCD) in the orbitrap with an NCE of 55% and a 2.5 *m/z* isolation window, 120 ms max IT, and 50,000 AGC target.

For label-free analysis of relative native abundances, each peptide sample was separated with 5-30% of Solvent B for 140 mins. Data-dependent scans at MS1 were collected at 60,000 resolution over 320-2000 *m/z* range with AGC target of 500,000 and max IT of 50 ms. Dynamic exclusion was allowed for 90 s. HCD fragmentation was performed at NCE of 38% with 1.5 *m/z* isolation window, AGC of 50,000, and max IT of 200 ms.

The MS2-based quantitative proteomic analyses of TMT-labeled peptides were performed using an Orbitrap Elite instrument (Thermo Fisher Scientific) equipped with RSLC Ultimate 3000 nano-UHPLC and the same gradients used in SPS-MS3 approach were employed. A data-dependent acquisition was performed for MS1 scans under 60,000 resolution in a 350-1600 *m/z* range, with an AGC target of 1,000,000 and a max IT of 50 ms. Precursors were fragmented at MS2 using HCD at NCE of 40% with a 1.5 *m/z* isolation window, an AGC target of 50,000, and a max IT of 500 ms at 15,000 resolution.

4.6.7. Proteomic data analysis

The .raw files were searched using Andromeda embedded in MaxQuant (version 1.6.2.10) against the non-redundant human (UP000005640) or mouse (UP0000000589) databases from Uniprot (EMBL-EBI, April 2018 release). The peptides identified were based on full

tryptic digestion with allowed missed cleavages of 3 with minimum peptide length of 7 residues. Fixed modifications were set for the TMT labels on both the N-terminal and lysine (229.163 Da) and variable modifications for methionine oxidation (15.995 Da) and N-term acetylation (42.010 Da). For label-free proteomic analysis, cysteine carbamidomethylation (57.021 Da) was used as a fixed modification instead. The unique + razor peptides were used for quantification. The default settings in the software for other parameters were used.

The resulting data were imported in Perseus (version 1.6.0.7) for filtering and statistical analysis. Proteins that were identified only by site, potential contaminant, or reversed were removed. The raw intensities were transformed to log2 values and proteins with less than 3 out of 6 values in each TMT channel were removed. Missing values were imputed based on a normal distribution. Reporter ion values were normalized by subtracting rows by means and columns by median. Statistical analysis was performed using two-sample t-tests with FDR = 0.01 and s0 = 0.5. Data were exported and processed in Microsoft Excel to generate volcano and fold-change correlation plots. For label-free proteomic analysis of the 20-30 kDa region proteins, LFQs were log2-transformed. Proteins identified in 2 out of 3 replicates were considered. Missing Log_2(LFQ) values were imputed, normalized to the internal standard, yeast ADH1, and mean values were calculated. Prenylated proteins were extracted from the list of proteins identified on the basis of the presence of CaaX-box, existing annotations or validated in previous studies.

4.6.8. Correlation analysis with published prenylation data

Previously reported prenylation data were used for correlation analyses. PrePS scores were obtained from http://mendel.imp.ac.at/PrePS/index.html and were adjusted by adding seven to obtain positive values. The FlexPepBind farnesylation scores were obtained from the complete list of 8000 CaaX-box peptide substrates published and provided by Dr. Ora Schueler-Furman.[329] The scores were adjusted by subtracting from three to obtain positive values. For both adjusted farnesylation scores, higher scores reflect greater propensity to farnesylation. The values for relative GGTase-I activity on peptide substrates were extracted from the thesis of Dr. Animesh V. Aditya from Purdue University. The percent prenylation on Rab protein substrates of RabGGTase determined *in vitro* were obtained from published data.[99] Kolmogorov-Smirnov (K-S) test was used to test for the normality of each variable. After assessing the normality of data, Spearman's rank correlation test was used to measure the monotonic association between variables. Spearman's rank correlation and regression analysis were performed on GraphPad Prism version 8.4.1. Graphs were formatted on Microsoft Excel.

4.7. Acknowledgements

This work was supported in part by the National Institute of Health grants RF1AG056976, R01GM084152, R01NS107442, R21AG056025 and RF1AG058081, and the National Science Foundation grant CHE-1308655. The authors would like to thank Dr. Hongwei Qin at the University of Alabama at Birmingham for providing BV2 cells, Dr. G. William Rebeck at Georgetown University for providing human APOE3 targeted-replacement immortalized mouse astrocytes, Elyse Froehling for generating the transcriptomic data

using next-generation sequencing at the University of Minnesota Genomics Center, and Dr. Yingchun Zhao for the assistance in LC-MS analysis in the Mass Spectrometry Core Facility of the Masonic Cancer Center, designated by the National Cancer Institute and supported by P30 CA77598. I would also personally like to thank the following for their contributions to this work: Angela Jeong for assistance in data analsysi; Mina Ahmadi and Caroline Brown for performing metabolic labeling and proteomic analysis on brain-derived cell lines, Wenhui Qu for isolating and preparing primary astrocytes, Ling Li and Mark Distefano for guiding the experimental designs.

Chapter 5: Thinking outside the CaaX-box: an unusual prenylation on ALDH9A1

5.1. Introduction

Protein prenylation is an essential post-translational modification (PTM) required for certain proteins to properly localize in cellular membranes and for mediating protein-protein interactions and protein trafficking.[543] In this type of PTM, a farnesyl or geranylgeranyl group(s) is irreversibly appended through a thioether linkage on a cysteine residue near the C-terminus of a protein. There are currently four characterized prenyltransferases that catalyze such modifications. Farnesyltransferase (FTase) attaches a 15-carbon farnesyl moiety from farnesyl diphosphate while geranylgeranyltransferase type 1 (GGTase-I) links a 20-carbon long geranylgeranyl moiety from geranylgeranyl diphosphate onto their substrates.[77] These substrates often bear a canonical CaaX-box prenylation sequence where C is the prenylated cysteine and a and X can be any amino acid. However, recent studies have shown that proteins terminating in CXXXX or CXX may potentially be substrates of prenylation.[83,84] The third type of prenylation involves geranylgeranyltransferase type II (GGTase-II or RabGGTase) that usually appends two geranylgeranyl units of on dual cysteine motifs on proteins, particularly those that belong to the Rab family. These substrates are often recognized first by the rab escort protein 1 or 2 (REP-1/2) and modified by GGTase-II at their C-terminal cysteines in their -CCXX, -CXC, or -XXCC canonical sequences.[328] Finally, the recently discovered GGTase-III appears to install a second isoprenoid geranylgeranyl moiety, in addition to a pre-farnesylated protein substrate.[108,383]

Identifying prenylated proteins and the lipid-modified proteome in general has been an important subject of interest for more than a decade.[14,18] Recent methods for high-throughput analysis of these lipid-modified proteins takes advantage of chemical proteomics that allows for selective identification of these substrates *via* an enrichment strategy.[353,360,366,368,373] In this scheme, a bio-orthogonal probe (usually containing an alkyne moiety) that mimics the native form of a small molecule substrate used for enzymatic protein modification is added to cells and is incorporated by the host machinery onto the PTM proteins. Alternatively, labeling of proteins can be achieved *in vitro* through the addition of the lipid probe and enzymes that catalyze the PTM.[369] These labeled proteins in lysates are then subjected to click reaction with a modified biotin for selective enrichment and subsequent proteomic identification of PTM proteins. Chemical proteomics approaches to identify prenylated proteins have been developed for more than a decade, wherein a bio-orthogonal isoprenoid analogue is synthesized and used to tag and identify the prenylated proteins in a given cell line.[18] The goal of defining the prenylome has been a challenge, reflected by the lesser number of proteins identified in prenylomic studies compared to the total number of prenylation substrates derived from predictions and annotations. Recently, two independent studies reported 80 prenylated proteins identified in a given cell line, which consists of known and novel prenylation substrates.[366,368] One study employed a dual labeling strategy where a farnesyl and a geranylgeranyl probe analogue was used, while our group used C15AlkOPP as a single probe that labels all classes of prenylation substrates. Despite the differences in these approaches, a comparable number of proteins were identified with slightly varying identities, particularly in the novel prenylated proteins discovered. In many cell lines our

group has studied, one peculiar protein, ALDH9A1, has been consistently enriched. In this chapter, we describe our discovery of ALDH9A1 as a potentially prenylated protein that has possible biological consequences in controlling this enzyme's function. Through the use of tools in chemical and molecular biology, we characterized this potentially novel lipid modification and proposed a plausible mechanism in which this may occur in nature.

5.2. Research Objectives

In this chapter, we describe our discovery of ALDH9A1 as a potentially prenylated protein that has possible biological consequence in controlling this enzyme's function. Through the use of tools in chemical and molecular biology, we characterized this potentially novel lipid modification and proposed a plausible mechanism in which this may occur in nature.

5.3. Results

5.3.1. Chemical proteomic analysis of prenylated proteins identified ALDH9A1

Recent advances in proteomic technologies have enabled high throughput profiling of post-translationally modified (PTM) proteins of interest. In particular, chemical proteomic approaches involve an enrichment strategy to identify a set of modified proteins such as the prenylated proteome. Along with other groups, we have conducted prenylomic profiling across multiple cell lines and showed that the scope of prenylated proteins varies to some extent in these various cell types (Fig. 5.1).[368] COS-7 (Fig. 5.1A) displayed the largest number of proteins profiled including novel prenylated proteins bearing the

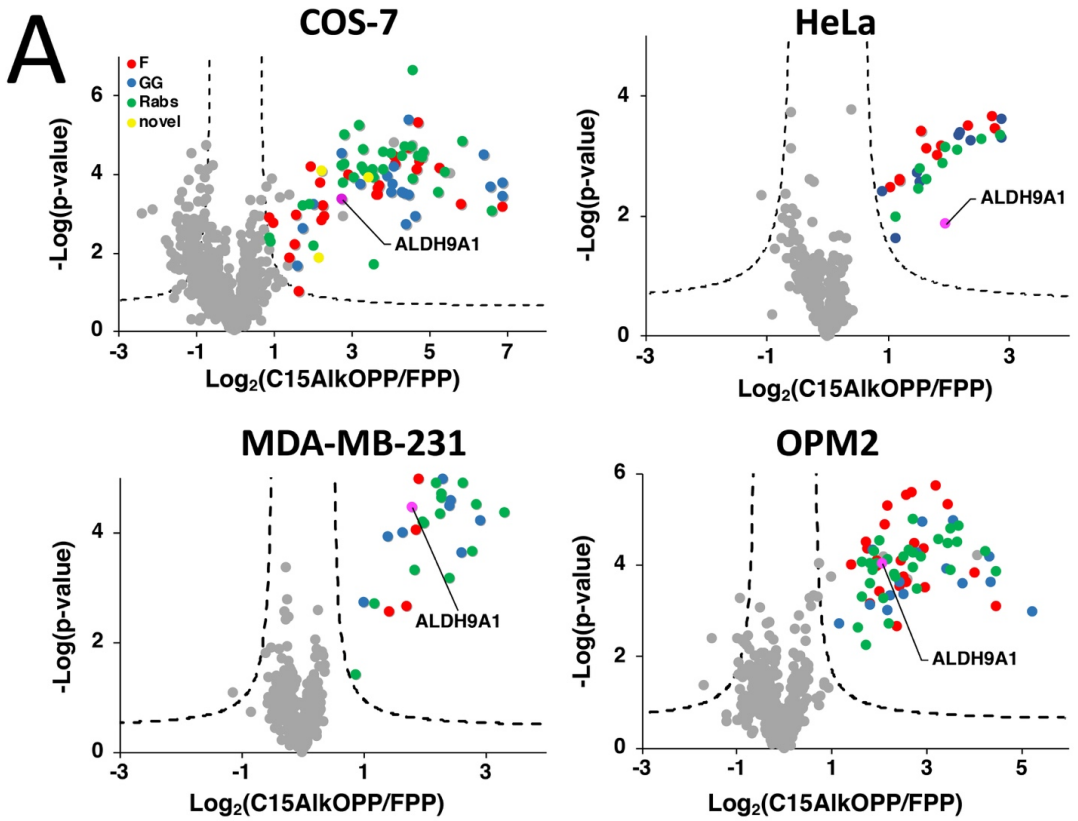

B

MSTGTFVVSQPLNYRGGARVEPADASGTEKAFEPATGRVIATFTCSGEKEVNLAVQNAKA
AFKIWSQKSGMERCRILLEAARIIREREDEIATMECINNGKSIFEARLDIDISWQCLEYYAGL
AASMAGEHIQLPGGSFGYTRREPLGVCVGIGAWNYPFQIASWKSAPALACGNAMVFKP
SPFTPVSALLLAEIYSEAGVPPGLFNVVQGGAATGQFLCQHPDVAKVSFTGSVPTGMKIM
EMSAKGIKPVTLELGGKSPLIIFSDCDMNNAVKGALMANFLTQGQVCCNGTRVFVQKEIL
DKFTEEVVKQTQRIKIGDPLLEDTRMGPLINRPHLERVLGFVKVAKEQGAKVLCGGDIYVP
EDPKLKDGYYMRPCVLTNCRDDMTCVKEEIFGPVMSILSFDTEAEVLERANDTTFGLAAG
VFTRDIQRAHRVVAELQAGTCFINNYNVSPVELPFGGYKKSGFGRENGRVTIEYYSQLKTV
CVEMGDVESAF

Figure 5. 1. ALDH9A1 in consistently enriched in prenylomic analyses in various cell lines.

A.) Volcano plots (FDR = 0.01, s0 = 0.5) of prenylomic analysis on various cell lines. ALDH9A1 is consistently enriched. **B.**) The complete protein sequence of the human ALDH9A1. Highlighted in yellow are the tryptic peptides identified in the prenylomic analyses.

canonical CaaX-box motifs but were not previously identified in other prenylomic studies reported. We have found that the differential labeling of the prenylomes on these various cell lines may be attributed to the levels of expression of their prenyltransferases and cognate substrates or their ability for probe uptake.[368]

Recent discoveries also suggest that the scope of the prenylome may be wider than the currently accepted paradigm since proteins terminating in the extended CXXXX or shorter CXX motifs can be potentially substrates of prenylation.[83,84] In our prenylomic studies, none of these types of proteins appeared to be enriched. However, ALDH9A1, an aldehyde dehydrogenase enzyme, has been consistently enriched in a number of cell lines we studied including COS-7, HeLa, MDA-MB-231, and OPM2 (Fig. 5.1A). This enzyme does not bear a canonical prenylation motif but rather contains two adjacent cysteines (Cys288/Cys289) within its protein sequence, with Cys288 ascribed as a catalytic residue (Fig. 5.1B).[583,584] We initially suspected that this protein may undergo proteolytic processing to reveal a nascent C-terminal Cys-Cys motif (Cys288 and Cys289) that could serve as a potential substrate for dual prenylation by RabGGTase. However, examining the peptides identified in our proteomic analysis revealed that residues downstream of Cys288/Cys289 are enriched, indicating that the intact full-length protein was isolated in our enrichment procedure. Therefore, labeling of ALDH9A1 with C15AlkOPP appears to deviate from the well-established rules for substrate recognition manifested by prenyltransferases.

5.3.2. C15AlkOPP labels ALDH9A1 but unresponsive to prenyltransferase inhibitors

In order to determine whether the C15AlkOPP probe indeed labels ALDH9A1 in our metabolic labeling experiments, the enzyme was overexpressed in COS-7 cells followed

by subsequent metabolic labeling. A plasmid expressing ALDH9A1 with a C-terminal GFP tag (ALDH9A1-GFP) was initially transfected in COS-7 cells followed by incubation with C15AlkOPP post-transfection. By placing the GFP tag in a C-terminal position downstream of ALDH9A1, it might have been possible to evaluate whether endoproteolytic cleavage to expose a C-terminal prenylation motif was occuring. However, this approach did not result in successful expression of the protein, perhaps owing to the fact that the C-terminal region of ALDH9A1 is important for it homotetramerization that is essential for its stability.[583] Instead, an N-terminal-tagged version (GFP-ALDH9A1) was used followed by metabolic labeling with C15AlkOPP and the lysates were subjected to click reaction with TAMRA-N_3. Importantly, that construct displayed an intense band near 75 kDa (Fig. 5.2A, lane 4), indicating successful labeling of the intact protein. Since C15AlkOPP has the ability to label all three classes of prenylation substrates, it is not clear whether the ALDH9A1 is potentially farnesylated or geranylgeranylated. Our lab has previously demonstrated that the shorter isoprenoid analogue C10AlkOPP is a good substrate in labeling farnesylated proteins *in vitro*.[333,585] On the other hand, the novel longer probe C20AlkOPP predominantly labels proteins near the 25 kDa region in lysates from HeLa where most geranylgeranylated proteins reside (data not shown). Treatment with C10AlkOPP does not result in effective labeling of ALDH9A1 (Fig. 5.2A, lane 5) while C20AlkOPP displays a diminished yet apparent labeling of GFP-ALDH9A1 (Fig. 5.2A, lane 6). This suggests that ALDH9A1 may be potentially geranylgeranylated.

To further establish the identity of the prenyl group modifying ALDH9A1, the C15AlkOPP probe was competed with the native isoprenoids. Co-treatment with 1.5-fold

excess of FPP or GGPP with C15AlkOPP significantly but not completely abolished the labeling on ALDH9A1 (Fig. 5.2B, lanes 5 and 7). Under these conditions, complete inhibition of the labeling of known prenylated proteins is readily achieved as indicated by the abolished signal in the 25 kDa region. Treatment with excess FPP inhibits both farnesylation and geranylgeranylation since FPP is elongated to GGPP by the GGPP synthase.[586] As both FPP and GGPP competition reduces its labeling, ALDH9A1 may indeed be geranylgeranylated. The prenyltransferases were also inhibited *in cellulo* by treating the transfected cells with known prenyltransferase inhibitors (Fig. 5.2C). Treatment with the FTase inhibitor L-744,832 (FTI) or GGTase-I inhibitor GGTI-286 (GGTI) did not significantly impact the labeling under concentrations previously reported to induce observable inhibition of intracellular prenylation.[379,587]

The absence of a CaaX-box motif in the full length ALDH9A1 is indicative that it is not a substrate of FTase and GGTase-I. However, this enzyme contains two adjacent cysteines Cys288/Cys289 with Cys288 shown to be the catalytic residue for its aldehyde dehydrogenase function. As previously mentioned, dual prenylation on adjacent cysteine residues is common among Rab family of proteins that are substrates of RabGGTase, albeit only when they are near the C-terminus. Interestingly, a dual cysteine motif of Rab5b in *Plasmodium falciparum* was shown be prenylated although these prenylatable cysteines are 65 amino acids upstream from the C-terminus of this protein.[365] We therefore examined the ability of known and novel RabGGTase inhibitors (RRGTI-1-3) in diminishing the C15AlkOPP-labeling on GFP-ALDH9A1. RGGTI-1 and RGGTI-2 were previously shown to be effective in inhibiting Rab geranylgeranylation at higher concentrations in HeLa cells

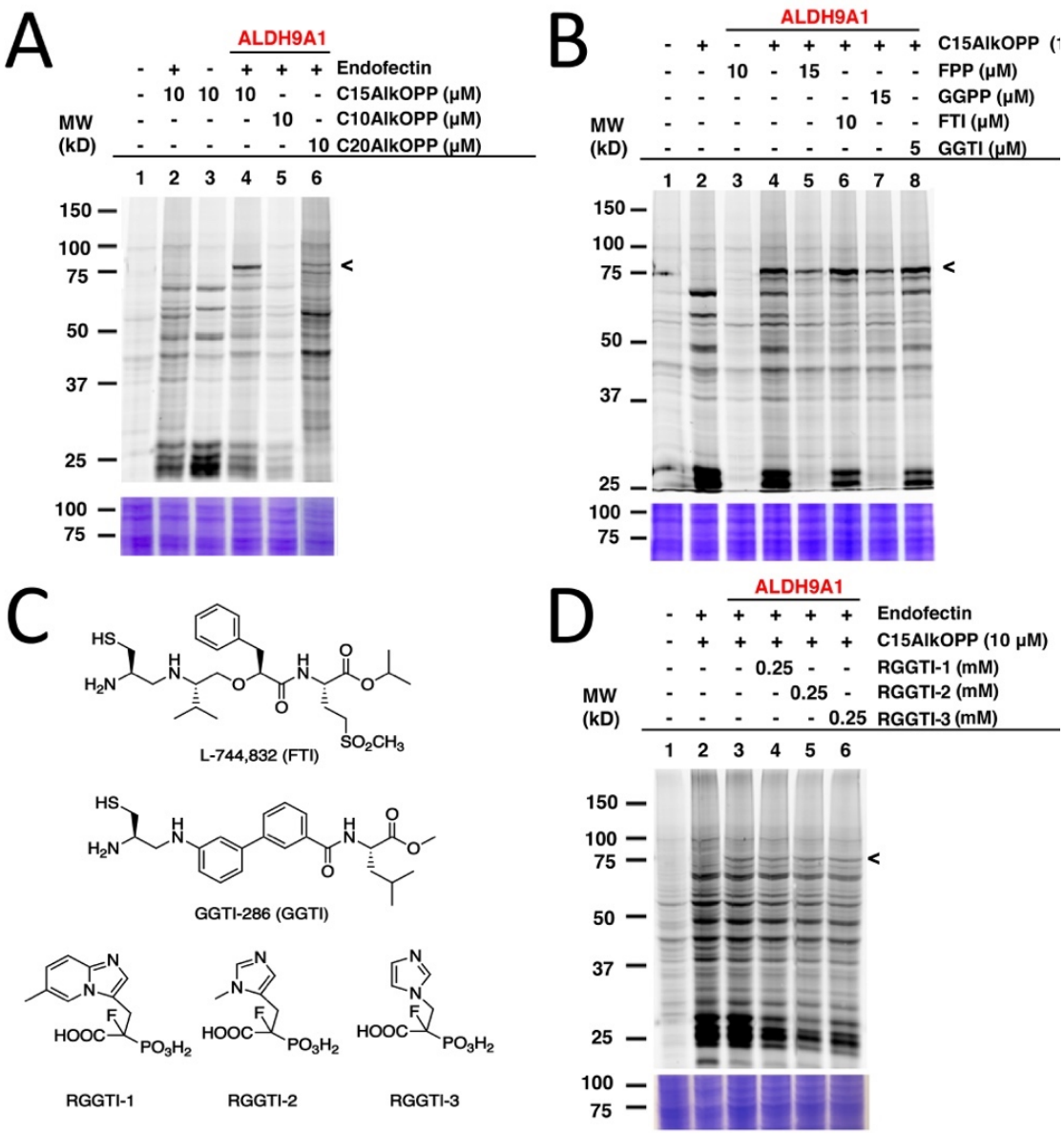

Figure 5. 2. The C15AlkOPP probe labels ALDH9A1 in cells.

A.) Labeling with isoprenoid probes with varying chain lengths in GFP-ALDH9A1 transfected in COS-7 cells. **B.**) Inhibition of the C15AlkOPP labeling with prenyltransferase inhibitors (FTI and GGTI) and competition with the native isoprenoids (FPP and GGPP). The C15AlkOPP labeling appears to be resistant in any of these inhibition/competition assays. **C.**) Structures of the prenyltransferase inhibitors used to inhibit the observed labeling on ALDH9A1. **D.**) Inhibition of the observed prenyl labeling on ALDH9A1 using RabGGTase inhibitors (RGGTIs). No apparent decrease in labeling was observed.

(IC_{50} = 358 μM and 297 μM, respectively).[588,589] On the other hand, RGGTI-3 displayed ineffective RabGGTase inhibition in HeLa with IC_{50} = 850 μM. Treatment with these

RGGT inhibitors in GFP-ALDH9A1-transfected COS-7 cells did not reduce the observed C15AlkOPP-labeling of GFP-ALDH9A1 (Fig. 5.2D). Under this RGGTI concentration (250 μM), the prenylome labeling in the 25 kDa region is significantly diminished where most Rab prenylation substrates migrate. If indeed RabGGTase prenylates ALDH9A1, a diminished labeling should have been observed in the presence of these RGGTIs. Therefore, ALDH9A1 does not appear to be a substrate of RabGGTase or any of the known prenyltransferases.

5.3.3. The key residues in ALDH9A1 function are involved in isoprenoid labeling

The aldehyde dehydrogenase (ALDH) superfamily is a family of NAD^+-dependent enzymes that catalyze the conversion of aldehydes to carboxylic acids with varying chain lengths.[590–592] ALDH9A1 in higher eukaryotes, especially in humans, is a homotetrameric enzyme that mediates the NAD^+-dependent oxidation of many aldehydes such as betaine aldehyde, the carnitine precursor 4-trimethylaminobuteraldehyde (TMABAL), the GABA precursor aminobutyraldehyde (ABAL).[593–595] The general mechanism of catalysis for ALDH9A1 and for most of these ALDHs initially involves NAD^+ co-factor binding that induces a conformational change resulting in activation of the thiol of a catalytic cysteine into a thiolate (Fig. 5.3A).[591] In ALDH9A1, NAD^+ binding in the coenzyme cavity is stabilized by many electrostatic interactions, which include the interaction between the pyrophosphate moiety of NAD^+ that interacts with the residues Trp156, Ser233, and Thr236.[584] The activated thiol then attacks the carbonyl of the aldehyde substrate, generating a thiohemiacetal intermediate stabilized by NH groups from the ALDH9A1 peptide chain. A hydride transfer to NAD^+ then follows, resulting in reduction of NAD^+ to

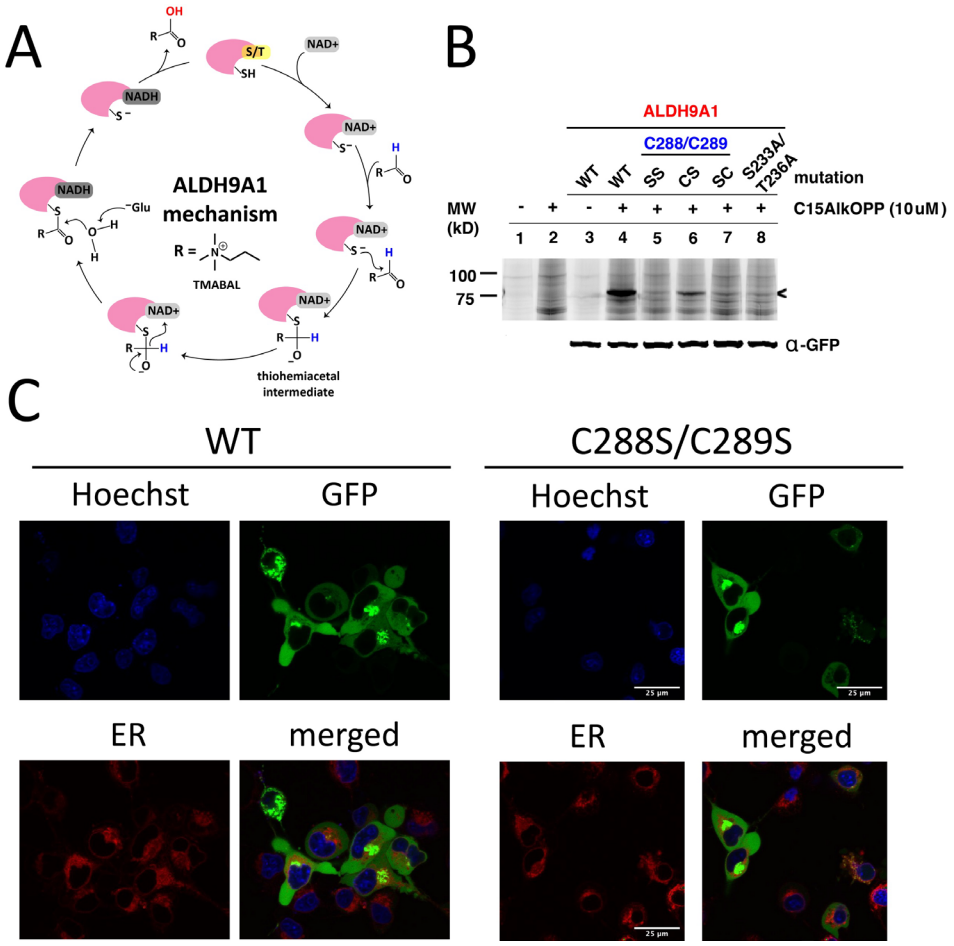

Figure 5. 3. Essential amino acids in ALDH9A1 function influence prenyl labeling.

A.) Mechanism of the ALDH9A1 activity. NAD^+ binds to ALDH9A1 in the coenzyme cavity stabilized by many interacting residues including Ser233 and Thr236. The catalytic Cys288 is activated and attacks the carbonyl of the aldehyde substrate. A thiohemiacetal intermediate is formed and subsequently oxidized by NAD^+ leaving a thioester bound substrate. A water molecule hydrolyzes the substrate assisted by an acidic amino acid (Glu). **B.**) Mutations on the residues essential to ALDH9A1 activity impacts the observed labeling. Labeling occurs on Cys288 and is affected by Cys289. Loss of the essential residues in the coenzyme cavity through double mutation Ser233A and Thr236A abolished labeling. **C.**) Fluorescent imaging of COS-7 cells transfected with wild-type or C288S/C289S mutant GFP-ALDH9A1. ALDH9A1 is distributed in the cytoplasm in both samples with observable puncta formation potentially resulted from aggregation. Hoechst, blue, nuclear stain; GFP, green, GFP-ALDH9A1; Endoplasmic reticulum (ER) tracker; red; ER.

NADH and oxidation of the substrate to a thioester. This bound substrate then undergoes hydrolysis with the aid of a charged amino acid (usually Glu) to release the carboxylic acid

product. The residue C288 is the known to be the catalytic cysteine in ALDH9A1 while an adjacent Cys289 has no currently known function in this enzyme. A related yeast enzyme ALDH4 also contains this dual cysteine motif Cys324/Cys325 with Cys324 being the catalytic residue. A recent study has shown Cys325 regulates the yeast enzyme's function by forming a disulfide bond with Cys324, in order to promote an oxidative stress response.[596] Similarly, the human ALDH1A1 exhibits the same disulfide bond formation between its active nucleophile Cys303 and the adjacent Cys302.[596]

Based on the mechanism described above, we decided to dissect the role of some of the amino acids essential for ALDH9A1-mediated catalysis. Therefore, site-directed mutagenesis was performed on the aforementioned protein construct to introduce mutations in some of these key residues and the resulting constructs transfected into COS-7 cells, followed by metabolic labeling with C15AlkOPP and click chemistry. Double mutation of the Cys288,Cys289 pair to serine residues (Cys288S,Cys289S, abbreviated SS) completely abolished labeling (Fig. 5.3B). Mutating the cysteine adjacent to the catalytic residue (C289S, CS) diminished the probe incorporation, whereas the mutating the catalytic cysteine only (C288S, SC) completely abrogated the signal. This suggests that probe labeling occurs on the catalytic Cys288 with Cys289 contributing in an indirect way. As a control experiment, metabolic labeling was also performed in cells transfected with GFP-ALDH1A1 bearing this dual cysteine motif (Cys302/Cys303) but no labeling was observed (data not shown). We also examined the potential participation of NAD^+ in the course of probe incorporation. Mutating residues Ser233 and Thr236, key amino acids essential to NAD^+ binding, into alanine also completely abolished the observed labeling.

Thus, these latter experiments suggest that NAD^+ may be involved in this process of isoprenoid labeling of the catalytic Cys288 of ALDH9A1.

Protein prenylation is often associated with membrane targeting of the modified substrates, with the prenyl moiety serving as an anchor.[77] Among the many protein prenylation substrates, mouse ALDH3B2 and ALDH3B3 are examples of aldehyde dehydrogenase enzymes known to be prenylated, both possessing the C-terminal sequence CTLL.[597] Although both are prenylated, they differ in their cellular localization—ALDH3B3 localizes in the plasma membrane while ALDH3B2 resides in lipid droplets—influenced by some key residues in their corresponding C-termini.[597] We therefore assessed the localization of the transfected GFP- ALDH9A1 fusion protein employed above and compared it with the corresponding double C288S/C289S mutant using fluorescence microscopy (Fig. 5.3C). There were no observable differences in the localization of the wild-type versus mutant. The protein appeared to be distributed across the cytoplasm, although discrete puncta were present in both samples. This protein species also did not localize in the endoplasmic reticulum (ER) where clusters of proteins reside during protein synthesis. Therefore, these puncta maybe protein aggregates, which is a common phenomenon in protein overexpression in cells, particularly with proteins bearing a considerable number of cysteine residues (16 Cys in ALDH9A1).[598] It is also possible that these puncta are lipid droplets, although the potential isoprenoid modification on ALDH9A1 may not necessarily influence this mechanism of localization. This hypothesis may be evaluated in future experiments.

5.3.4. *In vitro* assays do not support autoprenylation

The experiments above provide evidence that the C15AlkOPP probe modifies ALDH9A1 *in cellulo* most likely on its catalytic cysteine residue. In order to study this process in more detail, it was desirable to acquire a pure form of the enzyme and evaluate the isoprenoid probe labeling under varying conditions *in vitro*. Accordingly, a His-tagged form of ALDH9A1 was heterologously expressed in *E. coli* and purified to study the possible mechanism of prenylation in a cell-free system.

The purified enzyme was first incubated with the three different prenyltransferases in the presence of C15AlkOPP under conditions suitable for *in vitro* prenylation (Fig. 5.4A).[99,333] It is important to note that the contrast in these gel images was adjusted for clearer visualization but these were actually weak signals compared to bona fide prenylation substrates. As expected, none of the prenyltransferases efficiently catalyzed C15AlkOPP-labeling of ALDH9A1 (Fig. 5.4A lanes 4, 6, and 8), consistent with the observed *in cellulo* results in Fig. 5.2B and 5.2D. However, it appears that the presence of NAD^+ somehow increased the labeling (Fig. 5.4A lanes 5, 7, and 9), which was also apparent when the enzyme was incubated with the probe and NAD^+ in the absence of any prenyltransferase (Fig. 5.4A lane 3). We then evaluated if probe labeling could be increased by treating with C15AlkOPP at higher probe concentrations in the presence of NAD^+ (Fig. 5.4B). Indeed, significant labeling was observed at high probe concentrations (500 μM) in the presence of NAD^+ (Fig. 5.4B lane 7), which was not observed when NAD^+ was absent (Fig. 5.4B lane 6). While this high probe concentration is not physiologically relevant

compared to the actual FPP and GGPP concentrations inside cells, the highly specific requirement for NAD^+ and not NADH was noteworthy.

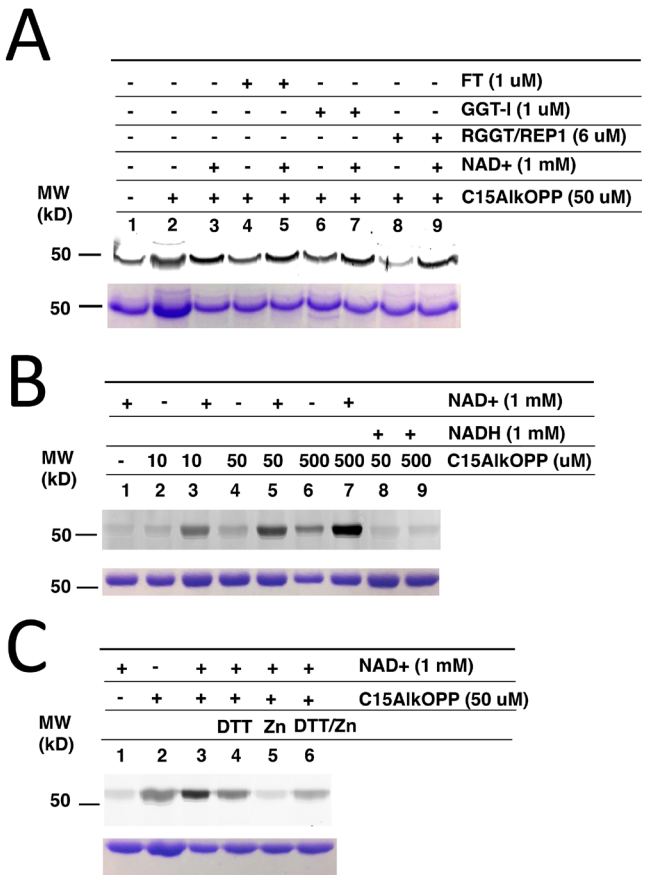

Figure 5. 4. *In vitro* labeling with C15AlkOPP.

A.) Incubation of His-ALDH9A1 with C15AlkOPP in the presence or absence of NAD^+ and various prenyltransferases. The intensities of labeling are weak and only observable after adjusting the contrast. NAD^+ appears to increase labeling on ALDH9A1. **B.**) Incubation of His-ALDH9A1 with increasing concentrations of C15AlkOPP. The observed labeling improves with concentration of C15AlkOPP and in the presence of NAD^+. **C.**) Incubation of His-ALDH9A1 with C15AlkOPP in the presence of reagents essential for prenyltransferase activity. ALDH9A1 did not exhibit autoprenylation.

Since probe labeling is achievable at high C15AlkOPP concentrations in the presence of NAD^+, we then speculated that ALDH9A1 may possess an inherent prenyltransferase activity. In *in vitro* prenylation assays, DTT is commonly added in order

retain the prenylatable cysteines of substrates as free thiols. A Zn^{2+} cofactor is also required to polarize the prenylatable thiol for a more efficient isoprenoid modification. We therefore evaluated the probe labeling in the presence of either DTT (Fig. 5.4C lane 4) or Zn^{2+} (Fig. 5.4C lane 5), or both (Fig. 5.4C lane 6). None of these additional components improved the C15AlkOPP labeling on ALDH9A1. In fact, they may have diminished the observed probe labeling. Therefore, ALDH9A1 may not proceed through an autoprenylation mechanism with C15AlkOPP under the conditions tested.

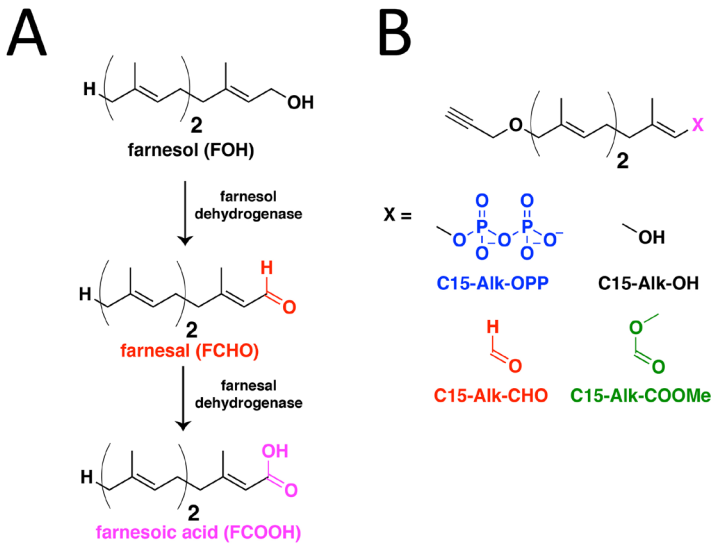

Figure 5. 5. Isoprenoids with varying functional groups.

A.) Conversion of farnesol (FOH) to farnesal (FCHO) and farnesoic acid (FCOOH) catalyzed by farnesol dehydrogenase and farnesal dehydrogenase, respectively. **B.**) Structures of alkyne-modified isoprenoid analogues with varying functional groups.

Although the isoprenoid analogue C15AlkOPP was used in the *in cellulo* labeling experiments to show that ALDH9A1 can be prenylated, this probe may be metabolized into other known forms of isoprenoids inside cells. For example, FPP can be hydrolyzed into products including farnesol (FOH) and farnesyl phosphate (FP), which can serve as non-sterol regulators of the mevalonate pathway.[599] Inhibition of the squalene synthesis

(downstream of FPP biosynthesis) also results in FPP hydrolysis to farnesol, leading to increased production of farnesoic acid in mouse liver.[600] Farnesol is first converted to farnesal and subsequently to farnesoic acid by the NAD^+-dependent enzymes farnesol and farnesal dehydrogenase, respectively (Fig. 5.5A).[601] This conversion of farnesol to farnesal and farnesoic acid is not well-characterized in higher eukaryotes but better understood in lower-order organisms such as in insects owing to its role in juvenile hormone biosynthesis.[602] However, extracts from mammalian tissues also exhibit juvenile hormone bioactivity and therefore these oxidized isoprenoid species may truly be present in higher eukaryotes.[603]

Due to the possibility that C15AlkOPP may be metabolized into products described above, we synthesized versions of the alkyne-containing isoprenoid with varying functional groups (Fig. 5.5B). We also synthesized farnesal and farnesoic acid according to published methods reported in the literature.[604] We evaluated these probes for their ability to inhibit the enzymatic activity of ALDH9A1, which could reflect their potential to modify the active site cysteine. In this assay, ALDH9A1 (1 μM) was incubated with the isoprenoid probe (100 μM) in a pyrophosphate buffer for one hour and the bona fide substrate TMABAL (1 mM) and NAD^+ (1 mM) were added to initiate oxidation of TMABAL (Fig. 5.3A). The enzymatic activity was recorded as changes in the absorbance at 340 nm where the NADH product absorbs. The resulting kinetic profiles showed that FPP, farnesol (FOH) and farnesoic acid (FCOOH) did not affect the enzymatic activity but farnesal (FCHO) completely impaired the reaction (Fig. 5.6A). Analogues of the longer isoprenoid GGPP and geranylgeraniol (GGOH) also did not affect the enzymatic activity

of ALDH9A1 (Fig. 5.6B). We were not able to generate geranylgeranal (GGCHO) and geranylgeranoic acid (GGCOOH) although these latter metabolites may exist *in vivo* as they have been detected in rat liver homogenates.[605]

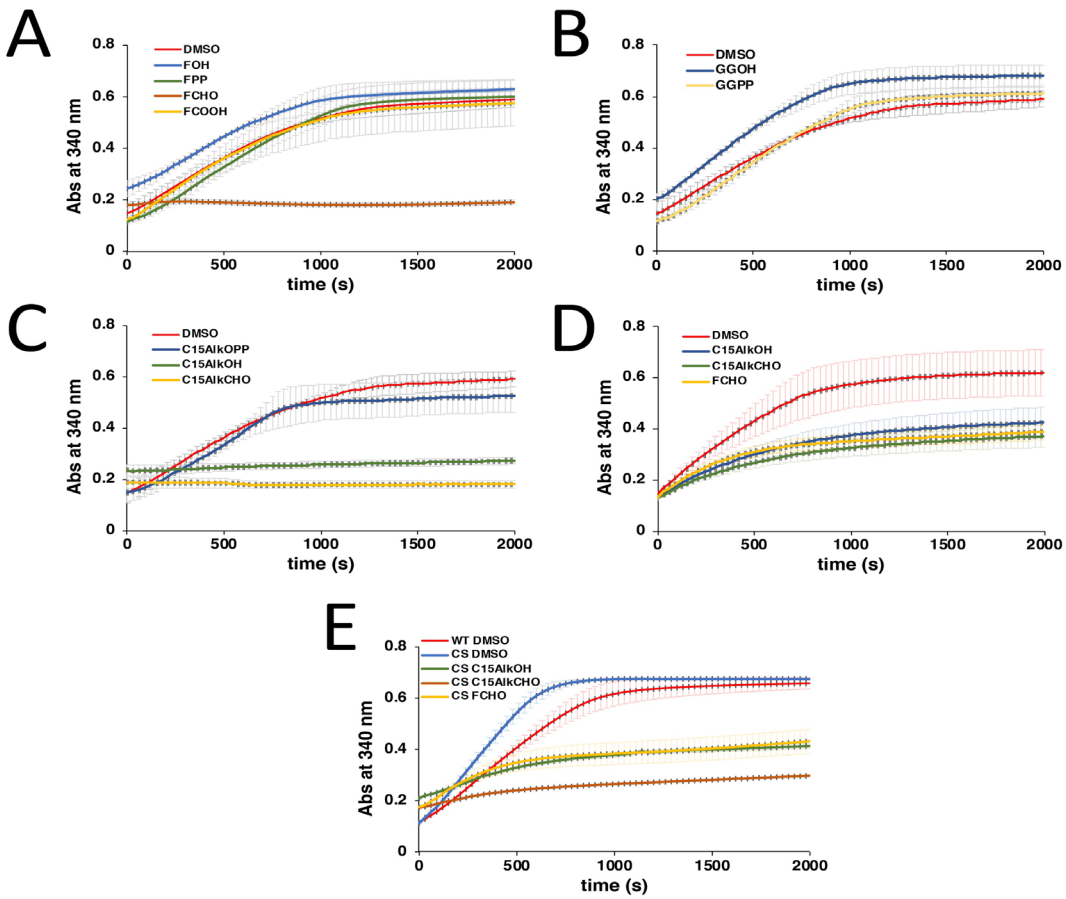

Figure 5. 6. Kinetic profiles of ALDH9A1 activity in the presence of isoprenoid analogues.

A.) Kinetics of ALDH9A1 activity with TMABAL (1 mM) in the presence of NAD^+ (1 mM) and analogues of farnesol (FOH). Absorbances were recorded at 340 nm where the NADH product absorbs. **B.**) Kinetics of ALDH9A1 activity in the presence of geranylgeraniol (GGOH) or geranylgeranyl diphosphate (GGPP). **C.**) Kinetics of ALDH9A1 activity in the presence alkyne-modified isoprenoid analogues. **D.**) Dilution assays of ALDH9A1 initially incubated with potential inhibitors and diluted 10-fold with TMABAL and NAD^+. **E.**) Kinetics of ALDH9A1 C289S mutant activity.

We also compared the alkyne-modified versions of this isoprenoid with varying functional groups (Fig. 5.6C). The diphosphate C15AlkOPP did not inhibit ALDH9A1

activity while both the alcohol C15AlkOH and aldehyde C15AlkCHO suppressed the enzymatic reaction. While the observed inhibition by C15AlkCHO is consistent with that observed with FCHO, the observed inhibition by C15AlkOH was unexpected since FOH did not result in diminished enzymatic activity (Fig. 5.6A). In order to determine whether these potential inhibitors are reversible and time-dependent inhibitors similar to diethylaminobenzaldehyde (DEAB), a known inhibitor of ALDH9A1,[584] we performed a dilution assay. In this assay, the isoprenoid was incubated with ALDH9A1 for one hour and diluted 10-fold with the pyrophosphate buffer containing both TMABAL and NAD^+ (ALDH9A1 and isoprenoid at 1 and 10 μM final concentrations, respectively). If the isoprenoid is a reversible, time-dependent inhibitor, a lag in the recovery of ALDH9A1 activity should be observed in the first few minutes after dilution. In our dilution assays, however, inhibition by the isoprenoids did not exhibit significant lag (no reaction) in enzymatic activity but displayed slow recovery of the TMABAL conversion (Fig. 5.6D). This may suggest that these isoprenoids can reversibly inhibit ALDH9A1 in a time-independent manner.

As previously mentioned, an adjacent cysteine to the catalytic cysteine residue may play an important function in controlling the enzyme's function such as in yeast ADLH4 and human ALDH1A1.[596] We therefore speculated that mutating Cys289 adjacent to the catalytic Cys288 in ALDH9A1 may impact the observed inhibition by the isoprenoids. We therefore expressed and purified ALDH9A1 with a C289S mutation (ALDH9A1 CS) and evaluated its response to isoprenoid inhibition. It appears that this mutation did not affect the observed inhibition in wild-type ALDH9A1 (Fig. 5.6E). However, we noticed that

ALDH9A1 CS displayed slightly improved activity compared with the wild-type, and therefore Cys289 may potentially play a role in preserving or impairing the ALHD9A1 function.

5.3.5. The isoprenoid modification is hydrolyzable

Results from *in vitro* assays with the alkyne-modified isoprenoid analogues varying in functional groups did not strongly support autoprenylation of ALDH9A1 under physiological isoprenoid concentrations. In order to test whether these analogues can be efficiently incorporated to ALDH9A1 inside the cells, we turned back into our metabolic labeling approach in COS-7 cells transfected with ALDH9A1. The C15AlkOH probe (FOH or GGOH analogue) displayed appreciable labeling with ALDH9A1 but slightly weaker compared to that observed with C15AlkOPP (Fig. 5.7A lane 3). A previous report of using this analogue in profiling prenylated proteins identified ALDH9A1 as one of the highly enriched prenylated proteins.[360] Although both C15AlkOPP and C15AlkOH can label ALDH9A1, a more intense band is observed with C15AlkOPP. Thus, the isoprenoid modification on ALDH9A1 may be derived from the diphosphate analogue and that C15AlkOH may have been converted by host cell kinases to C15AlkOPP.[347] We also evaluated the ability of the alkyne-modified analogue of farnesal (C15AlkCHO) and the methyl ester C15AlkCOOMe in labeling ALDH9A1. We rationalized that C15AlkCOOMe can efficiently penetrate the plasma membrane and be hydrolyzed by cellular esterases to C15AlkCOOH, an analogue of FCOOH or GGCOOH. However, none of these analogues efficiently modified ALDH9A1 (Fig. 5.7A lanes 4 and 5). It is possible that these analogues

were bound to or reacted with serum proteins in the media and were not able to enter the cells.

While our previous *in vitro* analyses showed that isoprenoids with different functional group did not directly modify ALDH9A1, it does not rule out the conversion of C15AlkOPP into this variety groups that could potentially result in a reversible modification on ALDH9A1 such as through a thioester or thiohemiacetal bond. We next investigated whether this observed modification can be hydrolyzed by hydroxylamine. Base hydrolysis is commonly employed to distinguish reversible modifications such as *S*-palmitoylation on proteins since the thioester bond on palmitoylated cysteines is labile to hydroxylamine. Treatment with hydroxylamine in C15AlkOPP-labeled GFP-ALDH9A1-expressing COS-7 cells completely abolished the isoprenoid labeling (Fig. 7B). Thus, C15AlkOPP-mediated labeling appears to involve a hydrolyzable modification on ALDH9A1 instead of a thioether linkage that is resistant to hydrolysis that typically occurs in farnesyl or geranylgeranyl protein modification.

The observed hydrolyzable modification on ALDH9A1 suggests that the isoprenoid modification may possibly involve a thioester or a thiohemiacetal functionality on a cysteine residue. Hence, we attempted to obtain a mass spectrum of the peptide modified with the alkyne-functionalized probe. COS-7 cells expressing the GFP-ALDH9A1 were treated with C15AlkOPP and the enzyme was immunoprecipitated using an anti-GFP resin. The immobilized protein was reduced, alkylated, and digested on-bead, generating tryptic peptides that were processed for LC-MS analysis. The reduced and

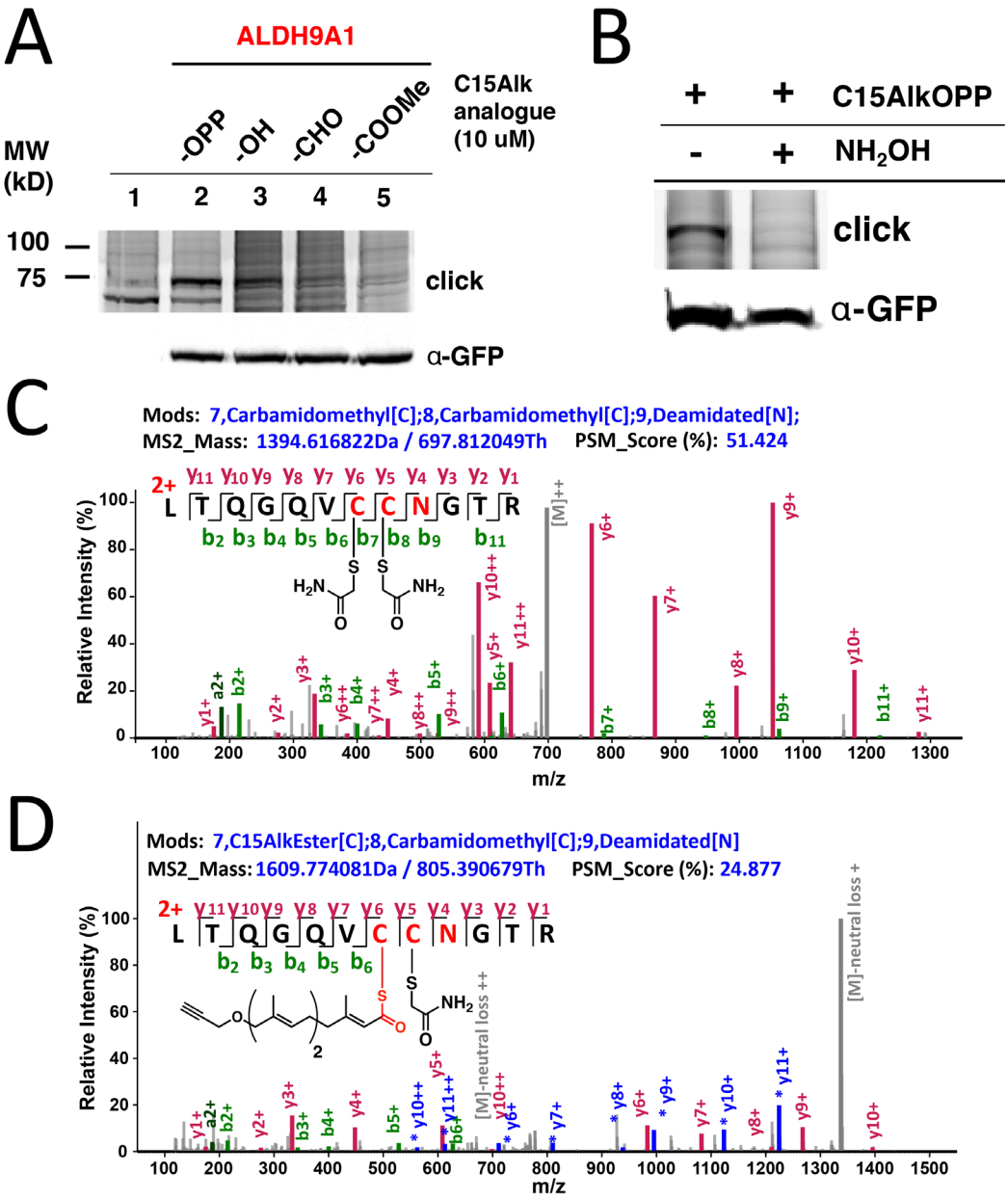

Figure 5. 7. Hydrolyzable modification on ALDH9A1

A.) In-gel fluorescence analysis on lysates from COS-7 cells transfected with GFP-ALDH9A1 and treated with various alkyne-modified isoprenoid analogues. **B.)** Hydrolysis of the observed labeling on C15AlkOPP-labeled GFP-ALDh9A1 using NH_2OH. **C.)** Mass spectrum of reduced/alkylated active site peptide of ALDH9A1. **D.)** Mass spectrum of the C15Alk-thioester-modified Cys288 of the active site peptide of ALDH9A1.

alkylated form of the peptide containing Cys288 and Cys289 was efficiently detected (Fig. 5.7C), indicating that a significant fraction of ALDH9A1 exists with the free Cys288 and

Cys289 thiols. In addition, we also detected the C15Alk thioester-modified ALDH9A1 with rather weaker signals (Fig. 5.7D). This MS data may suggest that the native isoprenoids may modify ALDH9A1 through a thioester bond. We therefore repeated the experiment in samples treated with FPP or GGPP instead. However, a mass spectrum for the thioester-modified Cys288 with the native farnesyl or geranylgeranyl isoprenoids could not be detected even after several attempts. If either farnesyl or geranylgeranyl truly modifies the active site through a thioester bond, obtaining their mass spectra is quite challenging owing to the sensitivity of thioester bonds to common proteomics sample processing, particularly in the reduction and alkylation step. Furthermore, the greasy modification from the isoprenoids on peptides commonly impacts their ionization efficiency in LC-MS analysis, thereby lowering the signal-to-noise ratio and complicating the detection of the lipid-modified peptide.[112]

5.4. Discussion

Chemical proteomic technologies has been proven to be a robust tool to identify novel post-translationally modified proteins. Here we report the discovery of ALDH9A1 initially identified through chemical proteomic profiling of prenylated proteins, followed by biochemical characterization of the isoprenoid modification on this enzyme.

In defining the scope of the prenylated proteome (prenylome), an isoprenoid analogue bearing an alkyne moiety has been commonly used to metabolically tag or label proteins *in vitro* in order to define the set of prenylated proteins, depending on the goal of the study. This strategy has led to the identification of known and novel proteins,

particularly those that are implicated in diseases such as choroideremia, Alzheimer's disease and parasitic and viral infections.[360,363,366,368,369] With our efforts to expand the scope of prenylated proteins, we have used this approach to search for proteins terminating in CXXXX sequences, which were shown to be substrates of farnesylation *in vitro* and inside the cells.[83] Despite their potential occurrence, we did not find any statistically enriched protein bearing such type of C-terminal sequence. Rather, in many of our prenylomic analysis in various cell lines, ALDH9A1 was consistently enriched, indicating that our isoprenoid probe modifies this enzyme. Overexpression of this enzyme in COS-7 cells combined with metabolic labeling with our isoprenoid probe indeed confirmed that this enzyme is prenylated. But the how and why this process occurs are the questions we attempted to address in this study.

We have shown through cellular and *in vitro* experiments that this observed isoprenoid modification on ALDH9A1 is not catalyzed by any of the known prenyltransferases. We initially suspected that this protein could be a substrate of RabGGTase owing to its dual cysteine motif in the center of its protein sequence. Rab5b in *P. falciparum* also contains this dual cysteine motif several amino acids upstream from its C-terminal and was shown to be labeled by C15AlkOH.[365] Although this protein is a member of the Rab family, it was not clear whether RabGGTase catalyzes the observed prenyl modification. Moreover, our results showed that ALDH9A1 acquires the isoprenoid modification while it is intact, indicating that the prenyl group is attached to an internal cysteine residue that is not recognized by any known prenyltransferase.

The ALDH superfamily constitutes an important class of enzymes that play key roles in modulating oxidative/electrophilic stress inside cells.[606] In fact, dysregulation in their expression and function has been implicated in a variety of cancers and inhibitors specific to these enzymes have been developed for cancer therapeutics.[607] Similar to sorbitol and alcohol dehydrogenases, ALDHs have been known to possess reactive nucleophilic cysteines in their active sites that drive the conversion of toxic aldehyde species to innocuous carboxylic acid derivatives, or in deactivating reactive aldehyde and oxygen species.[606,608] The recent developments in chemical proteomic strategies have allowed for profiling of proteins bearing reactive cysteines in which several ALDHs have been identified.[609–611] In particular, ALDH9A1 has been consistently identified in these chemical proteomic studies, underscoring the high reactivity of its active Cys288 residue. Given this information, it is plausible that this enzyme can acquire modifications under physiological conditions, either enzymatically or non-enzymatically.

Another salient characteristic of ALDH9A1 is the presence Cys289 adjacent to the nucleophilic Cys288. Other ALDHs also contain this dual (even triple) cysteine motif: ALDH2 (Cys318/Cys319*/Cys320), ALDH1A1 (Cys302/Cys303*), ALDH1A2 (Cys319/Cys320*), ALDH1A3 (Cys313/Cys314*), and ALDH1B1 (Cys318/Cys319*/Cys320), where * denotes the catalytic cysteine. Among these ALDHs, only ALDH9A1 was consistently enriched in our prenylomic analyses. Mutation of Cys289 to Ser in ALDH9A1 caused an appreciable decrease in isoprenoid labeling, indicating that it may participate in the mechanism of prenylation of Cys288. Previous studies in ALDH1A1 have shown that Cys302 adjacent to the nucleophilic Cys303 may control its

activity through disulfide bond formation and is potentially important for cellular response to oxidative stress.[596] This does not seem to be the case for ALDH9A1 since its isoprenoid labeling and activity does not improve in the presence of reducing reagents such as DTT. Interestingly, the mutant ALDH9A1 (C289S) appears to retain stability better than the wild-type as observed in our *in vitro* assays (Fig. 6E). Cys289 may modulate the nucleophilicity of Cys288 in some as of yet undiscovered manner.

ALDHs are classified as $NAD(P)^+$-dependent enzymes that require this cofactor as hydride acceptors in the oxidation of their aldehyde substrates.[612] These enzymes adopt a Rossman fold in their dinucleotide-binding domains that hosts the $NAD(P)^+$ cofactor.[613] In ALDH9A1, several essential residues that constitute to this coenzyme cavity interact and stabilize NAD^+ binding including Ser233 and Thr236, which form contacts with the pyrophosphate portion of NAD^+.[583,584] Mutations of these two essential residues into Ala resulted in loss of isoprenoid labeling *in cellulo*, suggesting NAD^+ may be involved in the mechanism of attaching the isoprenoid onto Cys288. Furthermore, our *in vitro* assays show that incubation of ALDH9A1 with the probe and NAD^+ exhibits labeling dependent on the probe concentration. Therefore, there must be a mechanism that requires NAD^+ for isoprenoid modification on ALDH9A1.

In cellulo, both C15AlkOPP and C15AlkOH can confer labeling on ALDH9A1 but not C15AlkCHO or C15AlkCOOMe, albeit the observed modification is hydrolyzable. Our attempts to identify the modified peptide using mass spectrometry provided evidence of isoprenoid modification through a thioester bond. However, we only observed this with the

probe but not with the native farnesyl nor geranylgeranyl diphosphate. If modification with either of these prenyl moieties truly occurs, their detection is particularly challenging owing to the inherent recalcitrant behavior of lipidated peptides in mass spectrometry.

Taking our data together, we propose the following model for how the prenyl modification can plausibly occur on ALDH9A1 (Fig. 5.8). The prenyl group from the isoprenoid diphosphate is appended to the reactive Cys288 via an unknown mechanism that results in a thioether linkage. This bond formation may be promoted by other cofactors or residues within ALDH9A1 that catalyze such a process. A one-electron oxidation then occurs wirth NAD^+ accepting a hydride from the prenyl group, leaving a thiohemiacetal species. A second oxidation catalyzed by NAD^+ then proceeds resulting in a thioester bond. The neighboring Cys289 may be involved in this process by forming an intermediate bond formation with the activated carbon or through enhancing the nucleophilicity of Cys288.

Our proposed mechanism may not accurately describe the actual isoprenoid labeling observed on ALDH9A1. If prenylation truly occurs in nature, the reversibility of the isoprenoid modification due to thioester formation may provide clues into the potential regulation of ALDH9A1 activity. Studies of the crystal structures of ALDH9A1 suggest that there could be a control mechanism that exists in order to regulate this enzyme's

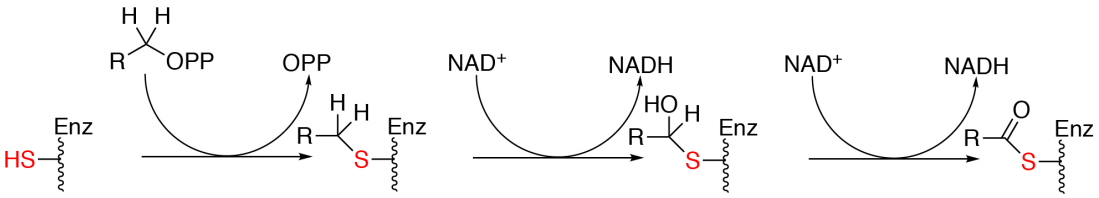

Figure 5. 8. Proposed mechanism for the observed isoprenoid modification on ALDH9A1.

The prenyl moiety is appended to the catalytic residue Cys288 via thioether bond through an unestablished mechanism. NAD^+ abstracts a hydride to oxidize the thioether into a thiohemiacetal. Another round of hydride transfer then results in a thioester modification on ALDH9A1.

function.[583] ALDH9A1 is involved in the hepatic biosynthesis of L-carnitine, an essential cofactor for the transfer of fatty acids to mitochondria for fatty acid oxidation.[614] Under conditions where the pool of isoprenoids is depleted, this modification of ALDH9A1 should be reduced and potentially increase L-carnitine production. However, studies have shown that treatment with statins—an inhibitor of isoprenoid biosynthesis—induces adverse effects through mitochondrial dysfunction in diabetes, which can be rescued by the addition of L-carnitine.[615] This implies that statin treatment may actually decrease L-carnitine biosynthesis, or perhaps induces the observed pleiotropic effects via mechanisms irrelevant to L-carnitine biosynthesis. Additional evidence concerning the actual identity of the isoprenoid or isoprenoid-derived modification is much needed to fully characterize this unusual modification and dissect the molecular mechanisms via which this process occurs. Delineating the biological consequence of this modification on ALDH9A1 activity could also expand our current knowledge of enzymatic activity regulation. While many of these questions remain unanswered, this work nonetheless describes a potential reversible isoprenoid or isoprenoid-derived modification on ALDH9A1 that may regulate its function.

5.5. Conclusion

In this work, we described the potential isoprenoid modification on ALDH9A1 discovered through chemical proteomics. Through the use of tools from chemical and molecular biology, we demonstrated that this isoprenoid or isoprenoid-like labeling on ALDH9A1 is robust but reversible. Characterizing through the use of isoprenoids bearing different functional groups in *in vitro* assays did not provide substantial evidence as to how this unusual modification occurs in nature. This potentially new type of isoprenoid modification opens new doors into the chemistry of lipid modifications on proteins, particularly in modifying the catalytic residue of an enzyme that may have functional roles in regulating its activity. The experiments described here set the stage for future work aimed in understanding this unusual post-translational modification on a protein. More evidence on characterizing this novel protein modification is therefore anticipated.

5.6. Methods

5.6.1. General Reagents

COS-7 and HeLa cells were generously provided by Dr. Elizabeth Wattenberg at the University of Minnesota, USA. The FTI L-744,832 was purchased from Merck and GGTI-286 from CalBiochem. The RabGGTase inhibitors 1, 2, and 3 were generously provided by Dr. Katarzyna Blazewska at Lodz Univeristy of Technology, Poland.[588,589]

5.6.2. Plasmid preparation

A plasmid expressing human ALDH9A1 was purchased from Genecopoeia. The ALDH9A1 gene was inserted in a vector (EX-Z3075-M29) to contain an N-terminal GFP tag controlled by the CMV promoter. Plasmids were transformed in 100 μL of competent DH5α *E. coli* (New England Biolabs) following the manufacturer's protocol. Transformed bacteria were plated in Luria broth (LB) agar plates containing ampicillin and colonies were isolated for bacterial cultures in 50 mL LB media. Cultures were grown overnight at 37 ºC and bacteria were pelleted by centrifugation at 6000 *x g* for 20 mins at 4 ºC. The bacterial pellets were suspended in sterile water and plasmids were extracted using PureYield™ Plasmid Miniprep System (Promega) following the manufacturer's protocol. Plasmid concentrations were determined by taking the absorbance at 260 and 280 nm using NanoPhotometer P330 (IMPLEN) and using the equation: concentration (μg/mL) = (A_{260} – A_{320}) x dilution factor x 50 μg/mL. Only good quality plasmids (A_{260}/A_{280} ~ 1.7 to 1.8) were used for transfection.

5.6.3. Transfection, in-gel fluorescence and cellular imaging

COS-7 cells were grown in 100-mm culture plates under DMEM media (Gibco) supplemented with 10% fetal bovine serum (Gibco) and 1% penicillin-streptomycin (Gibco). Cells were passaged before reaching 80% confluency and repeated at least three times prior to transfection. A day before transfection, cells (1.6 x 10^6) were seeded and grown overnight until 90% confluency is achieved. The media was removed and replaced with 10 mL of Opti-MEM™ Reduced Serum Media (Thermo Fisher Scientific). Plasmids (15 μg) and 50 μL of Endofectin Max (Genecopoeia) were each diluted to 750 μL with

Opti-MEM™ in separate tubes. The solutions were combined and added to the cells dropwise. After 8 hours post-transfection, 10 μM of C15AlkOPP, isoprenoid analogues, and inhibitors (when indicated) were added and allowed to incubate for 16 more hours. Cells were washed and collected by scraping and subjected to lysis in 1X PBS + 1% SDS as described in our previously reported protocol.[358] Protein concentrations were determined using BCA assay (Thermo Scientific).

For in-gel fluorescence analysis, 100 μg proteins were used for click reaction with 25 μM TAMRA-N_3, 1 mM TCEP, 0.1 mM TBTA, and 1 mM $CuSO_4$. Labeled proteins were resolved in a 12% SDS-PAGE gel. TAMRA fluorescence (542/568 nm excitation/emission) was detected using Typhoon FLA 9500 (GE Healthcare). Gels were stained with Coomassie blue and destained. For western blot analysis, proteins in gels were transferred to a PVDF membrane using Mini Trans-Blot® Electrophoretic Transfer Cell (Bio-Rad) and blocked with 5% milk. Membranes were incubated with mouse anti-GFP (ABclonal) overnight followed by incubation with a secondary goat HRP-conjugated anti-mouse (ABclonal) and treated with Clarity™ ECL (Bio-Rad). Chemiluminescence was detected using iBright (Thermo Fisher). Gel images were processed on ImageJ.

For fluorescence cellular imaging, cells (500,000) were seeded in 35-mm glass-bottomed dish (Ibidi USA) and grown overnight until 90% confluency. The DMEM media was replaced with 2 mL of Opti-MEM™. DNA plasmids (2.5 ng in 125 μL Opti-MEM™) and Endofectin (7.5 μL diluted to 125 μL with Opti-MEM™) were mixed and added dropwise to the cells. After 24 hrs, media was removed and cells were washed with cold

1X PBS (2 mL) twice, followed by staining with Hoechst 33342 (Thermo Scientific) and ER-Tracker™ Red (Invitrogen) following the manufacturers' protocols. Cells were washed twice with PBS and visualized under using FluoView FV1000IX2 Inverted Confocal Microscope (Olympus) with a 60X objective. The .oib files were imported in Fiji and formatted.

5.6.4. Site-directed mutagenesis

Human ALDH9A1 mutants were generated from template plasmid (EX-Z3075-M29) described above using QuickChange XL II Site-Directed Mutagenesis Kit (Agilent). Primers were designed with the corresponding mutations as prescribed by the QuickChange Primer Design tool (https://www.agilent.com/store/primerDesignProgram.jsp) with minor alterations at the 3' end and the oligos were purchased from Integrated DNA Technologies. In brief, the template plasmid (50 ng) was incubated with the forward (125 ng) and reverse (125 ng) primers, dNTP mix, and PfuTurbo DNA Polymerase (2.5 U). PCR mutagenesis was carried out in Arktik Thermal Cycler (Thermo Scientific) under the following thermal program: Initial denaturation (95 ºC, 1 min); 18 cycles of denaturation (95 ºC, 50 s), annealing (60 ºC, 50 s), and extension (68 ºC, 8 mins); final extension (68 ºC, 7 mins). Template plasmid was digested with DpnI and 5 µL of the mutagenesis reaction was transformed in XL10-Gold® Ultracompetent Cells (Agilent) and selected in amplicillin-containing LB-agar plates. Colonies were isolated, cultured and extracted with plasmids using PureYield™ Plasmid Miniprep System. Successful mutations were verified *via* Sanger-type DNA sequencing performed by the University of Minnesota Genomics Center. Purified plasmids

were transformed in DH5α *E. coli*, cloned, purified, and assayed for concentration using a nanodrop.

5.6.5. Protein expression and purification

Human ALDH9A1 with N-terminal His tag was generously provided by Dr. David Kopecny from Palacký University, Czech Republic. The hALDH9A1 gene was inserted in pETDuet under T7 promoter and transformed in Rosetta^{TM}(DE3) competent *E. coli* cells (Novagen) following the manufacturer's protocol. Bacterial colonies containing the plasmids resistant to ampicillin and chloramphenicol were grown in 20 mL LB media with 1% glucose overnight at 37 ºC with shaking at 220 rpm. Bacteria were pelleted by centrifugation at 4000 *x g* at 4 ºC for 5 mins and pellets were resuspended in 1 L LB media containing antibiotics. Bacteria were allowed to grow until OD_{600} reached ~0.7 and induction was carried out by adding 0.15 mM IPTG at 4 ºC followed by incubation overnight at 20 ºC with shaking. Bacteria were pelleted and resuspended in 50 mL lysis buffer: 50 mL Tris-HCl pH 7.5, two tables of cOmplete^{TM} EDTA-free protease inhibitor (Roche), 1 mM DNAse-I, 10% glycerol, 1 mM DTT, and 30 mM imidazole. Cells were lysed by sonication for 10 s with 10 s intervals for a total of 10 mins followed by centrifugation at 15000 *x g* for 30 mins at 4 ºC. The lysate was loaded in pre-washed Ni-NTA agarose column (Qiagen) followed by washing with 600 mL of the wash buffer: Tris-HCl pH 7.5, 10% glycerol, 1 mM DTT, and 30 mM imidazole. Bound His-ALDH9A1 was eluted with Tris-HCl pH 7.5, 10% glycerol, 1 mM DTT, and 250 mM imidazole in 5 mL fractions and samples containing the pure protein were pooled. The protein solution was

concentrated through buffer exchange with Tris-HCl pH 7.5, 10% glycerol, 1 mM DTT using Amicon spin filters with 30 kDa cut-off (Millipore). The glycerol concentration was adjusted to 30% and protein purity was assessed using SDS-PAGE and concentration was determined using Bradford assay. The pure His-ALDH9A1 was stored at -80 ºC.

5.6.7. Kinetic assays

The purified His-ALDH9A1 was used in kinetic assays to evaluate ALDH9A1 activity in the presence of isoprenoid analogues. ALDH9A1 (1 μM) was incubated with isoprenoid analogues (100 μM) in 100 mM sodium pyrophosphate pH 8.0 for 1 hr at 4 ºC. TMABAL and NAD^+ (both 1 mM final concentration) were added to initiate the reaction. These assays monitored the NADH production (340 nm) upon conversion from NAD^+ in a plate reader (GMI). Dilution assays were performed with ALDH9A1 (10 μM) and isoprenoid probes (100 μM) incubated in a 20 μL pyrophosphate buffer for 1 hr at 4 ºC. TMABAL (1 mM final) and NAD^+ (1 mM final) in pyrophosphate buffer (180 uL) was added to initiate the reaction and the absorbance was monitored over time. Data were exported and replotted in MS Excel.

5.6.8. Mapping of the modification site

Expressed GFP-ALDH9A1 were enriched using anti-GFP beads following the manufacturer's protocol for GFP-Trap (Chromotek). Briefly, COS-7 cells (~1 x 10^6) transfected with GFP-ALDH9A1 and treated with C15AlkOPP, FPP or GGPP were lysed

in lysis buffer (10 mM Tris-HCl pH 7.5, 10 mM NaCl, 0.5 mM EDTA, 0.5% Nonidet^{TM} P40 Subsitute (Sigma-Aldrich)) by pipetting in and out in syringe on ice. The lysates were separated from debris after centrifugation (20,000 *x g* at 4 ºC for 15 mins). Pre-washed GFP-Trap beads (25 uL) were added to the lysates and incubated for 1 hr at 4 ºC with head-to-tail mixing. The beads were then washed with the wash buffer (10 mM Tris-HCl pH 7.5, 10 mM NaCl, 0.5 mM EDTA) and the immobilized protein was reduced and digested in 50 mM Tris-HCl pH 7.5 containing 2 M urea, 10 ug/mL sequencing grade trypsin (Promega), 20 ug/ mL chymotrypsin (Promega), 1 mM $CaCl_2$, and 0.5 mM TCEP for 30 mins at 32 ºC. The supernatant was collected using spin trap (Pierce) and the beads were suspended in 50 mM Tris-HCl pH 67.5 containing 2 M urea and 5 mM iodoacetamide. The eluate was collected and pooled with the first eluate. Samples were dried lyophilization and redissolved in 2% acetonitrile in water with 0.1% formic acid. The peptides were cleaned up using STAGE tips following standard protocols. The recovered peptides were dried and redissolved in 0.1% formic acid in water.

The samples were resolved in a reversed-phase column and analyzed in Orbitrap Lumos. Separation was performed in 5-30% of 0.1% formic acid in acetonitrile for 140 mins. A targeted database determined using Skyline was used corresponding to the *m/z* of the active site peptide resulting from tryptic and chymotryptic digestion with maximum of 3 missed cleavages. MS1 scans were collected at 60,000 resolution over 320-2000 *m/z* range with AGC target of 500,000 and max IT of 50 ms. Dynamic exclusion was allowed for 90 s. HCD fragmentation was performed at NCE of 42% with 1.5 *m/z* isolation window, AGC of 50,000, and max IT of 200 ms. The .raw files were analyzed in pFind to search for

the following modifications on cysteine reisude: Carabamidomethylation (C_2H_3NO, 57.0215), C15Alk ($C_{18}H_{26}O$, 258.1984 Da), C15Alk-ester ($C_{18}H_{24}O_2$, 272.1776 Da), C15Alk-thiohemiacetal ($C_{18}H_{26}O_2$, 274.1933 Da), farnesyl ($C_{15}H_{24,}$ 204.1878 Da), farnesyl ester ($C_{15}H_{22}O$, 218.1671 Da), farnesyl thiohemiacetal ($C_{15}H_{24}O$, 220.1827 Da), geranylgeranyl ($C_{20}H_{32}$, 272.2504 Da), geranylgeranyl ester ($C_{20}H_{30}O$, 286.2297 Da), and geranylgeranyl thiohemiacetal ($C_{20}H_{32}O$, 288.2453 Da). Other dynamic modifications include methionine oxidation (16.0000 Da) and arginine and glutamine deamidation (0.9840 Da). Matching spectra were exported and formatted in Adobe Illustrator v. 24.2.1.

Bibliography

(1) Hentschel, A.; Zahedi, R. P.; Ahrends, R. Protein Lipid Modifications—More than Just a Greasy Ballast. *Proteomics* **2016**, *16*, 759–782.
(2) Wang, M.; Casey, P. J. Protein Prenylation: Unique Fats Make Their Mark on Biology. *Nat. Rev. Mol. Cell Biol.* **2016**, *17*, 110–122.
(3) Jiang, H.; Zhang, X.; Chen, X.; Aramsangtienchai, P.; Tong, Z.; Lin, H. Protein Lipidation: Occurrence, Mechanisms, Biological Functions, and Enabling Technologies. *Chem. Rev.* **2018**, *118*, 919–988.
(4) Resh, M. D. Fatty Acylation of Proteins: The Long and the Short of It. *Prog. Lipid Res.* **2016**, *63*, 120–131.
(5) Ciepla, P.; Magee, A. I.; Tate, E. W. Cholesterylation: A Tail of Hedgehog. *Biochem. Soc. Trans.* **2015**, *43*, 262–267.
(6) Running, M. The Role of Lipid Post–Translational Modification in Plant Developmental Processes. *Front. Plant Sci.* **2014**, *5*, 50.
(7) Resh, M. D. Covalent Lipid Modifications of Proteins. *Curr. Biol.* **2013**, *23*, R431–R435.
(8) Chen, B.; Sun, Y.; Niu, J.; Jarugumilli, G. K.; Wu, X. Protein Lipidation in Cell Signaling and Diseases: Function, Regulation, and Therapeutic Opportunities. *Cell Chem. Biol.* **2018**, *25*, 817–831.
(9) Ganesan, L.; Levental, I. Pharmacological Inhibition of Protein Lipidation. *J. Membr. Biol.* **2015**, *248*, 929–941.
(10) Fraser, N. J.; Howie, J.; Wypijewski, K. J.; Fuller, W. Therapeutic Targeting of Protein S-Acylation for the Treatment of Disease. *Biochem. Soc. Trans.* **2019**, *48*, 281–290.
(11) Palsuledesai, C. C.; Distefano, M. D. Protein Prenylation: Enzymes, Therapeutics, and Biotechnology Applications. *ACS Chem. Biol.* **2015**, *10*, 51–62.
(12) Rashidian, M.; Dozier, J. K.; Distefano, M. D. Enzymatic Labeling of Proteins: Techniques and Approaches. *Bioconjug. Chem.* **2013**, *24*, 1277–1294.
(13) Zhang, Y.; Park, K.-Y.; Suazo, K. F.; Distefano, M. D. Recent Progress in Enzymatic Protein Labelling Techniques and Their Applications. *Chem. Soc. Rev.* **2018**, *47*, 9106–9136.
(14) Tate, E. W.; Kalesh, K. A.; Lanyon-Hogg, T.; Storck, E. M.; Thinon, E. Global Profiling of Protein Lipidation Using Chemical Proteomic Technologies. *Curr. Opin. Chem. Biol.* **2015**, *24*, 48–57.
(15) Gao, X.; Hannoush, R. N. A Decade of Click Chemistry in Protein Palmitoylation: Impact on Discovery and New Biology. *Cell Chem. Biol.* **2018**, *25*, 236–246.
(16) Wang, Y.-C.; Distefano, M. D. Synthetic Isoprenoid Analogues for the Study of Prenylated Proteins: Fluorescent Imaging and Proteomic Applications. *Bioorg. Chem.* **2016**, *64*, 59–65.
(17) Peng, T.; Thinon, E.; Hang, H. C. Proteomic Analysis of Fatty-Acylated Proteins. *Curr. Opin. Chem. Biol.* **2016**, *30*, 77–86.
(18) Suazo, K. F.; Schey, G.; Schaber, C.; Odom John, A. R.; Distefano, M. D. Proteomic Analysis of Protein–Lipid Modifications: Significance and Application. *Mass Spectrometry-Based Chemical Proteomics*. August 13, 2019, pp 317–347.

(19) Minguez, P.; Letunic, I.; Parca, L.; Bork, P. PTMcode: A Database of Known and Predicted Functional Associations between Post-Translational Modifications in Proteins. *Nucleic Acids Res.* **2012**, *41*, D306–D311.
(20) Linder, M. E.; Deschenes, R. J. Palmitoylation: Policing Protein Stability and Traffic. *Nat Rev Mol Cell Biol* **2007**, *8*, 74–84.
(21) Schmidt, M. F. G.; Schlesinger, M. J. Fatty Acid Binding to Vesicular Stomatitis Virus Glycoprotein: A New Type of Post-Translational Modification of the Viral Glycoprotein. *Cell* **1979**, *17*, 813–819.
(22) O'Brien, P. J.; Zatz, M. Acylation of Bovine Rhodopsin by [3H]Palmitic Acid. *J. Biol. Chem.* **1984**, *259*, 5054–5057.
(23) Chen, Z. Q.; Ulsh, L. S.; DuBois, G.; Shih, T. Y. Posttranslational Processing of P21 Ras Proteins Involves Palmitylation of the C-Terminal Tetrapeptide Containing Cysteine-186. *J. Virol.* **1985**, *56*, 607–612.
(24) Jung, V.; Chen, L.; Hofmann, S. L.; Wigler, M.; Powers, S. Mutations in the SHR5 Gene of Saccharomyces Cerevisiae Suppress Ras Function and Block Membrane Attachment and Palmitoylation of Ras Proteins. *Mol. Cell. Biol.* **1995**, *15*, 1333–1342.
(25) Lobo, S.; Greentree, W. K.; Linder, M. E.; Deschenes, R. J. Identification of a Ras Palmitoyltransferase in Saccharomyces Cerevisiae . *J. Biol. Chem.* **2002**, *277*, 41268–41273.
(26) Uemura, T.; Mori, H.; Mishina, M. Isolation and Characterization of Golgi Apparatus-Specific GODZ with the DHHC Zinc Finger Domain. *Biochem. Biophys. Res. Commun.* **2002**, *296*, 492–496.
(27) Ohno, Y.; Kihara, A.; Sano, T.; Igarashi, Y. Intracellular Localization and Tissue-Specific Distribution of Human and Yeast DHHC Cysteine-Rich Domain-Containing Proteins. *Biochim. Biophys. Acta - Mol. Cell Biol. Lipids* **2006**, *1761*, 474–483.
(28) Tabaczar, S.; Czogalla, A.; Podkalicka, J.; Biernatowska, A.; Sikorski, A. F. Protein Palmitoylation: Palmitoyltransferases and Their Specificity. *Exp. Biol. Med. (Maywood).* **2017**, *242*, 1150–1157.
(29) Fukata, Y.; Iwanaga, T.; Fukata, M. Systematic Screening for Palmitoyl Transferase Activity of the DHHC Protein Family in Mammalian Cells. *Methods* **2006**, *40*, 177–182.
(30) Roth, A. F.; Feng, Y.; Chen, L.; Davis, N. G. The Yeast DHHC Cysteine-Rich Domain Protein Akr1p Is a Palmitoyl Transferase . *J. Cell Biol.* **2002**, *159*, 23–28.
(31) Huang, K.; Sanders, S. S.; Kang, R.; Carroll, J. B.; Sutton, L.; Wan, J.; Singaraja, R.; Young, F. B.; Liu, L.; El-Husseini, A.; et al. Wild-Type HTT Modulates the Enzymatic Activity of the Neuronal Palmitoyl Transferase HIP14. *Hum. Mol. Genet.* **2011**, *20*, 3356–3365.
(32) Mitchell, D. A.; Vasudevan, A.; Linder, M. E.; Deschenes, R. J. Thematic Review Series: Lipid Posttranslational Modifications. Protein Palmitoylation by a Family of DHHC Protein S-Acyltransferases. *J. Lipid Res.* **2006**, *47*, 1118–1127.
(33) Gottlieb, C. D.; Zhang, S.; Linder, M. E. The Cysteine-Rich Domain of the DHHC3 Palmitoyltransferase Is Palmitoylated and Contains Tightly Bound Zinc. *J. Biol. Chem.* **2015**.
(34) Rana, M. S.; Kumar, P.; Lee, C.-J.; Verardi, R.; Rajashankar, K. R.; Banerjee, A.

Fatty Acyl Recognition and Transfer by an Integral Membrane S-Acyltransferase. *Science (80-.).* **2018**, *359*, eaao6326.
(35) Rana, M. S.; Lee, C.-J.; Banerjee, A. The Molecular Mechanism of DHHC Protein Acyltransferases. *Biochem. Soc. Trans.* **2018**, *47*, 157–167.
(36) Dietrich, L. E. P.; Ungermann, C. On the Mechanism of Protein Palmitoylation. *EMBO Rep.* **2004**, *5*, 1053–1057.
(37) Lemonidis, K.; Gorleku, O. A.; Sanchez-Perez, M. C.; Grefen, C.; Chamberlain, L. H. The Golgi S-Acylation Machinery Comprises ZDHHC Enzymes with Major Differences in Substrate Affinity and S-Acylation Activity. *Mol. Biol. Cell* **2014**, *25*, 3870–3883.
(38) González Montoro, A.; Chumpen Ramirez, S.; Valdez Taubas, J. The Canonical DHHC Motif Is Not Absolutely Required for the Activity of the Yeast S-Acyltransferases Swf1 and Pfa4. *J. Biol. Chem.* **2015**, *290*, 22448–22459.
(39) Thomas, G. M.; Hayashi, T.; Chiu, S.-L.; Chen, C.-M.; Huganir, R. L. Palmitoylation by DHHC5/8 Targets GRIP1 to Dendritic Endosomes to Regulate AMPA-R Trafficking. *Neuron* **2012**, *73*, 482–496.
(40) Howie, J.; Reilly, L.; Fraser, N. J.; Vlachaki Walker, J. M.; Wypijewski, K. J.; Ashford, M. L. J.; Calaghan, S. C.; McClafferty, H.; Tian, L.; Shipston, M. J.; et al. Substrate Recognition by the Cell Surface Palmitoyl Transferase DHHC5. *Proc. Natl. Acad. Sci.* **2014**, *111*, 17534 LP – 17539.
(41) Zhou, F.; Xue, Y.; Yao, X.; Xu, Y. CSS-Palm: Palmitoylation Site Prediction with a Clustering and Scoring Strategy (CSS). *Bioinformatics* **2006**, *22*, 894–896.
(42) Won, S. J.; Cheung See Kit, M.; Martin, B. R. Protein Depalmitoylases. *Crit. Rev. Biochem. Mol. Biol.* **2018**, *53*, 83–98.
(43) Lin, D. T. S.; Conibear, E. ABHD17 Proteins Are Novel Protein Depalmitoylases That Regulate N-Ras Palmitate Turnover and Subcellular Localization. *Elife* **2015**, *4*, e11306.
(44) Rocks, O.; Peyker, A.; Kahms, M.; Verveer, P. J.; Koerner, C.; Lumbierres, M.; Kuhlmann, J.; Waldmann, H.; Wittinghofer, A.; Bastiaens, P. I. H. An Acylation Cycle Regulates Localization and Activity of Palmitoylated Ras Isoforms. *Science (80-.).* **2005**, *307*, 1746 LP – 1752.
(45) Won, S. J.; Martin, B. R. Temporal Profiling Establishes a Dynamic S-Palmitoylation Cycle. *ACS Chem. Biol.* **2018**, *13*, 1560–1568.
(46) Smotrys, J. E.; Linder, M. E. Palmitoylation of Intracellular Signaling Proteins: Regulation and Function. *Annu. Rev. Biochem.* **2004**, *73*, 559–587.
(47) Matt, L.; Kim, K.; Chowdhury, D.; Hell, J. W. Role of Palmitoylation of Postsynaptic Proteins in Promoting Synaptic Plasticity. *Front. Mol. Neurosci.* **2019**, *12*, 8.
(48) Sobocińska, J.; Roszczenko-Jasińska, P.; Ciesielska, A.; Kwiatkowska, K. Protein Palmitoylation and Its Role in Bacterial and Viral Infections. *Front. Immunol.* **2018**, *8*, 2003.
(49) Cho, E.; Park, M. Palmitoylation in Alzheimer's Disease and Other Neurodegenerative Diseases. *Pharmacol. Res.* **2016**, *111*, 133–151.
(50) Ko, P.-J.; Dixon, S. J. Protein Palmitoylation and Cancer. *EMBO Rep.* **2018**, *19*, e46666.
(51) Farazi, T. A.; Waksman, G.; Gordon, J. I. The Biology and Enzymology of

ProteinN-Myristoylation . *J. Biol. Chem.* **2001**, *276*, 39501–39504.
(52) Wright, M. H.; Heal, W. P.; Mann, D. J.; Tate, E. W. Protein Myristoylation in Health and Disease. *J. Chem. Biol.* **2010**, *3*, 19–35.
(53) Martin, D. D. O.; Beauchamp, E.; Berthiaume, L. G. Post-Translational Myristoylation: Fat Matters in Cellular Life and Death. *Biochimie* **2011**, *93*, 18–31.
(54) Castrec, B.; Dian, C.; Ciccone, S.; Ebert, C. L.; Bienvenut, W. V; Le Caer, J.-P.; Steyaert, J.-M.; Giglione, C.; Meinnel, T. Structural and Genomic Decoding of Human and Plant Myristoylomes Reveals a Definitive Recognition Pattern. *Nat. Chem. Biol.* **2018**, *14*, 671–679.
(55) Perinpanayagam, M. A.; Beauchamp, E.; Martin, D. D. O.; Sim, J. Y. W.; Yap, M. C.; Berthiaume, L. G. Regulation of Co- and Post-Translational Myristoylation of Proteins during Apoptosis: Interplay of N-Myristoyltransferases and Caspases. *FASEB J.* **2012**, *27*, 811–821.
(56) Rudnick, D. A.; McWherter, C. A.; Rocque, W. J.; Lennon, P. J.; Getman, D. P.; Gordon, J. I. Kinetic and Structural Evidence for a Sequential Ordered Bi Bi Mechanism of Catalysis by Saccharomyces Cerevisiae Myristoyl-CoA:Protein N-Myristoyltransferase. *J. Biol. Chem.* **1991**, *266*, 9732–9739.
(57) Dian, C.; Pérez-Dorado, I.; Rivière, F.; Asensio, T.; Legrand, P.; Ritzefeld, M.; Shen, M.; Cota, E.; Meinnel, T.; Tate, E. W.; et al. High-Resolution Snapshots of Human N-Myristoyltransferase in Action Illuminate a Mechanism Promoting N-Terminal Lys and Gly Myristoylation. *Nat. Commun.* **2020**, *11*, 1132.
(58) Towler, D.; Glaser, L. Protein Fatty Acid Acylation: Enzymatic Synthesis of an N-Myristoylglycyl Peptide. *Proc. Natl. Acad. Sci.* **1986**, *83*, 2812 LP – 2816.
(59) Farazi, T. A.; Waksman, G.; Gordon, J. I. Structures of Saccharomyces Cerevisiae N-Myristoyltransferase with Bound MyristoylCoA and Peptide Provide Insights about Substrate Recognition and Catalysis. *Biochemistry* **2001**, *40*, 6335–6343.
(60) Maurer-Stroh, S.; Eisenhaber, F. Myristoylation of Viral and Bacterial Proteins. *Trends Microbiol.* **2004**, *12*, 178–185.
(61) Giang, D. K.; Cravatt, B. F. A Second Mammalian N-Myristoyltransferase . *J. Biol. Chem.* **1998**, *273*, 6595–6598.
(62) Yang, S. H.; Shrivastav, A.; Kosinski, C.; Sharma, R. K.; Chen, M.-H.; Berthiaume, L. G.; Peters, L. L.; Chuang, P.-T.; Young, S. G.; Bergo, M. O. N-Myristoyltransferase 1 Is Essential in Early Mouse Development. *J. Biol. Chem.* **2005**, *280*, 18990–18995.
(63) Stevenson, F. T.; Bursten, S. L.; Locksley, R. M.; Lovett, D. H. Myristyl Acylation of the Tumor Necrosis Factor Alpha Precursor on Specific Lysine Residues. *J. Exp. Med.* **1992**, *176*, 1053 LP – 1062.
(64) Jing, H.; Zhang, X.; Wisner, S. A.; Chen, X.; Spiegelman, N. A.; Linder, M. E.; Lin, H. SIRT2 and Lysine Fatty Acylation Regulate the Transforming Activity of K-Ras4a. *Elife* **2017**, *6*, e32436.
(65) Zhang, X.; Spiegelman, N. A.; Nelson, O. D.; Jing, H.; Lin, H. SIRT6 Regulates Ras-Related Protein R-Ras2 by Lysine Defatty-Acylation. *Elife* **2017**, *6*, e25158.
(66) Spiegelman, N. A.; Zhang, X.; Jing, H.; Cao, J.; Kotliar, I. B.; Aramsangtienchai, P.; Wang, M.; Tong, Z.; Rosch, K. M.; Lin, H. SIRT2 and Lysine Fatty Acylation Regulate the Activity of RalB and Cell Migration. *ACS Chem. Biol.* **2019**, *14*,

2014–2023.
(67) Kosciuk, T.; Price, I. R.; Zhang, X.; Zhu, C.; Johnson, K. N.; Zhang, S.; Halaby, S. L.; Komaniecki, G. P.; Yang, M.; DeHart, C. J.; et al. NMT1 and NMT2 Are Lysine Myristoyltransferases Regulating the ARF6 GTPase Cycle. *Nat. Commun.* **2020**, *11*, 1067.
(68) Feldman, J. L.; Baeza, J.; Denu, J. M. Activation of the Protein Deacetylase SIRT6 by Long-Chain Fatty Acids and Widespread Deacylation by Mammalian Sirtuins. *J. Biol. Chem.* **2013**, *288*, 31350–31356.
(69) Nakagawa, T.; Guarente, L. Sirtuins at a Glance. *J. Cell Sci.* **2011**, *124*, 833 LP – 838.
(70) Park, S.-Y.; Kim, J.-S. A Short Guide to Histone Deacetylases Including Recent Progress on Class II Enzymes. *Exp. Mol. Med.* **2020**, *52*, 204–212.
(71) Cao, J.; Sun, L.; Aramsangtienchai, P.; Spiegelman, N. A.; Zhang, X.; Huang, W.; Seto, E.; Lin, H. HDAC11 Regulates Type I Interferon Signaling through Defatty-Acylation of SHMT2. *Proc. Natl. Acad. Sci.* **2019**, *116*, 5487 LP – 5492.
(72) Udenwobele, D. I.; Su, R.-C.; Good, S. V; Ball, T. B.; Varma Shrivastav, S.; Shrivastav, A. Myristoylation: An Important Protein Modification in the Immune Response. *Front. Immunol.* **2017**, *8*, 751.
(73) Martin, D. D. O.; Hayden, M. R. Post-Translational Myristoylation at the Cross Roads of Cell Death, Autophagy and Neurodegeneration. *Biochem. Soc. Trans.* **2015**, *43*, 229–234.
(74) Yuan, M.; Song, Z.; Ying, M.; Zhu, H.; He, Q.; Yang, B.; Cao, J. N-Myristoylation: From Cell Biology to Translational Medicine. *Acta Pharmacol. Sin.* **2020**.
(75) Kamiya, Y.; Sakurai, A.; Tamura, S.; Takahashi, N.; Abe, K.; Tsuchiya, E.; Fukui, S.; Kitada, C.; Fujino, M. Structure of Rhodotorucine A, a Novel Lipopeptide, Inducing Mating Tube Formation in Rhodosporidiumtoruloides. *Biochem. Biophys. Res. Commun.* **1978**, *83*, 1077–1083.
(76) Wolda, S. L.; Glomset, J. A. Evidence for Modification of Lamin B by a Product of Mevalonic Acid. *J. Biol. Chem.* **1988**, *263*, 5997–6000.
(77) Zhang, F. L.; Casey, P. J. Protein Prenylation: Molecular Mechanisms and Functional Consequences. *Annu. Rev. Biochem.* **1996**, *65*, 241–269.
(78) Liu, A.; Du, W.; Liu, J.-P.; Jessell, T. M.; Prendergast, G. C. RhoB Alteration Is Necessary for Apoptotic and Antineoplastic Responses to Farnesyltransferase Inhibitors. *Mol. Cell. Biol.* **2000**, *20*, 6105 LP – 6113.
(79) Hougland, J. L.; Lamphear, C. L.; Scott, S. A.; Gibbs, R. A.; Fierke, C. A. Context-Dependent Substrate Recognition by Protein Farnesyltransferase. *Biochemistry* **2009**, *48*, 1691–1701.
(80) Hougland, J. L.; Hicks, K. A.; Hartman, H. L.; Kelly, R. A.; Watt, T. J.; Fierke, C. A. Identification of Novel Peptide Substrates for Protein Farnesyltransferase Reveals Two Substrate Classes with Distinct Sequence Selectivities. *J. Mol. Biol.* **2010**, *395*, 176–190.
(81) Maurer-Stroh, S.; Eisenhaber, F. Refinement and Prediction of Protein Prenylation Motifs. *Genome Biol.* **2005**, *6*, 1–15.
(82) Hicks, K. A.; Hartman, H. L.; Fierke, C. A. Upstream Polybasic Region in Peptides Enhances Dual Specificity for Prenylation by Both Farnesyltransferase

and Geranylgeranyltransferase Type I. *Biochemistry* **2005**, *44*, 15325–15333.
(83) Blanden, M. J.; Suazo, K. F.; Hildebrandt, E. R.; Hardgrove, D. S.; Patel, M.; Saunders, W. P.; Distefano, M. D.; Schmidt, W. K.; Hougland, J. L. Efficient Farnesylation of an Extended C-Terminal C(x)3X Sequence Motif Expands the Scope of the Prenylated Proteome. *J. Biol. Chem.* **2017**, *293*, 2770–2785.
(84) Ashok, S.; Hildebrandt, E. R.; Ruiz, C. S.; Hardgrove, D. S.; Coreno, D. W.; Schmidt, W. K.; Hougland, J. L. Protein Farnesyltransferase Catalyzes Unanticipated Farnesylation and Geranylgeranylation of Shortened Target Sequences. *Biochemistry* **2020**, *59*, 1149–1162.
(85) Boyartchuk, V. L.; Ashby, M. N.; Rine, J. Modulation of Ras and A-Factor Function by Carboxyl-Terminal Proteolysis. *Science (80-.).* **1997**, *275*, 1796–1800.
(86) Dai, Q.; Choy, E.; Chiu, V.; Romano, J.; Slivka, S. R.; Steitz, S. A.; Michaelis, S.; Philips, M. R. Mammalian Prenylcysteine Carboxyl Methyltransferase Is in the Endoplasmic Reticulum. *J. Biol. Chem.* **1998**, *273*, 15030–15034.
(87) Hancock, J. F.; Paterson, H.; Marshall, C. J. A Polybasic Domain or Palmitoylation Is Required in Addition to the CAAX Motif to Localize P21ras to the Plasma Membrane. *Cell* **1990**, *63*, 133–139.
(88) Hildebrandt, E. R.; Cheng, M.; Zhao, P.; Kim, J. H.; Wells, L.; Schmidt, W. K. A Shunt Pathway Limits the CaaX Processing of Hsp40 Ydj1p and Regulates Ydj1p-Dependent Phenotypes. *Elife* **2016**, *5*, e15899.
(89) Rak, A.; Pylypenko, O.; Niculae, A.; Pyatkov, K.; Goody, R. S.; Alexandrov, K. Structure of the Rab7:REP-1 Complex: Insights into the Mechanism of Rab Prenylation and Choroideremia Disease. *Cell* **2004**, *117*, 749–760.
(90) Leung, K. F.; Baron, R.; Ali, B. R.; Magee, A. I.; Seabra, M. C. Rab GTPases Containing a CAAX Motif Are Processed Post-Geranylgeranylation by Proteolysis and Methylation. *J. Biol. Chem.* **2007**, *282*, 1487–1497.
(91) Calero, M.; Chen, C. Z.; Zhu, W.; Winand, N.; Havas, K. A.; Gilbert, P. M.; Burd, C. G.; Collins, R. N. Dual Prenylation Is Required for Rab Protein Localization and Function. *Mol. Biol. Cell* **2003**, *14*, 1852–1867.
(92) Long, S. B.; Casey, P. J.; Beese, L. S. Reaction Path of Protein Farnesyltransferase at Atomic Resolution. *Nature* **2002**, *419*, 645–650.
(93) Taylor, J. S.; Reid, T. S.; Terry, K. L.; Casey, P. J.; Beese, L. S. Structure of Mammalian Protein Geranylgeranyltransferase Type-I. *EMBO J.* **2003**, *22*, 5963–5974.
(94) Pompliano, D. L.; Schaber, M. D.; Mosser, S. D.; Omer, C. A.; Shafer, J. A.; Gibbs, J. B. Isoprenoid Diphosphate Utilization by Recombinant Human Farnesyl:Protein Transferase: Interactive Binding between Substrates and a Preferred Kinetic Pathway. *Biochemistry* **1993**, *32*, 8341–8347.
(95) Dolence, J. M.; Cassidy, P. B.; Mathis, J. R.; Poulter, C. D. Yeast Protein Farnesyltransferase: Steady-State Kinetic Studies of Substrate Binding. *Biochemistry* **1995**, *34*, 16687–16694.
(96) Stirtan, W. G.; Poulter, C. D. Yeast Protein Geranylgeranyltransferase Type-I: Steady-State Kinetics and Substrate Binding. *Biochemistry* **1997**, *36*, 4552–4557.
(97) Terry, K. L.; Casey, P. J.; Beese, L. S. Conversion of Protein Farnesyltransferase to a Geranylgeranyltransferase. *Biochemistry* **2006**, *45*, 9746–9755.

(98) Thomä, N. H.; Niculae, A.; Goody, R. S.; Alexandrov, K. Double Prenylation by RabGGTase Can Proceed without Dissociation of the Mono-Prenylated Intermediate. *J. Biol. Chem.* **2001**, *276*, 48631–48636.
(99) Köhnke, M.; Delon, C.; Hastie, M. L.; Nguyen, U. T. T.; Wu, Y.-W.; Waldmann, H.; Goody, R. S.; Gorman, J. J.; Alexandrov, K. Rab GTPase Prenylation Hierarchy and Its Potential Role in Choroideremia Disease. *PLoS One* **2013**, *8*, e81758.
(100) Ochocki, J. D.; Distefano, M. D. Prenyltransferase Inhibitors: Treating Human Ailments from Cancer to Parasitic Infections. *Medchemcomm* **2013**, *4*, 476.
(101) Berndt, N.; Hamilton, A. D.; Sebti, S. M. Targeting Protein Prenylation for Cancer Therapy. *Nat Rev Cancer* **2011**, *11*, 775–791.
(102) Young, S. G.; Yang, S. H.; Davies, B. S. J.; Jung, H.-J.; Fong, L. G. Targeting Protein Prenylation in Progeria. *Sci. Transl. Med.* **2013**, *5*, 171ps3-171ps3.
(103) Marakasova, E. S.; Eisenhaber, B.; Maurer-Stroh, S.; Eisenhaber, F.; Baranova, A. Prenylation of Viral Proteins by Enzymes of the Host: Virus-Driven Rationale for Therapy with Statins and FT/GGT1 Inhibitors. *BioEssays* **2017**, *39*, 1700014.
(104) Jeong, A.; Suazo, K. F.; Wood, W. G.; Distefano, M. D.; Li, L. Isoprenoids and Protein Prenylation: Implications in the Pathogenesis and Therapeutic Intervention of Alzheimer's Disease. *Crit. Rev. Biochem. Mol. Biol.* **2018**, *53*, 279–310.
(105) FDA Approves First Treatment for Hutchinson-Gilford Progeria Syndrome and Some Progeroid Laminopathies https://www.fda.gov/news-events/press-announcements/fda-approves-first-treatment-hutchinson-gilford-progeria-syndrome-and-some-progeroid-laminopathies.
(106) Gordon, L. B.; Kleinman, M. E.; Miller, D. T.; Neuberg, D. S.; Giobbie-Hurder, A.; Gerhard-Herman, M.; Smoot, L. B.; Gordon, C. M.; Cleveland, R.; Snyder, B. D.; et al. Clinical Trial of a Farnesyltransferase Inhibitor in Children with Hutchinson–Gilford Progeria Syndrome. *Proc. Natl. Acad. Sci.* **2012**, *109*, 16666–16671.
(107) Burai, L.; Fabian, I.; Kiraly, R.; Szilagyi, E.; Brucher, E. Equilibrium and Kinetic Studies on the Formation of the Lanthanide(III) Complexes, [Ce(Dota)]– and [Yb(Dota)]– (H4dota = 1,4,7,10-Tetraazacyclododecane-1,4,7,10-Tetraacetic Acid). *J. Chem. Soc.* **1998**, No. 2, 243–248.
(108) Kuchay, S.; Wang, H.; Marzio, A.; Jain, K.; Homer, H.; Fehrenbacher, N.; Philips, M. R.; Zheng, N.; Pagano, M. GGTase3 Is a Newly Identified Geranylgeranyltransferase Targeting a Ubiquitin Ligase. *Nat. Struct. Mol. Biol.* **2019**, *26*, 628–636.
(109) Veit, M.; Söllner, T. H.; Rothman, J. E. Multiple Palmitoylation of Synaptotagmin and the T-SNARE SNAP-25. *FEBS Lett.* **1996**, *385*, 119–123.
(110) Alland, L.; Peseckis, S. M.; Atherton, R. E.; Berthiaume, L.; Resh, M. D. Dual Myristylation and Palmitylation of Src Family Member P59fyn Affects Subcellular Localization. *J. Biol. Chem.* **1994**, *269*, 16701–16705.
(111) Maurer-Stroh, S.; Gouda, M.; Novatchkova, M.; Schleiffer, A.; Schneider, G.; Sirota, F. L.; Wildpaner, M.; Hayashi, N.; Eisenhaber, F. MYRbase: Analysis of Genome-Wide Glycine Myristoylation Enlarges the Functional Spectrum of Eukaryotic Myristoylated Proteins. *Genome Biol.* **2004**, *5*, R21.
(112) Tate, E. W. Recent Advances in Chemical Proteomics: Exploring the Post-

Translational Proteome. *J. Chem. Biol.* **2008**, *1*, 17–26.
(113) Hannoush, R. N.; Sun, J. The Chemical Toolbox for Monitoring Protein Fatty Acylation and Prenylation. *Nat. Chem. Biol.* **2010**, *6*, 498–506.
(114) Thinon, E.; Hang, H. C. Chemical Reporters for Exploring Protein Acylation. *Biochem. Soc. Trans.* **2015**, *43*, 253 LP – 261.
(115) Ong, S.-E.; Blagoev, B.; Kratchmarova, I.; Kristensen, D. B.; Steen, H.; Pandey, A.; Mann, M. Stable Isotope Labeling by Amino Acids in Cell Culture, SILAC, as a Simple and Accurate Approach to Expression Proteomics. *Mol. & Cell. Proteomics* **2002**, *1*, 376 LP – 386.
(116) Thompson, A.; Schäfer, J.; Kuhn, K.; Kienle, S.; Schwarz, J.; Schmidt, G.; Neumann, T.; Hamon, C. Tandem Mass Tags: A Novel Quantification Strategy for Comparative Analysis of Complex Protein Mixtures by MS/MS. *Anal. Chem.* **2003**, *75*, 1895–1904.
(117) Patterson, D. M.; Nazarova, L. A.; Prescher, J. A. Finding the Right (Bioorthogonal) Chemistry. *ACS Chem. Biol.* **2014**, *9*, 592–605.
(118) Saxon, E.; Bertozzi, C. R. Cell Surface Engineering by a Modified Staudinger Reaction. *Science (80-.).* **2000**, *287*, 2007–2010.
(119) Kolb, H. C.; Finn, M. G.; Sharpless, K. B. Click Chemistry: Diverse Chemical Function from a Few Good Reactions. *Angew. Chemie Int. Ed.* **2001**, *40*, 2004–2021.
(120) Rostovtsev, V. V; Green, L. G.; Fokin, V. V; Sharpless, K. B. A Stepwise Huisgen Cycloaddition Process: Copper(I)-Catalyzed Regioselective "Ligation" of Azides and Terminal Alkynes. *Angew. Chemie Int. Ed.* **2002**, *41*, 2596–2599.
(121) Sletten, E. M.; Bertozzi, C. R. Bioorthogonal Chemistry: Fishing for Selectivity in a Sea of Functionality. *Angew. Chemie Int. Ed.* **2009**, *48*, 6974–6998.
(122) Kennedy, D. C.; McKay, C. S.; Legault, M. C. B.; Danielson, D. C.; Blake, J. A.; Pegoraro, A. F.; Stolow, A.; Mester, Z.; Pezacki, J. P. Cellular Consequences of Copper Complexes Used To Catalyze Bioorthogonal Click Reactions. *J. Am. Chem. Soc.* **2011**, *133*, 17993–18001.
(123) Jewett, J. C.; Bertozzi, C. R. Cu-Free Click Cycloaddition Reactions in Chemical Biology. *Chem. Soc. Rev.* **2010**, *39*, 1272–1279.
(124) Broncel, M.; Serwa, R. A.; Ciepla, P.; Krause, E.; Dallman, M. J.; Magee, A. I.; Tate, E. W. Multifunctional Reagents for Quantitative Proteome-Wide Analysis of Protein Modification in Human Cells and Dynamic Profiling of Protein Lipidation During Vertebrate Development. *Angew. Chemie Int. Ed.* **2015**, *54*, 5948–5951.
(125) Wright, M. H.; Clough, B.; Rackham, M. D.; Rangachari, K.; Brannigan, J. A.; Grainger, M.; Moss, D. K.; Bottrill, A. R.; Heal, W. P.; Broncel, M.; et al. Validation of N-Myristoyltransferase as an Antimalarial Drug Target Using an Integrated Chemical Biology Approach. *Nat Chem* **2014**, *6*, 112–121.
(126) Hang, H. C.; Geutjes, E.-J.; Grotenbreg, G.; Pollington, A. M.; Bijlmakers, M. J.; Ploegh, H. L. Chemical Probes for the Rapid Detection of Fatty-Acylated Proteins in Mammalian Cells. *J. Am. Chem. Soc.* **2007**, *129*, 2744–2745.
(127) Charron, G.; Zhang, M. M.; Yount, J. S.; Wilson, J.; Raghavan, A. S.; Shamir, E.; Hang, H. C. Robust Fluorescent Detection of Protein Fatty-Acylation with Chemical Reporters. *J. Am. Chem. Soc.* **2009**, *131*, 4967–4975.
(128) Hannoush, R. N.; Arenas-Ramirez, N. Imaging the Lipidome: ω-Alkynyl Fatty

Acids for Detection and Cellular Visualization of Lipid-Modified Proteins. *ACS Chem. Biol.* **2009**, *4*, 581–587.
(129) Ourailidou, M. E.; Zwinderman, M. R. H.; Dekker, F. J. Bioorthogonal Metabolic Labelling with Acyl-CoA Reporters: Targeting Protein Acylation. *Medchemcomm* **2016**, *7*, 399–408.
(130) Yount, J. S.; Moltedo, B.; Yang, Y.-Y.; Charron, G.; Moran, T. M.; López, C. B.; Hang, H. C. Palmitoylome Profiling Reveals S-Palmitoylation–Dependent Antiviral Activity of IFITM3. *Nat Chem Biol* **2010**, *6*, 610–614.
(131) Yount, J. S.; Charron, G.; Hang, H. C. Bioorthogonal Proteomics of 15-Hexadecynyloxyacetic Acid Chemical Reporter Reveals Preferential Targeting of Fatty Acid Modified Proteins and Biosynthetic Enzymes. *Bioorg. Med. Chem.* **2012**, *20*, 650–654.
(132) Gao, X.; Hannoush, R. N. Single-Cell Imaging of Wnt Palmitoylation by the Acyltransferase Porcupine. *Nat. Chem. Biol.* **2014**, *10*, 61–68.
(133) Greaves, J.; Munro, K. R.; Davidson, S. C.; Riviere, M.; Wojno, J.; Smith, T. K.; Tomkinson, N. C. O.; Chamberlain, L. H. Molecular Basis of Fatty Acid Selectivity in the ZDHHC Family of S-Acyltransferases Revealed by Click Chemistry. *Proc. Natl. Acad. Sci.* **2017**, *114*, E1365 LP-E1374.
(134) Thiele, C.; Papan, C.; Hoelper, D.; Kusserow, K.; Gaebler, A.; Schoene, M.; Piotrowitz, K.; Lohmann, D.; Spandl, J.; Stevanovic, A.; et al. Tracing Fatty Acid Metabolism by Click Chemistry. *ACS Chem. Biol.* **2012**, *7*, 2004–2011.
(135) Thiele, C.; Wunderling, K.; Leyendecker, P. Multiplexed and Single Cell Tracing of Lipid Metabolism. *Nat. Methods* **2019**, *16*, 1123–1130.
(136) Lanyon-Hogg, T.; Faronato, M.; Serwa, R. A.; Tate, E. W. Dynamic Protein Acylation: New Substrates, Mechanisms, and Drug Targets. *Trends Biochem. Sci.* **2017**, *42*, 566–581.
(137) Haberkant, P.; Raijmakers, R.; Wildwater, M.; Sachsenheimer, T.; Brügger, B.; Maeda, K.; Houweling, M.; Gavin, A.-C.; Schultz, C.; van Meer, G.; et al. In Vivo Profiling and Visualization of Cellular Protein–Lipid Interactions Using Bifunctional Fatty Acids. *Angew. Chemie Int. Ed.* **2013**, *52*, 4033–4038.
(138) Peng, T.; Hang, H. C. Bifunctional Fatty Acid Chemical Reporter for Analyzing S-Palmitoylated Membrane Protein–Protein Interactions in Mammalian Cells. *J. Am. Chem. Soc.* **2015**, *137*, 556–559.
(139) Zhu, X. G.; Nicholson Puthenveedu, S.; Shen, Y.; La, K.; Ozlu, C.; Wang, T.; Klompstra, D.; Gultekin, Y.; Chi, J.; Fidelin, J.; et al. CHP1 Regulates Compartmentalized Glycerolipid Synthesis by Activating GPAT4. *Mol. Cell* **2019**, *74*, 45-58.e7.
(140) Drisdel, R. C.; Green, W. N. Labeling and Quantifying Sites of Protein Palmitoylation. *Biotechniques* **2004**, *36*, 276–285.
(141) Forrester, M. T.; Thompson, J. W.; Foster, M. W.; Nogueira, L.; Moseley, M. A.; Stamler, J. S. Proteomic Analysis of S-Nitrosylation and Denitrosylation by Resin-Assisted Capture. *Nat. Biotechnol.* **2009**, *27*, 557–559.
(142) Blanc, M.; David, F.; Abrami, L.; Migliozzi, D.; Armand, F.; Bürgi, J.; van der Goot, F. G. SwissPalm: Protein Palmitoylation Database. *F1000Research* **2015**, *4*, 261.
(143) Kostiuk, M. A.; Corvi, M. M.; Keller, B. O.; Plummer, G.; Prescher, J. A.;

Hangauer, M. J.; Bertozzi, C. R.; Rajaiah, G.; Falck, J. R.; Berthiaume, L. G. Identification of Palmitoylated Mitochondrial Proteins Using a Bio-Orthogonal Azido-Palmitate Analogue. *FASEB J.* **2008**, *22*, 721–732.
(144) Martin, B. R.; Cravatt, B. F. Large-Scale Profiling of Protein Palmitoylation in Mammalian Cells. *Nat Meth* **2009**, *6*, 135–138.
(145) Wilson, J. P.; Raghavan, A. S.; Yang, Y.-Y.; Charron, G.; Hang, H. C. Proteomic Analysis of Fatty-Acylated Proteins in Mammalian Cells with Chemical Reporters Reveals S-Acylation of Histone H3 Variants. *Mol. Cell. Proteomics* **2011**, *10*, M110.001198.
(146) Chesarino, N. M.; Hach, J. C.; Chen, J. L.; Zaro, B. W.; Rajaram, M. V. S.; Turner, J.; Schlesinger, L. S.; Pratt, M. R.; Hang, H. C.; Yount, J. S. Chemoproteomics Reveals Toll-like Receptor Fatty Acylation. *BMC Biol.* **2014**, *12*, 91.
(147) Sobocińska, J.; Roszczenko-Jasińska, P.; Zaręba-Kozioł, M.; Hromada-Judycka, A.; Matveichuk, O. V; Traczyk, G.; Łukasiuk, K.; Kwiatkowska, K. Lipopolysaccharide Upregulates Palmitoylated Enzymes of the Phosphatidylinositol Cycle: An Insight from Proteomic Studies. *Mol. & Cell. Proteomics* **2018**, *17*, 233 LP – 254.
(148) Cui, L.; Liu, M.; Lai, S.; Hou, H.; Diao, T.; Zhang, D.; Wang, M.; Zhang, Y.; Wang, J. Androgen Upregulates the Palmitoylation of EIF3L in Human Prostate LNCaP Cells. *Onco. Targets. Ther.* **2019**, *12*, 4451–4459.
(149) Buddelmeijer, N. The Molecular Mechanism of Bacterial Lipoprotein Modification—How, When and Why? *FEMS Microbiol. Rev.* **2015**, *39*, 246–261.
(150) Rangan, K. J.; Yang, Y.-Y.; Charron, G.; Hang, H. C. Rapid Visualization and Large-Scale Profiling of Bacterial Lipoproteins with Chemical Reporters. *J. Am. Chem. Soc.* **2010**, *132*, 10628–10629.
(151) Jones, M. L.; Collins, M. O.; Goulding, D.; Choudhary, J. S.; Rayner, J. C. Analysis of Protein Palmitoylation Reveals a Pervasive Role in Plasmodium Development and Pathogenesis. *Cell Host Microbe* **2012**, *12*, 246–258.
(152) Foe, I. T.; Child, M. A.; Majmudar, J. D.; Krishnamurthy, S.; van der Linden, W. A.; Ward, G. E.; Martin, B. R.; Bogyo, M. Global Analysis of Palmitoylated Proteins in Toxoplasma Gondii. *Cell Host Microbe* **2015**, *18*, 501–511.
(153) Santiago-Tirado, F. H.; Peng, T.; Yang, M.; Hang, H. C.; Doering, T. L. A Single Protein S-Acyl Transferase Acts through Diverse Substrates to Determine Cryptococcal Morphology, Stress Tolerance, and Pathogenic Outcome. *PLoS Pathog.* **2015**, *11*, e1004908.
(154) Serwa, R. A.; Abaitua, F.; Krause, E.; Tate, E. W.; O'Hare, P. Systems Analysis of Protein Fatty Acylation in Herpes Simplex Virus-Infected Cells Using Chemical Proteomics. *Chem. Biol.* **2015**, *22*, 1008–1017.
(155) Colquhoun, D. R.; Lyashkov, A. E.; Mohien, C. U.; Aquino, V. N.; Bullock, B. T.; Dinglasan, R. R.; Agnew, B. J.; Graham, D. R. M. Bioorthogonal Mimetics of Palmitoyl-CoA and Myristoyl-CoA and Their Subsequent Isolation by Click Chemistry and Characterization by Mass Spectrometry Reveal Novel Acylated Host-Proteins Modified by HIV-1 Infection. *Proteomics* **2015**, *15*, 2066–2077.
(156) Martin, B. R.; Wang, C.; Adibekian, A.; Tully, S. E.; Cravatt, B. F. Global Profiling of Dynamic Protein Palmitoylation. *Nat Meth* **2012**, *9*, 84–89.

(157) Liu, Y.; Patricelli, M. P.; Cravatt, B. F. Activity-Based Protein Profiling: The Serine Hydrolases. *Proc. Natl. Acad. Sci. U. S. A.* **1999**, *96*, 14694–14699.
(158) Medina-Cleghorn, D.; Nomura, D. K. Exploring Metabolic Pathways and Regulation through Functional Chemoproteomic and Metabolomic Platforms. *Chem. Biol.* **2014**, *21*, 1171–1184.
(159) Wei, X.; Adak, S.; Zayed, M.; Yin, L.; Feng, C.; Speck, S. L.; Kathayat, R. S.; Zhang, Q.; Dickinson, B. C.; Semenkovich, C. F. Endothelial Palmitoylation Cycling Coordinates Vessel Remodeling in Peripheral Artery Disease. *Circ. Res.* **2020**, *0*.
(160) Wright, M. H.; Paape, D.; Price, H. P.; Smith, D. F.; Tate, E. W. Global Profiling and Inhibition of Protein Lipidation in Vector and Host Stages of the Sleeping Sickness Parasite Trypanosoma Brucei. *ACS Infect. Dis.* **2016**, *2*, 427–441.
(161) Emmer, B. T.; Nakayasu, E. S.; Souther, C.; Choi, H.; Sobreira, T. J. P.; Epting, C. L.; Nesvizhskii, A. I.; Almeida, I. C.; Engman, D. M. Global Analysis of Protein Palmitoylation in African Trypanosomes. *Eukaryot. Cell* **2011**, *10*, 455 LP – 463.
(162) Hernandez, J. L.; Davda, D.; Majmudar, J. D.; Won, S. J.; Prakash, A.; Choi, A. I.; Martin, B. R. Correlated S-Palmitoylation Profiling of Snail-Induced Epithelial to Mesenchymal Transition. *Mol. Biosyst.* **2016**, *12*, 1799–1808.
(163) Miura, G. I.; Buglino, J.; Alvarado, D.; Lemmon, M. A.; Resh, M. D.; Treisman, J. E. Palmitoylation of the EGFR Ligand Spitz by Rasp Increases Spitz Activity by Restricting Its Diffusion. *Dev. Cell* **2006**, *10*, 167–176.
(164) Thinon, E.; Fernandez, J. P.; Molina, H.; Hang, H. C. Selective Enrichment and Direct Analysis of Protein S-Palmitoylation Sites. *J. Proteome Res.* **2018**, *17*, 1907–1922.
(165) Yount, J. S.; Zhang, M. M.; Hang, H. C. Visualization and Identification of Fatty Acylated Proteins Using Chemical Reporters. *Curr. Protoc. Chem. Biol.* **2011**, *3*, 65–79.
(166) Hannoush, R. N. Profiling Cellular Myristoylation and Palmitoylation Using ω-Alkynyl Fatty Acids BT - Chemical Genomics and Proteomics: Reviews and Protocols; Zanders, E. D., Ed.; Humana Press: Totowa, NJ, 2012; pp 85–94.
(167) Martin, B. R. Nonradioactive Analysis of Dynamic Protein Palmitoylation. *Curr. Protoc. Protein Sci.* **2013**, *73*, 14.15.1-14.15.9.
(168) Ji, Y.; Bachschmid, M. M.; Costello, C. E.; Lin, C. S- to N-Palmitoyl Transfer During Proteomic Sample Preparation. *J. Am. Soc. Mass Spectrom.* **2016**, *27*, 677–685.
(169) Percher, A.; Ramakrishnan, S.; Thinon, E.; Yuan, X.; Yount, J. S.; Hang, H. C. Mass-Tag Labeling Reveals Site-Specific and Endogenous Levels of Protein S-Fatty Acylation. *Proc. Natl. Acad. Sci.* **2016**, *113*, 4302 LP – 4307.
(170) Yount, J. S.; Karssemeijer, R. A.; Hang, H. C. S-Palmitoylation and Ubiquitination Differentially Regulate Interferon-Induced Transmembrane Protein 3 (IFITM3)-Mediated Resistance to Influenza Virus. *J. Biol. Chem.* **2012**, *287*, 19631–19641.
(171) McMichael, T. M.; Zhang, L.; Chemudupati, M.; Hach, J. C.; Kenney, A. D.; Hang, H. C.; Yount, J. S. The Palmitoyltransferase ZDHHC20 Enhances Interferon-Induced Transmembrane Protein 3 (IFITM3) Palmitoylation and Antiviral Activity. *J. Biol. Chem.* **2017**, *292*, 21517–21526.
(172) Spence, J. S.; He, R.; Hoffmann, H.-H.; Das, T.; Thinon, E.; Rice, C. M.; Peng, T.;

Chandran, K.; Hang, H. C. IFITM3 Directly Engages and Shuttles Incoming Virus Particles to Lysosomes. *Nat. Chem. Biol.* **2019**, *15*, 259–268.
(173) Benfield, C. T. O.; MacKenzie, F.; Ritzefeld, M.; Mazzon, M.; Weston, S.; Tate, E. W.; Teo, B. H.; Smith, S. E.; Kellam, P.; Holmes, E. C.; et al. Bat IFITM3 Restriction Depends on S-Palmitoylation and a Polymorphic Site within the CD225 Domain. *Life Sci. Alliance* **2020**, *3*, e201900542.
(174) Chesarino, N. M.; Compton, A. A.; McMichael, T. M.; Kenney, A. D.; Zhang, L.; Soewarna, V.; Davis, M.; Schwartz, O.; Yount, J. S. IFITM3 Requires an Amphipathic Helix for Antiviral Activity. *EMBO Rep.* **2017**, *18*, 1740–1751.
(175) Tsukamoto, T.; Li, X.; Morita, H.; Minowa, T.; Aizawa, T.; Hanagata, N.; Demura, M. Role of S-Palmitoylation on IFITM5 for the Interaction with FKBP11 in Osteoblast Cells. *PLoS One* **2013**, *8*, e75831–e75831.
(176) Hach, J. C.; McMichael, T.; Chesarino, N. M.; Yount, J. S. Palmitoylation on Conserved and Nonconserved Cysteines of Murine IFITM1 Regulates Its Stability and Anti-Influenza A Virus Activity. *J. Virol.* **2013**, *87*, 9923–9927.
(177) Hicks, S. W.; Charron, G.; Hang, H. C.; Galán, J. E. Subcellular Targeting of Salmonella Virulence Proteins by Host-Mediated S-Palmitoylation. *Cell Host Microbe* **2011**, *10*, 9–20.
(178) Melvin, W. J.; McMichael, T. M.; Chesarino, N. M.; Hach, J. C.; Yount, J. S. IFITMs from Mycobacteria Confer Resistance to Influenza Virus When Expressed in Human Cells. *Viruses* **2015**, *7*, 3035–3052.
(179) Zhang, M. M.; Wu, P.-Y. J.; Kelly, F. D.; Nurse, P.; Hang, H. C. Quantitative Control of Protein S-Palmitoylation Regulates Meiotic Entry in Fission Yeast. *PLOS Biol.* **2013**, *11*, e1001597.
(180) Roth, A. F.; Papanayotou, I.; Davis, N. G. The Yeast Kinase Yck2 Has a Tripartite Palmitoylation Signal. *Mol. Biol. Cell* **2011**, *22*, 2702–2715.
(181) Bhattacharyya, R.; Barren, C.; Kovacs, D. M. Palmitoylation of Amyloid Precursor Protein Regulates Amyloidogenic Processing in Lipid Rafts. *J. Neurosci.* **2013**, *33*, 11169–11183.
(182) Aramsangtienchai, P.; Spiegelman, N. A.; Cao, J.; Lin, H. S-Palmitoylation of Junctional Adhesion Molecule C Regulates Its Tight Junction Localization and Cell Migration. *J. Biol. Chem.* **2017**, *292*, 5325–5334.
(183) Konitsiotis, A. D.; Chang, S.-C.; Jovanović, B.; Ciepla, P.; Masumoto, N.; Palmer, C. P.; Tate, E. W.; Couchman, J. R.; Magee, A. I. Attenuation of Hedgehog Acyltransferase-Catalyzed Sonic Hedgehog Palmitoylation Causes Reduced Signaling, Proliferation and Invasiveness of Human Carcinoma Cells. *PLoS One* **2014**, *9*, e89899.
(184) Ampah, K. K.; Greaves, J.; Shun-Shion, A. S.; Asnawi, A. W.; Lidster, J. A.; Chamberlain, L. H.; Collins, M. O.; Peden, A. A. S-Acylation Regulates the Trafficking and Stability of the Unconventional Q-SNARE STX19. *J. Cell Sci.* **2018**, *131*, jcs212498.
(185) Zhang, M. M.; Tsou, L. K.; Charron, G.; Raghavan, A. S.; Hang, H. C. Tandem Fluorescence Imaging of Dynamic S-Acylation and Protein Turnover. *Proc. Natl. Acad. Sci.* **2010**, *107*, 8627 LP – 8632.
(186) Liu, K.; Yang, P.-Y.; Na, Z.; Yao, S. Q. Dynamic Monitoring of Newly Synthesized Proteomes: Up-Regulation of Myristoylated Protein Kinase A During

Butyric Acid Induced Apoptosis. *Angew. Chemie Int. Ed.* **2011**, *50*, 6776–6781.
(187) Akimzhanov, A. M.; Boehning, D. Rapid and Transient Palmitoylation of the Tyrosine Kinase Lck Mediates Fas Signaling. *Proc. Natl. Acad. Sci.* **2015**, *112*, 11876 LP – 11880.
(188) Holland, S. M.; Collura, K. M.; Ketschek, A.; Noma, K.; Ferguson, T. A.; Jin, Y.; Gallo, G.; Thomas, G. M. Palmitoylation Controls DLK Localization, Interactions and Activity to Ensure Effective Axonal Injury Signaling. *Proc. Natl. Acad. Sci.* **2016**, *113*, 763 LP – 768.
(189) Kim, Y.-C.; Lee, S. E.; Kim, S. K.; Jang, H.-D.; Hwang, I.; Jin, S.; Hong, E.-B.; Jang, K.-S.; Kim, H.-S. Toll-like Receptor Mediated Inflammation Requires FASN-Dependent MYD88 Palmitoylation. *Nat. Chem. Biol.* **2019**, *15*, 907–916.
(190) Segal-Salto, M.; Sapir, T.; Reiner, O. Reversible Cysteine Acylation Regulates the Activity of Human Palmitoyl-Protein Thioesterase 1 (PPT1). *PLoS One* **2016**, *11*, e0146466.
(191) Segal-Salto, M.; Hansson, K.; Sapir, T.; Kaplan, A.; Levy, T.; Schweizer, M.; Frotscher, M.; James, P.; Reiner, O. Proteomics Insights into Infantile Neuronal Ceroid Lipofuscinosis (CLN1) Point to the Involvement of Cilia Pathology in the Disease. *Hum. Mol. Genet.* **2017**, *26*, 1678.
(192) Pei, Z.; Xiao, Y.; Meng, J.; Hudmon, A.; Cummins, T. R. Cardiac Sodium Channel Palmitoylation Regulates Channel Availability and Myocyte Excitability with Implications for Arrhythmia Generation. *Nat. Commun.* **2016**, *7*, 12035.
(193) Zoltewicz, S. J.; Lee, S.; Chittoor, V. G.; Freeland, S. M.; Rangaraju, S.; Zacharias, D. A.; Notterpek, L. The Palmitoylation State of PMP22 Modulates Epithelial Cell Morphology and Migration. *ASN Neuro* **2012**, *4*, 409–421.
(194) Ramsey, J.; Renzi, E. C.; Arnold, R. J.; Trinidad, J. C.; Mukhopadhyay, S. Palmitoylation of Sindbis Virus TF Protein Regulates Its Plasma Membrane Localization and Subsequent Incorporation into Virions. *J. Virol.* **2017**, *91*, e02000-16.
(195) Lynes, E. M.; Raturi, A.; Shenkman, M.; Sandoval, C. O.; Yap, M. C.; Wu, J.; Janowicz, A.; Myhill, N.; Benson, M. D.; Campbell, R. E.; et al. Palmitoylation Is the Switch That Assigns Calnexin to Quality Control or ER Ca2+ Signaling. *J. Cell Sci.* **2013**, *126*, 3893 LP – 3903.
(196) Chan, P.; Han, X.; Zheng, B.; DeRan, M.; Yu, J.; Jarugumilli, G. K.; Deng, H.; Pan, D.; Luo, X.; Wu, X. Autopalmitoylation of TEAD Proteins Regulates Transcriptional Output of the Hippo Pathway. *Nat. Chem. Biol.* **2016**, *12*, 282–289.
(197) Noland, C. L.; Gierke, S.; Schnier, P. D.; Murray, J.; Sandoval, W. N.; Sagolla, M.; Dey, A.; Hannoush, R. N.; Fairbrother, W. J.; Cunningham, C. N. Palmitoylation of TEAD Transcription Factors Is Required for Their Stability and Function in Hippo Pathway Signaling. *Structure* **2016**, *24*, 179–186.
(198) Roberts, B. J.; Johnson, K. E.; McGuinn, K. P.; Saowapa, J.; Svoboda, R. A.; Mahoney, M. G.; Johnson, K. R.; Wahl, J. K. Palmitoylation of Plakophilin Is Required for Desmosome Assembly. *J. Cell Sci.* **2014**, *127*, 3782 LP – 3793.
(199) Antinone, S. E.; Ghadge, G. D.; Lam, T. T.; Wang, L.; Roos, R. P.; Green, W. N. Palmitoylation of Superoxide Dismutase 1 (SOD1) Is Increased for Familial Amyotrophic Lateral Sclerosis-Linked SOD1 Mutants. *J. Biol. Chem.* **2013**, *288*, 21606–21617.

(200) Jiang, M.; Hu, J.; White, F. K. H.; Williamson, J.; Klymchenko, A. S.; Murthy, A.; Workman, S. W.; Tseng, G.-N. S-Palmitoylation of Junctophilin-2 Is Critical for Its Role in Tethering the Sarcoplasmic Reticulum to the Plasma Membrane. *J. Biol. Chem.* **2019**, *294*, 13487–13501.
(201) Chen, B.; Zheng, B.; DeRan, M.; Jarugumilli, G. K.; Fu, J.; Brooks, Y. S.; Wu, X. ZDHHC7-Mediated S-Palmitoylation of Scribble Regulates Cell Polarity. *Nat. Chem. Biol.* **2016**, *12*, 686–693.
(202) Hernandez, J. L.; Davda, D.; Cheung See Kit, M.; Majmudar, J. D.; Won, S. J.; Gang, M.; Pasupuleti, S. C.; Choi, A. I.; Bartkowiak, C. M.; Martin, B. R. APT2 Inhibition Restores Scribble Localization and S-Palmitoylation in Snail-Transformed Cells. *Cell Chem. Biol.* **2017**, *24*, 87–97.
(203) Schroeder, G. N.; Aurass, P.; Oates, C. V; Tate, E. W.; Hartland, E. L.; Flieger, A.; Frankel, G. Legionella Pneumophila Effector LpdA Is a Palmitoylated Phospholipase D Virulence Factor. *Infect. Immun.* **2015**, *83*, 3989 LP – 4002.
(204) Ren, W.; Jhala, U. S.; Du, K. Proteomic Analysis of Protein Palmitoylation in Adipocytes. *Adipocyte* **2013**, *2*, 17–28.
(205) Ticho, A. L.; Malhotra, P.; Manzella, C. R.; Dudeja, P. K.; Saksena, S.; Gill, R. K.; Alrefai, W. A. S-Acylation Modulates the Function of the Apical Sodium-Dependent Bile Acid Transporter in Human Cells. *J. Biol. Chem.* **2020**.
(206) Kim, S. W.; Kim, D. H.; Park, K. S.; Kim, M. K.; Park, Y. M.; Muallem, S.; So, I.; Kim, H. J. Palmitoylation Controls Trafficking of the Intracellular Ca2+ Channel MCOLN3/TRPML3 to Regulate Autophagy. *Autophagy* **2019**, *15*, 327–340.
(207) Sada, R.; Kimura, H.; Fukata, Y.; Fukata, M.; Yamamoto, H.; Kikuchi, A. Dynamic Palmitoylation Controls the Microdomain Localization of the DKK1 Receptors CKAP4 and LRP6. *Sci. Signal.* **2019**, *12*, eaat9519.
(208) Yao, H.; Lan, J.; Li, C.; Shi, H.; Brosseau, J.-P.; Wang, H.; Lu, H.; Fang, C.; Zhang, Y.; Liang, L.; et al. Inhibiting PD-L1 Palmitoylation Enhances T-Cell Immune Responses against Tumours. *Nat. Biomed. Eng.* **2019**, *3*, 306–317.
(209) Yao, H.; Li, C.; He, F.; Song, T.; Brosseau, J.-P.; Wang, H.; Lu, H.; Fang, C.; Shi, H.; Lan, J.; et al. A Peptidic Inhibitor for PD-1 Palmitoylation Targets Its Expression and Functions. *RSC Chem. Biol.* **2021**.
(210) Ebersole, B.; Petko, J.; Woll, M.; Murakami, S.; Sokolina, K.; Wong, V.; Stagljar, I.; Lüscher, B.; Levenson, R. Effect of C-Terminal S-Palmitoylation on D2 Dopamine Receptor Trafficking and Stability. *PLoS One* **2015**, *10*, e0140661.
(211) Coleman, D. T.; Gray, A. L.; Kridel, S. J.; Cardelli, J. A. Palmitoylation Regulates the Intracellular Trafficking and Stability of C-Met. *Oncotarget* **2016**, *7*, 32664–32677.
(212) Runkle, K. B.; Kharbanda, A.; Stypulkowski, E.; Cao, X.-J.; Wang, W.; Garcia, B. A.; Witze, E. S. Inhibition of DHHC20-Mediated EGFR Palmitoylation Creates a Dependence on EGFR Signaling. *Mol. Cell* **2016**, *62*, 385–396.
(213) Wegleiter, T.; Buthey, K.; Gonzalez-Bohorquez, D.; Hruzova, M.; bin Imtiaz, M. K.; Abegg, A.; Mebert, I.; Molteni, A.; Kollegger, D.; Pelczar, P.; et al. Palmitoylation of BMPR1a Regulates Neural Stem Cell Fate. *Proc. Natl. Acad. Sci.* **2019**, *116*, 25688 LP – 25696.
(214) Zingler, P.; Särchen, V.; Glatter, T.; Caning, L.; Saggau, C.; Kathayat, R. S.; Dickinson, B. C.; Adam, D.; Schneider-Brachert, W.; Schütze, S.; et al.

Palmitoylation Is Required for TNF-R1 Signaling. *Cell Commun. Signal.* **2019**, *17*, 90.
(215) Poggi, M.; Kara, I.; Brunel, J.-M.; Landrier, J.-F.; Govers, R.; Bonardo, B.; Fluhrer, R.; Haass, C.; Alessi, M.-C.; Peiretti, F. Palmitoylation of TNF Alpha Is Involved in the Regulation of TNF Receptor 1 Signalling. *Biochim. Biophys. Acta - Mol. Cell Res.* **2013**, *1833*, 602–612.
(216) Wang, W.; Runkle, K. B.; Terkowski, S. M.; Ekaireb, R. I.; Witze, E. S. Protein Depalmitoylation Is Induced by Wnt5a and Promotes Polarized Cell Behavior. *J. Biol. Chem.* **2015**, *290*, 15707–15716.
(217) Stypulkowski, E.; Asangani, I. A.; Witze, E. S. The Depalmitoylase APT1 Directs the Asymmetric Partitioning of Notch and Wnt Signaling during Cell Division. *Sci. Signal.* **2018**, *11*, eaam8705.
(218) Zhang, M.; Zhou, L.; Xu, Y.; Yang, M.; Xu, Y.; Komaniecki, G. P.; Kosciuk, T.; Chen, X.; Lu, X.; Zou, X.; et al. A STAT3 Palmitoylation Cycle Promotes TH17 Differentiation and Colitis. *Nature* **2020**, *586*, 434–439.
(219) Cao, Y.; Qiu, T.; Kathayat, R. S.; Azizi, S.-A.; Thorne, A. K.; Ahn, D.; Fukata, Y.; Fukata, M.; Rice, P. A.; Dickinson, B. C. ABHD10 Is an S-Depalmitoylase Affecting Redox Homeostasis through Peroxiredoxin-5. *Nat. Chem. Biol.* **2019**, *15*, 1232–1240.
(220) Cui, Y.; Ma, L. Sequential Use of Milk and Bovine Serum Albumin for Streptavidin-Probed Western Blot. *Biotechniques* **2018**, *65*, 125–126.
(221) Fokin, V. V. Click Imaging of Biochemical Processes in Living Systems. *ACS Chem. Biol.* **2007**, *2*, 775–778.
(222) Ayana, R.; Yadav, P.; Kumari, R.; Ramu, D.; Garg, S.; Pati, S.; Singh, S. Identification and Characterization of a Novel Palmitoyl Acyltransferase as a Druggable Rheostat of Dynamic Palmitoylome in L. Donovani. *Front. Cell. Infect. Microbiol.* **2018**, *8*, 186.
(223) Siddiqui, M. A.; Singh, S.; Malhotra, P.; Chitnis, C. E. Protein S-Palmitoylation Is Responsive to External Signals and Plays a Regulatory Role in Microneme Secretion in Plasmodium Falciparum Merozoites. *ACS Infect. Dis.* **2020**, *6*, 379–392.
(224) Kilian, N.; Zhang, Y.; LaMonica, L.; Hooker, G.; Toomre, D.; Mamoun, C. Ben; Ernst, A. M. Palmitoylated Proteins in Plasmodium Falciparum-Infected Erythrocytes: Investigation with Click Chemistry and Metabolic Labeling. *BioEssays* **2020**, *42*, 1900145.
(225) Zaręba-Kozioł, M.; Bartkowiak-Kaczmarek, A.; Figiel, I.; Krzystyniak, A.; Wojtowicz, T.; Bijata, M.; Wlodarczyk, J. Stress-Induced Changes in the S-Palmitoylation and S-Nitrosylation of Synaptic Proteins. *Mol. Cell. ProteomicsCellular Proteomics* **2019**, *18*, 1916–1938.
(226) Dumoulin, A.; Dagane, A.; Dittmar, G.; Rathjen, F. G. S-Palmitoylation Is Required for the Control of Growth Cone Morphology of DRG Neurons by CNP-Induced CGMP Signaling. *Front. Mol. Neurosci.* **2018**, *11*, 345.
(227) Ernst, A. M.; Syed, S. A.; Zaki, O.; Bottanelli, F.; Zheng, H.; Hacke, M.; Xi, Z.; Rivera-Molina, F.; Graham, M.; Rebane, A. A.; et al. S-Palmitoylation Sorts Membrane Cargo for Anterograde Transport in the Golgi. *Dev. Cell* **2018**, *47*, 479-493.e7.

(228) Gao, X.; Arenas-Ramirez, N.; Scales, S. J.; Hannoush, R. N. Membrane Targeting of Palmitoylated Wnt and Hedgehog Revealed by Chemical Probes. *FEBS Lett.* **2011**, *585*, 2501–2506.
(229) Gao, X.; Hannoush, R. N. Method for Cellular Imaging of Palmitoylated Proteins with Clickable Probes and Proximity Ligation Applied to Hedgehog, Tubulin, and Ras. *J. Am. Chem. Soc.* **2014**, *136*, 4544–4550.
(230) Gao, X.; Hannoush, R. N. Single-Cell in Situ Imaging of Palmitoylation in Fatty-Acylated Proteins. *Nat. Protoc.* **2014**, *9*, 2607–2623.
(231) Yang, Y.; Dong, W.; Guo, Y.; Rioux, R. M. Cu(i)-Catalyzed Aerobic Cross-Dehydrogenative Coupling of Terminal Alkynes with Thiols for the Construction of Alkynyl Sulfides. *Green Chem.* **2013**, *15*, 3170–3175.
(232) Witten, A. J.; Ejendal, K. F. K.; Gengelbach, L. M.; Traore, M. A.; Wang, X.; Umulis, D. M.; Calve, S.; Kinzer-Ursem, T. L. Fluorescent Imaging of Protein Myristoylation during Cellular Differentiation and Development. *J. Lipid Res.* **2017**, *58*, 2061–2070.
(233) Coleman, D. T.; Soung, Y. H.; Surh, Y.-J.; Cardelli, J. A.; Chung, J. Curcumin Prevents Palmitoylation of Integrin B4 in Breast Cancer Cells. *PLoS One* **2015**, *10*, e0125399.
(234) Rodgers, U. R.; Lanyon-Hogg, T.; Masumoto, N.; Ritzefeld, M.; Burke, R.; Blagg, J.; Magee, A. I.; Tate, E. W. Characterization of Hedgehog Acyltransferase Inhibitors Identifies a Small Molecule Probe for Hedgehog Signaling by Cancer Cells. *ACS Chem. Biol.* **2016**, *11*, 3256–3262.
(235) Dodge, M. E.; Moon, J.; Tuladhar, R.; Lu, J.; Jacob, L. S.; Zhang, L.; Shi, H.; Wang, X.; Moro, E.; Mongera, A.; et al. Diverse Chemical Scaffolds Support Direct Inhibition of the Membrane Bound O-Acyltransferase Porcupine. *J. Biol. Chem.* **2012**.
(236) Proffitt, K. D.; Madan, B.; Ke, Z.; Pendharkar, V.; Ding, L.; Lee, M. A.; Hannoush, R. N.; Virshup, D. M. Pharmacological Inhibition of the Wnt Acyltransferase PORCN Prevents Growth of WNT-Driven Mammary Cancer. *Cancer Res.* **2013**, *73*, 502 LP – 507.
(237) Madan, B.; Ke, Z.; Harmston, N.; Ho, S. Y.; Frois, A. O.; Alam, J.; Jeyaraj, D. A.; Pendharkar, V.; Ghosh, K.; Virshup, I. H.; et al. Wnt Addiction of Genetically Defined Cancers Reversed by PORCN Inhibition. *Oncogene* **2016**, *35*, 2197–2207.
(238) Zhan, T.; Rindtorff, N.; Boutros, M. Wnt Signaling in Cancer. *Oncogene* **2017**, *36*, 1461–1473.
(239) Yadav, P.; Ayana, R.; Garg, S.; Jain, R.; Sah, R.; Joshi, N.; Pati, S.; Singh, S. Plasmodium Palmitoylation Machinery Engineered in E. Coli for High-Throughput Screening of Palmitoyl Acyl-Transferase Inhibitors. *FEBS Open Bio* **2019**, *9*, 248–264.
(240) Fukata, M.; Fukata, Y.; Adesnik, H.; Nicoll, R. A.; Bredt, D. S. Identification of PSD-95 Palmitoylating Enzymes. *Neuron* **2004**, *44*, 987–996.
(241) Zheng, B.; DeRan, M.; Li, X.; Liao, X.; Fukata, M.; Wu, X. 2-Bromopalmitate Analogues as Activity-Based Probes To Explore Palmitoyl Acyltransferases. *J. Am. Chem. Soc.* **2013**, *135*, 7082–7085.
(242) Davda, D.; El Azzouny, M. A.; Tom, C. T. M. B.; Hernandez, J. L.; Majmudar, J. D.; Kennedy, R. T.; Martin, B. R. Profiling Targets of the Irreversible

Palmitoylation Inhibitor 2-Bromopalmitate. *ACS Chem. Biol.* **2013**, *8*, 1912–1917.
(243) Zheng, B.; Zhu, S.; Wu, X. Clickable Analogue of Cerulenin as Chemical Probe to Explore Protein Palmitoylation. *ACS Chem. Biol.* **2015**, *10*, 115–121.
(244) Ganesan, L.; Shieh, P.; Bertozzi, C. R.; Levental, I. Click-Chemistry Based High Throughput Screening Platform for Modulators of Ras Palmitoylation. *Sci. Rep.* **2017**, *7*, 41147.
(245) Konitsiotis, A. D.; Jovanović, B.; Ciepla, P.; Spitaler, M.; Lanyon-Hogg, T.; Tate, E. W.; Magee, A. I. Topological Analysis of Hedgehog Acyltransferase, a Multipalmitoylated Transmembrane Protein. *J. Biol. Chem.* **2015**, *290*, 3293–3307.
(246) Lanyon-Hogg, T.; Masumoto, N.; Bodakh, G.; Konitsiotis, A. D.; Thinon, E.; Rodgers, U. R.; Owens, R. J.; Magee, A. I.; Tate, E. W. Click Chemistry Armed Enzyme-Linked Immunosorbent Assay to Measure Palmitoylation by Hedgehog Acyltransferase. *Anal. Biochem.* **2015**, *490*, 66–72.
(247) Lanyon-Hogg, T.; Patel, N. V; Ritzefeld, M.; Boxall, K. J.; Burke, R.; Blagg, J.; Magee, A. I.; Tate, E. W. Microfluidic Mobility Shift Assay for Real-Time Analysis of Peptide N-Palmitoylation. *SLAS Discov. Adv. Sci. Drug Discov.* **2017**, *22*, 418–424.
(248) Lanyon-Hogg, T.; Ritzefeld, M.; Sefer, L.; Bickel, J. K.; Rudolf, A. F.; Panyain, N.; Bineva-Todd, G.; Ocasio, C. A.; O'Reilly, N.; Siebold, C.; et al. Acylation-Coupled Lipophilic Induction of Polarisation (Acyl-CLIP): A Universal Assay for Lipid Transferase and Hydrolase Enzymes. *Chem. Sci.* **2019**, *10*, 8995–9000.
(249) Morrison, E.; Wegner, T.; Zucchetti, A. E.; Álvaro-Benito, M.; Zheng, A.; Kliche, S.; Krause, E.; Brügger, B.; Hivroz, C.; Freund, C. Dynamic Palmitoylation Events Following T-Cell Receptor Signaling. *Commun. Biol.* **2020**, *3*, 368.
(250) Salaun, C.; Greaves, J.; Tomkinson, N. C. O.; Chamberlain, L. H. The Linker Domain of the SNARE Protein SNAP25 Acts as a Flexible Molecular Spacer That Ensures Efficient S-Acylation. *J. Biol. Chem.* **2020**, *295*, 7501–7515.
(251) Martinez, A.; Traverso, J. A.; Valot, B.; Ferro, M.; Espagne, C.; Ephritikhine, G.; Zivy, M.; Giglione, C.; Meinnel, T. Extent of N-Terminal Modifications in Cytosolic Proteins from Eukaryotes. *Proteomics* **2008**, *8*, 2809–2831.
(252) Martin, D. D. O.; Vilas, G. L.; Prescher, J. A.; Rajaiah, G.; Falck, J. R.; Bertozzi, C. R.; Berthiaume, L. G. Rapid Detection, Discovery, and Identification of Post-Translationally Myristoylated Proteins during Apoptosis Using a Bio-Orthogonal Azidomyristate Analog. *FASEB J.* **2008**, *22*, 797–806.
(253) Yap, M. C.; Kostiuk, M. A.; Martin, D. D. O.; Perinpanayagam, M. A.; Hak, P. G.; Siddam, A.; Majjigapu, J. R.; Rajaiah, G.; Keller, B. O.; Prescher, J. A.; et al. Rapid and Selective Detection of Fatty Acylated Proteins Using ω-Alkynyl-Fatty Acids and Click Chemistry. *J. Lipid Res.* **2010**, *51*, 1566–1580.
(254) Storck, E. M.; Serwa, R. A.; Tate, E. W. Chemical Proteomics: A Powerful Tool for Exploring Protein Lipidation. *Biochem. Soc. Trans.* **2013**, *41*, 56 LP – 61.
(255) Martin, D. D. O.; Ahpin, C. Y.; Heit, R. J.; Perinpanayagam, M. A.; Yap, M. C.; Veldhoen, R. A.; Goping, I. S.; Berthiaume, L. G. Tandem Reporter Assay for Myristoylated Proteins Post-Translationally (TRAMPP) Identifies Novel Substrates for Post-Translational Myristoylation: PKC∈, a Case Study. *FASEB J.* **2012**, *26*, 13–28.

(256) Boyle, P. C.; Schwizer, S.; Hind, S. R.; Kraus, C. M.; De la Torre Diaz, S.; He, B.; Martin, G. B. Detecting N-Myristoylation and S-Acylation of Host and Pathogen Proteins in Plants Using Click Chemistry. *Plant Methods* **2016**, *12*, 38.
(257) Takamitsu, E.; Fukunaga, K.; Iio, Y.; Moriya, K.; Utsumi, T. Cell-Free Identification of Novel N-Myristoylated Proteins from Complementary DNA Resources Using Bioorthogonal Myristic Acid Analogues. *Anal. Biochem.* **2014**, *464*, 83–93.
(258) Rampoldi, F.; Sandhoff, R.; Owen, R. W.; Gröne, H.-J.; Porubsky, S. A New, Robust, and Nonradioactive Approach for Exploring N-Myristoylation. *J. Lipid Res.* **2012**, *53*, 2459–2468.
(259) Gao, H.; Sun, W.; Song, Z.; Yu, Y.; Wang, L.; Chen, X.; Zhang, Q. A Method to Generate and Analyze Modified Myristoylated Proteins. *Chembiochem* **2017**, *18*, 324–330.
(260) Goya Grocin, A.; Serwa, R. A.; Morales Sanfrutos, J.; Ritzefeld, M.; Tate, E. W. Whole Proteome Profiling of N-Myristoyltransferase Activity and Inhibition Using Sortase A. *Mol. & Cell. Proteomics* **2019**, *18*, 115 LP – 126.
(261) Kinoshita-Kikuta, E.; Tanikawa, A.; Hosokawa, T.; Kiwado, A.; Moriya, K.; Kinoshita, E.; Koike, T.; Utsumi, T. A Strategy to Identify Protein-N-Myristoylation-Dependent Phosphorylation Reactions of Cellular Proteins by Using Phos-Tag SDS-PAGE. *PLoS One* **2019**, *14*, e0225510.
(262) Kosciuk, T.; Lin, H. N-Myristoyltransferase as a Glycine and Lysine Myristoyltransferase in Cancer, Immunity, and Infections. *ACS Chem. Biol.* **2020**.
(263) Thinon, E.; Serwa, R. A.; Broncel, M.; Brannigan, J. A.; Brassat, U.; Wright, M. H.; Heal, W. P.; Wilkinson, A. J.; Mann, D. J.; Tate, E. W. Global Profiling of Co- and Post-Translationally N-Myristoylated Proteomes in Human Cells. *Nat Commun* **2014**, *5*.
(264) Thinon, E.; Morales-Sanfrutos, J.; Mann, D. J.; Tate, E. W. N-Myristoyltransferase Inhibition Induces ER-Stress, Cell Cycle Arrest, and Apoptosis in Cancer Cells. *ACS Chem. Biol.* **2016**, *11*, 2165–2176.
(265) Broncel, M.; Serwa, R. A.; Ciepla, P.; Krause, E.; Dallman, M. J.; Magee, A. I.; Tate, E. W. Myristoylation Profiling in Human Cells and Zebrafish. *Data Br.* **2015**, *4*, 379–383.
(266) Zhang, X.; Khan, S.; Jiang, H.; Antonyak, M. A.; Chen, X.; Spiegelman, N. A.; Shrimp, J. H.; Cerione, R. A.; Lin, H. Identifying the Functional Contribution of the Defatty-Acylase Activity of SIRT6. *Nat. Chem. Biol.* **2016**, *12*, 614–620.
(267) Jiang, H.; Khan, S.; Wang, Y.; Charron, G.; He, B.; Sebastian, C.; Du, J.; Kim, R.; Ge, E.; Mostoslavsky, R.; et al. SIRT6 Regulates TNF-[Agr] Secretion through Hydrolysis of Long-Chain Fatty Acyl Lysine. *Nature* **2013**, *496*, 110–113.
(268) Aramsangtienchai, P.; Spiegelman, N. A.; He, B.; Miller, S. P.; Dai, L.; Zhao, Y.; Lin, H. HDAC8 Catalyzes the Hydrolysis of Long Chain Fatty Acyl Lysine. *ACS Chem. Biol.* **2016**, *11*, 2685–2692.
(269) Spiegelman, N. A.; Hong, J. Y.; Hu, J.; Jing, H.; Wang, M.; Price, I. R.; Cao, J.; Yang, M.; Zhang, X.; Lin, H. A Small-Molecule SIRT2 Inhibitor That Promotes K-Ras4a Lysine Fatty-Acylation. *ChemMedChem* **2019**, *14*, 744–748.
(270) Heal, W. P.; Wickramasinghe, S. R.; Bowyer, P. W.; Holder, A. A.; Smith, D. F.; Leatherbarrow, R. J.; Tate, E. W. Site-Specific N-Terminal Labelling of Proteinsin

Vitro and in Vivo Using N-Myristoyl Transferase and Bioorthogonal Ligation Chemistry. *Chem. Commun.* **2008**, No. 4, 480–482.
(271) Meyer-Schaller, N.; Chou, Y.-C.; Sumara, I.; Martin, D. D. O.; Kurz, T.; Katheder, N.; Hofmann, K.; Berthiaume, L. G.; Sicheri, F.; Peter, M. The Human Dcn1-like Protein DCNL3 Promotes Cul3 Neddylation at Membranes. *Proc. Natl. Acad. Sci.* **2009**, *106*, 12365 LP – 12370.
(272) Govatati, S.; Pichavaram, P.; Janjanam, J.; Guo, L.; Virmani, R.; Rao, G. N. Myristoylation of LMCD1 Leads to Its Species-Specific Derepression of E2F1 and NFATc1 in the Modulation of CDC6 and IL-33 Expression During Development of Vascular Lesions. *Arterioscler. Thromb. Vasc. Biol.* **2020**, *40*, 1256–1274.
(273) Kumar, S.; Parameswaran, S.; Sharma, R. K. Novel Myristoylation of the Sperm-Specific Hexokinase 1 Isoform Regulates Its Atypical Localization. *Biol. Open* **2015**, *4*, 1679 LP – 1687.
(274) Rampoldi, F.; Bonrouhi, M.; Boehm, M. E.; Lehmann, W. D.; Popovic, Z. V; Kaden, S.; Federico, G.; Brunk, F.; Gröne, H.-J.; Porubsky, S. Immunosuppression and Aberrant T Cell Development in the Absence of N-Myristoylation. *J. Immunol.* **2015**, *195*, 4228 LP – 4243.
(275) Rampoldi, F.; Brunk, F.; Bonrouhi, M.; Federico, G.; Krunic, D.; Porubsky, S.; Gröne, H.-J.; Popovic, Z. V. Deficiency of N-Myristoylation Reveals Calcineurin Activity as Regulator of IFN-γ-Producing Γδ T Cells. *J. Leukoc. Biol.* **2017**, *101*, 1005–1014.
(276) Stackpole, E. E.; Akins, M. R.; Fallon, J. R. N-Myristoylation Regulates the Axonal Distribution of the Fragile X-Related Protein FXR2P. *Mol. Cell. Neurosci.* **2014**, *62*, 42–50.
(277) Demetriadou, A.; Morales-Sanfrutos, J.; Nearchou, M.; Baba, O.; Kyriacou, K.; Tate, E. W.; Drousiotou, A.; Petrou, P. P. Mouse Stbd1 Is N-Myristoylated and Affects ER–Mitochondria Association and Mitochondrial Morphology. *J. Cell Sci.* **2017**, *130*, 903 LP – 915.
(278) Liang, J.; Xu, Z.-X.; Ding, Z.; Lu, Y.; Yu, Q.; Werle, K. D.; Zhou, G.; Park, Y.-Y.; Peng, G.; Gambello, M. J.; et al. Myristoylation Confers Noncanonical AMPK Functions in Autophagy Selectivity and Mitochondrial Surveillance. *Nat. Commun.* **2015**, *6*, 7926.
(279) Kallemeijn, W. W.; Lueg, G. A.; Faronato, M.; Hadavizadeh, K.; Goya Grocin, A.; Song, O.-R.; Howell, M.; Calado, D. P.; Tate, E. W. Validation and Invalidation of Chemical Probes for the Human N-Myristoyltransferases. *Cell Chem. Biol.* **2019**, *26*, 892-900.e4.
(280) Zhu, F.; Xie, N.; Jiang, Z.; Li, G.; Ma, L.; Tong, T. The Cellular Senescence-Inhibited Gene Is Essential for PPM1A Myristoylation To Modulate Transforming Growth Factor β Signaling. *Mol. Cell. Biol.* **2018**, *38*, e00414-18.
(281) Zha, J.; Weiler, S.; Oh, K. J.; Wei, M. C.; Korsmeyer, S. J. Posttranslational N-Myristoylation of BID as a Molecular Switch for Targeting Mitochondria and Apoptosis. *Science (80-.).* **2000**, *290*, 1761 LP – 1765.
(282) Martin, D. D. O.; Heit, R. J.; Yap, M. C.; Davidson, M. W.; Hayden, M. R.; Berthiaume, L. G. Identification of a Post-Translationally Myristoylated Autophagy-Inducing Domain Released by Caspase Cleavage of Huntingtin. *Hum. Mol. Genet.* **2014**, *23*, 3166–3179.

(283) Martin, D. D. O.; Kay, C.; Collins, J. A.; Nguyen, Y. T.; Slama, R. A.; Hayden, M. R. A Human Huntingtin SNP Alters Post-Translational Modification and Pathogenic Proteolysis of the Protein Causing Huntington Disease. *Sci. Rep.* **2018**, *8*, 8096.
(284) Das, U.; Kumar, S.; Sharma, J. R. D. and R. K. Inhibition of Protein N-Myristoylation: A Therapeutic Protocol in Developing Anticancer Agents. *Current Cancer Drug Targets*. 2012, pp 667–692.
(285) Kim, S.; Yang, X.; Li, Q.; Wu, M.; Costyn, L.; Beharry, Z.; Bartlett, M. G.; Cai, H. Myristoylation of Src Kinase Mediates Src-Induced and High-Fat Diet–Accelerated Prostate Tumor Progression in Mice. *J. Biol. Chem.* **2017**, *292*, 18422–18433.
(286) Kim, S.; Alsaidan, O. A.; Goodwin, O.; Li, Q.; Sulejmani, E.; Han, Z.; Bai, A.; Albers, T.; Beharry, Z.; Zheng, Y. G. G.; et al. Blocking Myristoylation of Src Inhibits Its Kinase Activity and Suppresses Prostate Cancer Progression. *Cancer Res.* **2017**, canres.0981.2017.
(287) Beauchamp, E.; Yap, M. C.; Iyer, A.; Perinpanayagam, M. A.; Gamma, J. M.; Vincent, K. M.; Lakshmanan, M.; Raju, A.; Tergaonkar, V.; Tan, S. Y.; et al. Targeting N-Myristoylation for Therapy of B-Cell Lymphomas. *Nat. Commun.* **2020**, *11*, 5348.
(288) Li, Q.; Alsaidan, O. A.; Ma, Y.; Kim, S.; Liu, J.; Albers, T.; Liu, K.; Beharry, Z.; Zhao, S.; Wang, F.; et al. Pharmacologically Targeting the Myristoylation of the Scaffold Protein FRS2α Inhibits FGF/FGFR-Mediated Oncogenic Signaling and Tumor Progression. *J. Biol. Chem.* **2018**, *293*, 6434–6448.
(289) Bowyer, P. W.; Tate, E. W.; Leatherbarrow, R. J.; Holder, A. A.; Smith, D. F.; Brown, K. A. N-Myristoyltransferase: A Prospective Drug Target for Protozoan Parasites. *ChemMedChem* **2008**, *3*, 402–408.
(290) Tate, E. W.; Bell, A. S.; Rackham, M. D.; Wright, M. H. N-Myristoyltransferase as a Potential Drug Target in Malaria and Leishmaniasis. *Parasitology* **2014**, *141*, 37–49.
(291) Ritzefeld, M.; Wright, M. H.; Tate, E. W. New Developments in Probing and Targeting Protein Acylation in Malaria, Leishmaniasis and African Sleeping Sickness. *Parasitology* **2018**, *145*, 157–174.
(292) Poulin, B.; Patzewitz, E.-M.; Brady, D.; Silvie, O.; Wright, M. H.; Ferguson, D. J. P.; Wall, R. J.; Whipple, S.; Guttery, D. S.; Tate, E. W.; et al. Unique Apicomplexan IMC Sub-Compartment Proteins Are Early Markers for Apical Polarity in the Malaria Parasite. *Biol. Open* **2013**, *2*, 1160 LP – 1170.
(293) Schlott, A. C.; Mayclin, S.; Reers, A. R.; Coburn-Flynn, O.; Bell, A. S.; Green, J.; Knuepfer, E.; Charter, D.; Bonnert, R.; Campo, B.; et al. Structure-Guided Identification of Resistance Breaking Antimalarial N-Myristoyltransferase Inhibitors. *Cell Chem. Biol.* **2019**, *26*, 991-1000.e7.
(294) Price, H. P.; Hodgkinson, M. R.; Wright, M. H.; Tate, E. W.; Smith, B. A.; Carrington, M.; Stark, M.; Smith, D. F. A Role for the Vesicle-Associated Tubulin Binding Protein ARL6 (BBS3) in Flagellum Extension in Trypanosoma Brucei. *Biochim. Biophys. Acta - Mol. Cell Res.* **2012**, *1823*, 1178–1191.
(295) Roberts, A. J.; Torrie, L. S.; Wyllie, S.; Fairlamb, A. H. Biochemical and Genetic Characterization of Trypanosoma Cruzi N-Myristoyltransferase. *Biochem. J.* **2014**,

459, 323–332.
(296) Herrera, L. J.; Brand, S.; Santos, A.; Nohara, L. L.; Harrison, J.; Norcross, N. R.; Thompson, S.; Smith, V.; Lema, C.; Varela-Ramirez, A.; et al. Validation of N-Myristoyltransferase as Potential Chemotherapeutic Target in Mammal-Dwelling Stages of Trypanosoma Cruzi. *PLoS Negl. Trop. Dis.* **2016**, *10*, e0004540.
(297) Roberts, A. J.; Fairlamb, A. H. The N-Myristoylome of Trypanosoma Cruzi. *Sci. Rep.* **2016**, *6*, 31078.
(298) Wright, M. H.; Paape, D.; Storck, E. M.; Serwa, R. A.; Smith, D. F.; Tate, E. W. Global Analysis of Protein N-Myristoylation and Exploration of N-Myristoyltransferase as a Drug Target in the Neglected Human Pathogen Leishmania Donovani. *Chem. Biol.* **2015**, *22*, 342–354.
(299) Rackham, M. D.; Yu, Z.; Brannigan, J. A.; Heal, W. P.; Paape, D.; Barker, K. V.; Wilkinson, A. J.; Smith, D. F.; Leatherbarrow, R. J.; Tate, E. W. Discovery of High Affinity Inhibitors of Leishmania Donovani N-Myristoyltransferase. *Medchemcomm* **2015**, *6*, 1761–1766.
(300) Corpas-Lopez, V.; Moniz, S.; Thomas, M.; Wall, R. J.; Torrie, L. S.; Zander-Dinse, D.; Tinti, M.; Brand, S.; Stojanovski, L.; Manthri, S.; et al. Pharmacological Validation of N-Myristoyltransferase as a Drug Target in Leishmania Donovani. *ACS Infect. Dis.* **2019**, *5*, 111–122.
(301) Bell, A. S.; Yu, Z.; Hutton, J. A.; Wright, M. H.; Brannigan, J. A.; Paape, D.; Roberts, S. M.; Sutherell, C. L.; Ritzefeld, M.; Wilkinson, A. J.; et al. Novel Thienopyrimidine Inhibitors of Leishmania N-Myristoyltransferase with On-Target Activity in Intracellular Amastigotes. *J. Med. Chem.* **2020**, *63*, 7740–7765.
(302) Broncel, M.; Dominicus, C.; Vigetti, L.; Nofal, S. D.; Bartlett, E. J.; Touquet, B.; Hunt, A.; Wallbank, B. A.; Federico, S.; Matthews, S.; et al. Profiling of Myristoylation in Toxoplasma Gondii Reveals an N-Myristoylated Protein Important for Host Cell Penetration. *Elife* **2020**, *9*, e57861.
(303) Foe, I. T.; Onguka, O.; Amberg-Johnson, K.; Garner, R. M.; Amara, N.; Beatty, W.; Yeh, E.; Bogyo, M. The Toxoplasma Gondii Active Serine Hydrolase 4 Regulates Parasite Division and Intravacuolar Parasite Architecture. *mSphere* **2018**, *3*, e00393-18.
(304) Kemp, L. E.; Rusch, M.; Adibekian, A.; Bullen, H. E.; Graindorge, A.; Freymond, C.; Rottmann, M.; Braun-Breton, C.; Baumeister, S.; Porfetye, A. T.; et al. Characterization of a Serine Hydrolase Targeted by Acyl-Protein Thioesterase Inhibitors in Toxoplasma Gondii . *J. Biol. Chem.* **2013**, *288*, 27002–27018.
(305) Lodge, J. K.; Jackson-Machelski, E.; Toffaletti, D. L.; Perfect, J. R.; Gordon, J. I. Targeted Gene Replacement Demonstrates That Myristoyl-CoA: Protein N-Myristoyltransferase Is Essential for Viability of Cryptococcus Neoformans. *Proc. Natl. Acad. Sci.* **1994**, *91*, 12008 LP – 12012.
(306) Lodge, J. K.; Johnson, R. L.; Weinberg, R. A.; Gordon, J. I. Comparison of Myristoyl-CoA:Protein N-Myristoyltransferases from Three Pathogenic Fungi: Cryptococcus Neoformans, Histoplasma Capsulatum, and Candida Albicans. *J. Biol. Chem.* **1994**, *269*, 2996–3009.
(307) Weinberg, R. A.; McWherter, C. A.; Freeman, S. K.; Wood, D. C.; Gordon, J. I.; Lee, S. C. Genetic Studies Reveal That MyristoylCoA:Protein N-Myristoyltransferase Is an Essential Enzyme in Candida Albicans. *Mol. Microbiol.*

1995, *16*, 241–250.
(308) Fang, W.; Robinson, D. A.; Raimi, O. G.; Blair, D. E.; Harrison, J. R.; Lockhart, D. E. A.; Torrie, L. S.; Ruda, G. F.; Wyatt, P. G.; Gilbert, I. H.; et al. N-Myristoyltransferase Is a Cell Wall Target in Aspergillus Fumigatus. *ACS Chem. Biol.* **2015**, *10*, 1425–1434.
(309) Fedoryshchak, R. O.; Ocasio, C. A.; Strutton, B.; Mattocks, J.; Corran, A. J.; Tate, E. W. Wheat Pathogen Zymoseptoria Tritici N-Myristoyltransferase Inhibitors: On-Target Antifungal Activity and an Unusual Metabolic Defense Mechanism. *RSC Chem. Biol.* **2020**.
(310) Zhu, A. Y.; Zhou, Y.; Khan, S.; Deitsch, K. W.; Hao, Q.; Lin, H. Plasmodium Falciparum Sir2A Preferentially Hydrolyzes Medium and Long Chain Fatty Acyl Lysine. *ACS Chem. Biol.* **2012**, *7*, 155–159.
(311) Charlton, T. M.; Kovacs-Simon, A.; Michell, S. L.; Fairweather, N. F.; Tate, E. W. Quantitative Lipoproteomics in Clostridium Difficile Reveals a Role for Lipoproteins in Sporulation. *Chem. Biol.* **2015**, *22*, 1562–1573.
(312) Nimchuk, Z.; Marois, E.; Kjemtrup, S.; Leister, R. T.; Katagiri, F.; Dangl, J. L. Eukaryotic Fatty Acylation Drives Plasma Membrane Targeting and Enhances Function of Several Type III Effector Proteins from Pseudomonas Syringae. *Cell* **2000**, *101*, 353–363.
(313) Boyle, P. C.; Martin, G. B. Greasy Tactics in the Plant–Pathogen Molecular Arms Race. *J. Exp. Bot.* **2015**, *66*, 1607–1616.
(314) Ribet, D.; Cossart, P. Pathogen-Mediated Posttranslational Modifications: A Re-Emerging Field. *Cell* **2010**, *143*, 694–702.
(315) Burnaevskiy, N.; Fox, T. G.; Plymire, D. A.; Ertelt, J. M.; Weigele, B. A.; Selyunin, A. S.; Way, S. S.; Patrie, S. M.; Alto, N. M. Proteolytic Elimination of N-Myristoyl Modifications by the Shigella Virulence Factor IpaJ. *Nature* **2013**, *496*, 106–109.
(316) Burnaevskiy, N.; Peng, T.; Reddick, L. E.; Hang, H. C.; Alto, N. M. Myristoylome Profiling Reveals a Concerted Mechanism of ARF GTPase Deacylation by the Bacterial Protease IpaJ. *Mol. Cell* **2015**, *58*, 110–122.
(317) Kim, B. S.; Satchell, K. J. F. MARTX Effector Cross Kingdom Activation by Golgi-Associated ADP-Ribosylation Factors. *Cell. Microbiol.* **2016**, *18*, 1078–1093.
(318) Li, H.; Dou, J.; Ding, L.; Spearman, P. Myristoylation Is Required for Human Immunodeficiency Virus Type 1 Gag-Gag Multimerization in Mammalian Cells. *J. Virol.* **2007**, *81*, 12899 LP – 12910.
(319) P, G.; Le Seyec, J.; Rumin, S.; Guguen-Guillouzo, C. Myristylation of the Hepatitis B Virus Large Surface Protein Is Essential for Viral Infectivity. *Virology* **1995**, *213*, 292–299.
(320) MacLean, C. A.; Clark, B.; McGeoch, D. J. Gene UL11 of Herpes Simplex Virus Type 1 Encodes a Virion Protein Which Is Myristylated. *J. Gen. Virol.* **1989**, *70*, 3147–3157.
(321) Ohta, H.; Takamune, N.; Kishimoto, N.; Shoji, S.; Misumi, S. N-Myristoyltransferase 1 Enhances Human Immunodeficiency Virus Replication through Regulation of Viral RNA Expression Level. *Biochem. Biophys. Res. Commun.* **2015**, *463*, 988–993.

(322) Marc, D.; Masson, G.; Girard, M.; van der Werf, S. Lack of Myristoylation of Poliovirus Capsid Polypeptide VP0 Prevents the Formation of Virions or Results in the Assembly of Noninfectious Virus Particles. *J. Virol.* **1990**, *64*, 4099–4107.
(323) Corbic Ramljak, I.; Stanger, J.; Real-Hohn, A.; Dreier, D.; Wimmer, L.; Redlberger-Fritz, M.; Fischl, W.; Klingel, K.; Mihovilovic, M. D.; Blaas, D.; et al. Cellular N-Myristoyltransferases Play a Crucial Picornavirus Genus-Specific Role in Viral Assembly, Virion Maturation, and Infectivity. *PLoS Pathog.* **2018**, *14*, e1007203–e1007203.
(324) Mousnier, A.; Bell, A. S.; Swieboda, D. P.; Morales-Sanfrutos, J.; Pérez-Dorado, I.; Brannigan, J. A.; Newman, J.; Ritzefeld, M.; Hutton, J. A.; Guedán, A.; et al. Fragment-Derived Inhibitors of Human N-Myristoyltransferase Block Capsid Assembly and Replication of the Common Cold Virus. *Nat. Chem.* **2018**, *10*, 599–606.
(325) Bell, A. S.; Mills, J. E.; Williams, G. P.; Brannigan, J. A.; Wilkinson, A. J.; Parkinson, T.; Leatherbarrow, R. J.; Tate, E. W.; Holder, A. A.; Smith, D. F. Selective Inhibitors of Protozoan Protein N-Myristoyltransferases as Starting Points for Tropical Disease Medicinal Chemistry Programs. *PLoS Negl. Trop. Dis.* **2012**, *6*, e1625–e1625.
(326) Casey, P. J.; Solski, P. A.; Der, C. J.; Buss, J. E. P21ras Is Modified by a Farnesyl Isoprenoid. *Proc. Natl. Acad. Sci. U. S. A.* **1989**, *86*, 8323–8327.
(327) Casey, P. J.; Thissen, J. A.; Moomaw, J. F. Enzymatic Modification of Proteins with a Geranylgeranyl Isoprenoid. *Proc. Natl. Acad. Sci. U. S. A.* **1991**, *88*, 8631–8635.
(328) Kinsella, B. T.; Maltese, W. A. Rab GTP-Binding Proteins with Three Different Carboxyl-Terminal Cysteine Motifs Are Modified in Vivo by 20-Carbon Isoprenoids. *J. Biol. Chem.* **1992**, *267*, 3940–3945.
(329) London, N.; Lamphear, C. L.; Hougland, J. L.; Fierke, C. A.; Schueler-Furman, O. Identification of a Novel Class of Farnesylation Targets by Structure-Based Modeling of Binding Specificity. *PLOS Comput. Biol.* **2011**, *7*, e1002170.
(330) Wang, Y.-C.; Dozier, J. K.; Beese, L. S.; Distefano, M. D. Rapid Analysis of Protein Farnesyltransferase Substrate Specificity Using Peptide Libraries and Isoprenoid Diphosphate Analogues. *ACS Chem. Biol.* **2014**, *9*, 1726–1735.
(331) Berger, B. M.; Kim, J. H.; Hildebrandt, E. R.; Davis, I. C.; Morgan, M. C.; Hougland, J. L.; Schmidt, W. K. Protein Isoprenylation in Yeast Targets COOH-Terminal Sequences Not Adhering to the CaaX Consensus. *Genetics* **2018**, *210*, 1301 LP – 1316.
(332) Krzysiak, A. J.; Rawat, D. S.; Scott, S. A.; Pais, J. E.; Handley, M.; Harrison, M. L.; Fierke, C. A.; Gibbs, R. A. Combinatorial Modulation of Protein Prenylation. *ACS Chem. Biol.* **2007**, *2*, 385–389.
(333) Zhang, Y.; Blanden, M. J.; Sudheer, C.; Gangopadhyay, S. A.; Rashidian, M.; Hougland, J. L.; Distefano, M. D. Simultaneous Site-Specific Dual Protein Labeling Using Protein Prenyltransferases. *Bioconjug. Chem.* **2015**, *26*, 2542–2553.
(334) Hovlid, M. L.; Edelstein, R. L.; Henry, O.; Ochocki, J.; DeGraw, A.; Lenevich, S.; Talbot, T.; Young, V. G.; Hruza, A. W.; Lopez-Gallego, F.; et al. Synthesis, Properties, and Applications of Diazotrifluropropanoyl-Containing Photoactive

Analogs of Farnesyl Diphosphate Containing Modified Linkages for Enhanced Stability. *Chem. Biol. Drug Des.* **2010**, *75*, 51–67.
(335) Kyro, K.; Manandhar, S. P.; Mullen, D.; Schmidt, W. K.; Distefano, M. D. Photoaffinity Labeling of Ras Converting Enzyme Using Peptide Substrates That Incorporate Benzoylphenylalanine (Bpa) Residues: Improved Labeling and Structural Implications. *Bioorg. Med. Chem.* **2011**, *19*, 7559–7569.
(336) Vervacke, J. S.; Funk, A. L.; Wang, Y.-C.; Strom, M.; Hrycyna, C. A.; Distefano, M. D. Diazirine-Containing Photoactivatable Isoprenoid: Synthesis and Application in Studies with Isoprenylcysteine Carboxyl Methyltransferase. *J. Org. Chem.* **2014**, *79*, 1971–1978.
(337) Davies, B. S. J.; Yang, S. H.; Farber, E.; Lee, R.; Buck, S. B.; Andres, D. A.; Spielmann, H. P.; Agnew, B. J.; Tamanoi, F.; Fong, L. G.; et al. Increasing the Length of Progerin's Isoprenyl Anchor Does Not Worsen Bone Disease or Survival in Mice with Hutchinson-Gilford Progeria Syndrome. *J. Lipid Res.* **2009**, *50*, 126–134.
(338) Onono, F. O.; Morgan, M. A.; Spielmann, H. P.; Andres, D. A.; Subramanian, T.; Ganser, A.; Reuter, C. W. M. A Tagging-via-Substrate Approach to Detect the Farnesylated Proteome Using Two-Dimensional Electrophoresis Coupled with Western Blotting. *Mol. Cell. Proteomics* **2010**, *9*, 742–751.
(339) Nguyen, U. T. T.; Guo, Z.; Delon, C.; Wu, Y.; Deraeve, C.; Fränzel, B.; Bon, R. S.; Blankenfeldt, W.; Goody, R. S.; Waldmann, H.; et al. Analysis of the Eukaryotic Prenylome by Isoprenoid Affinity Tagging. *Nat. Chem. Biol.* **2009**, *5*, 227–235.
(340) Hougland, J. L.; Fierke, C. A. Getting a Handle on Protein Prenylation. *Nat. Chem. Biol.* **2009**, *5*, 197–198.
(341) Ali, N.; Jurczyluk, J.; Shay, G.; Tnimov, Z.; Alexandrov, K.; Munoz, M. A.; Skinner, O. P.; Pavlos, N. J.; Rogers, M. J. A Highly Sensitive Prenylation Assay Reveals in Vivo Effects of Bisphosphonate Drug on the Rab Prenylome of Macrophages Outside the Skeleton. *Small GTPases* **2015**, *6*, 202–211.
(342) Kho, Y.; Kim, S. C.; Jiang, C.; Barma, D.; Kwon, S. W.; Cheng, J.; Jaunbergs, J.; Weinbaum, C.; Tamanoi, F.; Falck, J.; et al. A Tagging-via-Substrate Technology for Detection and Proteomics of Farnesylated Proteins. *Proc. Natl. Acad. Sci. U. S. A.* **2004**, *101*, 12479–12484.
(343) Rose, M. W.; Xu, J.; Kale, T. A.; O'Doherty, G.; Barany, G.; Distefano, M. D. Enzymatic Incorporation of Orthogonally Reactive Prenylazide Groups into Peptides Using Geranylazide Diphosphate via Protein Farnesyltransferase: Implications for Selective Protein Labeling. *Pept. Sci.* **2005**, *80*, 164–171.
(344) Labadie, G. R.; Viswanathan, R.; Poulter, C. D. Farnesyl Diphosphate Analogues with ω-Bioorthogonal Azide and Alkyne Functional Groups for Protein Farnesyl Transferase-Catalyzed Ligation Reactions. *J. Org. Chem.* **2007**, *72*, 9291–9297.
(345) Hosokawa, A.; Wollack, J. W.; Zhang, Z.; Chen, L.; Barany, G.; Distefano, M. D. Evaluation of an Alkyne-Containing Analogue of Farnesyl Diphosphate as a Dual Substrate for Protein-Prenyltransferases. *Int. J. Pept. Res. Ther.* **2007**, *13*, 345–354.
(346) Crick, D. C.; Andres, D. A.; Waechter, C. J. Farnesol Is Utilized for Protein Isoprenylation and the Biosynthesis of Cholesterol in Mammalian Cells. *Biochem.*

Biophys. Res. Commun. **1995**, *211*, 590–599.
(347) Bentinger, M.; Grünler, J.; Peterson, E.; Swiezewska, E.; Dallner, G. Phosphorylation of Farnesol in Rat Liver Microsomes: Properties of Farnesol Kinase and Farnesyl Phosphate Kinase. *Arch. Biochem. Biophys.* **1998**, *353*, 191–198.
(348) Meigs, T. E.; Simoni, R. D. Farnesol as a Regulator of HMG-CoA Reductase Degradation: Characterization and Role of Farnesyl Pyrophosphatase. *Arch. Biochem. Biophys.* **1997**, *345*, 1–9.
(349) Rizzo, W. B. Fatty Aldehyde and Fatty Alcohol Metabolism: Review and Importance for Epidermal Structure and Function. *Biochim. Biophys. Acta* **2014**, *1841*, 377–389.
(350) Rose, M. W.; Rose, N. D.; Boggs, J.; Lenevich, S.; Xu, J.; Barany, G.; Distefano, M. D. Evaluation of Geranylazide and Farnesylazide Diphosphate for Incorporation of Prenylazides into a CAAX Box-Containing Peptide Using Protein Farnesyltransferase. *J. Pept. Res.* **2005**, *65*, 529–537.
(351) Chan, L. N.; Hart, C.; Guo, L.; Nyberg, T.; Davies, B. S. J.; Fong, L. G.; Young, S. G.; Agnew, B. J.; Tamanoi, F. A Novel Approach to Tag and Identify Geranylgeranylated Proteins. *Electrophoresis* **2009**, *30*, 3598–3606.
(352) Berry, A. F. H.; Heal, W. P.; Tarafder, A. K.; Tolmachova, T.; Baron, R. A.; Seabra, M. C.; Tate, E. W. Rapid Multilabel Detection of Geranylgeranylated Proteins by Using Bioorthogonal Ligation Chemistry. *ChemBioChem* **2010**, *11*, 771–773.
(353) DeGraw, A. J.; Palsuledesai, C.; Ochocki, J. D.; Dozier, J. K.; Lenevich, S.; Rashidian, M.; Distefano, M. D. Evaluation of Alkyne-Modified Isoprenoids as Chemical Reporters of Protein Prenylation. *Chem. Biol. Drug Des.* **2010**, *76*, 460–471.
(354) Placzek, A. T.; Gibbs, R. A. New Synthetic Methodology for the Construction of 7-Substituted Farnesyl Diphosphate Analogs. *Org. Lett.* **2011**, *13*, 3576–3579.
(355) Jennings, B. C.; Danowitz, A. M.; Wang, Y.-C.; Gibbs, R. A.; Distefano, M. D.; Fierke, C. A. Analogs of Farnesyl Diphosphate Alter CaaX Substrate Specificity and Reactions Rates of Protein Farnesyltransferase. *Bioorg. Med. Chem. Lett.* **2016**, *26*, 1333–1336.
(356) Goldstein, J. L.; Brown, M. S. Regulation of the Mevalonate Pathway. *Nature* **1990**, *343*, 425.
(357) Ahmadi, M.; Suazo, K. F.; Distefano, M. D. Optimization of Metabolic Labeling with Alkyne-Containing Isoprenoid Probes BT - Protein Lipidation: Methods and Protocols; Linder, M. E., Ed.; Springer New York: New York, NY, 2019; pp 35–43.
(358) Suazo, K. F.; Hurben, A. K.; Liu, K.; Xu, F.; Thao, P.; Sudheer, C.; Li, L.; Distefano, M. Metabolic Labeling of Prenylated Proteins Using Alkyne- Modified Isoprenoid Analogues. *Curr. Protoc. Chem. Biol.* **2018**, *In Press*.
(359) Charron, G.; Tsou, L. K.; Maguire, W.; Yount, J. S.; Hang, H. C. Alkynyl-Farnesol Reporters for Detection of Protein S-Prenylation in Cells. *Mol. Biosyst.* **2011**, *7*, 67–73.
(360) Charron, G.; Li, M. M. H.; MacDonald, M. R.; Hang, H. C. Prenylome Profiling Reveals S-Farnesylation Is Crucial for Membrane Targeting and Antiviral Activity

of ZAP Long-Isoform. *Proc. Natl. Acad. Sci.* **2013**, *110*, 11085–11090.
(361) Ochocki, J. D.; Distefano, M. D. Prenyltransferase Inhibitors: Treating Human Ailments from Cancer to Parasitic Infections. *Med. Chem. Commun.* **2013**, *4*, 476–492.
(362) Nallan, L.; Bauer, K. D.; Bendale, P.; Rivas, K.; Yokoyama, K.; Hornéy, C. P.; Pendyala, P. R.; Floyd, D.; Lombardo, L. J.; Williams, D. K.; et al. Protein Farnesyltransferase Inhibitors Exhibit Potent Antimalarial Activity. *J. Med. Chem.* **2005**, *48*, 3704–3713.
(363) Suazo, K. F.; Schaber, C.; Palsuledesai, C. C.; Odom John, A. R.; Distefano, M. D. Global Proteomic Analysis of Prenylated Proteins in Plasmodium Falciparum Using an Alkyne-Modified Isoprenoid Analogue. *Sci. Rep.* **2016**, *6*, 38615.
(364) Mathews, E. S.; Jezewski, A. J.; Odom John, A. R. Protein Prenylation and Hsp40 in Thermotolerance of Plasmodium Falciparum Malaria Parasites. *bioRxiv* **2019**, 842468.
(365) Gisselberg, J. E.; Zhang, L.; Elias, J. E.; Yeh, E. The Prenylated Proteome of Plasmodium Falciparum Reveals Pathogen-Specific Prenylation Activity and Drug Mechanism-of-Action. *Mol. Cell. Proteomics* **2017**, *16*, S54–S64.
(366) Storck, E. M.; Morales-Sanfrutos, J.; Serwa, R. A.; Panyain, N.; Lanyon-Hogg, T.; Tolmachova, T.; Ventimiglia, L. N.; Martin-Serrano, J.; Seabra, M. C.; Wojciak-Stothard, B.; et al. Dual Chemical Probes Enable Quantitative System-Wide Analysis of Protein Prenylation and Prenylation Dynamics. *Nat. Chem.* **2019**, *11*, 552–561.
(367) Seabra, M. C.; Brown, M. S.; Goldstein, J. L. Retinal Degeneration in Choroideremia: Deficiency of Rab Geranylgeranyl Transferase. *Science (80-.).* **1993**, *259*, 377 LP – 381.
(368) Suazo, K. F.; Jeong, A.; Ahmadi, M.; Brown, C.; Qu, W.; Li, L.; Distefano, M. D. Metabolic Labeling with an Alkyne Probe Reveals Similarities and Differences in the Prenylomes of Several Brain-Derived Cell Lines and Primary Cells. *Sci. Rep.* **2021**, *11*, 4367.
(369) Qu, W.; Suazo, K. F.; Liu, W.; Cheng, S.; Jeong, A.; Hottman, D.; Yuan, L.-L.; Distefano, M. D.; Li, L. Neuronal Protein Farnesylation Regulates Hippocampal Synaptic Plasticity and Cognitive Function. *Mol. Neurobiol.* **2020**.
(370) Palsuledesai, C. C.; Ochocki, J. D.; Markowski, T. W.; Distefano, M. D. A Combination of Metabolic Labeling and 2D-DIGE Analysis in Response to a Farnesyltransferase Inhibitor Facilitates the Discovery of New Prenylated Proteins. *Mol. Biosyst.* **2014**, *10*, 1094–1103.
(371) Berg, T. J.; Gastonguay, A. J.; Lorimer, E. L.; Kuhnmuench, J. R.; Li, R.; Fields, A. P.; Williams, C. L. Splice Variants of SmgGDS Control Small GTPase Prenylation and Membrane Localization. *J. Biol. Chem.* **2010**, *285*, 35255–35266.
(372) Schuld, N. J.; Vervacke, J. S.; Lorimer, E. L.; Simon, N. C.; Hauser, A. D.; Barbieri, J. T.; Distefano, M. D.; Williams, C. L. The Chaperone Protein SmgGDS Interacts with Small GTPases Entering the Prenylation Pathway by Recognizing the Last Amino Acid in the CAAX Motif. *J. Biol. Chem.* **2014**, *289*, 6862–6876.
(373) Brandt, A. C.; McNally, L.; Lorimer, E. L.; Unger, B.; Koehn, O. J.; Suazo, K. F.; Rein, L.; Szabo, A.; Tsaih, S.-W.; Distefano, M. D.; et al. Splice Switching an Oncogenic Ratio of SmgGDS Isoforms as a Strategy to Diminish Malignancy.

Proc. Natl. Acad. Sci. **2020**, *117*, 3627 LP – 3636.
(374) ten Klooster, J. P.; Hordijk, P. L. Targeting and Localized Signalling by Small GTPases. *Biol. Cell* **2007**, *99*, 1–12.
(375) Akula, M. K.; Ibrahim, M. X.; Ivarsson, E. G.; Khan, O. M.; Kumar, I. T.; Erlandsson, M.; Karlsson, C.; Xu, X.; Brisslert, M.; Brakebusch, C.; et al. Protein Prenylation Restrains Innate Immunity by Inhibiting Rac1 Effector Interactions. *Nat. Commun.* **2019**, *10*, 3975.
(376) Kang, R.; Wan, J.; Arstikaitis, P.; Takahashi, H.; Huang, K.; Bailey, A. O.; Thompson, J. X.; Roth, A. F.; Drisdel, R. C.; Mastro, R.; et al. Neural Palmitoyl-Proteomics Reveals Dynamic Synaptic Palmitoylation. *Nature* **2008**, *456*, 904–909.
(377) Nishimura, A.; Linder, M. E. Identification of a Novel Prenyl and Palmitoyl Modification at the CaaX Motif of Cdc42 That Regulates RhoGDI Binding. *Mol. Cell. Biol.* **2013**, *33*, 1417 LP – 1429.
(378) Wilkins, J. A.; Kaasik, K.; Chalkley, R. J.; Burlingame, A. L. Characterization of Prenylated C-Terminal Peptides Using a Thiopropyl-Based Capture Technique and LC-MS/MS. *Mol. Cell. Proteomics* **2020**, *19*, 1005 LP – 1016.
(379) Palsuledesai, C. C.; Ochocki, J. D.; Kuhns, M. M.; Wang, Y.-C.; Warmka, J. K.; Chernick, D. S.; Wattenberg, E. V; Li, L.; Arriaga, E. A.; Distefano, M. D. Metabolic Labeling with an Alkyne-Modified Isoprenoid Analog Facilitates Imaging and Quantification of the Prenylome in Cells. *ACS Chem. Biol.* **2016**, *11*, 2820–2828.
(380) Diaz-Rodriguez, V.; Hsu, E.-T.; Ganusova, E.; Werst, E. R.; Becker, J. M.; Hrycyna, C. A.; Distefano, M. D. A-Factor Analogues Containing Alkyne- and Azide-Functionalized Isoprenoids Are Efficiently Enzymatically Processed and Retain Wild-Type Bioactivity. *Bioconjug. Chem.* **2018**, *29*, 316–323.
(381) Gaebler, A.; Penno, A.; Kuerschner, L.; Thiele, C. A Highly Sensitive Protocol for Microscopy of Alkyne Lipids and Fluorescently Tagged or Immunostained Proteins. *J. Lipid Res.* **2016**, *57*, 1934–1947.
(382) Scott-Solomon, E.; Kuruvilla, R. Prenylation of Axonally Translated Rac1 Controls NGF-Dependent Axon Growth. *Dev. Cell* **2020**, *53*, 691–705.
(383) Shirakawa, R.; Goto-Ito, S.; Goto, K.; Wakayama, S.; Kubo, H.; Sakata, N.; Trinh, D. A.; Yamagata, A.; Sato, Y.; Masumoto, H.; et al. A SNARE Geranylgeranyltransferase Essential for the Organization of the Golgi Apparatus. *EMBO J.* e104120.
(384) Moudgil, D. K.; Westcott, N.; Famulski, J. K.; Patel, K.; Macdonald, D.; Hang, H.; Chan, G. K. T. A Novel Role of Farnesylation in Targeting a Mitotic Checkpoint Protein, Human Spindly, to Kinetochores. *J. Cell Biol.* **2015**, *208*, 881–896.
(385) Silva, P. M. A.; Delgado, M. L.; Ribeiro, N.; Florindo, C.; Tavares, Á. A.; Ribeiro, D.; Lopes, C.; do Amaral, B.; Bousbaa, H.; Monteiro, L. S. Spindly and Bub3 Expression in Oral Cancer: Prognostic and Therapeutic Implications. *Oral Dis.* **2019**, *25*, 1291–1301.
(386) Ivanov, S. S.; Charron, G.; Hang, H. C.; Roy, C. R. Lipidation by the Host Prenyltransferase Machinery Facilitates Membrane Localization of Legionella Pneumophila Effector Proteins. *J. Biol. Chem.* **2010**, *285*, 34686–34698.
(387) Reinicke, A. T.; Hutchinson, J. L.; Magee, A. I.; Mastroeni, P.; Trowsdale, J.;

Kelly, A. P. A Salmonella Typhimurium Effector Protein SifA Is Modified by Host Cell Prenylation and S-Acylation Machinery. *J. Biol. Chem.* **2005**, *280*, 14620–14627.
(388) DeMar, J. C.; Anderson, R. E. Identification and Quantitation of the Fatty Acids Composing the CoA Ester Pool of Bovine Retina, Heart, and Liver. *J. Biol. Chem.* **1997**, *272*, 31362–31368.
(389) Fujimoto, T.; Stroud, E.; Whatley, R. E.; Prescott, S. M.; Muszbek, L.; Laposata, M.; McEver, R. P. P-Selectin Is Acylated with Palmitic Acid and Stearic Acid at Cysteine 766 through a Thioester Linkage. *J. Biol. Chem.* **1993**, *268*, 11394–11400.
(390) Zeng, F.-Y.; Kaphalia, B. S.; Ansari, G. A. S.; Weigel, P. H. Fatty Acylation of the Rat Asialoglycoprotein Receptor: The Three Subunits From Active Receptors Contain Covalently Bound Palmitate and Stearate. *J. Biol. Chem.* **1995**, *270*, 21382–21387.
(391) Liang, X.; Lu, Y.; Neubert, T. A.; Resh, M. D. Mass Spectrometric Analysis of GAP-43/Neuromodulin Reveals the Presence of a Variety of Fatty Acylated Species. *J. Biol. Chem.* **2002**, *277*, 33032–33040.
(392) Kordyukova, L. V; Serebryakova, M. V; Baratova, L. A.; Veit, M. Site-Specific Attachment of Palmitate or Stearate to Cytoplasmic versus Transmembrane Cysteines Is a Common Feature of Viral Spike Proteins. *Virology* **2010**, *398*, 49–56.
(393) Wang, M.; Ludwig, K.; Böttcher, C.; Veit, M. The Role of Stearate Attachment to the Hemagglutinin-Esterase-Fusion Glycoprotein HEF of Influenza C Virus. *Cell. Microbiol.* **2016**, *18*, 692–704.
(394) Alvarez, E.; Gironès, N.; Davis, R. J. Inhibition of the Receptor-Mediated Endocytosis of Diferric Transferrin Is Associated with the Covalent Modification of the Transferrin Receptor with Palmitic Acid. *J. Biol. Chem.* **1990**, *265*, 16644–16655.
(395) Senyilmaz, D.; Virtue, S.; Xu, X.; Tan, C. Y.; Griffin, J. L.; Miller, A. K.; Vidal-Puig, A.; Teleman, A. A. Regulation of Mitochondrial Morphology and Function by Stearoylation of TFR1. *Nature* **2015**, *525*, 124–128.
(396) Senyilmaz-Tiebe, D.; Pfaff, D. H.; Virtue, S.; Schwarz, K. V; Fleming, T.; Altamura, S.; Muckenthaler, M. U.; Okun, J. G.; Vidal-Puig, A.; Nawroth, P.; et al. Dietary Stearic Acid Regulates Mitochondria in Vivo in Humans. *Nat. Commun.* **2018**, *9*, 3129.
(397) Chen, B.; Niu, J.; Kreuzer, J.; Zheng, B.; Jarugumilli, G. K.; Haas, W.; Wu, X. Auto-Fatty Acylation of Transcription Factor RFX3 Regulates Ciliogenesis. *Proc. Natl. Acad. Sci.* **2018**, *115*, E8403 LP-E8412.
(398) Liu, W.; Zhou, Y.; Peng, T.; Zhou, P.; Ding, X.; Li, Z.; Zhong, H.; Xu, Y.; Chen, S.; Hang, H. C.; et al. Nε-Fatty Acylation of Multiple Membrane-Associated Proteins by Shigella IcsB Effector to Modulate Host Function. *Nat. Microbiol.* **2018**, *3*, 996–1009.
(399) Zhou, Y.; Huang, C.; Yin, L.; Wan, M.; Wang, X.; Li, L.; Liu, Y.; Wang, Z.; Fu, P.; Zhang, N.; et al. Nε-Fatty Acylation of Rho GTPases by a MARTX Toxin Effector. *Science (80-.).* **2017**, *358*, 528 LP – 531.
(400) Parisi, L. R.; Li, N.; Atilla-Gokcumen, G. E. Very Long Chain Fatty Acids Are

Functionally Involved in Necroptosis. *Cell Chem. Biol.* **2017**, *24*, 1445-1454.e8.
(401) Parisi, L. R.; Sowlati-Hashjin, S.; Berhane, I. A.; Galster, S. L.; Carter, K. A.; Lovell, J. F.; Chemler, S. R.; Karttunen, M.; Atilla-Gokcumen, G. E. Membrane Disruption by Very Long Chain Fatty Acids during Necroptosis. *ACS Chem. Biol.* **2019**, *14*, 2286–2294.
(402) Rivera-Chávez, F.; Zhang, L. F.; Faber, F.; Lopez, C. A.; Byndloss, M. X.; Olsan, E. E.; Xu, G.; Velazquez, E. M.; Lebrilla, C. B.; Winter, S. E.; et al. Depletion of Butyrate-Producing Clostridia from the Gut Microbiota Drives an Aerobic Luminal Expansion of Salmonella. *Cell Host Microbe* **2016**, *19*, 443–454.
(403) Zhang, Z. J.; Pedicord, V. A.; Peng, T.; Hang, H. C. Site-Specific Acylation of a Bacterial Virulence Regulator Attenuates Infection. *Nat. Chem. Biol.* **2020**, *16*, 95–103.
(404) Ali, I.; Conrad, R. J.; Verdin, E.; Ott, M. Lysine Acetylation Goes Global: From Epigenetics to Metabolism and Therapeutics. *Chem. Rev.* **2018**, *118*, 1216–1252.
(405) Yang, C.; Mi, J.; Feng, Y.; Ngo, L.; Gao, T.; Yan, L.; Zheng, Y. G. Labeling Lysine Acetyltransferase Substrates with Engineered Enzymes and Functionalized Cofactor Surrogates. *J. Am. Chem. Soc.* **2013**, *135*, 7791–7794.
(406) Yu-Ying, Y.; Markus, G.; Howard, H. C. Identification of Lysine Acetyltransferase P300 Substrates Using 4-Pentynoyl-Coenzyme A and Bioorthogonal Proteomics. *Bioorg. Med. Chem. Lett.* **2011**, *21*, 4976–4979.
(407) Han, Z.; Chou, C.; Yang, X.; Bartlett, M. G.; Zheng, Y. G. Profiling Cellular Substrates of Lysine Acetyltransferases GCN5 and P300 with Orthogonal Labeling and Click Chemistry. *ACS Chem. Biol.* **2017**, *12*, 1547–1555.
(408) Heppner, K. M.; Tong, J.; Kirchner, H.; Nass, R.; Tschöp, M. H. The Ghrelin O-Acyltransferase–Ghrelin System: A Novel Regulator of Glucose Metabolism. *Curr. Opin. Endocrinol. Diabetes Obes.* **2011**, *18*.
(409) Hougland, J. L. Ghrelin Octanoylation by Ghrelin O-Acyltransferase: Unique Protein Biochemistry Underlying Metabolic Signaling. *Biochem. Soc. Trans.* **2019**, *47*, 169–178.
(410) Cleverdon, E. R.; McGovern-Gooch, K. R.; Hougland, J. L. The Octanoylated Energy Regulating Hormone Ghrelin: An Expanded View of Ghrelin's Biological Interactions and Avenues for Controlling Ghrelin Signaling. *Mol. Membr. Biol.* **2016**, *33*, 111–124.
(411) Garner, A. L.; Janda, K. D. Cat-ELCCA: A Robust Method To Monitor the Fatty Acid Acyltransferase Activity of Ghrelin O-Acyltransferase (GOAT). *Angew. Chemie Int. Ed.* **2010**, *49*, 9630–9634.
(412) Garner, A. L.; Janda, K. D. A Small Molecule Antagonist of Ghrelin O-Acyltransferase (GOAT). *Chem. Commun.* **2011**, *47*, 7512–7514.
(413) Ibrahim Abdalla, M. M. Ghrelin - Physiological Functions and Regulation. *Eur. Endocrinol.* **2015**, *11*, 90–95.
(414) Eubanks, L. M.; Stowe, G. N.; De Lamo Marin, S.; Mayorov, A. V; Hixon, M. S.; Janda, K. D. Identification of A2 Macroglobulin as a Major Serum Ghrelin Esterase. *Angew. Chemie Int. Ed.* **2011**, *50*, 10699–10702.
(415) Liang, X.; Nazarian, A.; Erdjument-Bromage, H.; Bornmann, W.; Tempst, P.; Resh, M. D. Heterogeneous Fatty Acylation of Src Family Kinases with Polyunsaturated Fatty Acids Regulates Raft Localization and Signal Transduction.

J. Biol. Chem. **2001**, *276*, 30987–30994.
(416) Takada, R.; Satomi, Y.; Kurata, T.; Ueno, N.; Norioka, S.; Kondoh, H.; Takao, T.; Takada, S. Monounsaturated Fatty Acid Modification of Wnt Protein: Its Role in Wnt Secretion. *Dev. Cell* **2006**, *11*, 791–801.
(417) Flock, M. R.; Kris-Etherton, P. M. Diverse Physiological Effects of Long-Chain Saturated Fatty Acids: Implications for Cardiovascular Disease. *Curr. Opin. Clin. Nutr. Metab. Care* **2013**, *16*.
(418) Mikels, A. J.; Nusse, R. Wnts as Ligands: Processing, Secretion and Reception. *Oncogene* **2006**, *25*, 7461–7468.
(419) Ching, W.; Hang, H. C.; Nusse, R. Lipid-Independent Secretion of a Drosophila Wnt Protein. *J. Biol. Chem.* **2008**, *283*, 17092–17098.
(420) Miranda, M.; Galli, L. M.; Enriquez, M.; Szabo, L. A.; Gao, X.; Hannoush, R. N.; Burrus, L. W. Identification of the WNT1 Residues Required for Palmitoylation by Porcupine. *FEBS Lett.* **2014**, *588*, 4815–4824.
(421) Tuladhar, R.; Yarravarapu, N.; Ma, Y.; Zhang, C.; Herbert, J.; Kim, J.; Chen, C.; Lum, L. Stereoselective Fatty Acylation Is Essential for the Release of Lipidated WNT Proteins from the Acyltransferase Porcupine (PORCN). *J. Biol. Chem.* **2019**.
(422) Schey, K. L.; Gutierrez, D. B.; Wang, Z.; Wei, J.; Grey, A. C. Novel Fatty Acid Acylation of Lens Integral Membrane Protein Aquaporin-0. *Biochemistry* **2010**, *49*, 9858–9865.
(423) Montigny, C.; Decottignies, P.; Le Maréchal, P.; Capy, P.; Bublitz, M.; Olesen, C.; Møller, J. V.; Nissen, P.; le Maire, M. S-Palmitoylation and S-Oleoylation of Rabbit and Pig Sarcolipin. *J. Biol. Chem.* **2014**, *289*, 33850–33861.
(424) Gaebler, A.; Milan, R.; Straub, L.; Hoelper, D.; Kuerschner, L.; Thiele, C. Alkyne Lipids as Substrates for Click Chemistry-Based in Vitro Enzymatic Assays. *J. Lipid Res.* **2013**, *54*, 2282–2290.
(425) Thinon, E.; Percher, A.; Hang, H. C. Bioorthogonal Chemical Reporters for Monitoring Unsaturated Fatty-Acylated Proteins. *ChemBioChem* **2016**, *17*, 1800–1803.
(426) Muszbek, L.; Laposata, M. Covalent Modification of Proteins by Arachidonate and Eicosapentaenoate in Platelets. *J. Biol. Chem.* **1993**, *268*, 18243–18248.
(427) Hallak, H.; Muszbek, L.; Laposata, M.; Belmonte, E.; Brass, L. F.; Manning, D. R. Covalent Binding of Arachidonate to G Protein Alpha Subunits of Human Platelets. *J. Biol. Chem.* **1994**, *269*, 4713–4716.
(428) Puca, A. A.; Andrew, P.; Novelli, V.; Anselmi, C. V.; Somalvico, F.; Cirillo, N. A.; Chatgilialoglu, C.; Ferreri, C. Fatty Acid Profile of Erythrocyte Membranes As Possible Biomarker of Longevity. *Rejuvenation Res.* **2007**, *11*, 63–72.
(429) Refsgaard, H. H. F.; Tsai, L.; Stadtman, E. R. Modifications of Proteins by Polyunsaturated Fatty Acid Peroxidation Products. *Proc. Natl. Acad. Sci.* **2000**, *97*, 611 LP – 616.
(430) Beavers, W. N.; Serwa, R.; Shimozu, Y.; Tallman, K. A.; Vaught, M.; Dalvie, E. D.; Marnett, L. J.; Porter, N. A. ω-Alkynyl Lipid Surrogates for Polyunsaturated Fatty Acids: Free Radical and Enzymatic Oxidations. *J. Am. Chem. Soc.* **2014**, *136*, 11529–11539.
(431) Beavers, W. N.; Rose, K. L.; Galligan, J. J.; Mitchener, M. M.; Rouzer, C. A.;

Tallman, K. A.; Lamberson, C. R.; Wang, X.; Hill, S.; Ivanova, P. T.; et al. Protein Modification by Endogenously Generated Lipid Electrophiles: Mitochondria as the Source and Target. *ACS Chem. Biol.* **2017**, *12*, 2062–2069.

(432) Isobe, Y.; Kawashima, Y.; Ishihara, T.; Watanabe, K.; Ohara, O.; Arita, M. Identification of Protein Targets of 12/15-Lipoxygenase-Derived Lipid Electrophiles in Mouse Peritoneal Macrophages Using Omega-Alkynyl Fatty Acid. *ACS Chem. Biol.* **2018**, *13*, 887–893.

(433) Robichaud, P. P.; Poirier, S. J.; Boudreau, L. H.; Doiron, J. A.; Barnett, D. A.; Boilard, E.; Surette, M. E. On the Cellular Metabolism of the Click Chemistry Probe 19-Alkyne Arachidonic Acid. *J. Lipid Res.* **2016**, *57*, 1821–1830.

(434) Schopfer, F. J.; Cipollina, C.; Freeman, B. A. Formation and Signaling Actions of Electrophilic Lipids. *Chem. Rev.* **2011**, *111*, 5997–6021.

(435) Vila, A.; Tallman, K. A.; Jacobs, A. T.; Liebler, D. C.; Porter, N. A.; Marnett, L. J. Identification of Protein Targets of 4-Hydroxynonenal Using Click Chemistry for Ex Vivo Biotinylation of Azido and Alkynyl Derivatives. *Chem. Res. Toxicol.* **2008**, *21*, 432–444.

(436) Galligan, J. J.; Rose, K. L.; Beavers, W. N.; Hill, S.; Tallman, K. A.; Tansey, W. P.; Marnett, L. J. Stable Histone Adduction by 4-Oxo-2-Nonenal: A Potential Link between Oxidative Stress and Epigenetics. *J. Am. Chem. Soc.* **2014**, *136*, 11864–11866.

(437) Sun, R.; Fu, L.; Liu, K.; Tian, C.; Yang, Y.; Tallman, K. A.; Porter, N. A.; Liebler, D. C.; Yang, J. Chemoproteomics Reveals Chemical Diversity and Dynamics of 4-Oxo-2-Nonenal Modifications in Cells. *Mol. & Cell. Proteomics* **2017**, *16*, 1789 LP – 1800.

(438) Long, M. J. C.; Parvez, S.; Zhao, Y.; Surya, S. L.; Wang, Y.; Zhang, S.; Aye, Y. Akt3 Is a Privileged First Responder in Isozyme-Specific Electrophile Response. *Nat. Chem. Biol.* **2017**, *13*, 333–338.

(439) Long, M. J. C.; Rogg, C.; Aye, Y. An Oculus to Profile and Probe Target Engagement In Vivo: How T-REX Was Born and Its Evolution into G-REX. *Acc. Chem. Res.* **2020**.

(440) Cui, Y.; Li, X.; Lin, J.; Hao, Q.; Li, X. D. Histone Ketoamide Adduction by 4-Oxo-2-Nonenal Is a Reversible Posttranslational Modification Regulated by Sirt2. *ACS Chem. Biol.* **2017**, *12*, 47–51.

(441) Ullery, J. C.; Marnett, L. J. Protein Modification by Oxidized Phospholipids and Hydrolytically Released Lipid Electrophiles: Investigating Cellular Responses. *Biochim. Biophys. Acta - Biomembr.* **2012**, *1818*, 2424–2435.

(442) Wright, M. H.; Sieber, S. A. Chemical Proteomics Approaches for Identifying the Cellular Targets of Natural Products. *Nat. Prod. Rep.* **2016**, *33*, 681–708.

(443) Mann, R. K.; Beachy, P. A. Novel Lipid Modifications of Secreted Protein Signals. *Annu. Rev. Biochem.* **2004**, *73*, 891–923.

(444) Heretsch, P.; Tzagkaroulaki, L.; Giannis, A. Modulators of the Hedgehog Signaling Pathway. *Bioorg. Med. Chem.* **2010**, *18*, 6613–6624.

(445) Sasai, N.; Toriyama, M.; Kondo, T. Hedgehog Signal and Genetic Disorders. *Front. Genet.* **2019**, *10*, 1103.

(446) Rubin, L. L.; de Sauvage, F. J. Targeting the Hedgehog Pathway in Cancer. *Nat. Rev. Drug Discov.* **2006**, *5*, 1026–1033.

(447) Hall, T. M. T.; Porter, J. A.; Young, K. E.; Koonin, E. V; Beachy, P. A.; Leahy, D. J. Crystal Structure of a Hedgehog Autoprocessing Domain: Homology between Hedgehog and Self-Splicing Proteins. *Cell* **1997**, *91*, 85–97.
(448) Heal, W. P.; Jovanovic, B.; Bessin, S.; Wright, M. H.; Magee, A. I.; Tate, E. W. Bioorthogonal Chemical Tagging of Protein Cholesterylation in Living Cells. *Chem. Commun.* **2011**, *47*, 4081–4083.
(449) Ciepla, P.; Konitsiotis, A. D.; Serwa, R. A.; Masumoto, N.; Leong, W. P.; Dallman, M. J.; Magee, A. I.; Tate, E. W. New Chemical Probes Targeting Cholesterylation of Sonic Hedgehog in Human Cells and Zebrafish. *Chem. Sci.* **2014**, *5*, 4249–4259.
(450) Porter, J. A.; Young, K. E.; Beachy, P. A. Cholesterol Modification of Hedgehog Signaling Proteins in Animal Development. *Science (80-.).* **1996**, *274*, 255 LP – 259.
(451) Byrne, E. F. X.; Sircar, R.; Miller, P. S.; Hedger, G.; Luchetti, G.; Nachtergaele, S.; Tully, M. D.; Mydock-McGrane, L.; Covey, D. F.; Rambo, R. P.; et al. Structural Basis of Smoothened Regulation by Its Extracellular Domains. *Nature* **2016**, *535*, 517–522.
(452) Xiao, X.; Tang, J.-J.; Peng, C.; Wang, Y.; Fu, L.; Qiu, Z.-P.; Xiong, Y.; Yang, L.-F.; Cui, H.-W.; He, X.-L.; et al. Cholesterol Modification of Smoothened Is Required for Hedgehog Signaling. *Mol. Cell* **2017**, *66*, 154-162.e10.
(453) Tukachinsky, H.; Kuzmickas, R. P.; Jao, C. Y.; Liu, J.; Salic, A. Dispatched and Scube Mediate the Efficient Secretion of the Cholesterol-Modified Hedgehog Ligand. *Cell Rep.* **2012**, *2*, 308–320.
(454) Hulce, J. J.; Cognetta, A. B.; Niphakis, M. J.; Tully, S. E.; Cravatt, B. F. Proteome-Wide Mapping of Cholesterol-Interacting Proteins in Mammalian Cells. *Nat. Methods* **2013**, *10*, 259–264.
(455) Porter, N. A.; Xu, L.; Pratt, D. A. Reactive Sterol Electrophiles: Mechanisms of Formation and Reactions with Proteins and Amino Acid Nucleophiles. *Chemistry* . 2020.
(456) Windsor, K.; Genaro-Mattos, T. C.; Kim, H.-Y. H.; Liu, W.; Tallman, K. A.; Miyamoto, S.; Korade, Z.; Porter, N. A. Probing Lipid-Protein Adduction with Alkynyl Surrogates: Application to Smith-Lemli-Opitz Syndrome. *J. Lipid Res.* **2013**, *54*, 2842–2850.
(457) Tallman, K. A.; Kim, H.-Y. H.; Korade, Z.; Genaro-Mattos, T. C.; Wages, P. A.; Liu, W.; Porter, N. A. Probes for Protein Adduction in Cholesterol Biosynthesis Disorders: Alkynyl Lanosterol as a Viable Sterol Precursor. *Redox Biol.* **2017**, *12*, 182–190.
(458) Mayor, S.; Riezman, H. Sorting GPI-Anchored Proteins. *Nat. Rev. Mol. Cell Biol.* **2004**, *5*, 110–120.
(459) Paulick, M. G.; Bertozzi, C. R. The Glycosylphosphatidylinositol Anchor: A Complex Membrane-Anchoring Structure for Proteins. *Biochemistry* **2008**, *47*, 6991–7000.
(460) Poisson, G.; Chauve, C.; Chen, X.; Bergeron, A. FragAnchor: A Large-Scale Predictor of Glycosylphosphatidylinositol Anchors in Eukaryote Protein Sequences by Qualitative Scoring. *Genomics Proteomics Bioinforma.* **2007**, *5*.
(461) Pierleoni, A.; Martelli, P. L.; Casadio, R. PredGPI: A GPI-Anchor Predictor. *BMC*

Bioinformatics **2008**, *9*, 392.
(462) Taylor, D. R.; Hooper, N. M. GPI-Anchored Proteins in Health and Disease BT - Post-Translational Modifications in Health and Disease; Vidal, C. J., Ed.; Springer New York: New York, NY, 2011; pp 39–55.
(463) Paul, K. S.; Jiang, D.; Morita, Y. S.; Englund, P. T. Fatty Acid Synthesis in African Trypanosomes: A Solution to the Myristate Mystery. *Trends Parasitol.* **2001**, *17*, 381–387.
(464) Ferguson, M. A. J.; Hart, G. W.; Kinoshita, T. *Glycosylphosphatidylinositol Anchors*, 3rd ed.; Cold Spring Harbor Laboratory Press, Cold Spring Harbor (NY), 2015.
(465) Vainauskas, S.; Cortes, L. K.; Taron, C. H. In Vivo Incorporation of an Azide-Labeled Sugar Analog to Detect Mammalian Glycosylphosphatidylinositol Molecules Isolated from the Cell Surface. *Carbohydr. Res.* **2012**, *362*, 62–69.
(466) Lu, L.; Gao, J.; Guo, Z. Labeling Cell Surface GPIs and GPI-Anchored Proteins through Metabolic Engineering with Artificial Inositol Derivatives. *Angew. Chemie Int. Ed.* **2015**, *54*, 9679–9682.
(467) Mateos-Gil, P.; Letschert, S.; Doose, S.; Sauer, M. Super-Resolution Imaging of Plasma Membrane Proteins with Click Chemistry. *Front. Cell Dev. Biol.* **2016**, *4*, 98.
(468) Elortza, F.; Mohammed, S.; Bunkenborg, J.; Foster, L. J.; Nuhse, T. S.; Brodbeck, U.; Peck, S. C.; Jensen, O. N. Modification-Specific Proteomics of Plasma Membrane Proteins: Identification and Characterization of Glycosylphosphatidylinositol-Anchored Proteins Released upon Phospholipase D Treatment. *J Proteome Res* **2006**, *5*.
(469) Cortes, L. K.; Vainauskas, S.; Dai, N.; McClung, C. M.; Shah, M.; Benner, J. S.; Corrêa Jr., I. R.; VerBerkmoes, N. C.; Taron, C. H. Proteomic Identification of Mammalian Cell Surface Derived Glycosylphosphatidylinositol-Anchored Proteins through Selective Glycan Enrichment. *Proteomics* **2014**, *14*, 2471–2484.
(470) Swarts, B. M.; Guo, Z. Chemical Synthesis and Functionalization of Clickable Glycosylphosphatidylinositol Anchors. *Chem. Sci.* **2011**, *2*, 2342–2352.
(471) Ding, N.; Li, X.; Chinoy, Z. S.; Boons, G.-J. Synthesis of a Glycosylphosphatidylinositol Anchor Derived from Leishmania Donovani That Can Be Functionalized by Cu-Catalyzed Azide-Alkyne Cycloadditions. *Org. Lett.* **2017**, *19*, 3827–3830.
(472) Feachem, R. G. A.; Phillips, A. A.; Hwang, J.; Cotter, C.; Wielgosz, B.; Greenwood, B. M.; Sabot, O.; Rodriguez, M. H.; Abeyasinghe, R. R.; Ghebreyesus, T. A.; et al. Shrinking the Malaria Map: Progress and Prospects. *Lancet* **2010**, *376*, 1566–1578.
(473) World Health Organization. World Malaria Report 2014. Geneva: WHO; 2014. **2014**.
(474) Ashley, E. A.; Dhorda, M.; Fairhurst, R. M.; Amaratunga, C.; Lim, P.; Suon, S.; Sreng, S.; Anderson, J. M.; Mao, S.; Sam, B.; et al. Spread of Artemisinin Resistance in Plasmodium Falciparum Malaria. *N. Engl. J. Med.* **2014**, *371*, 411–423.
(475) von Seidlein, L.; Dondorp, A. Fighting Fire with Fire: Mass Antimalarial Drug Administrations in an Era of Antimalarial Resistance. *Expert Rev. Anti. Infect.*

Ther. **2015**, *13*, 715–730.
(476) Eastman, R. T.; Buckner, F. S.; Yokoyama, K.; Gelb, M. H.; Van Voorhis, W. C. Fighting Parasitic Disease by Blocking Protein Farnesylation. *J. Lipid Res.* **2006**, *47*, 233–240.
(477) Gelb, M. H.; Van Voorhis, W. C.; Buckner, F. S.; Yokoyama, K.; Eastman, R.; Carpenter, E. P.; Panethymitaki, C.; Brown, K. A.; Smith, D. F. Protein Farnesyl and N-Myristoyl Transferases: Piggy-Back Medicinal Chemistry Targets for the Development of Antitrypanosomatid and Antimalarial Therapeutics. *Mol. Biochem. Parasitol.* **2003**, *126*, 155–163.
(478) Bos, J. L. Ras Oncogenes in Human Cancer: A Review. *Cancer Res.* **1989**, *49*, 4682–4689.
(479) Chakrabarti, D.; Azam, T.; DelVecchio, C.; Qiu, L.; Park, Y.; Allen, C. M. Protein Prenyl Transferase Activities of Plasmodium Falciparum. *Mol. Biochem. Parasitol.* **1998**, *94*, 175–184.
(480) Chakrabarti, D.; Silva, T. Da; Barger, J.; Paquette, S.; Patel, H.; Patterson, S.; Allen, C. M. Protein Farnesyltransferase and Protein Prenylation in Plasmodium Falciparum. *J. Biol. Chem.* **2002**, *277*, 42066–42073.
(481) Howe, R.; Kelly, M.; Jimah, J.; Hodge, D.; Odom, A. R. Isoprenoid Biosynthesis Inhibition Disrupts Rab5 Localization and Food Vacuolar Integrity in Plasmodium Falciparum. *Eukaryot. Cell* **2013**, *12*, 215–223.
(482) Wiesner, J.; Kettler, K.; Sakowski, J.; Ortmann, R.; Katzin, A. M.; Kimura, E. A.; Silber, K.; Klebe, G.; Jomaa, H.; Schlitzer, M. Farnesyltransferase Inhibitors Inhibit the Growth of Malaria Parasites In Vitro and In Vivo. *Angew. Chemie Int. Ed.* **2004**, *43*, 251–254.
(483) Glenn, M. P.; Chang, S.-Y.; Hucke, O.; Verlinde, C. L. M. J.; Rivas, K.; Hornéy, C.; Yokoyama, K.; Buckner, F. S.; Pendyala, P. R.; Chakrabarti, D.; et al. Structurally Simple Farnesyltransferase Inhibitors Arrest the Growth of Malaria Parasites. *Angew. Chemie Int. Ed.* **2005**, *44*, 4903–4906.
(484) Glenn, M. P.; Chang, S.-Y.; Hornéy, C.; Rivas, K.; Yokoyama, K.; Pusateri, E. E.; Fletcher, S.; Cummings, C. G.; Buckner, F. S.; Pendyala, P. R.; et al. Structurally Simple, Potent, Plasmodium Selective Farnesyltransferase Inhibitors That Arrest the Growth of Malaria Parasites. *J. Med. Chem.* **2006**, *49*, 5710–5727.
(485) Buckner, F. S.; Eastman, R. T.; Yokoyama, K.; Gelb, M. H.; Van Voorhis, W. C. Protein Farnesyl Transferase Inhibitors for the Treatment of Malaria and African Trypanosomiasis. *Curr. Opin. Investig. Drugs* **2005**, *6*, 791.
(486) Palsuledesai, C. C.; Ochocki, J. D.; Markowski, T. W.; Distefano, M. D. A Combination of Metabolic Labeling and 2D-DIGE Analysis in Response to a Farnesyltransferase Inhibitor Facilitates the Discovery of New Prenylated Proteins. *Mol. BioSyst.* **2014**, *10*, 1094–1103.
(487) Jomaa, H.; Wiesner, J.; Sanderbrand, S.; Altincicek, B.; Weidemeyer, C.; Hintz, M.; Türbachova, I.; Eberl, M.; Zeidler, J.; Lichtenthaler, H. K.; et al. Inhibitors of the Nonmevalonate Pathway of Isoprenoid Biosynthesis as Antimalarial Drugs. *Science (80-.).* **1999**, *285*, 1573–1576.
(488) Zhang, B.; Watts, K. M.; Hodge, D.; Kemp, L. M.; Hunstad, D. A.; Hicks, L. M.; Odom, A. R. A Second Target of the Antimalarial and Antibacterial Agent Fosmidomycin Revealed by Cellular Metabolic Profiling. *Biochemistry* **2011**, *50*,

3570–3577.
(489) Kakhniashvili, D. G.; Bulla, L. A.; Goodman, S. R. The Human Erythrocyte Proteome: Analysis by Ion Trap Mass Spectrometry . *Mol. Cell. Proteomics* **2004**, *3*, 501–509.
(490) Chiancone, E.; Gilbert, L. M.; Gilbert, G. A.; Kellett, G. L. Dissociation of Hemoglobin into Subunits: II. HUMAN OXYHEMOGLOBIN: GEL FILTRATION STUDIES . *J. Biol. Chem.* **1968**, *243*, 1212–1219.
(491) Artz, J. D.; Wernimont, A. K.; Dunford, J. E.; Schapira, M.; Dong, A.; Zhao, Y.; Lew, J.; Russell, R. G. G.; Ebetino, F. H.; Oppermann, U.; et al. Molecular Characterization of a Novel Geranylgeranyl Pyrophosphate Synthase from Plasmodium Parasites. *J. Biol. Chem.* **2011**, *286*, 3315–3322.
(492) Jordão, F. M.; Gabriel, H. B.; Alves, J. M. P.; Angeli, C. B.; Bifano, T. D.; Breda, A.; de Azevedo, M. F.; Basso, L. A.; Wunderlich, G.; Kimura, E. A.; et al. Cloning and Characterization of Bifunctional Enzyme Farnesyl Diphosphate/Geranylgeranyl Diphosphate Synthase from Plasmodium Falciparum. *Malar. J.* **2013**, *12*, 1–15.
(493) Struck, N. S.; Herrmann, S.; Schmuck-Barkmann, I.; De Souza Dias, S.; Haase, S.; Cabrera, A. L.; Treeck, M.; Bruns, C.; Langer, C.; Cowman, A. F.; et al. Spatial Dissection of the Cis- and Trans-Golgi Compartments in the Malaria Parasite Plasmodium Falciparum. *Mol. Microbiol.* **2008**, *67*, 1320–1330.
(494) Pendyala, P. R.; Ayong, L.; Eatrides, J.; Schreiber, M.; Pham, C.; Chakrabarti, R.; Fidock, D. A.; Allen, C. M.; Chakrabarti, D. Characterization of a PRL Protein Tyrosine Phosphatase from Plasmodium Falciparum. *Mol. Biochem. Parasitol.* **2008**, *158*, 1–10.
(495) Ayong, L.; DaSilva, T.; Mauser, J.; Allen, C. M.; Chakrabarti, D. Evidence for Prenylation-Dependent Targeting of a Ykt6 SNARE in Plasmodium Falciparum. *Mol. Biochem. Parasitol.* **2011**, *175*, 162–168.
(496) Soni, R.; Sharma, D.; Patel, S.; Sharma, B.; Bhatt, T. K. Structure-Based Binding between Protein Farnesyl Transferase and PRL-PTP of Malaria Parasite: An Interaction Study of Prenylation Process in Plasmodium. *J. Biomol. Struct. Dyn.* **2016**, 1–12.
(497) Ohkanda, J.; Lockman, J. W.; Yokoyama, K.; Gelb, M. H.; Croft, S. L.; Kendrick, H.; Harrell, M. I.; Feagin, J. E.; Blaskovich, M. A.; Sebti, S. M.; et al. Peptidomimetic Inhibitors of Protein Farnesyltransferase Show Potent Antimalarial Activity. *Bioorg. Med. Chem. Lett.* **2001**, *11*, 761–764.
(498) Olepu, S.; Suryadevara, P. K.; Rivas, K.; Yokoyama, K.; Verlinde, C. L. M. J.; Chakrabarti, D.; Van Voorhis, W. C.; Gelb, M. H. 2-Oxo-Tetrahydro-1,8-Naphthyridines as Selective Inhibitors of Malarial Protein Farnesyltransferase and as Anti-Malarials. *Bioorg. Med. Chem. Lett.* **2008**, *18*, 494–497.
(499) Jordão, F. M.; Saito, A. Y.; Miguel, D. C.; de Jesus Peres, V.; Kimura, E. A.; Katzin, A. M. In Vitro and In Vivo Antiplasmodial Activities of Risedronate and Its Interference with Protein Prenylation in Plasmodium Falciparum. *Antimicrob. Agents Chemother.* **2011**, *55*, 2026–2031.
(500) Casey, P. J.; Seabra, M. C. Protein Prenyltransferases. *J. Biol. Chem.* **1996**, *271*, 5289–5292.
(501) Maurer-Stroh, S.; Koranda, M.; Benetka, W.; Schneider, G.; Sirota, F. L.;

Eisenhaber, F. Towards Complete Sets of Farnesylated and Geranylgeranylated Proteins. *PLoS Comput. Biol.* **2007**, *3*, e66.
(502) Moura, I. C.; Wunderlich, G.; Uhrig, M. L.; Couto, A. S.; Peres, V. J.; Katzin, A. M.; Kimura, E. A. Limonene Arrests Parasite Development and Inhibits Isoprenylation of Proteins in Plasmodium Falciparum. *Antimicrob. Agents Chemother.* **2001**, *45*, 2553–2558.
(503) Quevillon, E.; Spielmann, T.; Brahimi, K.; Chattopadhyay, D.; Yeramian, E.; Langsley, G. The Plasmodium Falciparum Family of Rab GTPases. *Gene* **2003**, *306*, 13–25.
(504) Dacks, J. B.; Field, M. C. Evolution of the Eukaryotic Membrane-Trafficking System: Origin, Tempo and Mode. *J. Cell Sci.* **2007**, *120*, 2977–2985.
(505) Rojas, A. M.; Fuentes, G.; Rausell, A.; Valencia, A. The Ras Protein Superfamily: Evolutionary Tree and Role of Conserved Amino Acids. *J. Cell Biol.* **2012**, *196*, 189–201.
(506) Botha, M.; Chiang, A. N.; Needham, P. G.; Stephens, L. L.; Hoppe, H. C.; Külzer, S.; Przyborski, J. M.; Lingelbach, K.; Wipf, P.; Brodsky, J. L.; et al. Plasmodium Falciparum Encodes a Single Cytosolic Type I Hsp40 That Functionally Interacts with Hsp70 and Is Upregulated by Heat Shock. *Cell Stress Chaperones* **2011**, *16*, 389–401.
(507) Pesce, E.-R.; Cockburn, I. L.; Goble, J. L.; Stephens, L. L.; Blatch, G. L. Malaria Heat Shock Proteins: Drug Targets That Chaperone Other Drug Targets. *Infect. Disord. - Drug TargetsDisorders)* **2010**, *10*, 147–157.
(508) Flom, G. A.; Lemieszek, M.; Fortunato, E. A.; Johnson, J. L. Farnesylation of Ydj1 Is Required for In Vivo Interaction with Hsp90 Client Proteins. *Mol. Biol. Cell* **2008**, *19*, 5249–5258.
(509) Summers, D. W.; Douglas, P. M.; Ren, H.-Y.; Cyr, D. M. The Type I Hsp40 Ydj1 Utilizes a Farnesyl Moiety and Zinc Finger-like Region to Suppress Prion Toxicity. *J. Biol. Chem.* **2009**, *284*, 3628–3639.
(510) Pesce, E.; Blatch, G. L. The Hsp40-Hsp70 Chaperone Machinery of Plasmodium Falciparum. *African J. Biochem. Res.* **2009**, *3*, 154–163.
(511) Trager, W.; Jensen, J. B. Human Malaria Parasites in Continuous Culture. *Science (80-.).* **1976**, *193*, 673–675.
(512) Mehlin, C.; Boni, E.; Buckner, F. S.; Engel, L.; Feist, T.; Gelb, M. H.; Haji, L.; Kim, D.; Liu, C.; Mueller, N.; et al. Heterologous Expression of Proteins from Plasmodium Falciparum: Results from 1000 Genes. *Mol. Biochem. Parasitol.* **2006**, *148*, 144–160.
(513) Imlay, L. S.; Armstrong, C. M.; Masters, M. C.; Li, T.; Price, K. E.; Edwards, R. L.; Mann, K. M.; Li, L. X.; Stallings, C. L.; Berry, N. G.; et al. Plasmodium IspD (2-C-Methyl-d-Erythritol 4-Phosphate Cytidyltransferase), an Essential and Druggable Antimalarial Target. *ACS Infect. Dis.* **2015**, *1*, 157–167.
(514) Kalli, A.; Smith, G. T.; Sweredoski, M. J.; Hess, S. Evaluation and Optimization of Mass Spectrometric Settings during Data-Dependent Acquisition Mode: Focus on LTQ-Orbitrap Mass Analyzers. *J. Proteome Res.* **2013**, *12*, 3071–3086.
(515) Consortium, T. U. Reorganizing the Protein Space at the Universal Protein Resource (UniProt). *Nucleic Acids Res.* **2012**, *40*, D71–D75.
(516) Nesvizhskii, A. I.; Keller, A.; Kolker, E.; Aebersold, R. A Statistical Model for

Identifying Proteins by Tandem Mass Spectrometry. *Anal. Chem.* **2003**, *75*, 4646–4658.
(517) Lerner, E. C.; Zhang, T.-T.; Knowles, D. B.; Qian, Y.; Hamilton, A. D.; Sebti, S. M. Inhibition of the Prenylation of K-Ras, but Not H- or N-Ras, Is Highly Resistant to CAAX Peptidomimetics and Requires Both a Farnesyltransferase and a Geranylgeranyltransferase I Inhibitor in Human Tumor Cell Lines. *Oncogene* **1997**, *15*, 1283.
(518) Rashidian, M.; Dozier, J. K.; Lenevich, S.; Distefano, M. D. Selective Labeling of Polypeptides Using Protein Farnesyltransferase via Rapid Oxime Ligation. *Chem. Commun.* **2010**, *46*, 8998–9000.
(519) Henry, O.; Lopez-Gallego, F.; Agger, S. A.; Schmidt-Dannert, C.; Sen, S.; Shintani, D.; Cornish, K.; Distefano, M. D. A Versatile Photoactivatable Probe Designed to Label the Diphosphate Binding Site of Farnesyl Diphosphate Utilizing Enzymes. *Bioorg. Med. Chem.* **2009**, *17*, 4797–4805.
(520) Duckworth, B. P.; Chen, Y.; Wollack, J. W.; Sham, Y.; Mueller, J. D.; Taton, T. A.; Distefano, M. D. A Universal Method for the Preparation of Covalent Protein–DNA Conjugates for Use in Creating Protein Nanostructures. *Angew. Chemie Int. Ed.* **2007**, *46*, 8819–8822.
(521) Rashidian, M.; Kumarapperuma, S. C.; Gabrielse, K.; Fegan, A.; Wagner, C. R.; Distefano, M. D. Simultaneous Dual Protein Labeling Using a Triorthogonal Reagent. *J. Am. Chem. Soc.* **2013**, *135*, 16388–16396.
(522) Rashidian, M.; Song, J. M.; Pricer, R. E.; Distefano, M. D. Chemoenzymatic Reversible Immobilization and Labeling of Proteins without Prior Purification. *J. Am. Chem. Soc.* **2012**, *134*, 8455–8467.
(523) Mahmoodi, M. M.; Rashidian, M.; Dozier, J. K.; Distefano, M. D. Chemoenzymatic Site-Specific Reversible Immobilization and Labeling of Proteins from Crude Cellular Extract Without Prior Purification Using Oxime and Hydrazine Ligation. *Curr. Protoc. Chem. Biol.* **2013**, *5*, 89–109.
(524) Cravatt, B. F.; Sorensen, E. J. Chemical Strategies for the Global Analysis of Protein Function. *Curr. Opin. Chem. Biol.* **2000**, *4*, 663–668.
(525) Speers, A. E.; Cravatt, B. F. Profiling Enzyme Activities In Vivo Using Click Chemistry Methods. *Chem. Biol.* **2004**, *11*, 535–546.
(526) Diaz-Rodriguez, V.; Hsu, E.-T.; Ganusova, E.; Werst, E.; Becker, J. M.; Hrycyna, C. A.; Distefano, M. D. A-Factor Analogues Containing Alkyne- and Azide Functionalized Isoprenoids Are Efficiently Enzymatically Processed and Retain Wild Type Bioactivity. *Bioconjug. Chem.* **2017**, Just Accepted.
(527) Gisselberg, J. E.; Zhang, L.; Elias, J. E.; Yeh, E. The Prenylated Proteome of Plasmodium Falciparum Reveals Pathogen-Specific Prenylation Activity and Drug Mechanism-of-Action. *Mol. Cell. Proteomics* **2016**.
(528) Scandinavian Simvastatin Survival Study Group. Randomised Trial of Cholesterol Lowering in 4444 Patients with Coronary Heart Disease: The Scandinavian Simvastatin Survival Study (4S). *Lancet* **1994**, *344*, 1383–1389.
(529) Goldstein, J. L.; Brown, M. S. A Century of Cholesterol and Coronaries: From Plaques to Genes to Statins. *Cell* **2015**, *161*, 161–172.
(530) Sacks, F. M.; Pfeffer, M. A.; Moye, L. A.; Rouleau, J. L.; Rutherford, J. D.; Cole, T. G.; Brown, L.; Warnica, J. W.; Arnold, J. M. O.; Wun, C.-C.; et al. The Effect

of Pravastatin on Coronary Events after Myocardial Infarction in Patients with Average Cholesterol Levels. *N. Engl. J. Med.* **1996**, *335*, 1001–1009.
(531) Endo, A.; Kuroda, M.; Tanzawa, K. Competitive Inhibition of 3-Hydroxy-3-Methylglutaryl Coenzyme a Reductase by ML-236A and ML-236B Fungal Metabolites, Having Hypocholesterolemic Activity. *FEBS Lett.* **1976**, *72*, 323–326.
(532) Endo, A. The Discovery and Development of HMG-CoA Reductase Inhibitors. *J. Lipid Res.* **1992**, *33*, 1569–1582.
(533) Li, L.; Zhang, W.; Cheng, S.; Cao, D.; Parent, M. Isoprenoids and Related Pharmacological Interventions: Potential Application in Alzheimer's Disease. *Mol. Neurobiol.* **2012**, *46*, 64–77.
(534) Istvan, E. S.; Deisenhofer, J. Structural Mechanism for Statin Inhibition of HMG-CoA Reductase. *Science (80-.).* **2001**, *292*, 1160 LP – 1164.
(535) Suazo, K. F.; Schaber, C.; Palsuledesai, C. C.; Odom John, A. R.; Distefano, M. D.; Feachem, R. G. A.; Ashley, E. A.; Seidlein, L. Von; Dondorp, A.; Eastman, R. T.; et al. Global Proteomic Analysis of Prenylated Proteins in Plasmodium Falciparum Using an Alkyne-Modified Isoprenoid Analogue. *Sci. Rep.* **2016**, *6*, 38615.
(536) Davisson, V. J.; Woodside, A. B.; Neal, T. R.; Stremler, K. E.; Muehlbacher, M.; Poulter, C. D. Phosphorylation of Isoprenoid Alcohols. *J. Org. Chem.* **1986**, *51*, 4768–4779.
(537) Feld, B. K.; Weiss, G. A. Convenient Methods for the Synthesis of P1-Farnesyl-P2-Indicator Diphosphates. *Bioorg. Med. Chem. Lett.* **2006**, *16*, 1665–1667.
(538) Stremler, K. E.; Poulter, C. D. Methane- and Difluoromethanediphosphonate Analogs of Geranyl Diphosphate: Hydrolysis-Inert Alternate Substrates. *J. Am. Chem. Soc.* **1987**, *109*, 5542–5544.
(539) Kavalipati, N.; Shah, J.; Ramakrishan, A.; Vasnawala, H. Pleiotropic Effects of Statins. *Indian J. Endocrinol. Metab.* **2015**, *19*, 554–562.
(540) Leitmeyer, K.; Glutz, A.; Setz, C.; Wieland, L.; Egloff, S.; Bodmer, D.; Brand, Y. Simvastatin Results in a Dose-Dependent Toxic Effect on Spiral Ganglion Neurons in an *In Vitro* Organotypic Culture Assay. *Biomed Res. Int.* **2016**, *2016*, 3580359.
(541) Fatehi Hassanabad, A. Current Perspectives on Statins as Potential Anti-Cancer Therapeutics: Clinical Outcomes and Underlying Molecular Mechanisms. *Transl. lung cancer Res.* **2019**, *8*, 692–699.
(542) Beck-Sickinger, A. G.; Mörl, K. Posttranslational Modification of Proteins. Expanding Nature's Inventory. By Christopher T. Walsh. *Angew. Chemie Int. Ed.* **2006**, *45*, 1020.
(543) Marshall, C. J. Protein Prenylation: A Mediator of Protein-Protein Interactions. *Science (80-.).* **1993**, *259*, 1865–1866.
(544) Safety and Efficacy of Tipifarnib in Head and Neck Cancer With HRAS Mutations and Impact of HRAS on Response to Therapy - ClinicalTrials https://www.clinicaltrials.gov/ct2/show/NCT03719690?term=NCT03719690&draw=2&rank=1.
(545) Maltese, W. A.; Sheridan, K. M.; Repko, E. M.; Erdman, R. A. Post-Translational Modification of Low Molecular Mass GTP-Binding Proteins by Isoprenoid. *J.*

Biol. Chem. **1990**, *265*, 2148–2155.
(546) Farnsworth, C. C.; Casey, P. J.; Howald, W. N.; Glomset, J. A.; Gelb, M. H. Structural Characterization of Prenyl Groups Attached to Proteins. *Methods* **1990**, *1*, 231–240.
(547) Berndt, N.; Sebti, S. M. Measurement of Protein Farnesylation and Geranylgeranylation in Vitro, in Cultured Cells and in Biopsies, and the Effects of Prenyl Transferase Inhibitors. *Nat. Protoc.* **2011**, *6*, 1775–1791.
(548) Lin, H. P.; Hsu, S. C.; Wu, J. C.; Sheen, I. J.; Yan, B. S.; Syu, W. J. Localization of Isoprenylated Antigen of Hepatitis Delta Virus by Anti-Farnesyl Antibodies. *J. Gen. Virol.* **1999**, *80*, 91–96.
(549) Baron, R.; Fourcade, E.; Lajoie-Mazenc, I.; Allal, C.; Couderc, B.; Barbaras, R.; Favre, G.; Faye, J.-C.; Pradines, A. RhoB Prenylation Is Driven by the Three Carboxyl-Terminal Amino Acids of the Protein: Evidenced in Vivo by an Anti-Farnesyl Cysteine Antibody. *Proc. Natl. Acad. Sci.* **2000**, *97*, 11626 LP – 11631.
(550) Suazo, K. F.; Hurben, A. K.; Liu, K.; Xu, F.; Thao, P.; Sudheer, C.; Li, L.; Distefano, M. D. Metabolic Labeling of Prenylated Proteins Using Alkyne-Modified Isoprenoid Analogues. *Curr. Protoc. Chem. Biol.* **2018**, *0*, e46.
(551) Raghu, V. K.; Beckwitt, C. H.; Warita, K.; Wells, A.; Benos, P. V; Oltvai, Z. N. Biomarker Identification for Statin Sensitivity of Cancer Cell Lines. *Biochem. Biophys. Res. Commun.* **2018**, *495*, 659–665.
(552) McAlister, G. C.; Nusinow, D. P.; Jedrychowski, M. P.; Wühr, M.; Huttlin, E. L.; Erickson, B. K.; Rad, R.; Haas, W.; Gygi, S. P. MultiNotch MS3 Enables Accurate, Sensitive, and Multiplexed Detection of Differential Expression across Cancer Cell Line Proteomes. *Anal. Chem.* **2014**, *86*, 7150–7158.
(553) Aditya, A. V. Investigation of Peptide Substrate Specificity and Design of Novel Bisubstrate Inhibitors of Protein Geranylgeranyl Transferase-I, Purdue University, 2010.
(554) Barrowman, J.; Hamblet, C.; Kane, M. S.; Michaelis, S. Requirements for Efficient Proteolytic Cleavage of Prelamin A by ZMPSTE24. *PLoS One* **2012**, *7*, e32120–e32120.
(555) Holstein, S. A.; Wohlford-Lenane, C. L.; Hohl, R. J. Isoprenoids Influence Expression of Ras and Ras-Related Proteins. *Biochemistry* **2002**, *41*, 13698–13704.
(556) Wong, W. W.-L.; Clendening, J. W.; Martirosyan, A.; Boutros, P. C.; Bros, C.; Khosravi, F.; Jurisica, I.; Stewart, A. K.; Bergsagel, P. L.; Penn, L. Z. Determinants of Sensitivity to Lovastatin-Induced Apoptosis in Multiple Myeloma. *Mol. Cancer Ther.* **2007**, *6*, 1886 LP – 1897.
(557) Gbelcová, H.; Rimpelová, S.; Ruml, T.; Fenclová, M.; Kosek, V.; Hajšlová, J.; Strnad, H.; Kolář, M.; Vítek, L. Variability in Statin-Induced Changes in Gene Expression Profiles of Pancreatic Cancer. *Sci. Rep.* **2017**, *7*, 44219.
(558) Tabb, D. L.; Vega-Montoto, L.; Rudnick, P. A.; Variyath, A. M.; Ham, A.-J. L.; Bunk, D. M.; Kilpatrick, L. E.; Billheimer, D. D.; Blackman, R. K.; Cardasis, H. L.; et al. Repeatability and Reproducibility in Proteomic Identifications by Liquid Chromatography-Tandem Mass Spectrometry. *J. Proteome Res.* **2010**, *9*, 761–776.
(559) Zhang, Y.; Chen, K.; Sloan, S. A.; Bennett, M. L.; Scholze, A. R.; O'Keeffe, S.; Phatnani, H. P.; Guarnieri, P.; Caneda, C.; Ruderisch, N.; et al. An RNA-

Sequencing Transcriptome and Splicing Database of Glia, Neurons, and Vascular Cells of the Cerebral Cortex. *J. Neurosci.* **2014**, *34*, 11929 LP – 11947.
(560) Furfine, E. S.; Leban, J. J.; Landavazo, A.; Moomaw, J. F.; Casey, P. J. Protein Farnesyltransferase: Kinetics of Farnesyl Pyrophosphate Binding and Product Release. *Biochemistry* **1995**, *34*, 6857–6862.
(561) Yokoyama, K.; Zimmerman, K.; Scholten, J.; Gelb, M. H. Differential Prenyl Pyrophosphate Binding to Mammalian Protein Geranylgeranyltransferase-I and Protein Farnesyltransferase and Its Consequence on the Specificity of Protein Prenylation. *J. Biol. Chem.* **1997**, *272*, 3944–3952.
(562) Thomä, N. H.; Iakovenko, A.; Owen, D.; Scheidig, A. S.; Waldmann, H.; Goody, R. S.; Alexandrov, K. Phosphoisoprenoid Binding Specificity of Geranylgeranyltransferase Type II. *Biochemistry* **2000**, *39*, 12043–12052.
(563) Schwanhäusser, B.; Busse, D.; Li, N.; Dittmar, G.; Schuchhardt, J.; Wolf, J.; Chen, W.; Selbach, M. Global Quantification of Mammalian Gene Expression Control. *Nature* **2011**, *473*, 337–342.
(564) Eliuk, S.; Makarov, A. Evolution of Orbitrap Mass Spectrometry Instrumentation. *Annu. Rev. Anal. Chem.* **2015**, *8*, 61–80.
(565) Ting, L.; Rad, R.; Gygi, S. P.; Haas, W. MS3 Eliminates Ratio Distortion in Isobaric Multiplexed Quantitative Proteomics. *Nat. Methods* **2011**, *8*, 937–940.
(566) Mathur, B. N.; Caprioli, R. M.; Deutch, A. Y. Proteomic Analysis Illuminates a Novel Structural Definition of the Claustrum and Insula. *Cereb. Cortex* **2009**, *19*, 2372–2379.
(567) Pirone, A.; Cozzi, B.; Edelstein, L.; Peruffo, A.; Lenzi, C.; Quilici, F.; Antonini, R.; Castagna, M. Topography of Gng2- and NetrinG2-Expression Suggests an Insular Origin of the Human Claustrum. *PLoS One* **2012**, *7*, e44745–e44745.
(568) de Curtis, I. The Rac3 GTPase in Neuronal Development, Neurodevelopmental Disorders, and Cancer. *Cells* **2019**, *8*, 1063.
(569) Hottman, D. A.; Li, L. Protein Prenylation and Synaptic Plasticity: Implications for Alzheimer's Disease. *Mol. Neurobiol.* **2014**, *50*, 177–185.
(570) Thornton, C.; Yaka, R.; Dinh, S.; Ron, D. H-Ras Modulates N-Methyl-D-Aspartate Receptor Function via Inhibition of Src Tyrosine Kinase Activity. *J. Biol. Chem.* **2003**, *278*, 23823–23829.
(571) Manabe, T.; Aiba, A.; Yamada, A.; Ichise, T.; Sakagami, H.; Kondo, H.; Katsuki, M. Regulation of Long-Term Potentiation by H-Ras through NMDA Receptor Phosphorylation. *J. Neurosci.* **2000**, *20*, 2504 LP – 2511.
(572) Fivaz, M.; Bandara, S.; Inoue, T.; Meyer, T. Robust Neuronal Symmetry Breaking by Ras-Triggered Local Positive Feedback. *Curr. Biol.* **2008**, *18*, 44–50.
(573) Oinuma, I.; Katoh, H.; Negishi, M. R-Ras Controls Axon Specification Upstream of Glycogen Synthase Kinase-3β through Integrin-Linked Kinase. *J. Biol. Chem.* **2007**, *282*, 303–318.
(574) Iwasawa, N.; Negishi, M.; Oinuma, I. R-Ras Controls Axon Branching through Afadin in Cortical Neurons. *Mol. Biol. Cell* **2012**, *23*, 2793–2804.
(575) Goldenberg, N. M.; Grinstein, S.; Silverman, M. Golgi-Bound Rab34 Is a Novel Member of the Secretory Pathway. *Mol. Biol. Cell* **2007**, *18*, 4762–4771.
(576) Kasmapour, B.; Gronow, A.; Bleck, C. K. E.; Hong, W.; Gutierrez, M. G. Size-Dependent Mechanism of Cargo Sorting during Lysosome-Phagosome Fusion Is

Controlled by Rab34. *Proc. Natl. Acad. Sci.* **2012**, *109*, 20485 LP – 20490.
(577) Wang, H.; Gao, Y.; Chen, L.; Li, Y.; Jiang, C. RAB34 Was a Progression- and Prognosis-Associated Biomarker in Gliomas. *Tumor Biol.* **2015**, *36*, 1573–1578.
(578) Murga, C.; Zohar, M.; Teramoto, H.; Gutkind, J. S. Rac1 and RhoG Promote Cell Survival by the Activation of PI3K and Akt, Independently of Their Ability to Stimulate JNK and NF-KB. *Oncogene* **2002**, *21*, 207–216.
(579) Lee, J.; Park, B.; Kim, G.; Kim, K.; Pak, J.; Kim, K.; Ye, M. B.; Park, S.-G.; Park, D. Arhgef16, a Novel Elmo1 Binding Partner, Promotes Clearance of Apoptotic Cells via RhoG-Dependent Rac1 Activation. *Biochim. Biophys. Acta - Mol. Cell Res.* **2014**, *1843*, 2438–2447.
(580) Morikawa, M.; Fryer, J. D.; Sullivan, P. M.; Christopher, E. A.; Wahrle, S. E.; DeMattos, R. B.; O'Dell, M. A.; Fagan, A. M.; Lashuel, H. A.; Walz, T.; et al. Production and Characterization of Astrocyte-Derived Human Apolipoprotein E Isoforms from Immortalized Astrocytes and Their Interactions with Amyloid-β. *Neurobiol. Dis.* **2005**, *19*, 66–76.
(581) Chernick, D.; Ortiz-Valle, S.; Jeong, A.; Swaminathan, S. K.; Kandimalla, K. K.; Rebeck, G. W.; Li, L. High-Density Lipoprotein Mimetic Peptide 4F Mitigates Amyloid-β-Induced Inhibition of Apolipoprotein E Secretion and Lipidation in Primary Astrocytes and Microglia. *J. Neurochem.* **2018**, *147*, 647–662.
(582) Kim, J. H.; Lukowicz, A.; Qu, W.; Johnson, A.; Cvetanovic, M. Astroglia Contribute to the Pathogenesis of Spinocerebellar Ataxia Type 1 (SCA1) in a Biphasic, Stage-of-Disease Specific Manner. *Glia* **2018**, *66*, 1972–1987.
(583) Končitíková, R.; Vigouroux, A.; Kopečná, M.; Šebela, M.; Moréra, S.; Kopečný, D. Kinetic and Structural Analysis of Human ALDH9A1. *Biosci. Rep.* **2019**, *39*, BSR20190558.
(584) Wyatt, J. W.; Korasick, D. A.; Qureshi, I. A.; Campbell, A. C.; Gates, K. S.; Tanner, J. J. Inhibition, Crystal Structures, and in-Solution Oligomeric Structure of Aldehyde Dehydrogenase 9A1. *Arch. Biochem. Biophys.* **2020**, *691*, 108477.
(585) Duckworth, B. P.; Zhang, Z.; Hosokawa, A.; Distefano, M. D. Selective Labeling of Proteins by Using Protein Farnesyltransferase. *ChemBioChem* **2007**, *8*, 98–105.
(586) Kuzuguchi, T.; Morita, Y.; Sagami, I.; Sagami, H.; Ogura, K. Human Geranylgeranyl Diphosphate Synthase: CDNA CLONING AND EXPRESSION*. *J. Biol. Chem.* **1999**, *274*, 5888–5894.
(587) Lerner, E. C.; Qian, Y.; Hamilton, A. D.; Sebti, S. M. Disruption of Oncogenic K-Ras4B Processing and Signaling by a Potent Geranylgeranyltransferase I Inhibitor. *J. Biol. Chem.* **1995**, *270*, 26770–26773.
(588) Kaźmierczak, A.; Kusy, D.; Niinivehmas, S. P.; Gmach, J.; Joachimiak, Ł.; Pentikäinen, O. T.; Gendaszewska-Darmach, E.; Błażewska, K. M. Identification of the Privileged Position in the Imidazo[1,2-a]Pyridine Ring of Phosphonocarboxylates for Development of Rab Geranylgeranyl Transferase (RGGT) Inhibitors. *J. Med. Chem.* **2017**, *60*, 8781–8800.
(589) Joachimiak, Ł.; Marchwicka, A.; Gendaszewska-Darmach, E.; Błażewska, K. M. Synthesis and Biological Evaluation of Imidazole-Bearing α-Phosphonocarboxylates as Inhibitors of Rab Geranylgeranyl Transferase (RGGT). *ChemMedChem* **2018**, *13*, 842–851.
(590) Sophos, N. A.; Vasiliou, V. Aldehyde Dehydrogenase Gene Superfamily: The

2002 Update. *Chem. Biol. Interact.* **2003**, *143–144*, 5–22.
(591) Marchitti, S. A.; Brocker, C.; Stagos, D.; Vasiliou, V. Non-P450 Aldehyde Oxidizing Enzymes: The Aldehyde Dehydrogenase Superfamily. *Expert Opin. Drug Metab. Toxicol.* **2008**, *4*, 697–720.
(592) Koppaka, V.; Thompson, D. C.; Chen, Y.; Ellermann, M.; Nicolaou, K. C.; Juvonen, R. O.; Petersen, D.; Deitrich, R. A.; Hurley, T. D.; Vasiliou, V. Aldehyde Dehydrogenase Inhibitors: A Comprehensive Review of the Pharmacology, Mechanism of Action, Substrate Specificity, and Clinical Application. *Pharmacol. Rev.* **2012**, *64*, 520 LP – 539.
(593) Chern, M. K.; Pietruszko, R. Human Aldehyde Dehydrogenase E3 Isozyme Is a Betaine Aldehyde Dehydrogenase. *Biochem. Biophys. Res. Commun.* **1995**, *213*, 561–568.
(594) Vaz, F. M.; Fouchier, S. W.; Ofman, R.; Sommer, M.; Wanders, R. J. A. Molecular and Biochemical Characterization of Rat γ-Trimethylaminobutyraldehyde Dehydrogenase and Evidence for the Involvement of Human Aldehyde Dehydrogenase 9 in Carnitine Biosynthesis*. *J. Biol. Chem.* **2000**, *275*, 7390–7394.
(595) Kurys, G.; Ambroziak, W.; Pietruszko, R. Human Aldehyde Dehydrogenase: Purification and Characterization of a Third Isozyme with Low Km for γ-Aminobutyraldehyde. *J. Biol. Chem.* **1989**, *264*, 4715–4721.
(596) Zhang, Y.; Wang, M.; Lin, H. A Regulatory Cysteine Residue Mediates Reversible Inactivation of NAD+-Dependent Aldehyde Dehydrogenases to Promote Oxidative Stress Response. *ACS Chem. Biol.* **2020**, *15*, 28–32.
(597) Kitamura, T.; Takagi, S.; Naganuma, T.; Kihara, A. Mouse Aldehyde Dehydrogenase ALDH3B2 Is Localized to Lipid Droplets via Two C-Terminal Tryptophan Residues and Lipid Modification. *Biochem. J.* **2014**, *465*, 79–87.
(598) Fink, A. L. Protein Aggregation: Folding Aggregates, Inclusion Bodies and Amyloid. *Fold. Des.* **1998**, *3*, R9–R23.
(599) Petras, S. F.; Lindsey, S.; Harwood Jr., H. J. HMG-CoA Reductase Regulation: Use of Structurally Diverse First Half-Reaction Squalene Synthetase Inhibitors to Characterize the Site of Mevalonate-Derived Nonsterol Regulator Production in Cultured IM-9 Cells. *J. Lipid Res.* **1999**, *40*, 24–38.
(600) Vaidya, S.; Bostedor, R.; Kurtz, M. M.; Bergstrom, J. D.; Bansal, V. S. Massive Production of Farnesol-Derived Dicarboxylic Acids in Mice Treated with the Squalene Synthase Inhibitor Zaragozic Acid A. *Arch. Biochem. Biophys.* **1998**, *355*, 84–92.
(601) Baker, F. C.; Mauchamp, B.; Tsai, L. W.; Schooley, D. A. Farnesol and Farnesal Dehydrogenase(s) in Corpora Allata of the Tobacco Hornworm Moth, Manduca Sexta. *J. Lipid Res.* **1983**, *24*, 1586–1594.
(602) Sperry, A. E.; Sen, S. E. Farnesol Oxidation in Insects: Evidence That the Biosynthesis of Insect Juvenile Hormone Is Mediated by a Specific Alcohol Oxidase. *Insect Biochem. Mol. Biol.* **2001**, *31*, 171–178.
(603) De Loof, A.; Marchal, E.; Rivera-Perez, C.; Noriega, F. G.; Schoofs, L. Farnesol-like Endogenous Sesquiterpenoids in Vertebrates: The Probable but Overlooked Functional "Inbrome" Anti-Aging Counterpart of Juvenile Hormone of Insects? *Front. Endocrinol. (Lausanne).* **2015**, *5*, 222.

(604) Kim, S.; Kim, E.; Shin, D.-S.; Kang, H.; Oh, K.-B. Evaluation of Morphogenic Regulatory Activity of Farnesoic Acid and Its Derivatives against Candida Albicans Dimorphism. *Bioorg. Med. Chem. Lett.* **2002**, *12*, 895–898.
(605) Mitake, M.; Shidoji, Y. Geranylgeraniol Oxidase Activity Involved in Oxidative Formation of Geranylgeranoic Acid in Human Hepatoma Cells. *Biomed. Res.* **2012**, *33*, 15–24.
(606) Singh, S.; Brocker, C.; Koppaka, V.; Chen, Y.; Jackson, B. C.; Matsumoto, A.; Thompson, D. C.; Vasiliou, V. Aldehyde Dehydrogenases in Cellular Responses to Oxidative/Electrophilic Stress. *Free Radic. Biol. Med.* **2013**, *56*, 89–101.
(607) Dinavahi, S. S.; Bazewicz, C. G.; Gowda, R.; Robertson, G. P. Aldehyde Dehydrogenase Inhibitors for Cancer Therapeutics. *Trends Pharmacol. Sci.* **2019**, *40*, 774–789.
(608) Johansson, J.; Fleetwood, L.; Jörnvall, H. Cysteine Reactivity in Sorbitol and Aldehyde Dehydrogenases Differences towards the Pattern in Alcohol Dehydrogenase. *FEBS Lett.* **1992**, *303*, 1–3.
(609) Ford, B.; Bateman, L. A.; Gutierrez-Palominos, L.; Park, R.; Nomura, D. K. Mapping Proteome-Wide Targets of Glyphosate in Mice. *Cell Chem. Biol.* **2017**, *24*, 133–140.
(610) Whitby, L. R.; Obach, R. S.; Simon, G. M.; Hayward, M. M.; Cravatt, B. F. Quantitative Chemical Proteomic Profiling of the in Vivo Targets of Reactive Drug Metabolites. *ACS Chem. Biol.* **2017**, *12*, 2040–2050.
(611) Huang, Z.; Ogasawara, D.; Seneviratne, U. I.; Cognetta 3rd, A. B.; Am Ende, C. W.; Nason, D. M.; Lapham, K.; Litchfield, J.; Johnson, D. S.; Cravatt, B. F. Global Portrait of Protein Targets of Metabolites of the Neurotoxic Compound BIA 10-2474. *ACS Chem. Biol.* **2019**, *14*, 192–197.
(612) Sellés Vidal, L.; Kelly, C. L.; Mordaka, P. M.; Heap, J. T. Review of NAD(P)H-Dependent Oxidoreductases: Properties, Engineering and Application. *Biochim. Biophys. Acta - Proteins Proteomics* **2018**, *1866*, 327–347.
(613) Kutzenko, A. S.; Lamzin, V. S.; Popov, V. O. Conserved Supersecondary Structural Motif in NAD-Dependent Dehydrogenases. *FEBS Lett.* **1998**, *423*, 105–109.
(614) Strijbis, K.; Vaz, F. M.; Distel, B. Enzymology of the Carnitine Biosynthesis Pathway. *IUBMB Life* **2010**, *62*, 357–362.
(615) David, S. J.; K., D. G. Overcoming Challenges With Statin Therapy. *J. Am. Heart Assoc.* **2021**, *5*, e002497.
(616) Kuleshov, M. V; Jones, M. R.; Rouillard, A. D.; Fernandez, N. F.; Duan, Q.; Wang, Z.; Koplev, S.; Jenkins, S. L.; Jagodnik, K. M.; Lachmann, A.; et al. Enrichr: A Comprehensive Gene Set Enrichment Analysis Web Server 2016 Update. *Nucleic Acids Res.* **2016**, *44*, W90–W97.

Appendix

Table A. 1. List of prenylated proteins identified from COS-7 cells.

Proteins are categorized into substrates of FTase (red), GGTase-I (blue), and RabGGTase (green).

-LOG(P-value)	Log2(fold change)	Majority protein IDs	Gene names	Peptides	Sequence coverage [%]	Mol. weight [kDa]
2.96	1.60	G3V3G9;Q5TAQ9	DCAF8	2	2.7	84.8
4.25	4.16	O15498	YKT6	10	61.1	22.4
4.11	4.70	O60884	DNAJA2	11	26	45.7
3.18	2.27	O75781	PALM	9	25.6	42.1
5.31	4.73	P01111	NRAS	6	44.4	21.2
3.22	5.84	P01116	KRAS	5	37	21.7
4.44	4.09	P20700	LMNB1	34	48.6	66.4
3.63	3.69	P31689	DNAJA1	10	34.8	44.9
3.68	3.74	P40855	PEX19	4	13.4	32.8
2.17	1.54	P49454	CENPF	10	3.2	367.8
4.12	5.29	P55209	NAP1L1	7	21.2	45.4
4.65	4.47	Q03252	LMNB2	28	40.5	69.9
3.97	2.92	Q12974;Q93096	PTP4A2;PTP4A1	4	22.8	19.1
3.45	3.68	Q14642	INPP5A	2	3.9	47.8
3.13	6.91	Q15382	RHEB	6	33.2	20.5
3.75	2.22	Q16644;P49137	MAPKAPK3;MAPKAPK2	3	8.4	43.0
2.73	1.00	Q27J81	INF2	2	1.7	135.6
4.31	4.77	Q5VW32	BROX	9	21.7	46.5
2.81	2.23	Q6P2H3	CEP85	3	4.7	85.6
4.17	1.96	Q7Z2W4	ZC3HAV1	1	1	101.4
2.90	2.31	Q8NDI1	EHBP1	4	3.2	140.0
3.44	3.67	Q99733	NAP1L4	8	21.6	42.8
2.87	0.89	P02545	LMNA	23	39.2	74.1
1.65	1.61	A0A024R161;P50151	hCG_1994888;GNG10	1	9.8	16.5
2.71	4.43	A0A0J9YXB3;A6NIZ1		6	36.4	18.9
3.53	4.05	O14807	MRAS	3	16.8	23.8
2.61	1.76	O95164	UBL3	2	17.9	13.2
3.72	3.26	P09543	CNP	14	25.9	47.6
3.46	4.47	P10301	RRAS	7	39.4	23.5
3.93	3.94	P11233	RALA	5	35.9	23.6
3.22	2.05	P11234	RALB	5	34	23.4
1.84	1.42	P32456;P32455	GBP2;GBP1	1	2	67.2
3.77	6.89	P60953	CDC42	3	16.8	21.3
3.43	6.90	P61224	RAP1B	6	32.6	20.8
3.50	4.38	P61225	RAP2B	6	39.3	20.5
4.49	6.42	P61586;P08134	RHOA;RHOC	4	19.2	21.8
5.37	4.50	P62745;U3KQV3	RHOB	2	12.8	22.1
2.92	4.67	P62834	RAP1A	6	32.6	21.0
3.65	6.60	P63000;P15153	RAC1;RAC2	6	27.1	21.5

3.51	4.33	P63218	GNG5	5	42.6	7.3
4.50	2.77	P84095	RHOG	6	36.6	21.3
4.19	4.10	Q9UBI6	GNG12	3	47.2	8.0
3.74	4.07	Q9Y3L5	RAP2C	4	31.1	20.7
4.21	2.77	O95716	RAB3D	3	12.8	24.3
4.83	5.86	P20338	RAB4A	2	11.5	24.4
3.53	5.25	P20339	RAB5A	9	54	23.7
4.02	5.42	P20340	RAB6A	7	37	23.6
3.89	3.58	P51148;K7ERQ8	RAB5C	9	58.8	23.5
4.11	3.54	P51149	RAB7A	12	59.4	23.5
3.04	6.62	P51151;Q9NP90	RAB9A;RAB9B	4	23.4	22.8
4.54	4.86	P51153	RAB13	6	30.5	22.8
3.91	3.06	P51157	RAB28	4	20.4	24.8
4.09	3.83	P61006	RAB8A	12	50.7	23.7
5.22	3.20	P61018	RAB4B	3	19.2	23.6
4.16	3.28	P61019	RAB2A	11	58.5	23.5
4.45	4.73	P61020	RAB5B	8	53.5	23.7
4.42	4.84	P61026	RAB10	11	53	22.5
4.70	4.56	P61106	RAB14	12	70.2	23.9
5.00	2.82	P62491	RAB11A	11	59.7	24.4
4.61	3.33	P62820	RAB1A	13	65.4	22.7
3.87	4.59	Q13636	RAB31	3	16.5	21.6
3.20	1.92	Q13637	RAB32	6	32	25.0
4.07	3.37	Q15286	RAB35	7	31.3	23.0
6.62	4.60	Q15907	RAB11B	11	51.8	24.5
4.44	4.30	Q92930	RAB8B	8	39.6	23.6
1.69	3.60	Q969Q5	RAB24	1	4.4	23.1
3.77	2.80	Q9BZG1	RAB34	4	20.1	29.0
2.27	0.94	Q9H082	RAB33B	2	11.8	25.7
2.37	0.91	Q9H0N0	RAB6C	2	13	28.4
4.53	3.84	Q9H0U4;Q92928	RAB1B;RAB1C	11	56.2	22.2
4.70	4.40	Q9NP72	RAB18	10	48.1	23.0
2.15	2.05	Q9NRW1	RAB6B	6	32.2	23.5
4.52	4.03	Q9UL25	RAB21	5	20.4	24.3
3.19	1.78	Q9UL26	RAB22A	4	25.8	21.9
4.23	2.83	Q9ULC3	RAB23	3	16	26.7
4.07	2.25	O75475	PSIP1	4	7.7	60.1
3.91	3.46	Q53S48;Q9Y6Q2	ALF;STON1	2	2.1	132.1
1.86	2.17	Q7L7V1	DHX32	1	1.1	84.4
0.99	1.65	P62070	RRAS2	6	33.3	23.4